Structural and functional characterization of the rotor rings from a *Fusobacterium* F-type and a *Burkholderia* N-type rotary ATPase

Dissertation
zur Erlangung des Doktorgrades
der Naturwissenschaften

vorgelegt beim Fachbereich 14
Biochemie, Chemie, Pharmazie
der Johann Wolfgang Goethe-Universität
in Frankfurt am Main

von
Sarah Schulz
aus Heidelberg, Deutschland

Frankfurt am Main, 2015
(D30)

Diese Arbeit wurde in der Arbeitsgruppe von Prof. Dr. Thomas Meier der Abteilung Strukturbiologie des Max-Planck-Institutes für Biophysik in Frankfurt am Main durchgeführt und vom Fachbereich 14 Biochemie, Chemie und Pharmazie der Johann Wolfgang Goethe-Universität als Dissertation angenommen.

Dekan: Prof. Dr. Michael Karas

1. Gutachter: Prof. Dr. Klaas Martinus Pos
2. Gutachter: Prof. Dr. Werner Kühlbrandt

Datum der Disputation: _____

Table of contents

List of figures

List of tables

List of abbreviations

°C	degrees Celsius
2D	two dimensional
3D	three dimensional
Å	Angstrom(s)
ADP	adenosine-5`-diphosphate
AEX	anion exchange chromatography
AFM	atomic force microscopy
AMP-PNP	5`-adenylyl-imidodiphosphate
Amp	ampicillin
APS	ammonium persulfate
ATP	adenosine-5`-triphosphate
BCA	bicinchoninic acid
BN	blue native
bp	base pairs
BSA	bovine serum albumin
B. pseudomallei	*Burkholderia pseudomallei*
B. thailandensis	*Burkholderia thailandensis*
CCD	charge coupled device
CCCP	carbonylcyanid-*m*-chlorophenylhydrazon
CTF	contrast transfer function
CV	column volume
DCCD	dicyclohexylcarbodiimide
DDM	n-dodecyl-ß-D-maltoside
DM	n-decyl-ß-D-maltoside
DMSO	dimethyl-sulfoxide
(c)DNA	(complementary) deoxyribonucleic acid
dNTP	deoxyribonucleotide triphosphate
E. coli	*Escherichia coli*
EDTA	ethylendiaminetetraacetic acid
EM	elecron microscope
ESI-MS	Electrospray Ionization Mass Spectrometry

ESRF	European Synchrotron Radiation Facility
et al.	*et alii*
g	gram(s)
$His_{6/10}$	hexameric/decameric histidin tag
IPTG	isopropyl-ß-D-1-thiogalactopyranoside
I. tartaricus	*Ilyobacter tartaricus*
kDa	kilo Dalton
kJ	kilo Joule
l	liter
LB	Luria Bertani
LDAO	lauryldimethylamide-N-oxide
LS	laurylsarcosine
m	milli
MALDI-MS	Matrix Assisted Laser Desorption Ionization Mass Spectrometry
min	minute(s)
M	molar
MPD	2-methyl-2,4-pentanediol
MWCO	molecular weight cutoff
m/z	mass-to-charge ratio
NaN_3	sodium azide
NADH	nicotinamide adenine dinucleotide
NCD-4	*N*-cyclohexyl-*N`*-(4-dimethylamino-α-naphtyl)carbodiimide
NMR	nuclear magnetic resonance
NTA	nitrilotriacetic acid
OG	n-octyl-ß-D-glucoside
OD	optical density
PAGE	polyacrylamide gelelectrophoresis
PCR	polymerase chain reaction
pdb	protein data base
P_i	inorganic phosphate
pKa	acid dissociation constant
pmf	*proton motive force*
PEG	polyethylene glycol

PVDF	polyvinylidene fluoride
RELION	REgularized LIkelihood OptimizatioN
(r)RNA	(ribosomale) ribonucleic acid
rpm	rotations per minute
SEC	size exclusion chromatography
SDS	sodium dodecyl sulfate
sec	second(s)
SLS	Swiss Light Source
SNR	Signal-to-Noise Ratio
smf	*sodium motive force*
T	temperature
t	time
TBT-Cl	tributyltin chloride
TCA	trichloroacetic acid
TEMED	tetramethylethylenediamine
TMH	transmembrane helix
Tris	2-amino-2-hydroxymethyl-propane-1,3-diol
v/v	volume/volume
v/w	volume/weight
w/v	weight/volume
w/w	weight/weight
wt	wildtype
µ	micro

Abstract

Rotary adenosine triphosphate (ATP)ases are ubiquitous, membrane-bound enzyme complexes involved in biological energy conversion. The first subtype, the so-called F_1F_o ATP synthase, predominantly functions as an ATP synthesizing machinery in most bacteria, mitochondria and chloroplasts. The vacuolar subtype of enzyme, the V_1V_o ATPase, operates as an ATP driven ion-pump in eukaryotic membranes. The third subtype found in archaea and some bacteria is called A_1A_o ATP (synth)ase and is capable of working in both directions either to synthesize ATP or to generate an ion motive force by consuming the same.

All the three above-mentioned subtypes of rotary ATPases work as nanomolecular machines sharing a conserved mechanism to perform the energy conservation process. The simplest form of these enzymes is the bacterial F_1F_o ATP synthase. Here, ions are channelled via the membrane stator a-subunit to the rotor ring of the enzyme. After almost a complete rotation of the ring the ions are released again on the other side of the membrane. This rotation is further transmitted via the central stalk to the soluble part of the enzyme, the F_1-complex, where conformational changes within the nucleotide binding sites result in the synthesis of ATP from ADP and P_i.

The rotor or c-ring of the enzyme is the key protein complex in mediating transmembrane ion translocation. Several structural and biochemical methods have been applied in the past years to study the rotor rings from many different organisms. The results revealed that the stoichiometry of a c-ring of a given species is constant while it can vary between different species within a range of 8 to 15 c-subunits. The c-ring stoichiometry determines directly the number of ions transported through F_o per rotation whereby three molecules of ATP are concurrently synthesized in the water-soluble F_1 headgroup. Hence the number of c-subunits has an important influence on the bioenergetics of the corresponding enzyme and thus the entire organism.

The c-ring of a rotary ATPase is able to specifically bind either protons (H^+) or sodium ions (Na^+) as a coupling ion for the enzyme. Several structures are already available revealing the coordination network of both types of rotor rings. In each case ion-binding includes a highly-conserved carboxylic acid residue (glutamate or aspartate), in addition to a more varying combination of amino acid residues, whereby Na^+-coordination is structurally more demanding than H^+-binding.

In the first part of my PhD thesis, I aimed to characterize the F_1F_o ATP synthase rotor ring of the opportunistic pathogenic bacterium *Fusobacterium nucleatum* on a functional and structural level. *F. nucleatum* is an anaerobic bacterium which uses peptides and amino acids as a primary energy source. It is one of the most frequently occuring bacteria in human body infections and involved in human periodontal diseases.

The protein complex was heterologously expressed within a hybrid ATP synthase in *Escherichia coli* and purified without an affinity tag for further analysis. Two high resolution X-ray structures of the c-ring were solved at low (5.3) and high (8.7) pH to 2.2 Å and 2.64 Å, respectively. In both structures, the conserved glutamate is in an ion-locked conformation, revealing that the conformational state of the ion-binding carboxylate is not depending on the pH of the crystallization condition, which is in good agreement with previous structural and biochemical studies of other c-rings.

A Na^+-ion is present within the c-ring binding site and directly coordinated by four amino acid residues and a structural water molecule. Remarkably, the Na^+ is bound by two glutamate residues instead of one as is the case in the *I. tartaricus* Na^+-binding c-ring, of which the first high resolution X-ray structure of a c-ring has been solved in 2005. Thus, a new type of Na^+-coordination in an ATP synthase rotor ring with a two-carboxylate ion-binding motif is described here, which also occurs in other bacteria, including several pathogens. Na^+-specificity of the investigated c-ring was further confirmed by a competitive biochemical labeling reaction performed with a fluorescent ATP synthase inhibitor molecule (N-cyclohexyl-N`-[4(dimethylamino)-α-naphtyl] carbodiimide, NCD-4).

We furthermore complemented our functional and structural data of the *F. nucleatum* c-ring by computational studies to explore the ion translocation mechanism of this enzyme in more details. We therefore analyzed the protonation state of the second, additional glutamate in the ion-binding site. Molecular dynamics (MD) simulations and free-energy calculations indicated that this glutamate is constitutively protonated, in the ion-locked as well as in a simulated, more hydrated open-conformation of the ion-binding glutamate as when it is travelling through the a/c-ring interface upon c-ring rotation.

Concerning the stoichiometry of the *F. nucleatum* c-ring, our structural investigations revealed that the complex is composed of eleven identical c-subunits. They assemble

into an hourglass-shaped ring into the membrane. While it is remarkable that also in this case the c-ring has an undecameric stoichiometry, like all previously described Na^+-specific rings, the reason for this observation is not yet fully understood.

In the second part of my PhD thesis, I aimed to characterize another, new subtype of rotary ATPase. In addition to the three subtypes of rotary ATPases, which were already described above, a novel (N), distinct subtype, found in the genomes of several Bacteria and Archaea, has been recently identified in a bioinformatics study and was thus referred to as N-type ATPase. While the subunit composition of this N-ATPase is not known, it is postulated that at least some of the corresponding rotor rings are Na^+-specific and that the enzyme is physiologically working as an ATP-driven ion-pump. It has been shown that this type of enzyme is encoded by an operon, which occurs always as a second and accompanying type of the conventional F-type ATP synthase-encoding *atp* operon in those genomes. Interestingly, many bacteria encoding for an N-ATPase are either marine or grow in the presence of salt. Besides, the N-*atp* operon is also present in *Burkholderia* species, which include different soil bacteria like *Burkholderia thailandensis* as well as some pathogenic representatives as *Burkholderia pseudomallei*, the causative agent of melioidosis.

Here, I aimed to characterize this novel subtype of enzyme to gain information about its structure and function. My first goal was to provide evidence for the phenotypic existence of this new type of rotary ATPase in native *B. thailandensis* cells. To produce the entire N-ATPase of *B. pseudomallei* for subsequent purification trials two different heterologous expression systems were used.

In addition, a heterologous expression and purification system for the *B. pseudomallei* N-ATPase rotor ring was established. The enzyme complex was isolated without an affinity tag and used for functional and structural studies. Biochemical competition assays, in which either the ATPase inhibitor DCCD or its fluorescent analogue NCD-4 competes with the coupling ions for the c-ring ion-binding site, indicated that the isolated c-ring binds H^+ but not Na^+-ions. To explore this feature in more details, site-directed-mutagenesis within the predicted ion-binding site was performed, which revealed that even if all ion-binding residues were substituted by the corresponding residues present in the Na^+-binding *F. nucleatum* c-ring, the N-ATPase rotor ring still remained H^+-specific. These results indicated that apparently more parameters than

just the primary sequence of this c-subunit alone are required to ultimately determine the ion specificity of this oligomeric complex.

To obtain structural information about the rotor ring of this novel subtype of ATPase, I used two alternative approaches. The isolated, detergent-solubilized c-ring was crystallized in 3D for subsequent X-ray crystallographic experiments. Reproducible crystals were obtained which diffract X-rays to a resolution of 6-7 Å. For the determination of the 3D structure of this membrane protein complex, these crystals require further optimization. Besides the X-ray crystallographic study, the purified protein complex was analyzed by single-particle electron cryo-microscopy (cryo-EM). In the past, this method has generally been applied for structure determination of protein complexes in the megadalton size range. However, a recent "revolution" in structure determination by single-particle cryo-EM is due to the development of new and more sensitive direct electron detector cameras for data collection as well as new and more powerful software packages for data processing thus enabling structure determination of continuously smaller protein complexes. Despite the fact that the *B. pseudomallei* N-ATPase c-ring is still very small to investigate it by EM, it bears, as all other homomeric c-rings so far, the probable advantage of an intrinsically high symmetry, which could be applied to improve the resolution. We obtained 2-dimensional class averages from the protein particles indicating that the N-ATPase c-ring consists of a previously unseen, new stoichiometry of 17 identical c-subunits. In total, three cryo-EM data sets were collected and processed with the c-ring in amphipol (A8-35) and in the detergents n-dodecyl-β-D-maltoside (DDM) and lauryl-dimethylamine-N-oxide (LDAO). The results of these three data sets were compared with each other revealing a large impact of the detergent on the structural analysis of a small membrane protein by single-particle cryo-EM. Finally a structural model of the *B. pseudomallei* N-ATPase c-ring was created. It shows a c_{17} ring with a diameter and height comparable to those of the 2-dimensional class averages obtained from the cryo-EM data of the protein.

The results presented here provide first functional and structural insights into an N-type ATPase rotor ring. Assuming a stoichiometry of 17 subunits the corresponding c-ring has a molecular weight of 141 kDa. To date, no high resolution structure of such a small protein complex has been determined by cryo-EM leading to the necessity of optimizing the 3D structure determination process of the rotor ring by this method.

Zusammenfassung

Rotierende Adenosintriphosphat (ATP)asen sind ubiquitäre, membrangebundene Enzymkomplexe, die eine essenzielle Rolle bei der biologischen Energieumwandlung spielen. Die erste Untergruppe, die sogenannte F_1F_o ATP-Synthase, fungiert hauptsächlich als ATP-bildende Maschine in vielen Bakterien, Mitochondrien und Chloroplasten. Der vakuoläre Subtyp, die V_1V_o ATPase, arbeitet hingegen als ATP betriebene Ionenpumpe in eukaryotischen Membranen. Die dritte Untergruppe, die in Archaeen sowie in einigen Bakterien vorkommt, wird als A_1A_o ATP-(Synth)ase bezeichnet und ist fähig in beide Richtungen zu arbeiten, entweder um ATP zu synthetisieren oder um eine Ionenmotorische Kraft aufzubauen, indem sie ATP verbraucht.

Alle drei oben genannten Subtypen von rotierenden ATPasen arbeiten als nanomolekulare Maschinen, die einen gemeinsamen, konservierten Mechanismus zur Energieumwandlung verwenden. Die einfachste Form dieser Enzyme ist die bakterielle F_1F_o ATP-Synthase. Hier werden Ionen durch die statische a-Untereinheit zu dem Rotor-Ring des Enzyms geleitet. Nach einer fast vollständigen Umdrehung des Rings werden die Ionen auf der anderen Seite der Membran schließlich wieder entlassen. Diese Drehung wird über den zentralen Schaft zu dem löslichen Teil des Enzyms, dem F_1 Komplex, weiter geleitet, wo Konformationsänderungen in den Nukleotidbindestellen die Synthese von ATP aus ADP und P_i bewirken.

Der Rotor oder c-Ring des Enzyms ist der Schlüsselproteinkomplex bei der Ionentranslokation über die Membran. Einige biochemische und strukturelle Methoden wurden in den letzten Jahren angewendet, um die Rotor Ringe vieler verschiedener Organismen zu untersuchen. Die erhaltenen Ergebnisse zeigen, dass die Stöchiometrie eines solchen c-Rings innerhalb einer Spezies konstant ist, während sie zwischen verschiedenen Spezies innerhalb von 8 bis 15 Untereinheiten variieren kann. Die c-Ring Stöchiometrie bestimmt direkt die Anzahl an Ionen, die durch den membrangebundenen F_o Teil während einer Umdrehung transportiert werden, während gleichzeitig drei ATP Moleküle in der wasserlöslichen F_1 Kopfgruppe synthetisiert werden. Somit hat die Anzahl der c-Untereinheiten einen großen Einfluss auf die Bioenergetik des jeweiligen Enzyms und damit des gesamten Organismus.

Der c-Ring einer rotierenden ATPase bindet spezifisch entweder Protonen (H^+) oder Natriumionen (Na^+) als Kopplungsion für das Enzym. Es existieren bereits einige

Strukturen, die das Koordinationsnetzwerk in beiden Arten von Rotor Ringen zeigen. In jedem dieser Fälle ist eine hoch konservierte Carboxylgruppe (Glutamat oder Aspartat) sowie eine variablere Kombination aus Aminosäureresten beteiligt, wobei die Koordination von Na^+ strukturell eine größere Herausforderung darstellt als die H^+-Bindung.

Das erste Ziel dieser Doktorarbeit bestand darin, den F_1F_o ATP-Synthase Rotor Ring des opportunistisch pathogenen Bakeriums *Fusobacterium nucleatum* auf funktionaler und struktureller Ebene zu charakterisieren. *F. nucleatum* ist ein anaerobes Bakterium, das Peptide und Aminosäuren als primäre Energiequelle verwendet. Es ist eines der am häufigsten in menschlichen Infektionen vorkommenden Bakterien und an der Entstehung von Zahnfleischerkrankungen beteiligt.
Für die Charakterisierung wurde der Rotor Ring heterolog innerhalb eines hybriden Enzyms in *Escherichia coli* hergestellt und daraus gereinigt ohne Verwendung eines Affinitätstags. Zwei hochauflösende Röntgenstrukturen des c-Rings bei tiefem (5.3) und hohem (8.7) pH-Wert wurden mit einer Auflösung von 2.2 Å beziehungsweise 2.64 Å gelöst. In beiden Strukturen befindet sich das konservierte Glutamat in einer geschlossenen, ionengebundenen Konformation, was zeigt, dass der Konformations-zustand dieses ionenbindenden Carboxylatrestes nicht von dem pH-Wert der Kristallisationsbedingung abhängt, was gut mit zuvor veröffentlichten strukturellen und biochemischen Daten von anderen c-Ringen übereinstimmt.
In der c-Ring Ionenbindestelle befindet sich jeweils ein Natriumion, wo es von vier Aminosäureresten und einem strukturellen Wassermolekül direkt koordiniert wird. Bemerkenswert ist, dass das Na^+ hier von zwei Glutamatresten gebunden wird und nicht nur von einem, wie es in der c-Ring Na^+ Bindestelle von *Ilyobacter tartaricus* der Fall ist, von dem die erste hochauflösende Röntgenstruktur eines c-Rings im Jahr 2005 gelöst wurde. Demzufolge wird hier eine neue Art von Na^+-Koordination in einem ATP-Synthase Rotor Ring mit einem Zwei-Carboxylat Ionenbindemotif beschrieben, die auch in anderen Bakterien einschließlich einigen Pathogenen zu finden ist. Die Na^+-Spezifität des untersuchten Rings wurde außerdem biochemisch durch eine kompetitive Bindereaktion des c-Rings mit einem fluoreszierenden ATP-Synthase Inhibitor (N-cyclohexyl-N`-[4(dimethylamino)-α-naphtyl]carbodiimide, NCD-4) bestätigt.

In diesem Zuge haben wir anschließend unsere funktionalen und strukturellen Daten des c-Rings von *F. nucleatum* durch computergestützte Untersuchungen ergänzt, um den Mechanismus der Ionentranslokation dieses Enzyms genauer zu untersuchen. Wir haben dazu den Protonierungszustand des zweiten, zusätzlichen Glutamatrests in der Ionenbindestelle analysiert. Molekulardynamische (MD) Simulationen und freie-Energie-Berechnungen deuten darauf hin, dass dieses Glutamat konstitutiv und unabhängig vom pH-Wert des umgebenden Lösungsmittels protoniert vorliegt, das heißt sowohl in der geschlossenen, ionengebundenen Form, als auch in einer simulierten, hydratisierten offenen Konformation des ionenbindenden Glutamatrests, wie sie auftritt, wenn dieses Glutamat die a/c-Ring Grenzfläche während der Drehung des Rings passiert.
Bezüglich der Stöchiometrie des c-Rings von *F. nucleatum* haben die Untersuchungen gezeigt, dass der Komplex aus elf identischen Untereinheiten aufgebaut ist, die sich zu einem sanduhrförmigen Ring in der Membran zusammenlagern. Interessanterweise hat auch in diesem Fall der c-Ring eine Stöchiometry von elf Untereinheiten, genau wie die bereits zuvor untersuchten Na^+-spezifischen c-Ringe. Der Grund für diese Beobachtung konnte allerdings noch nicht vollständig geklärt werden.

Das zweite Ziel meiner Doktorarbeit bestand darain eine weitere, neue Untergruppe von rotierenden ATPasen zu charakterisieren. Zusätzlich zu den drei Subtypen von ATPasen, die oben bereits beschrieben wurden, wurde kürzlich in bioinformatischen Studien eine neue Untergruppe des Enzyms in den Genomen einiger Bakterien und Archaeen identifiziert, die daraufhin als N-Typ bezeichnet wurde. Während die Zusammensetzung der einzelnen Untereinheiten dieser N-ATPase noch nicht bekannt ist, wird postuliert, dass zumindest einige der entsprechenden Rotor Ringe spezifisch für Na^+ sind und das Enzym physiologisch betrachtet als ATP betriebene Ionenpumpe arbeitet. Es konnte außerdem gezeigt werden, dass dieses Enzym von einem Operon kodiert wird, das jeweils als zweites *atp* Operon in einem bestimmten Genom vorkommt und zwar zusätzlich zu einem *atp* Operon, das für eine gewöhnliche F_1F_o ATP-Synthase kodiert. Interessanterweise sind viele Bakterien, die für eine N-Typ ATPase kodieren, entweder marin oder wachsen in salzhaltiger Umgebung. Daneben ist das N-*atp* Operon auch in der *Burkholderia* Gattung zu finden, welche verschiedene Bodenbakterien wie *Burkholderia thailandensis* sowie einige pathogene

Vertreter, unter anderem *Burkholderia pseudomallei*, den Verursacher von Melioidose, beinhaltet.

Hier sollte dieser neue Subtyp von Enzym charakterisiert werden, um Informationen über seine Struktur und Funktion zu erhalten. Das erste Ziel war hierbei die phänotypische Existenz dieses neuen Typs von Enzym in nativen *B. thailandensis* Zellen nachzuweisen. Um die vollständige N-typ ATPase von *B. pseudomallei* herzustellen und sie anschließend reinigen zu können wurden zwei verschiedenene heterologe Expressionssysteme angewendet.

Daneben wurde ein heterologes Expressions- sowie ein Reinigungssystem für den N-ATPase Rotor Ring von *B. pseudomallei* etabliert. Der Enzymkomplex wurde ohne Verwendung eines Affinitätstags isoliert und für biochemische und strukturelle Studien eingesetzt. Biochemische, kompetetive Bindereaktionen, bei welcher der ATPase Inhibitor DCCD und sein fluoreszierendes Analog NCD-4 mit dem Kopplungsion um die Ionenbindestelle des c-Rings konkurrieren, zeigen, dass der isolierte c-Ring Protonen aber nicht Nartiumionen bindet. Um diese Eigenschaft des Rings genauer zu untersuchen, führten wir ortsgerichtete Mutagenesen an der vorausgesagten Ionenbindestelle dieses c-Rings durch, die zeigen, dass der N-ATPase Rotor Ring spezifisch für Protonen bleibt, selbst wenn alle Aminosäurereste innnerhalb der Ionenbindestelle durch die entsprechenden Reste, wie sie in dem Na^+-spezifischen c-Ring von *F. nucleatum* vorkommen, ausgetauscht werden. Diese Ergebnisse deuteten an, dass offensichtlich mehrere Parameter und nicht nur die Primärsequenz der c-Untereinheit letztlich für die Ionenspezifität dieses Rings verantwortlich sind.

Um strukturelle Informationen über den Rotor Ring dieses neuen Subtypes von ATPase zu erhalten wählte ich zwei verschiedene Herangehensweisen. Der isolierte und in Detergens gelöste c-Ring wurde in 3D kristallisiert und anschließend röntgenkristallographisch vermessen. Hierbei konnten reproduzierbare Kristalle erhalten werden, die Röntgenstrahlung mit einer Auflösung von 6-7 Å beugten. Eine weitere Optimierung der Kristalle ist hier notwendig, um die dreidimensionale Struktur dieses Membranproteinkomplexes zu bestimmen.

Neben der Röntgenstrukturanalyse wurde der gereinigte Proteinkomplex mithilfe von Einzelpartikel Elektronen Kryo-Mikroskopie (Kryo-EM) untersucht. In der Vergangenheit wurde diese Methode generell zur Strukturbestimmung von Proteinen

im Megadalton Größenbereich angewendet. Die Entwicklung von neuen und sensitiveren Direkt-Elektronen-Detektor Kameras für die Datenaufnahme sowie von neuen und leistungsfähigeren Software-Paketen für die Datenverarbeitung verbesserte jedoch kürzlich die Strukturbestimmung mittels Einzelpartikel Kryo-EM. Demzufolge können Strukturen von stetig kleineren Proteinkomplexen damit bestimmt werden. Auch wenn der Rotor Ring immer noch sehr klein ist, um ihn anhand dieser Methode zu untersuchen, birgt er dennoch den möglichen Vorteil einer intrinsisch hohen Symmetrie, die bisher bei allen aus identischen Untereinheiten aufgebauten c-Ringen vorhanden war und die bei der Datenverabreitung genutzt werden kann, um die Auflösung zu verbessern. Wir haben hier zweidimensionale Klassendurchschnitte von den Protein Partikeln erhalten, die zeigen, dass der N-ATPase c-Ring eine bisher noch nicht für einen c-Ring beschriebene, neue Stöchiometrie von 17 identischen Untereinheiten aufweist. Insgesamt wurden drei Kryo-EM Datensätze aufgenommen und bearbeitet, bei denen der c-Ring in Amphipol (A8-35) und in den beiden Detergenzien n-Dodecyl-β-D-maltosid (DDM) und Lauryldimethylamin-N-oxid (LDAO) untersucht wurde. Die Ergebnisse dieser drei Datensätze wurden miteinander verglichen und zeigen den großen Einfluss des jeweiligen Detergenz auf die strukturelle Analyse eines kleinen Membranproteins mittels Einzelpartikel Kryo-EM. Anschließend wurde ein strukturelles Model des N-ATPase c-Rings erstellt. Dieses zeigt einen c_{17} Ring mit einem Durchmesser und einer Höhe vergleichbar zu denen der 2-dimensionalen Klassendurchschnitte, die von den Kryo-EM Daten des Proteins erhalten wurden.

Die hier dargestellten Ergebnisse liefern erste funktionelle und strukturelle Erkenntnisse über einen N-ATPase Rotor Ring. Unter der Annahme einer Stöchiometrie von 17 Untereinheiten weist der entsprechende c-Ring ein molekulares Gewicht von 141 kDa auf. Bis zum heutigen Zeitpunkt wurde noch keine hochauflösende Struktur eines so kleinen Proteins mittels Kryo-EM bestimmt, sodass die 3-dimensionale Strukturbestimung des Rotor Rings unter Anwendung dieser Methode Optimierung bedarf.

1 Introduction

1.1 ATP - the universal energy currency

All living cells require energy to drive many different active processes. These include biochemical activities as the biosynthesis of organic molecules, cell division and active transport of compounds across membranes. Mechanical processes like motion of single cells by a flagellum or muscle contraction via the actin-myosin complexes also need to be energized. The universal energy currency for all these processes is adenosine-5`-triphosphate (ATP). It is a nucleotide composed of an adenine moiety, a pentose monosaccharide ribose and three phosphate groups (at α, β and γ position, abducent from the ribose), which contain two high-energy phospho-anhydride bonds within the β and γ phosphate groups (figure 1). Upon ATP hydrolysis the γ phosphate is released leading to the formation of adenosine-5`-diphosphate (ADP) and inorganic phosphate (P_i); this chemical reaction provides the cell free energy usable for the catalysis of many types of cellular reactions.

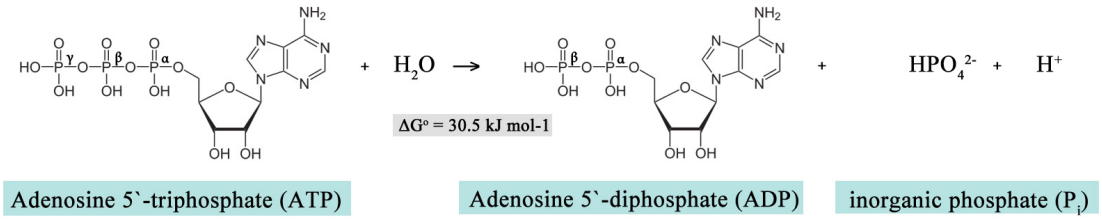

Figure 1. Structure of adenosine-5`-triphosphate (ATP) and ATP hydrolysis reaction.
Hydrolytic cleavage of the γ phosphate group of ATP releases free energy of 30.5 kJ mol^{-1} resulting in the formation of adenosine-5`-diphosphate (ADP) and inorganic phosphate (HPO_4^{2-}, P_i). This reaction is reversible; ATP can be generated from ADP and P_i.

ATP was already discovered in 1929 by Karl Lohmann (Langen & Hucho, 2008) but claimed to be the main energy transfer molecule not before more than one decade later, in 1941, by Fritz Albert Lipmann (Lipman, 1941). There are three different ways of synthesizing most of the ATP in a cell: (1) photophosphorylation, (2) substrate level phosphorylation and (3) oxidative phosphorylation. During the latter one electrons are transported via several carriers from the reduced form of

nicotinamide adenine dinucleotide (NADH) to oxygen, while protons are pumped across the membrane producing an electrochemical pH gradient (ΔpH) as well as a transmembrane electrical potential (ΔΨ). This ion motive force (see chapter 1.3.3.3) can then in turn be used by the last complex during oxidative phosphorylation, the ATP synthase, to produce ATP from ADP and P_i (figure 2). This cycle of synthesizing and hydrolyzing ATP is the fundamental mechanism of energy transfer in all living cells and coupled to many biochemical reactions in the cell.

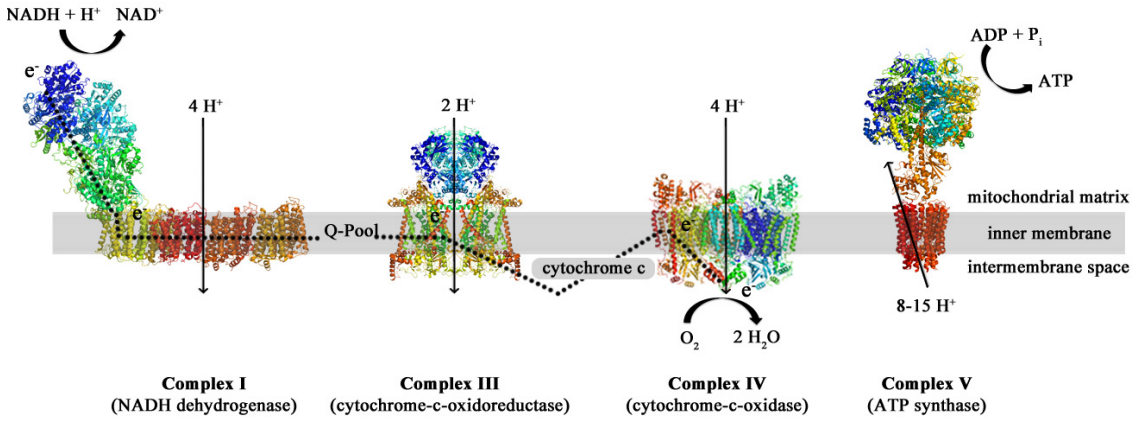

Figure 2. Respiratory chain complexes in the inner mitochondrial membrane.
The scheme shows Complex I, III, IV and V (ATP Synthase). Electrons are transported from NADH through three large membrane protein complexes (I, III, IV) to O_2 (black dotted lines) as a terminal acceptor thus reducing it to H_2O. The electron transfer reaction is coupled to proton pumping across the membrane (black arrows) thereby establishing a proton motive force (*pmf*) consisting of a pH gradient (ΔpH) and an electrical membrane potential (ΔΨ). Backflow of protons into the cytoplasm then fuels the last protein complex, the F_1F_o ATP synthase, which uses the energy to synthesize ATP from ADP and P_i. Complex II (succinate-dehydrogenase, not shown), another respiratory chain complex, does not pump protons itself, but delivers additional electrons from $FADH_2$ via the Q-Pool to the respiratory chain. The protein structures were extracted from the RCSB Protein Data Bank (www.rcsb.org): Complex I, pdb 4hea (Baradaran *et al*, 2013); Complex III (a dimer of 11 subunits), pdb 1ezv (Hunte *et al*, 2000); Complex IV (a dimer of 13 ubunits), pdb 1occ (Tsukihara *et al*, 1996); Part of Complex V (F_1c_{10}), pdb 2xok (Stock *et al*, 1999).

1.2 Rotary ATPases

Rotary ATPases play an important role in all three domains of life (Bacteria, Archaea and Eukarya) and act as molecular machines involved in many different bioenergetic processes. They either synthesize ATP by using a transmembrane ion gradient, or

hydrolyze ATP to generate an electrochemical driving force, namely a proton- (or sodium-) motive force (*pmf* or *smf*). In the meantime, several X-ray crystallographic structures of single subunits or subcomplexes of rotary ATPases have become available, including recently also a complete cryo-EM structure of an intact complex from the *Polytomella* mitochondrial ATP synthase (Allegretti *et al*, 2015). Taken together, these data reveal a common ATPase architecture. In general, a water-soluble subcomplex catalyzes the ATP synthesis and hydrolysis reaction, whereas ions (H^+ or Na^+) are translocated through a membrane-bound subcomplex. Both parts are connected to each other by central and peripheral stalks and act as reversible motors.

Different types of rotary ATPases were assigned according to their exact subunit composition whereby the number of peripheral stalks is a typical attribute for each of them. F-type ATP synthases possess just one peripheral stalk, whereas A-type ATP(synth)ases have two and V-type ATPases usually have three, respectively (figure 3).

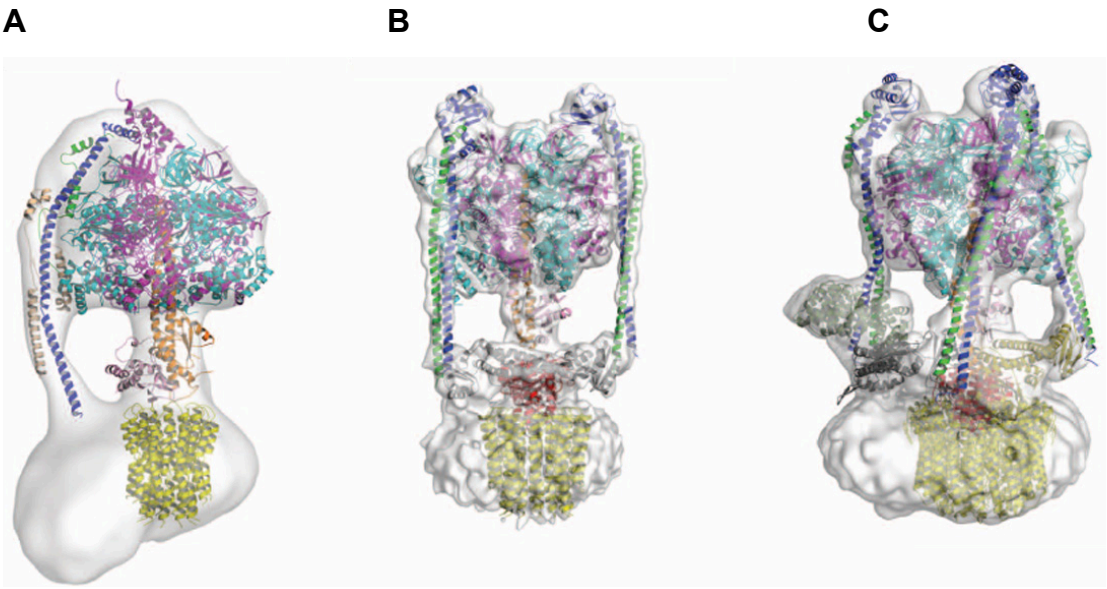

Figure 3. Models of the three types of rotary ATPases.

Overall structures of the enzymes obtained by electron microscopy experiments are supplemented with available X-ray structures of individual subunits or subcomplexes. **(A)** The F-type ATP synthase from *Bos taurus* with one peripheral stalk, **(B)** the A-type ATPase/ ATP synthase from *Thermus thermophilus* with two peripheral stalks and **(C)** the V-type ATPase from *Saccharomyces cerevisiae* with three outer stalks. The figure was taken from (Stewart *et al*, 2013).

The different types of rotary ATPases can also be distinguished according to their physiological functions. F-type ATP synthases residue in mitochondrial, chloroplast or bacterial membranes using an ion motive force to synthesize ATP. A-type ATP (synth)ases can be found in bacterial and archaeal membranes where they work either in ATP synthesis or hydrolysis direction. V-type ATPases are exclusively located in eukaryotic membranes (e.g. in vacuoles or lysosomes) functioning as ATP-driven ion-pumps for intracellular acidification.

1.3 The F-type ATP synthase - a well-studied type of rotary ATPase

In 1956, the simplest form of an F_1F_o ATP synthase was found in bacterial membranes and initially described as soluble factor that activates coupled oxidative phosphorylation (Brodie & Gray, 1956). Subsequently, the mitochondrial enzyme was characterized suggesting that coupling and ATPase activity are catalyzed by the same protein (Conover *et al*, 1963; Kagawa & Racker, 1966; Penefsky *et al*, 1960; Pullmann *et al*, 1960). The bacterial enzyme is composed of eight structural subunits with $\alpha_3\beta_3\gamma\delta\varepsilon$ building the water-soluble F_1-domain (named after coupling factor 1, (Conover *et al*, 1963; Penefsky *et al*, 1960; Pullman *et al*, 1960; Pullmann *et al*, 1960)) and $ab_2c_{10\text{-}15}$ forming the membrane-bound F_o-part (named after oligomycin sensitivity-conferring coupling factor o (Kagawa & Racker, 1966)). Later, the indirect coupling mechanism of ATP synthesis by a mechanical rotation of the enzyme has been explored (Abrahams *et al*, 1994; Boyer, 1975; Boyer, 1993).

Under physiological conditions the enzyme uses the energy stored in a transmembrane ion gradient to synthesize ATP. Thereby electrochemical energy (the *pmf* or the *smf*; see chapter 1.3.3.3) is converted into mechanical energy (rotation of parts of the enzyme) and finally back into chemical energy (ATP formation). Ions become bound to the rotary part of the F_o-domain, the c-ring, which rotates within the membrane against a stator domain thereby translocating the ions across the membrane. This rotation is further transferred via the central stalk consisting of the $\gamma\varepsilon$-subunits to the soluble F_1-part where ATP is formed in the catalytic sites of three individual β-subunits. This mechanism is consistent with the chemiosmotic theory described by Peter Mitchell who claimed already in 1961 that ATP synthesis is coupled to transmembrane ion translocation (Mitchell, 1961).

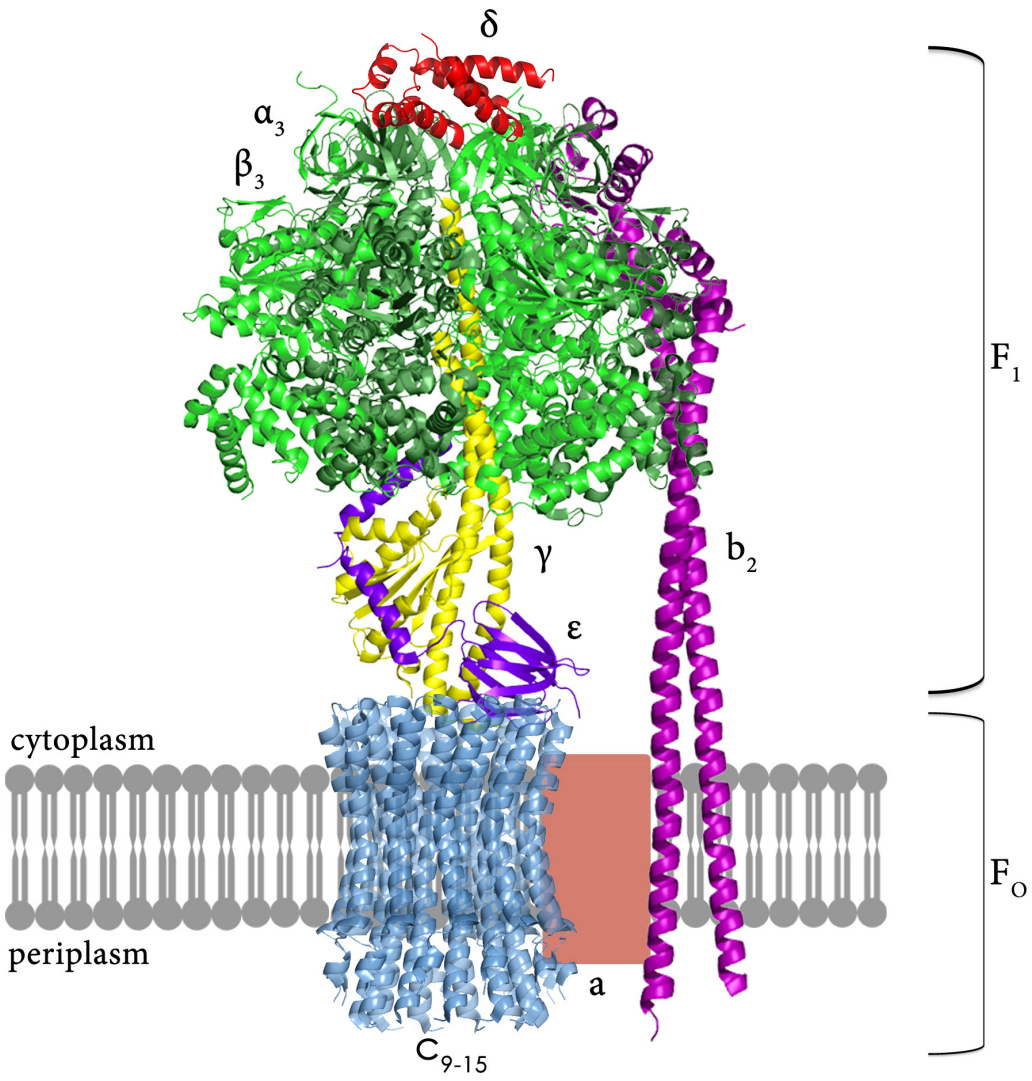

Figure 4. Mosaic structure of the bacterial F_1F_o ATP synthase.
This model of the enzyme was created using X-ray protein structures extracted from the RCSB protein data bank (www.rcsb.org). It includes the F_1-subcomplex ($\alpha_3\beta_3\gamma\varepsilon$) and the δ-subunit from *E. coli* (pdb 1jnv (Hausrath *et al*, 2001) and pdb 1abv (Wilkens *et al*, 1997)), the b_2 outer stalk from *T. thermophilus* (pdb 3k5b (Lee *et al*, 2010)) and the rotor (c)-ring from *I. tartaricus* (pdb 1yce (Meier *et al*, 2005)). The stator a-subunit is shown schematically as there is no X-ray structure available. Stoichiometries of all subunits are indicated as they can be found in bacterial F-type ATP synthases.

1.3.1 Structure and function of the water-soluble F_1-domain

1.3.1.1 General architecture of the F_1-subcomplex

The F_1-subcomplex of the ATP synthase is a pseudo-symmetric hexamer of alternating α and β-subunits around an elongated α-helical structure of the central

stalk, the γ-subunit, which connects this domain with the membrane-bound F_o-part (Abrahams *et al*, 1994). Besides the subunits which form the catalytic core of the bacterial F_1 ($\alpha_3\beta_3\gamma$), two additional subunits, namely ε and δ, are present in the water-soluble subcomplex. Subunit ε consists of an N-terminal β-barrel domain and two C-terminal α-helices (Uhlin *et al*, 1997; Wilkens *et al*, 1995) and is forming the central stalk together with the γ-subunit. The function of subunit ε is described in more detail below. The δ-subunit is sitting on top of the α-β-hexamer being part of the peripheral stalk connecting both parts of the enzyme. It is composed of a globular N-terminal domain and a rather disordered C-terminus, including one α-helix (Wilkens *et al*, 1997).

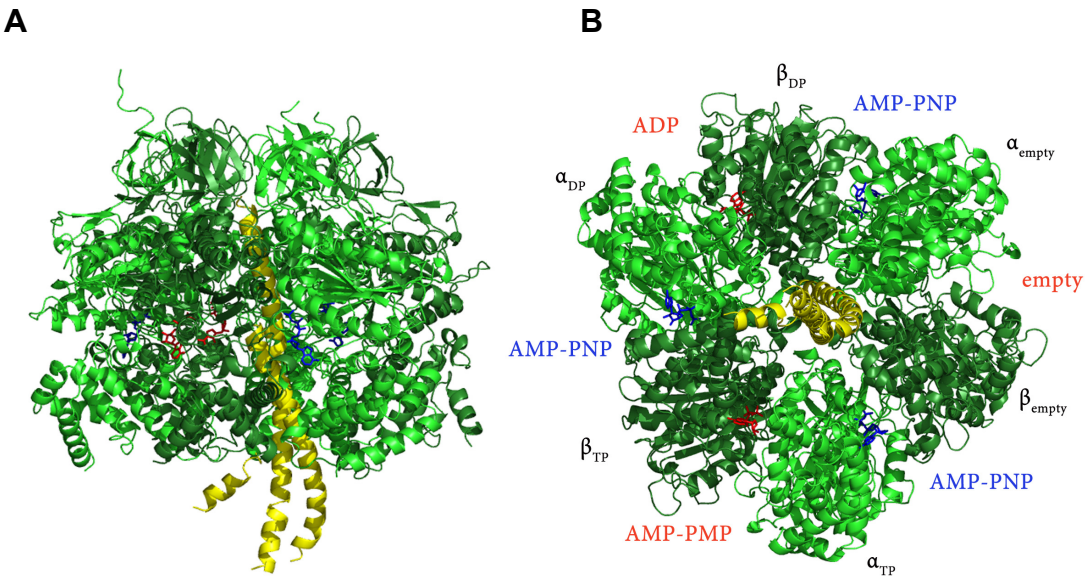

Figure 5. X-ray structure of the mitochondrial F_1-subcomplex without the δε-subunits ($\alpha_3\beta_3\gamma$). **(A)** View of the F_1-subcomplex perpendicular to the membrane**. (B)** Periplasmic view of the F_1-subcomplex. The nucleotide binding sites are localized at the interfaces of the α (light green) and β-subunits (dark green) of the enzyme, which are alternatingly arranged around the central stalk γ-subunit (yellow). The subunit termed β_{TP} as well as all three α-subunits bind the non-hydrolyzable ATP analogue 5`-adenylyl-imidodiphosphate (AMP-PNP) whereas ADP is bound to β_{DP} and the nucleotide binding site in β_E is empty. The three non-catalytically active α-subunits are specified as α_{TP}, α_{DP} and α_E in relation to the three catalytically active β-subunits. The structure was extracted from the RCSB protein data bank (www.rcsb.org; pdb 1bmf (Abrahams *et al*, 1994)).

Each α- and β-subunit comprises a nucleotide binding site at their interfaces, whereby only the ones corresponding to the β-subunits are catalytically active (Cross & Nalin, 1982; Yoshida & Allison, 1986). Figure 5 shows the mitochondrial F_1-subcomplex without subunits δε ($\alpha_3\beta_3\gamma$) with the catalytically active sites in red, having either 5`-adenylyl-imidodiphosphate (AMP-PNP), ADP or no nucleotide (empty) bound. The non-catalytical sites are marked in blue. They bind AMP-PNP, but neither hydrolyze nor synthesize it.

1.3.1.2 The ATP synthesis reaction: the binding change mechanism

Under physiological conditions in the cell allowing ATP synthesis, the energy stored in a transmembrane ion gradient (in most cases a *pmf*) induces rotation of the c-ring within the F_o-domain. This rotation is further transmitted to the helical γ-subunit leading to conformational changes in the catalytic nucleotide binding sites on the three β-subunits. The central stalk thereby specifies the affinity and function of each catalytic site at a given time point during operation of the enzyme.

Very early biochemical experiments on this enzyme showed that enzyme-bound ATP can be synthesized also in the absence of a *pmf*, but ATP can not be released from the catalytic center of the enzyme, indicating that the energy requiring step in this process is not the formation of ATP but rather its release from the nucleotide binding site (Boyer *et al*, 1973). Based on these experimental facts, Paul Boyer proposed the so-called "binding change mechanism" for the proton driven ATP synthesis reaction (Boyer, 1993). According to this hypothesis each β-subunit can adapt three different conformational states within one enzyme at a given time point (figure 6). One β-subunit is in a loose (L) conformation having ADP and P_i bound. Another subunit can bind ATP in a tight (T) conformation, whereas the third β-subunit is in an open (O) conformation not binding any nucleotide, therefore being empty. Counterclockwise 120° rotation of the γ-subunit (as seen from the cytoplasm) provokes the interconversion of the β-subunit in the tight conformation (ATP bound) into the open conformation. Coincidentially, the subunit in the loose conformation changes into the tight conformation, leading to the formation of ATP from ADP and P_i. Subsequently, the ATP molecule previously synthesized and still bound to the subunit in the open conformation is released from the binding site being replaced by further ADP and P_i

molecules. The proximate 120° rotational step of the γ-subunit leads to the interconversion of the open conformation into the loose one, thereby fixing the two substrates ADP and P_i. Upon one complete 360° rotation three molecules of ATP are synthesized as a result (Yasuda *et al*, 1998). The binding change mechanism is illustrated in figure 6. The structure of the mitochondrial F_1-subcomplex solved in 1994 (Abrahams *et al*, 1994) was in very good agreement with Boyer`s proposal of an ATP synthesis reaction as it showed asymmetric structures of the three catalytic nucleotide binging sites which can alternatingly adapt an open, loose and tight state.

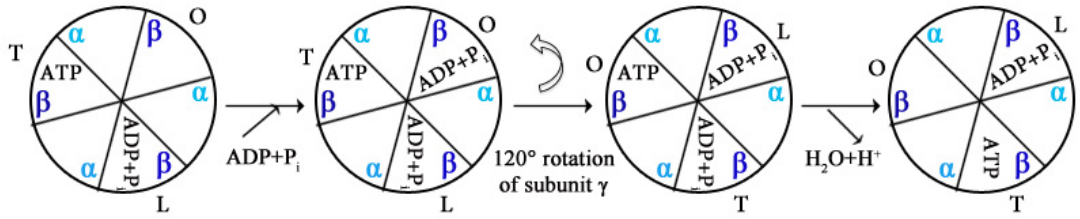

Figure 6. Model of the binding change mechanism for the ATP synthesis reaction.
The mechanism was proposed by Paul Boyer in 1977, stating that ATP is synthesized in each catalytically active site within the β-subunits (dark blue), which alternatingly undergo three different conformational states. In the loose state ADP and P_i are bound whereby counterclockwise rotation of the γ-subunit by 120° leads to a conformational change into the tight state forming ATP. Upon conversion of the tight into the open state the ATP molecule is released from the binding site and replaced by further ADP and P_i molecules. The non-catalytically active sites in the three α-subunits can also bind ATP, but not hydrolyze it and are therefore left blank in this scheme.

1.3.1.3 Rotational studies of the F_1-subcomplex

The rotation of F_1 was verified by a number of remarkable experiments including (direct) single molecule observations. The rotational motion of the γ-subunit was first shown biochemically by crosslinking studies between the *E. coli* β- and ε-subunits (Duncan *et al*, 1995). Biophysical experiments revealed intersubunit rotation in the active spinach chloroplast F_1-ATPase (Sabbert *et al*, 1996). Finally, direct visualization of ATP-driven rotation of the γ-subunit was possible in the *Bacillus* PS3 F_1-ATPase by a single-molecule approach using a fluorescently labeled actin filament attached to the γ-subunit (Noji *et al*, 1997). Besides the actin filament, gold beads

(Nakanishi-Matsui *et al*, 2006; Yasuda *et al*, 2001) were used showing that the rotational direction is always counterclockwise (when viewed from the membrane) which measured up to the rotational direction expected from the crystal structure (Abrahams *et al*, 1994). Additionally, single-molecule FRET experiments revealed rotation of the γ-subunit also in ATP synthesis direction (Diez *et al*, 2004).

The high reversibility of mechanochemical coupling is a dominant attribute of the ATP synthase allowing ATP synthesis when movements are enforced in the reverse direction (Itoh *et al*, 2004). However, the high efficiency of ATP synthesis is only given in a $\alpha_3\beta_3\gamma\varepsilon$-subunit composition, whereas the absence of subunit ε dramatically decreases the efficiency, emphasizing its stabilizing function (Rondelez *et al*, 2005). Subunit ε is important for coupling between transmembrane ion translocation through F_o and ATP synthesis/hydrolysis in F_1 (Giraud & Velours, 1997; Klionsky *et al*, 1984; Kuki *et al*, 1988; Patrie & McCarty, 1984; Richter *et al*, 1984; Sternweis, 1978). Besides, it plays an important role in inhibition of ATP hydrolysis. The functional findings of the ε-subunit arise from numerous studies summarized in (Feniouk & Yoshida, 2008).

1.3.1.4 Regulation of ATP (synth)ase activity

The activity of F_1F_o ATP synthases is regulated by several mechanisms in different species as the conditions under which the enzyme operates vary considerably among them. The rate of ATP production is universally regulated by modifying the transmembrane electrochemical potential difference of the coupling ion ($\Delta\mu_{H^+/Na^+}$) in the particular cell (Feniouk & Yoshida, 2008). ATP hydrolysis activity is regulated in another way. In mitochondria, chloroplasts and bacteria MgADP (without P_i) binds tightly to a high affinity catalytically active site provoking ATPase inhibition (Carmeli & Lifshitz, 1972; Minkov *et al*, 1979; Yoshida & Allison, 1986).

As already mentioned above, subunit ε plays an important role in controlling the ATPase activity. On the one hand it enhances inhibition by ADP as it stabilizes the ADP-inhibited state (Feniouk *et al*, 2007). On the other hand, subunit ε modulates ATPase activity also in the absence of ADP. It can adapt two different conformational states. In the contracted form the C-terminal α-helices are folded in a hairpin-like-structure not influencing the ATP(synth)ase activity (Suzuki *et al*, 2003). Upon

conformational changes triggered by diverse stimuli including nucleotides and $\Delta\mu_{H^+/Na^+}$, the C-terminal α-helices become more extended and inhibit the ATPase activity (Suzuki *et al*, 2003; Tsunoda *et al*, 2001) probably via interacting with negatively-charged residues within a so-called DELSEED motif within the β-subunits (Hara *et al*, 2001).

In chloroplasts an additional regulation mechanism was described involving a disulfide bond between two cysteine residues within the γ-subunit, stabilizing the ADP-inhibited state of the β-subunit and precluding γ-subunit rotation necessary to expel ADP from the high-affinity catalytic site. Upon daylight, the disulfide bond becomes reduced thereby stimulating ATPase activity. This kind of regulation is supposed to be a day-night switch in the plant enzyme (Kramer & Crofts, 1989).

In mitochondria, a small α-helical basic protein, called IF1, plays a crucial role in ATPase activity regulation. It inhibits ATP hydrolysis below pH 8, where it occurs as a dimer, whereas ATP synthesis activity is not affected (Pullman & Monroy, 1963).

1.3.2 Structure and function of the membrane-bound F_o-domain

1.3.2.1 General architecture of the F_o-subcomplex

In bacteria and chloroplasts, the F_o-subcomplex is composed of a single copy of subunit a, a dimer of subunit b and an oligomeric complex of a varying number of c-subunits forming the rotor (c_{9-15}) ring. The F_1- and F_o-subcomplexes are connected by two stalks (Wilkens & Capaldi, 1998), a peripheral or outer stalk (subunits b and δ) and a central stalk (subunits γ and ε). All F_o-subunits are membrane-bound and hydrophobic accounting for the rare structural information available for the complete subcomplex. Progress with respect to structure determination of the entire enzyme was made in 2012 by obtaining a cryo-EM single-particle structure of the related V_1V_o ATPase of *Thermus thermophilus* at 9.7 Å resolution (Lau & Rubinstein, 2012) (figure 7). The map reveals only a small contact between the stator I-subunit (equivalent to the F_o a-subunit) and the L-ring (corresponding to the F_o c-ring). Helix bundles of subunit I are supposed to form two aqueous half-channels for transmembrane ion translocation, which was already proposed in earlier studies (Angevine & Fillingame, 2003; Angevine *et al*, 2007; Cain, 2000).

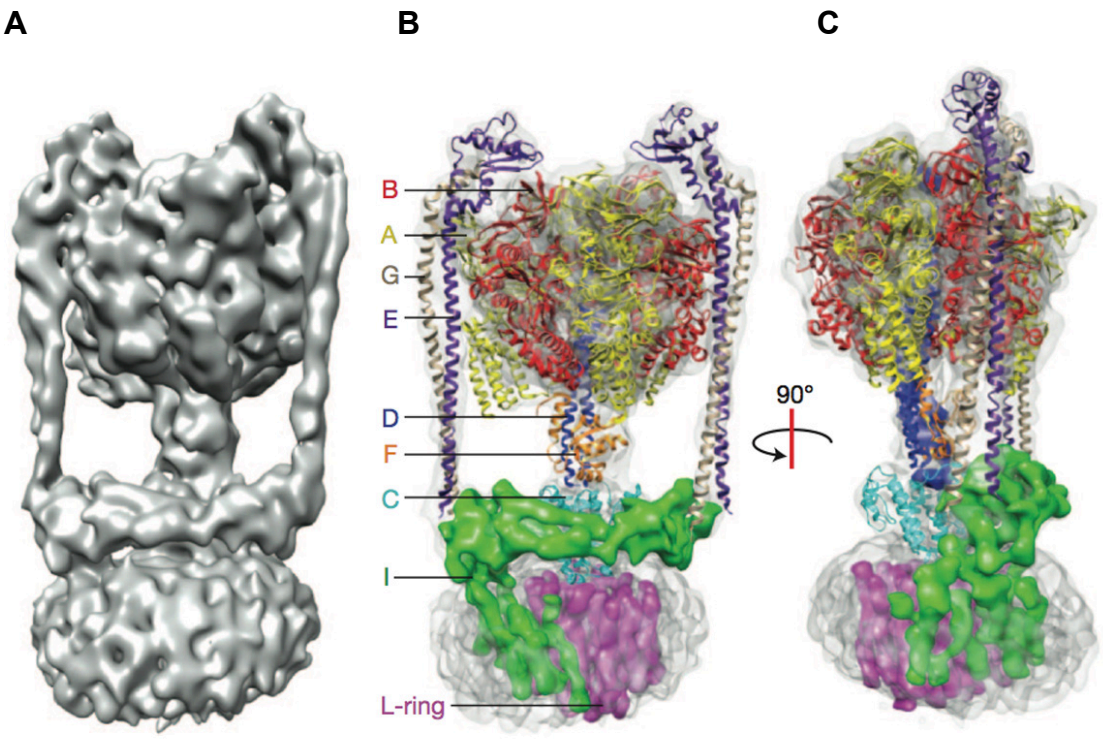

Figure 7. Structure of the intact V_1V_o ATPase of *Thermus thermophilus* determined by single-particle electron cryo-microscopy.

(A) A surface view of the three-dimensional map at 9.7 Å, **(B)** and **(C)** the map with fitted crystal structures of individual subunits (B, A, G, E, D, F) and residual cryo-EM densities for the subunits of which no crystal structures are available (C, I, L-ring). The figure was taken from (Lau & Rubinstein, 2012).

Besides these data on the V_o, a 2D crystallization approach of the intact F_o complex of *Ilyobacter tartaricus* revealed the arrangement of the 22 α-helices of the rotor ring and a four-helix bundle of the stator a-subunit in close proximity (Hakulinen *et al*, 2012). Three more helices were visible in the 2D projection map, which could not be assigned unambiguously. They could either all represent the outer stalk b_2-subunits or also all correspond to the a-subunit or partially contribute to both (figure 8).

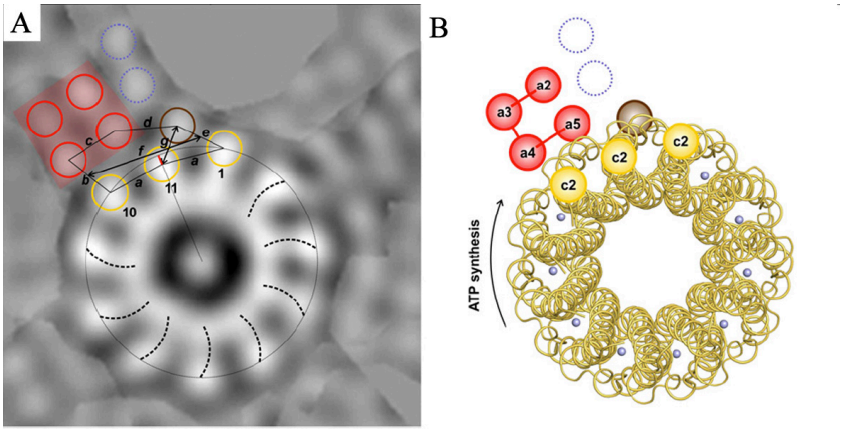

Figure 8. Electron density map of the F_o complex of *I. tartaricus* obtained by 2D crystallization. **(A)** Map and **(B)** model interpretation with three densities corresponding to the hairpin-like-subunits of the c_{11} ring (yellow) and a four-helix bundle assigned to build the stator a-subunit (red). Helices shown in brown and blue could be part of the b_2 or the a-subunit. The figure was taken from (Hakulinen *et al*, 2012).

Very recently, the structure of a native mitochondrial ATP synthase dimer was determined by single-particle electron cryo-microscopy at 6.2 Å resolution showing a twofold symmetrical V-shaped complex (Allegretti *et al*, 2015) (figure 9 A). The cryo-EM map revealed details about the F_o structure of the enzyme. Four long, horizontal membrane-intrinsic α-helices in subunit a are arranged in two hairpins almost perpendicular to the c-ring. Two aqueous half-channels could be observed in the F_o-subcomplex (figure 9 B, see also 1.3.3.3).

A

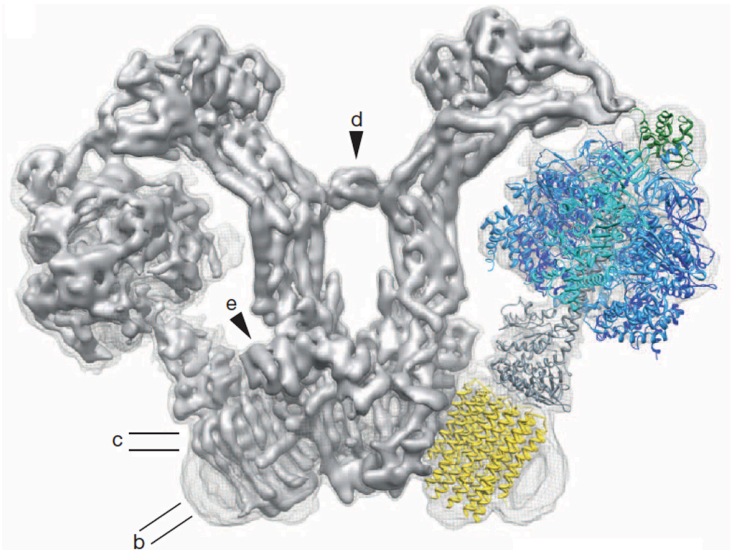

B

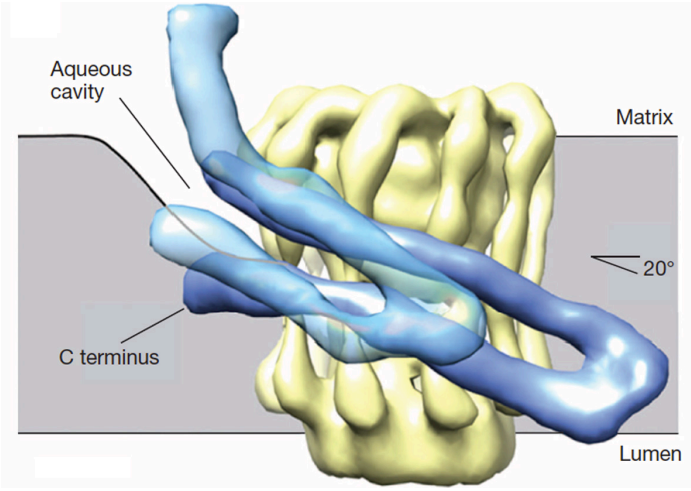

Figure 9. Cryo-EM map of the *Polytomella* F_1F_o ATP synthase dimer and the arrangement of subunit a and the c-ring.

(A) Side view of the ATP synthase dimer with fitted atomic models of the F_1-subcomplex (pdb 2WSS) (Rees *et al*, 2009) and the c-ring (pdb 3U2Y) (Symersky *et al*, 2012). **(B)** Organization of membrane-intrinsic hairpins of subunit a (blue) next to the rotor ring (yellow) viewed from the dimer interface. The figure was taken from (Allegretti *et al*, 2015).

1.3.2.2 The b-subunit

The peripheral stalk of the bacterial F_1F_o ATP synthase is formed by subunits b and δ. A purified, soluble form of the *E. coli* b-subunit was analyzed by circular dichroism (CD) and shown to have an elongated α-helical extension (Dunn, 1992). The native protein forms a homodimer as confirmed by cross-linking studies (McLachlin & Dunn, 1997; Rodgers *et al*, 1997). Besides, a heterodimer of one b and a related b`-subunit is found in some bacteria and chloroplasts (Dunn *et al*, 2001; McCarn *et al*, 1988; Walker *et al*, 1987). Dimerization was shown to be crucial for interaction with F_1 (Dunn & Chandler, 1998; Sorgen *et al*, 1998). In addition, subunit δ is essential for binding of F_1 to F_o (Jounouchi *et al*, 1992).

The amphiphilic b-subunit is membrane-anchored via its N-terminal α-helix (Dmitriev *et al*, 1999) while its C-terminus extends along the entire F_1-part of the ATP synthase and interacts with it (Rodgers & Capaldi, 1998). Interaction of the two b-subunits occurs via their C-terminal regions and was independent from the presence

of other ATP synthase subunits (Dunn & Chandler, 1998; McLachlin *et al*, 1998; Rodgers *et al*, 1997; Sawada *et al*, 1997).

Later, an X-ray structure of the dimerization domain of the monomeric b-subunit of *E. coli* revealed a right-handed twist (Del Rizzo *et al*, 2002) and further analyses presented an 11-residue repeat in the protein sequence suggesting a right-handed coiled coil dimer structure for subunit b with the two helices parallel offset to each other by half of the hendecad (Del Rizzo *et al*, 2006).

The bacterial outer stalk was first imaged by single-particle cryo-EM (Bottcher *et al*, 1998; Wilkens & Capaldi, 1998). Several experiments were carried out elucidating that the peripheral stalk of the enzyme is rather stiff keeping both subcomplexes together, whereas the rotor ring is more elastic, being essential for power transmission between the two stepping motors, F_1 and F_o (Wachter *et al*, 2011).

1.3.2.3 The a-subunit

The largest and most hydrophobic subunit of the F_o-subcomplex is subunit a (Nielsen *et al*, 1981). Early experiments revealed that over-expression and membrane insertion of subunit a leads to a partial collapse of $\Delta\psi$ and inhibition of proton-driven transport systems, indicating a protonophoric activity of the protein (von Meyenburg *et al*, 1985). The more hydrophilic N-terminus of subunit a was shown to be important for membrane insertion and F_o assembly (Lewis and Simoni, 1992), whereas the C-terminal region is interacting with subunit b (Vik and Simoni, 1987) and the rotor ring (Steffens *et al*, 1988).

Differing secondary structure models suggest that subunit a is composed of five (Hatch *et al*, 1995; Long *et al*, 1998; Valiyaveetil & Fillingame, 1998; Vik & Ishmukhametov, 2005; Wada *et al*, 1999) or six transmembrane helices (Deckers-Hebestreit *et al*, 2000; Jager *et al*, 1998; Yamada *et al*, 1996). While all these models coincide in the location of the two C-terminal helices, the topology of the N-terminus is controversial.

Subunit a has been postulated to play a key role in transmembrane ion translocation (Deckers-Hebestreit & Altendorf, 1996; Fillingame *et al*, 1998; Howitt *et al*, 1996; Nakamoto, 1996). Site-directed mutagenesis revealed that a conserved arginine residue (Arg210 in *E. coli*) in TMH 4 of subunit a is important (Cain & Simoni, 1989;

Eya *et al*, 1991; Lightowlers *et al*, 1987), but not essential (Valiyaveetil & Fillingame, 1997). Partial retention of the *E. coli* enzyme activity was observed when the R210 was transferred to a close position (Hatch *et al*, 1995). Mutants of the corresponding arginine in *P. modestum* showed ATP driven Na^+-transport only under particular conditions of pH and [Na^+] suggesting that the stator a-subunit facilitates the dissociation of a Na^+ from the approaching rotor ring binding site (Wehrle *et al*, 2002). Mutational studies of the *Bacillus* PS3 aR169 revealed loss of H^+-coupled ATPase activity while passive H^+-transport was observed. The corresponding arginine was suggested to prevent a proton shortcut on the one hand and facilitate proton transfer between the stator a-subunit and the rotor ring on the other hand (Mitome *et al*, 2010). In addition, E219 and H245 have been shown to be important in the *E. coli* a-subunit (Cain & Simoni, 1986; Cain & Simoni, 1988; Eya *et al*, 1991; Hartzog & Cain, 1994; Howitt *et al*, 1990; Lightowlers *et al*, 1988).

Projection maps of two-dimensional crystals suggested that TMH 2-5 form a four-helix bundle (Hakulinen *et al*, 2012; Schwem & Fillingame, 2006) (figure 8). In the proposed model residues from TMH 2, 4 and 5 at the center of the bundle are involved in translocation of ions from the periplasm to the center of the membrane forming a first half-channel. In addition, TMH 4 and 5 as well as TMH 2 of the rotor ring were thought to mediate translocation from the membrane center to the cytoplasm building a second half-channel (Angevine *et al*, 2007).

The recently obtained cryo-EM map of the *Polytomella* ATP synthase dimer at 6.2 Å resolution showed the actual arrangement of subunit a in the membrane (Allegretti *et al*, 2015) (figure 9 A). A bundle of four long, horizontal membrane-intrinsic α-helices is arranged almost perpendicular to the c-ring. The longest helix (80 Å) is forming a hairpin with another helix of 65 Å, which are both in contact with the c-ring. A second, shorter hairpin is build by the two residual horizontal α-helices and is continuous with a density that extends into the peripheral stalk of the enzyme.

1.3.2.4 The c-subunit

The third component of the bacterial and chloroplast F_o-subcomplex is the c-subunit. The highly hydrophobic c-monomer was initially extracted from membranes with chloroform/methanol and therefore designated as proteolipid (Agarwal & Kalra, 1983; Hoppe *et al*, 1980; Hoppe & Sebald, 1980). The c-subunit isolated from *E. coli*

was first structurally investigated by NMR studies (Girvin *et al*, 1998). It consists of two α-helices that are connected by a short cytoplasmatic loop and form a hairpin. The loop region is highly conserved consisting of a common RQPE-motif and interacts with the central stalk proteins (Stock *et al*, 1999), whereas both termini of the protein reside in the periplasm.

The most prominent attribute of every c-subunit is, besides its loop region, a highly conserved carboxylic residue (D or E) within TMH 2, being localized approximately at the middle of the membrane (von Ballmoos *et al*, 2002a). It was shown that this carboxylic residue can specifically and covalently react with the ATP synthase inhibitor dicyclohexylcarbodiimide (DCCD) (Hoppe *et al*, 1980; Sebald *et al*, 1980). In the intact ATP synthase the c-subunits assemble into a ring-shaped oligomeric complex of 8 to 15 copies (Pogoryelov *et al*, 2010) (table 1) building the enzyme`s rotary element responsible for transmembrane ion translocation together with the stator a-subunit.

1.3.3 Structure and function of the rotor (c)-ring

Today, 16 years after the first three-dimensional structure of a c-ring (in the yeast F_1c_{10} complex) was solved by X-ray crystallography (Stock *et al*, 1999), a lot of structural information about c-rings from different species has become available. Generally, all c-rings have an overall height, which ranges from 55 to 70 Å, and a variable diameter of 50 to 65 Å depending on their individual stoichiometry. Some of these rings are rather straight in their outer shape, like the one isolated from *Bacillus pseudofirmus* OF4 (Preiss *et al*, 2010) (figure 10 B) whereas other rings have a prominent kink in the α-helices, approximately in the middle of the membrane, as the one from *Ilyobacter tartaricus* resembling the shape of an hour-glass (Meier *et al*, 2005) (figure 10 A).

In a lipid environment such as the membrane c-rings have a phospholipid plug on their periplasmatic side (Meier *et al*, 2001; Oberfeld *et al*, 2006) replaced by detergent molecules if the protein is isolated and crystallized in 3D (Meier *et al*, 2005; Pogoryelov *et al*, 2009; Preiss *et al*, 2010; Schulz *et al*, 2013). Most experimental investigations of c-rings are focused on the question of ring stoichiometry, their ion specificity and, in context with the stator a-subunit, the ion translocation mechanism.

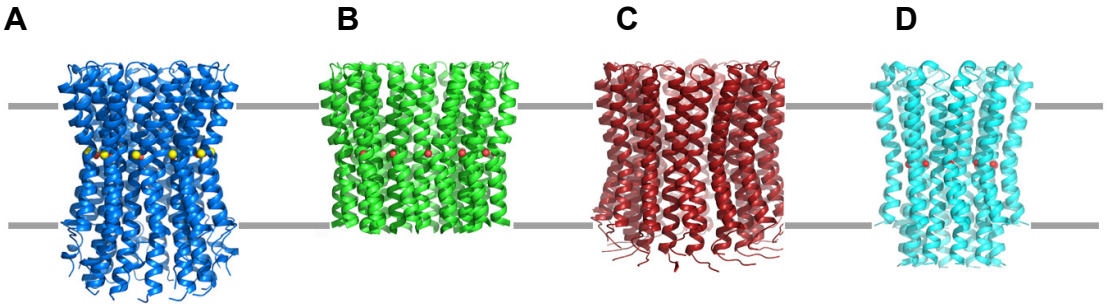

Figure 10. X-ray structures of the c-rings from *I. tartaricus*, *B. pseudofirmus* OF4, *S. platensis* and *S. cerevisiae*.

(A) The Na^+-binding c_{11} ring from *I. tartaricus* (pdb 2wgm), **(B)** the H^+-binding c_{13} ring from *B. pseudofirmus* OF4 (pdb 2x2v) , **(C)** the H^+-binding c_{15} ring from *S. platensis* (pdb 2wie) and **(D)** the H^+-binding c_{10} ring from *S. cerevisiae* (pdb 3u2y). The different c-rings are displayed from the membrane plane. The structures were extracted from the RCSB protein data bank (www.rcsb.org).

1.3.3.1 The c-ring stoichiometry

Atomic force microscopy (AFM) studies (Fritz *et al*, 2008; Matthies *et al*, 2009; Pogoryelov *et al*, 2007; Pogoryelov *et al*, 2005; Preiss *et al*, 2013; Seelert *et al*, 2000; Stahlberg *et al*, 2001), projection maps calculated from 2-dimensional crystals (Fritz *et al*, 2008; Matthies *et al*, 2009; Meier *et al*, 2006; Meier *et al*, 2003; Stahlberg *et al*, 2001; Toei *et al*, 2007) and X-ray structures of 3-dimensional crystals (Matthies *et al*, 2014; Meier *et al*, 2005; Pogoryelov *et al*, 2009; Preiss *et al*, 2010; Saroussi *et al*, 2012; Symersky *et al*, 2012; Vollmar *et al*, 2009; Watt *et al*, 2010) revealed different c-ring stoichiometries (table 1).

Formerly, it was proposed that the number of c-subunits varies depending on the carbon source and that this variability represents a regulatory mechanism for ATP synthesis activity (Schemidt *et al*, 1995; Schemidt *et al*, 1998). Later, several structural investigations indicated that the c-ring stoichiometry varies between different species despite the highly conserved primary sequences, but is constant within one species, independent of external parameters (Meier *et al*, 2011). The fact that heterologously expressed c-rings assemble in their native stoichiometry supports the hypothesis that the oligomeric size of the rotor ring is intrinsically determined by the primary amino acid sequence (Arechaga *et al*, 2002; Muller *et al*, 2001). These findings indicate that c-rings are highly adapted to the specific bioenergetic needs of a given organism (Hicks *et al*, 2010; Liu *et al*, 2011; Matthies *et al*, 2009; Pogoryelov *et al*, 2005).

Table 1. Overview of all determined c-ring structures.

Species	Stoichiometry	Specificity	Method	Reference
Bos taurus	c_8	H^+	X-ray crystallography	(Watt *et al*, 2010)
Mycobacterium phlei	c_9	H^+	X-ray crystallography	(Preiss *et al*, 2010)
Saccharomyces cerevisiae	c_{10}	H^+	X-ray crystallography	(Stock *et al*, 1999; Symersky *et al*, 2012)
Enterococcus hirae (V-type)	c_{10} (2x hairpins)	Na^+	X-ray crystallography	(Murata *et al*, 2005)
Ilyobacter tartaricus	c_{11}	Na^+	Atomic force microscopy Electron crystallography X-ray crystallography	(Meier *et al*, 2009; Meier *et al*, 2005; Stahlberg *et al*, 2001; Vonck *et al*, 2002)
Propionigenium modestum	c_{11}	Na^+	Electron crystallography	(Meier *et al*, 2003)
Clostridium paradoxum	c_{11}	Na^+	Electron crystallography	(Meier *et al*, 2006)
Acetobacterium woodii	c_{11}	Na^+	Atomic force microscopy Electron crystallography X-ray crystallography	(Fritz *et al*, 2008; Matthies *et al*, 2014)
Thermus thermophilus	c_{12}	H^+	Electron crystallography	(Toei *et al*, 2007)
Synechococcus elongatus	c_{13}	H^+	Atomic force microscopy	(Pogoryelov *et al*, 2007)
Caldalkalibacillus thermarum strain TA2.A1	c_{13}	H^+	Atomic force microscopy Electron crystallography	(Matthies *et al*, 2009)
Bacillus pseudofirmus OF4	c_{13}	H^+	Atomic force microscopy X-ray crystallography	(Preiss *et al*, 2013; Preiss *et al*, 2010)
Spinacia oleracea	c_{14}	H^+	Atomic force microscopy X-ray crystallography	(Seelert *et al*, 2000; Vollmar *et al*, 2009)
Spirulina platensis strain C1	c_{15}	H^+	Atomic force microscopy X-ray crystallography	(Pogoryelov *et al*, 2009; Pogoryelov *et al*, 2005)

As mentioned above the primary c-subunit sequences are highly conserved raising the question of what exactly determines the size of the particular oligomeric complex. A motif of repeating glycine residues (GxGxGxG) within TMH 1 was described to be involved in defining the c-ring stoichiometry, as it represents a typical dimerization domain in transmembrane α-helices (MacKenzie *et al*, 1997). Mutations within this motif, e.g. by replacing one or several glycine residues by alanines indeed have been shown to alter the stoichiometry of the respective c-ring either up or down (Pogoryelov *et al*, 2012; Preiss *et al*, 2013).

The number of c-subunits in the ring has a substantial bioenergetic impact on the efficiency of the particular ATP synthase. Considering the fact that 3 ATP molecules are synthesized in the F_1-subcomplex per 360° rotation (Abrahams *et al*, 1994) and assuming that the enzyme is tightly coupled, the ion-to-ATP ratio is just determined by the number of c-subunits. Considering ATP synthesis lower c-ring stoichiometries are more beneficial as less ions need to be transported per ATP molecule. For the enzyme working in ATP hydrolysis mode larger c-rings are more profitable for generating a transmembrane ion gradient, as they translocate more ions per ATP (Meier *et al*, 2011).

1.3.3.2 The c-ring structure and the ion-binding site

In the last years a lot of progress was made in structure determination of c-rings by X-ray crystallography. The first c-ring structure of a bacterial F_1F_o ATP synthase was the one from *Ilyobacter tartaricus*, solved in 2005, revealing an hour-glass shaped oligomeric complex of eleven subunits (Meier *et al*, 2005). In the same Journal issue the K-ring structure of the *Enterococcus hirae* V_1V_o ATPase was also published, being composed of ten subunits and having a comparable height but a much wider diameter as the subunits build four instead of only two transmembrane α-helices (Murata *et al*, 2005). Today, several medium and high resolution c-ring structures are available. Besides the homomeric c-ring from *I. tartaricus*, other structures of bacterial rings isolated from *Spirulina platensis* (Pogoryelov *et al*, 2009), *Bacillus pseudofirmus* OF4 (Preiss *et al*, 2010) and the heteromeric c-ring of *Acetobacterium woodii* (Matthies *et al*, 2014) were determined. Further, the bovine c_8 ring (*B. taurus) (Watt et al, 2010)*, the yeast c_{10} ring (*Saccharomyces cerevisiae)* (Symersky *et al*, 2012) as well as two chloroplast c_{14} rings ((*Spinacia oleracea*) (Vollmar *et al*, 2009)

and (*Pisum sativum*) (Saroussi *et al*, 2012)) were solved. The high resolution structures (Matthies *et al*, 2014; Pogoryelov *et al*, 2009; Preiss *et al*, 2010; Symersky *et al*, 2012) provide insights into the ion specificities of the rings and atomic details how the corresponding ions are coordinated in the binding sites (figure 11).

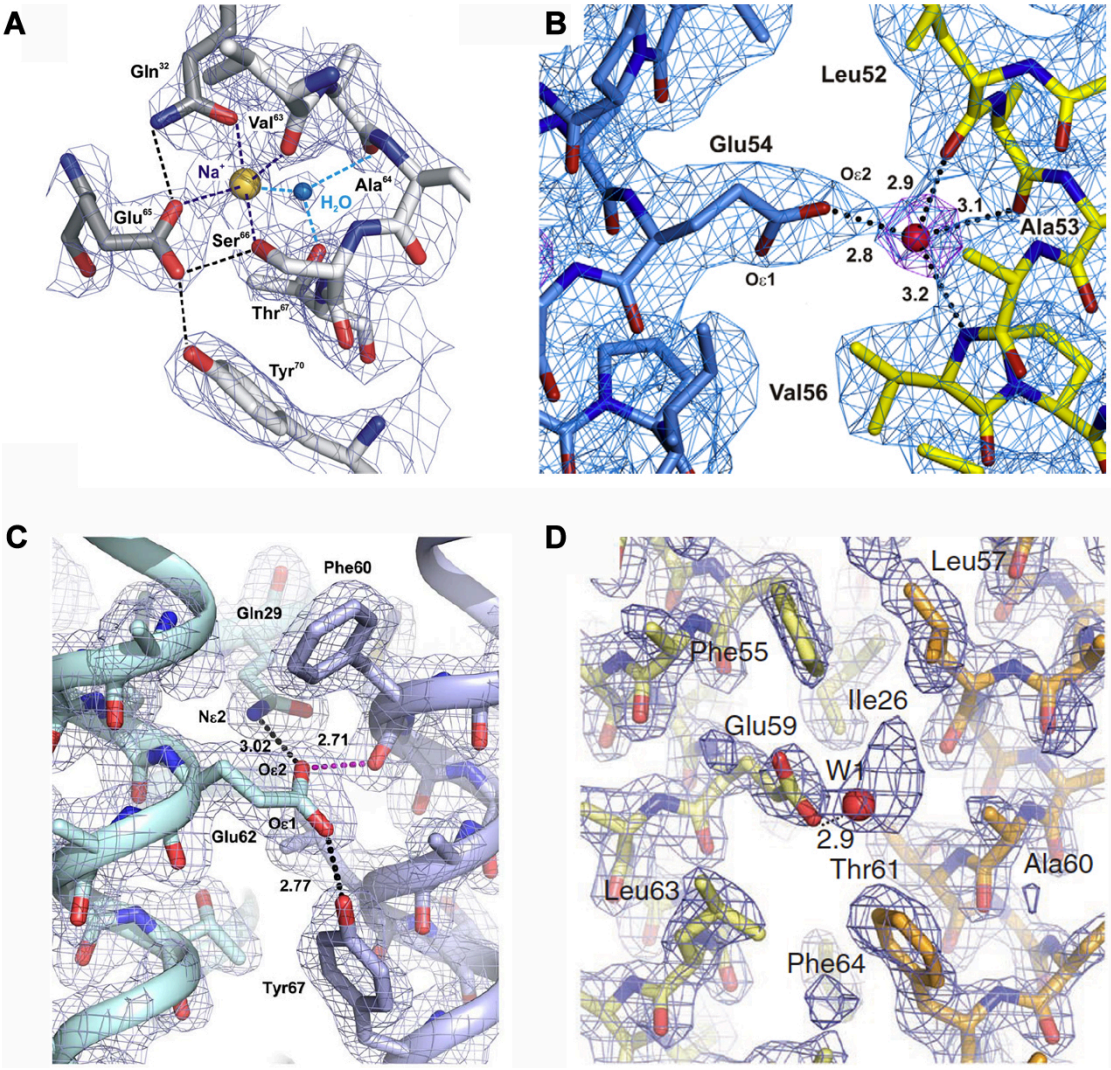

Figure 11. The ion-binding site of the c-rings from *I. tartaricus*, *B. pseudofirmus* OF4, *S. platensis* and *S. cerevisiae*.

(A) The Na^+-binding site of the c_{11} ring from *I. tartaricus*, which involves a Na^+ and a structural water molecule (yellow and blue spheres, respectively) (Meier *et al*, 2009). **(B)** The H^+-binding site of the c_{13} ring from *B. pseudofirmus* OF4, where a H_2O (red sphere) is also involved in H^+-coordination (Preiss *et al*, 2010). **(C)** The H^+-binding site of the c_{15} ring from *S. platensis* lacking a water molecule (Pogoryelov *et al*, 2009) and **(D)** the H^+-binding site of the c_{10} ring from *S. cerevisiae* including a H_2O (red sphere) (Symersky *et al*, 2012). The binding sites of the *I. tartaricus*, *S. platensis* and *B. pseudofirmus* OF4 c-rings are shown in the closed, ion-locked conformation, whereas the site of the *S. cerevisae* c-ring is represented in the open, unlocked state with the glutamate facing outwards.

The high resolution structure of the *I. tartaricus* c-ring revealed a tight coordination of the Na^+ in each of the eleven binding sites, situated approximately at the middle of the membrane (Meier *et al*, 2005). Four amino acid residues were identified to be involved in Na^+-coordination at each ion-binding site. Later, by re-processing these data, a structural water molecule was found to complement the Na^+-coordination as a fifth ligand, which could also be confirmed by molecular dynamics simulations (Meier *et al*, 2009). The Na^+-binding site is arranged between two adjacent c-subunits and directly coordinated by side chain oxygens of E65 and Q32 corresponding to one subunit, the hydroxyl oxygen of S66 and the backbone carbonyl hydrogen of V63 of the neighbouring c-subunit. The structural water molecule is also binding the Na^+, being itself further coordinated by the carbonyl oxygen of A64 and the hydrogen oxygen of T67 of the adjacent subunit. Besides, hydrogen bonds exists between E65 and Q32 as well as between E65 and S66 and between E65 and T70. This constellation represents the ion-locked conformation of the Na^+ (figure 11 A).

In contrast to this complex network providing a stable locked conformation for the Na^+, a H^+-binding site is simpler to engineer, as illustrated in the c-ring of *S. platensis* (Pogoryelov *et al*, 2009). The H^+ is directly coordinated by the side chain oxygen of E62, which alongside is forming hydrogen bonds with the side chain oxygen of Q32 from the same subunit as well as with the hydroxyl oxygen of T67 and the backbone carbonyl oxygen of F60 from the adjacent c-subunit. This constellation corresponds to the stable ion-locked conformation for a proton, similar to the locked conformation as seen in the Na^+-binding site (figure 11 C).

Besides the chemical nature of the residues itself, the size of a particular binding site plays an additional role in defining the ion specificity of a c-ring. Comparing the Na^+ and H^+-binding c-rings described here (Meier *et al*, 2005; Pogoryelov *et al*, 2009) reveals that the H^+-specific ring is less kinked than the Na^+-binding one. Hence, the distances between the residues defining the ion-binding sites are shorter in the latter one geometrically excluding Na^+-coordination.

A second type of H^+-coordination was described in the c-ring of *Bacillus pseudofirmus* OF4 where the ion is coordinated by the side chain carboxyl oxygen of

the conserved glutamate (E54) as well as the backbone carbonyl oxygens of L52 and A53 and the backbone nitrogen of V63 (Preiss *et al*, 2010). Additionally, a water molecule is involved in the coordination, which is not present in the H^+-binding c_{15} ring (figure 11 B).

1.3.3.3 The ion translocation mechanism

As described previously (1.3), ATP synthesis is tightly coupled to a rotational mechanism of the enzyme, whereby torque is generated by an ion motive force (proton motive force, *pmf* or sodium motive force, *smf*). The *pmf* or *smf* consists of an electrical potential ($\Delta\Psi$) and a transmembrane H^+- or Na^+-gradient (ΔpH or ΔNa^+) as described in the following equation(s):

$$pmf = \Delta\Psi + 2.3RT/F\ \Delta pH$$
$$(smf = \Delta\Psi + 2.3RT/F\ \Delta Na^+)$$

(R: gas constant, F: Faraday`s constant, T: absolute temperature)

It was shown that $\Delta\Psi$ is compulsory for ATP synthesis, whereas ΔpH was suggested to be not essential but accelerates the reaction (Kaim & Dimroth, 1999). Nevertheless, both, $\Delta\Psi$ and ΔpH, are required for efficient ATP synthesis. Besides, it is widely accepted that for ion translocation a conserved glutamate or aspartate residue of the rotor ring binding site (figure 10) must interact with a conserved arginine of the stator a-subunit. Further, it is proposed that the ion reaches the binding site by a periplasmic half channel and leaves through a cytoplasmic gate.

Two prominent models of an ion translocation mechanism were proposed (Dimroth *et al*, 2006; Junge *et al*, 1997; Vik & Antonio, 1994), differing in the resulting driving force for torque generation and the localization of the ion exit gate (figure 12).
The first model describes a " push-and-pull" mechanism in a Na^+-translocating c-ring with the a-subunit arginine functioning as a regulator for opening and closing the access for the ion to and from the binding sites in the c-ring (Dimroth *et al*, 2006) (figure 12 A). During counterclockwise rotation (ATP synthesis), a Na^+ tightly bound to a glutamate in the locked conformation reaches the a/c-ring interface where it is

repelled by the positively charged arginine, thereby leaving the binding site towards the cytoplasm. The electrostatic attraction between the negatively charged glutamate (in the open conformation) and the positively charged arginine keeps the gate open for binding of another ion from the periplasm. After having been neutralized, the glutamate adopts again the locked conformation, transporting the Na^+ into the lipid environment of the membrane. As a prerequisite for the directed rotation of the c-ring, a membrane potential ($\Delta\Psi$) is needed to move the glutamate from which the ion was just repelled towards the periplasm where it can accept another ion. This model suggests the entrance pathway for the Na^+ being in subunit a and the exit pathway to be localized in the c-ring. This assumption is in agreement with several experiments which revealed that the ring is accessible for ions even in the absence of subunit a (Dimroth *et al*, 2006; Meier *et al*, 2003; von Ballmoos *et al*, 2002a).

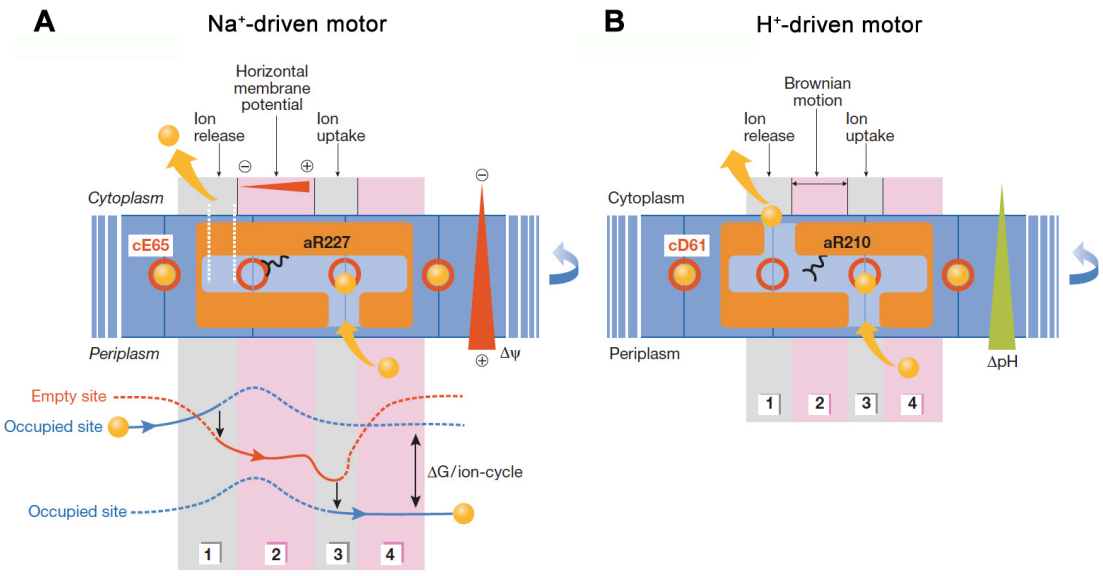

Figure 12. Two models for torque generation in the c-ring and the ion translocation mechanism. **(A)** The "push-and-pull"-mechanism model for a Na^+-translocating c-ring. The substeps as well as calculated free energy profiles of empty and ion bound sites are presented. **(B)** The "ratchet"-mechanism model for a H^+-translocating c-ring. Four substeps during ion translocation in ATP synthesis direction are shown. The figure was taken from (Dimroth *et al*, 2006).

The second model was proposed for a H^+-translocating c-ring attributing the interaction between the glutamate and the arginine to regulate access to the binding sites (figure 12 B). Unlike in the first model, both access channels are supposed to be localized in subunit a (Aksimentiev *et al*, 2004; Feniouk & Yoshida, 2008; Junge *et*

al, 1997; Vik & Antonio, 1994). The H^+ reaches the glutamate of the binding site through the periplasmic channel and leaves it after almost a complete rotation of the c-ring through the cytoplasmic channel. While being deprotonated, the negatively-charged glutamate is coordinated by the positively-charged arginine of subunit a, compensating its charge. Directional rotation is mediated by a transmembrane proton gradient, protonating the glutamate from the side with a higher proton concentration (periplasm). Hence in this model, ΔpH is the driving force for ion translocation. After having released the H^+, the glutamate acts as a ratchet, preventing backwards movement which would be energetically disfavoured. Therefore this model describes the so-called "ratchet"-mechanism for ion translocation.

The cryo-EM map recently obtained from the *Polytomella* ATP synthase dimer (figure 9 A) showed four long, horizontal membrane-intrinsic α-helices in subunit a arranged in two hairpins almost perpendicular to the c-ring (Allegretti *et al*, 2015) (figure 9 B). By fitting the C-terminus of subunit a, the conserved stator arginine becomes situated next to the conserved ion-binding glutamate of a c-subunit. Two aqueous half-channels can be observed here: The cavity on the matrix side is build by the N-terminal part of a longer helix of subunit a, which is partly hydrophilic or amphiphatic. A second cavity can be found on the luminal side and is supposed to be the entrance channel for protons translocated across the membrane. Accordingly, protons reach the conserved glutamate in subunit c via the hydrophilic luminal half-channel and after almost a complete rotation of the c-ring the bound proton approaches the second half-channel where it is released into the matrix (figure 13).

All the previously described c-ring structures (1.3.3.2) showed the corresponding ion (Na^+ or H^+) in a stable, locked conformation which is the energetically most favored state within the hydrophobic environment of a lipid membrane. However in 2012, the structure of the mitochondrial c_{10} ring from *S. cerevisiae* was solved showing the binding sites in an open conformation with the ion coordinating glutamate facing outwards (Symersky *et al*, 2012). Here, the isolated c-ring was crystallized in a buffer containing a 2-methyl-2,4-pentadiol (MPD)/propylene glycol mixture instead of detergent and polyethylene glycol (PEG) as precipitant which was used in the previous crystallization trials obtaining c-ring structures with the ion-binding sites in a

closed, ion locked state. The conformation in the yeast c-ring is due to the local hydration of the MPD molecules building multiple hydrogen bonds with the side chain oxygens of the glutamate (figure 11 D). This state was already observed in a c-ring co-crystallized with DCCD which covalently binds to the glutamate (Mizutani *et al*, 2011) thereby inducing an open conformation (Pogoryelov *et al*, 2010). The open conformation represents the binding site in the a/c-ring interface, when the glutamate is interacting with the arginine of the a-subunit during ion translocation.

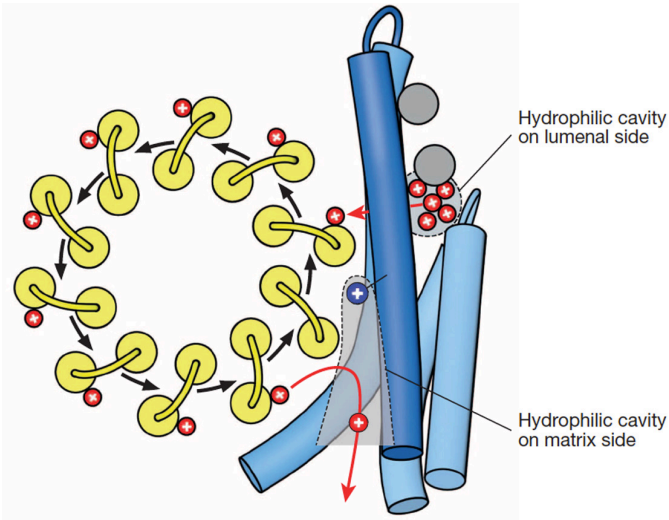

Figure 13. Ion translocation in the *Polytomella* ATP synthase.
Protons (red) reach the conserved glutamate of a c-subunit via a lumenal half-channel (dashed grey circle) and after almost a complete rotation of the c-ring (yellow), the bound proton approaches the second half-channel on the matrix side (dashed grey outline) where it is released. The figure was taken from (Allegretti *et al*, 2015).

1.3.4 The bacterium *Fusobacterium nucleatum*

Fusobacterium nucleatum was first described in 1922 (Knorr, 1922). It is the type species of the genus *Fusobacterium*, belonging to the family *Bacteroidaceae*. Its designation refers to the fact that it is a spindle-shaped rod (*fusus*: spindle, *bacterion*: small rod) with a nucleated appearance in light and electron microscopy due to intracellular granules (Hofstadt, 1981; Moore *et al*, 1984b; Robrish *et al*, 1987) (figure 14). The gram-negative bacterium is non-sporeforming and non-motile (Bolstadt *et al*, 1994).

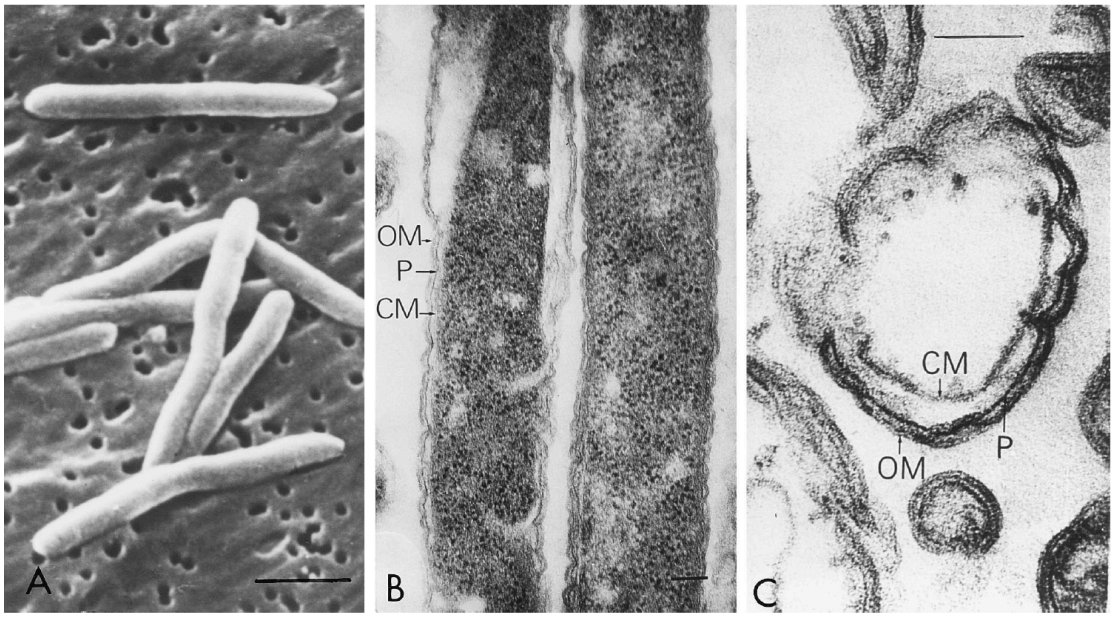

Figure 14. Electron microscopy (EM) of *F. nucleatum*.
(A) Scanning EM (bar 1 um), **(B** and **C)** Transmission EM of sections through intact and French pressed cells, respectively (bar 100 nm). The figure was taken from (Bolstadt *et al*, 1996). OM: outer membrane, P: periplasmic space, CM: cytoplasmic membrane.

F. nucleatum is one of the most common species in human infections (Moore & Moore, 1994), frequently isolated from dental plaque in humans and has been implicated in the aetiology of periodontal diseases (Bolstadt *et al*, 1996; Dzink *et al*, 1988; Dzink *et al*, 1985; Haffajee *et al*, 1988; Moore & Moore, 1994; Moore *et al*, 1985; Signat *et al*, 2011; Socransky *et al*, 1998). Beyond this, it regularly occurs in infections of other human body sites such as for example the lung, liver and brain (Moore *et al*, 1984a; Moore & Moore, 1994).

F. nucleatum grows under anaerobic conditions using peptides and amino acids as a primary energy source (Bolstadt *et al*, 1996; Gharbia & Shah, 1991) whereby glucose is just utilized to a low extent (Gharbia & Shah, 1988; Robrish *et al*, 1987; Robrish & Thompson, 1990; Rogers *et al*, 1991). Besides, it possesses a transport system for carbohydrates (glucose, galactose and fructose) for which energy is derived from anaerobic amino acid fermentation. The ability of intracellular polymer synthesis and subsequent fermentation of these sugar reserves in case of an amino acid depletion may support the survival of these cells in the human oral cavity where availability of nutriments changes rapidly.

It was reported that *F. nucleatum* grows as planktonic culture between pH 6 and pH 8 (Rogers *et al*, 1991), whereas at increased pH biofilm growth was observed (Zilm & Rogers, 2007). This alkaline pH-induced phenotypic switch may be an adaption to an altered, unfavoured environmental pH as it occurs during periodontal diseases *in vivo* (Chew *et al*, 2012).

To date *F. nucleatum* seems to be the only known gram-negative bacterium able to ferment glutamate to acetate and butyrate via the 2-hydroxyglutarate pathway (Buckel & Barker, 1974). The key enzyme of this pathway is a biotin-dependent sodium ion-pump, the glutaconyl-Coenzyme A decarboxylase, catalyzing the decarboxylation reaction of glutaconyl-CoA to crotonyl-CoA thereby generating a transmembrane Na^+-gradient (Beatrix *et al*, 1990; Boiangiu *et al*, 2005; Buckel, 2001).

1.3.4.1 The Na^+-binding signature and the *F. nucleatum* F_1F_o ATP synthase

Early biochemical studies have already identified several Na^+-coupled F_1F_o ATP synthases (Laubinger & Dimroth, 1987; Laubinger & Dimroth, 1988; Neumann *et al*, 1998; Reidlinger & Muller, 1994). Subsequently, the corresponding Na^+-binding c-rings were biochemically investigated, revealing ligands which are involved in Na^+-coordination (Kaim *et al*, 1997; Zhang & Fillingame, 1995) and showing that Na^+ has a stabilizing effect on the stability of the rotor ring (Meier & Dimroth, 2002).

Due to the high resolution X-ray structures of different c-rings (Matthies *et al*, 2014; Pogoryelov *et al*, 2009; Preiss *et al*, 2010; Symersky *et al*, 2012) (figure 10 and 11), all the amino acid residues involved in Na^+- and H^+-coordination are now exactly known. A typical signature for Na^+-binding, as it is found in the *I. tartaricus* c-subunit, consists of a series of conserved amino acid residues, namely E32, V63, A64, E65, S66, T67 and T70 (*I. tartaricus* numbering).

Many species possess a selection of the previously mentioned residues or sometimes even the same residues. For example, a similar motif can be found in some species, in which the glutamine residue in the first TMH (Q32 in *I. tartaricus*) is replaced by a glutamate meaning that two instead of one carboxyl side chains are involved in ion-coordination (figure 15). This could be interpreted as a “two-carboxylate-motif” in a c-ring ion-binding site. From a structural point of view, it is questionable if a second ion is bound to this glutamate side chain to compensate the additional charge in the binding site. Moreover, assuming this ion can also be translocated during enzyme

operation, this would result in an ion-to-ATP ratio twice as large as expected from the c-ring stoichiometry (see chapter 1.3.3.1).

Figure 15. Alignment of c-subunit sequences from F-ATP synthases of selected species.
The individual sequences were aligned according to their cytoplasmic loop region shown in highlighted black. The single c-subunits form α-helical hairpins, the N- and C-terminal helices are indicated. The type of ion-coordination (Na^+ or H^+) is stated on the right side, the question marks in color indicate the predicted type of coordinated ion, respectively. The residues involved in (Na^+-) coordination (Meier *et al*, 2005; Murata *et al*, 2005) are indicated in colors. Species names: *Fusobacterium nucleatum* subsp. *nucleatum* (numbering), *Ruminococcus albus, Thermotoga maritima, Eubacterium siraeum* DSM 15702, *Butyrivibrio proteoclasticus* B316, *Stomatobaculum longum*, *Oribacterium* sp. *oral* taxon 078 str. F0262, *Azotobacter vinelandii*, *Gluconobacter oxydans*, *Ilyobacter tartaricus*, *Propionigenium modestum*, *Clostridium paradoxum*, *Acetobacterium woodii, Mycoplasma genitalium, Streptococccus pneumonia*, *Mycobacterium tuberculosis, Aquifex aeolicus, Gloeobacter violaceus* PCC 7421, *Synechocystis* sp. strain PCC 6803, *Synoechococcus* sp. strain PCC 6716, *Arthrospira* sp. strain PCC 9438, Spinach chloroplast, *Bacillus* sp. strain PS3, *Caldalkalibacillus thermarum* (*Bacillus* sp. strain TA2.A1), *Saccharomyces cerevisiae*, *Bos taurus*, *Haemophilus influenza, Escherichia coli*. The figure was adapted from (Schulz *et al*, 2013).

One of the species showing this just described "two-carboxylate-motif" in the c-subunit sequence is *F. nucleatum* possessing a glutamate at positions 32 in addition to the conserved one at position 65 (figure 15). As the other residues in the *F. nucleatum* c-subunits are identical to the corresponding residues in the *I. tartaricus* c-subunits it

suggests that the *F. nucleatum* ATP synthase is likewise physiologically coupled to Na^+ and hence the *smf*. Nevertheless, it is also conceivable that the second glutamate changes the c-ring ion specificity and along with it possibly also its actual driving force (e.g. the *smf*). Therefore this assumption needs to be experimentally tested. Besides that, the bioenergetic and mechanistic implications of an altered amino acid constellation in the ion-binding sites are not clear. Having said that a *smf* is produced by the glutaconyl-CoA decarboxylase involved in the amino acid fermentation in *F. nucleatum* (figure 16), it is feasible that this transmembrane sodium gradient could directly be used for energy conversion by its ATP synthase.

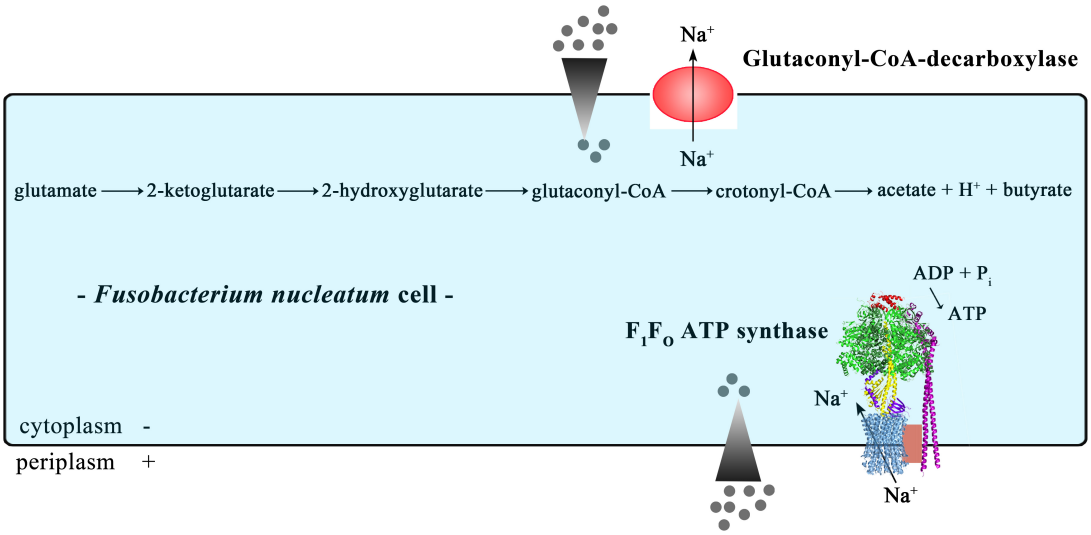

Figure 16. A hypothetical proposal for the energy metabolism in *F. nucleatum*.
Fermentation of glutamate via the hydroxyglutarate pathway involves a membrane-bound glutaconyl-CoA decarboxylase. The enzyme catalyzes the formation of crotonyl-CoA from glutaconyl-CoA thereby generating a transmembrane sodium ion gradient (*smf*). This *smf* could potentially then fuel a Na^+-coupled F_1F_o ATP synthase.

1.4 The N-type ATPase - a Novel type of rotary ATPase

In 2012, bioinformatics studies were performed to evaluate the distribution of Na^+-translocating ATPases among bacterial genomes. In the course of this, a novel (N) type of enzyme was found being present always as a second copy of rotary ATPase in various phylogenetically independent species (Dibrova *et al*, 2010).

1.4.1 The N-*atp* operon and the enzyme subunits

Bacterial ATPases are encoded by a conserved *atp* (formerly *unc*) operon (figure 15) (Gay & Walker, 1981a; Gay & Walker, 1981b; Kanazawa *et al*, 1981a; Kanazawa *et al*, 1981b; McCarn *et al*, 1988; Saraste *et al*, 1981; Walker *et al*, 1984), which is likewise true for the novel enzyme, always occurring alongside with a common F-*atp* operon in a particular genome. As this novel enzyme is always present next to a H^+-translocating F- or A-type ATP synthase, while itself suggested to have a Na^+-binding c-ring, it was designated as N-type ATPase (Dibrova *et al*, 2010).

There are several conspicuous features of the N-*atp* operon. Lacking the *atpH* gene which in F-*atp* operons encodes for the δ-subunit, the N-*atp* operon has an unusually long *atpF* gene. However, the C-terminus of the N-type *atpF* can be aligned with an F-type *atpH*, implicating that *atpF* and *atpH* have probably been fused in the N-*atp* operon (Saum *et al*, 2009). This constellation also appears, occasionally, in some F-*atp* operons, for example in *Mycobacteria* species, where a common *atpF* gene can be found alongside with an *atpF-atpH* fusion gene (Preiss, 2013).

Further, an unrivaled characteristic of the N-*atp* operon is the presence of a gene named *atpR*, which encodes for a hydrophobic membrane protein with three predicted TMH and a theoretical molecular weight between 10 and 13 kDa. Remarkably, this gene product carries two conserved arginine residues, each in the middle of the second and third TMH, respectively. Charged residues within the hydrophobic core of the membrane often have a functional purpose. In this case, it was proposed that the positively charged residues could interact with the negatively charged glutamate residues of the c-subunits thereby assisting c-ring assembly (Dibrova *et al*, 2010). In F-type ATP synthases subunit i probably takes over this function, also having a conserved arginine residue in the second TMH (Suzuki *et al*, 2007). The corresponding *atpI* gene, however, is not present in the N-*atp* operon. Due to the fact that the *atpR* gene occurs in all N-*atp* operons assigned, but in no classical *atp* operon known so far, it can be used as a hallmark for these enzymes.

Another gene constituting this operon is called *atpQ*, as well assumed to encode for a hydrophobic membrane protein of yet unknown function having a theoretical

molecular weight between 11 and 18 kDa. Unlike *atpR*, the latter one is not limited to the N-*atp* operon.

Figure 17 shows a comparison of the N-*atp* operon as it was found in *Burkholderia pseudomallei* with a common F-*atp* operon as it occurs in *I. tartaricus*.

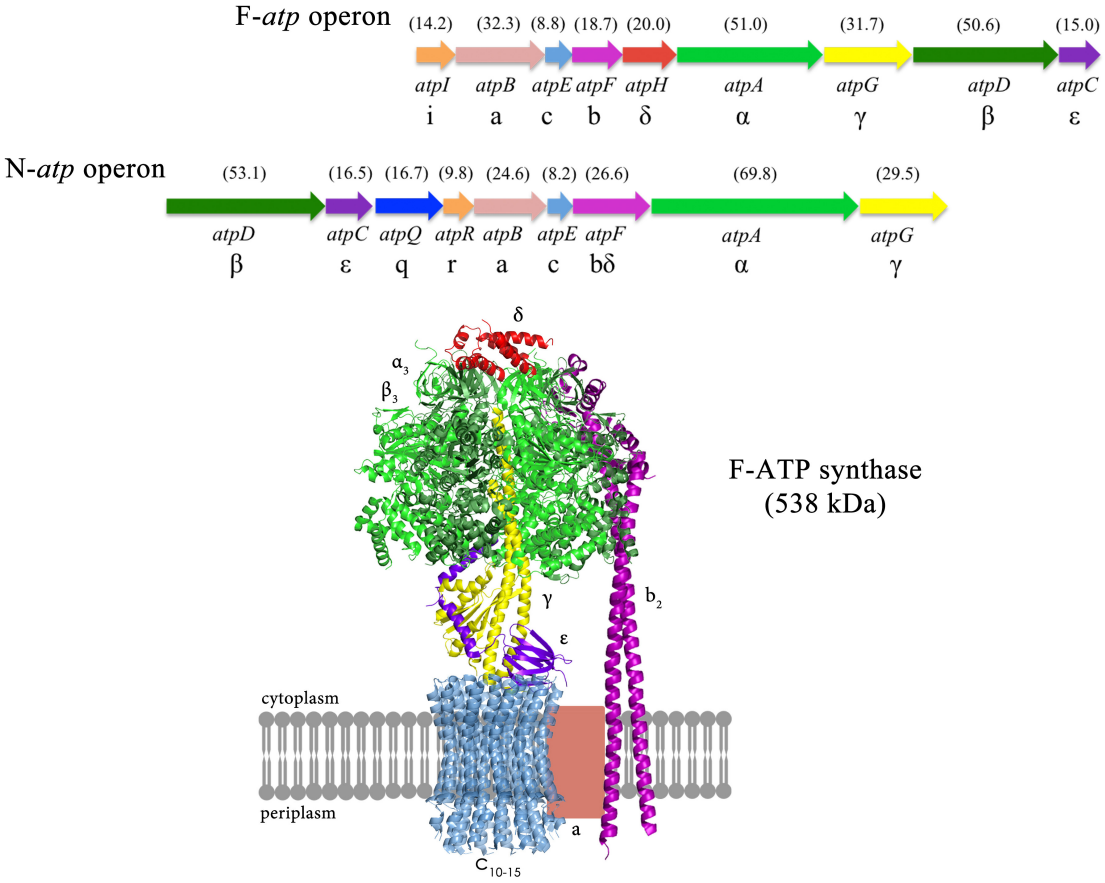

Figure 17. The gene organization in the F- and N-type *atp* operon and the enzyme subunits.
The upper part shows the gene order of both *atp* operons encoding for a common F-type ATP synthase (top) and the novel N-type ATPase (bottom). The gene arrangement is altered in the N-*atp* operon where *atpD* and *atpC* precede the *atpB* being followed by *atpQ* and *atpR*, which are not present in the F-*atp* operon. The arrows reflect the actual gene lengths. The theoretical molecular masses of the *I. tartaricus* F-ATP synthase and the *B. pseudomallei* N-ATPase gene products are given in kDa above the corresponding genes. The lower part of the figure shows a model of the bacterial F-ATP synthase. The colour code for the single subunits of the assembled enzyme is the same as in the F-*atp* operon above. *AtpI* does not encode for a structural subunit and is therefore absent in the ATP synthase model.

1.4.2 The phylogenetic distribution and properties of the N-ATPase

Analyses of the phylogenetic distribution of the N-*atp* operon revealed that it is present in the genomes of different bacterial phyla including *Aquificae*, *Chlorobi*, *Cyanobacteria*, *Planktomycetes* and *Proteobacteria* as well as in the archaeal genus *Methanosarcina*. The fact that it can be found in the Archaea *M. barkeri* and *M. acetivorans* while being absent in other closely related Archaea leads to the assumption that the operon was acquired via lateral gene transfer (Dibrova *et al*, 2010). In support of this notion, the GC-content of the N-*atp* operons also correlates with the average GC-content of the host genomes and moreover the gene neighborhoods of the operons are also well conserved among these species (Dibrova *et al*, 2010).

These bioinformatics data can be related to findings from prior biochemical investigations. Already in 1994, two types of ATPases were detected in the genome of the Archaeon *Methanosarcina mazei*: an A-type ATPase suggested to translocate H^+ and an F-type enzyme using Na^+ as the coupling ion (Becher & Muller, 1994). Whereas the A-ATPase is encoded in the archaeal genome, the F-ATPase was found to be plasmid-borne just like some N-ATPases in cyanobacteria are (Dibrova *et al*, 2010). Furthermore, in 1997, an "archaebacterial" F_1F_o ATPase was described to be present in the *Methanosarcina barkeri* genome. However, attempts to confirm the expression of this enzyme on mRNA or protein level failed. For this reason it remains ambiguous if these genes are actually expressed in the cells (Sumi *et al*, 1997).

The N *atp*-operon was also found in several bacterial genomes, although the function of these enzymes was never conclusively determined (Glockner *et al*, 2003; McInerney *et al*, 2007; Swingley *et al*, 2008). Due to the remaining question about a possible existence of two structurally and functionally different ATPases in archaea, mutational studies of both enzymes (A- and the F-type ATPase) from *M. acetivorans* were performed. While the deletion of the "archaebacterial" F-type ATPase had no significant effect on cell growth and ATP synthesis rate, a ΔA-ATPase mutant could not be obtained (Saum *et al*, 2009). It therefore seems obvious that this "archaebacterial" F-type ATPase, probably represening an N-type ATPase, does not have a physiological role in ATP synthesis whereas the A-ATPase does.

In 2011, a second type of rotary ATPase was also claimed to exist in the halotolerant, alkaliphilic cyanobacterium *Aphanothece halophytica*, which can grow in alkaline media of up to 3 M NaCl and pH 11 (Soontharapirakkul *et al*, 2011). Having expressed it in the Δ*atp* strain *E. coli* DK8 the authors could show that this enzyme can support growth on the non-fermentable carbon source succinate. Besides, Na^+ stimulated ATP hydrolysis activity in inverted *E. coli* membrane vesicles was observed. This activity could be inhibited by the Na^+/H^+-antiporter monensin, the F_o-ATP synthase inhibitor dicyclohexylcarbodiimide (DCCD), the F_1-ATPase inhibitors sodium azide (NaN_3) and tributylin chloride (TBT-Cl), but not by the protonophore carbonylcyanid-*m*-chlorophenylhydrazon (CCCP).
Moreover, Na^+ protected against DCCD-inhibition. When expressed in a salt-sensitive *E. coli* mutant, cells only grew when transformed with a plasmid expressing the Na^+-ATPase from *A. halophytica*. Additionally, expression tests of the enzyme in the cyanobacterium *Synechococcus* sp. PCC 7002 revealed that expression increased with increasing NaCl concentrations in the medium and the enzyme could impair growth of the cells at high salinity.

These findings point at a potential function of the enzyme as ATP-driven Na^+ pump in salt-stress tolerance, besides the well-characterized Na^+-extruding mechanisms involving Na^+/H^+-antiporters and P-type Na^+-ATPases (Soontharapirakkul *et al*., 2011). These results are consistent with the observation that the c-subunit of *A. halophytica* carries a complete set of Na^+-binding ligands (Meier *et al*, 2009) (see chapter 1.3.3). Continuing this train of thought, this N-type ATPases would operate by either using a *smf* to generate ATP or by consuming the same in order to generate a transmembrane sodium gradient. However, it is not clear what the actual ion specificity of the N-type ATPases is or if all N-ATPases have the same ion specificity. The fact that an N-ATPase never occurs as the only ATPase within a genome but always additional to an F- or V/A-type enzyme implies that it cannot functionally replace these proteins.
As only very few experimental data concerning the N-ATPase are available to date, its actual physiological function is still under debate. Besides, recurrent deviations in the nomenclature of these enzymes preclude a common assignment for them. Obtaining further functional and first structural information about the N-ATPases

would be beneficial for both, a common classification of this type of enzyme as well as a better understanding of the evolution and function of all rotary ATPases.

1.4.3 The genus *Burkholderia* and melioidosis

In 1992, the genus *Burkholderia* was defined within the β-proteobacteria with initially comprising seven bacteria until then belonging to the rRNA group II of *Pseudomonas* (Yabuuchi *et al*, 1992). Nowadays, the genus comprises more than 30 characterized species being ubiquitous in terrestrial ecosystems and having been isolated from these as well as from industrial areas and infected humans (Coenye & Vandamme, 2003). Important representatives are biotechnologically relevant strains concerning bioremediation and biocontrol (O'Sullivan & Mahenthiralingam, 2005) as well as primary pathogens.

One pathogenic representative is *Burkholderia pseudomallei*, the causative agent of melioidosis (Chaowagul *et al*, 1989; Yabuuchi *et al*, 1992), formerly also called Whitmore`s disease, named after its discoverer (Whitmore, 1913). Melioidosis occurs in humans and animals and is characterized by pneumonia, sometimes also multiple organ abscesses exhibiting a morbidity rate of up to 40 % (Jabbar & Currie, 2013). Melioidosis is endemic in Southeast Asia, northern Australia, Africa, the Middle East, China, India and South America (Cheng *et al*, 2005; White, 2003) with the highest morbidity and mortality in Thailand (Leelarasamee & Bovornkitti, 1989; Susaengrat *et al*, 1987). Infections are supposed to be transferred via skin lesions or by particle inhalation. Immunocompromised persons are most likely to be affected by *B. pseudomallei* infections. At present there are no vaccines available to treat melioidosis.

A major problem is the fact that *B. pseudomallei* is intrinsically resistant to many kinds of antibiotics, including β-lactams, aminoglycosides, macrolides and polymyxins (Dance *et al*, 1989; Eickhoff *et al*, 1970), whereby intrinsic multidrug resistance mechanisms have already partially been elucidated (Moore *et al*, 1999) and are still under intensive investigation. However, conventional antibiotic treatment comprises a combination of chloramphenicol, doxycycline, trimethoprim-sulfamethoxazole or amoxiciilin-clavulanate for children and pregnant women

(Cheng, 2010; Peacock *et al*, 2008). Besides, ceftazidime, imipenem and meropenem are successfully used for therapy (Jabbar & Currie, 2013).

A laboratory model organism to evade working with the highly virulent strain *B. pseudomallei* is the closely-related but non-pathogenic strain *B. thailandensis* (Haraga *et al*, 2008). This bacterium was isolated from rice field soil in Thailand (Smith *et al*, 1995; Wuthiekanun *et al*, 1995) and primarily classified as a lowly virulent *B. pseudomallei* strain separate from the highly virulent "true" *B. pseudomallei* strains (Brett *et al*, 1998). Upon a 16S rRNA phylogenetic analysis of a highly virulent and the recently isolated lowly virulent strain, the latter one was designated as a new species of *Burkholderia* (Brett *et al*, 1998), which was further confirmed after having shown prominent differences concerning their genomes and biochemistry (Kim *et al*, 2005) (figure 18).

In general, *Burkholderia* have a large genome conferring them broad and flexible genetic resources which enables them to adapt to different environments. As the genomes of *B. pseudomallei* (K96243) and *B. thailandensis* (E264) have been sequenced (Holden *et al*, 2004; Kim *et al*, 2005) thus allowing genetic manipulation, these species were considered for functional and structural investigations of the N-ATPase in this work.

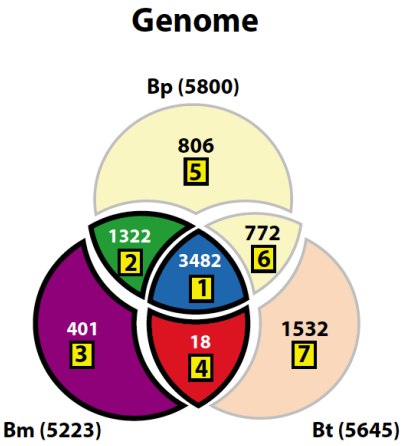

Figure 18. Comparison of the genomes from *B. pseudomallei* (Bp), *B. mallei* (Bm) and *B. thailandensis* (Bt).

Most genes are conserved between Bp and Bm (blue and green). The conservation is less between Bp and Bt (blue and yellow) and least between Bm and Bt (blue and red). The figure was taken from (Kim *et al*, 2005).

1.5 Aims of this work

In this work, two different aspects of bacterial rotary ATPases were examined: The first aim was to investigate the rotor ring from the opportunistic pathogenic bacterium *Fusobacterium nucleatum*, which has a two-carboxylate-motif within the predicted ion binding site. For this purpose, the c-ring has to be expressed and purified in amounts and quality suitable for biochemical and structural studies. The ion specificity should be determined by analyzing the influence of Na^+ on the reaction of the purified, detergent-solubilized c-ring with the ATP synthase inhibitor dicyclohexylcarbodiimide (DCCD) and its fluorescent analogue N-cyclohexyl-N`-[4(dimethylamino)-α-naphtyl]carbodiimide (NCD-4).

However, the exact coordination of the particular ion in the binding site as well as the protonation states of all residues involved can only be obtained by a high-resolution X-ray structure. Finally, the oligomeric state of the protein complex can also be determined and with it, the ion-to-ATP ratio of this enzyme. Therefore, high-quality three-dimensional crystals of the purified *F. nucleatum* c-ring should be grown to perform X-ray crystallographic experiments.

The second goal of this thesis was to characterize the N-ATPase of *Burkholderia pseudomallei* using the model organism *Burkholderia thailandensis*. After the introduction of a novel type of rotary ATPase in the literature, referred to as N-type ATPase, which was suggested to work as an ATP-driven ion pump, a proper biochemical characterization of this enzyme according to its structure and physiological function is needed (Dibrova *et al.*, 2010). The N-type ATPase can be found in different bacteria and archaea but is always accompanying the F-type (or A-type) ATP(synth)ase thereby representing a second type of rotary ATPase in these genomes.

To find out if the N-type ATPases are actually phenotypically expressed in the corresponding cells, transcriptional analysis should be performed first. The genus of *Burkholderia* was chosen for investigating the enzyme, including the pathogenic *B. pseudomallei* and the closely-related non-pathogenic model organism *B. thailandensis*. In the course of these investigations, a heterologous expression system as well as a purification protocol for the N-ATPase from native *B. thailandensis* cells has to be developed.

Besides the investigation of the complete enzyme, the rotor ring of the N-type ATPase was of particular interest. Therefore the c-ring of *B. pseudomallei* should be expressed and purified in order to determine its biochemical properties, including its oligomeric size and its particular ion specificity. We further aimed to obtain structural information of the protein complex by applying two different approaches: three-dimensional crystallization for X-ray crystallographic experiments and single particle electron cryo-microscopy of the purified c-ring.

2 Materials and Methods

2.1 Materials

2.1.1 Instruments

Microfluidizer (Microfluidics Corporation)
French Press (SIM AMINCO SLM Instruments Inc.)
Cary 50 UV-Vis Spectrometer (Varian)
F-450 Fluorescence Spectrophotometer (Hitachi)
Äkta Purifier System (GE Healthcare)
Mosquito™ pipetting robot (TTPLabtech)

2.1.2 Kits

QIAquick PCR purification Kit (Qiagen)
Quiaprep Spin Miniprep Kit (Qiagen)
QIEX II Gel extraction Kit (Qiagen)
GeneMatrix Universal RNA Purification Kit (Roboklon)
dART 2-Step RT-PCR Kit (Roboklon)

2.1.3 Chemicals

All chemicals used in this work were purchased from Anatrace, Avanti, Biorad, Glycon, Life technologies (Invitrogen), Merck-Millipore, New England Biolabs, Roche, Roth, Serva, Sigma-Aldrich and Thermo Scientific Molecular Biology.

2.1.4 Media and antibiotics

Table 2. LB medium

Component	Concentration
Bacto-yeast extract	5 g/l
Bacto-tryptone	10 g/l
NaCl	10 g/l

Table 3. 2YT-glucose medium

Component	Concentration
Bacto-yeast extract	10 g/l
Bacto-tryptone	16 g/l
NaCl	5 g/l
Glucose	5 g/l

Table 4. TB medium

Component	Concentration
Bacto-yeast extract	24 g/l
Bacto-tryptone	12 g/l
Glycerol	4 ml /l
Phosphate buffer (KH_2PO_4/K_2HPO_4 pH 6)	100 ml/l

Table 5. SOC medium

Component	Concentration
Bacto-yeast extract	5 g/l
Bacto-tryptone	20 g/l
Glucose	3.6 g/l
$MgCl_2$	0.95 g/l
$MgSO_4$	1.20 g/l
NaCl	0.58 g/l
KCl	0.186 g/l

Table 6. Antibiotics

Component	Concentration
Ampicillin	200 mg/ml
Trimethoprim	50 mg/ml

2.1.5 Bacterial strains and plasmids

Table 7. Bacterial strains used for cloning and protein expression

Strain	Description
E. coli DH5α	F- 80dlacZ M15 (lacZYA-argF) U169 recA1 endA1 hsdR17(rk-, mk+) phoAsupE44 –thi-1 gyrA96 relA1 - (Sambrook *et al*, 1989)-
E. coli DK8	K-12 strain 1100 Δ(uncB-uncC) ilv::Tn10 (Klionsky *et al*., 1984)
E. coli BL21 (DE3)	F– ompT gal dcm lon hsdSB(rB- mB-) λ(DE3(*lacI lac*UV5-T7 gene 1 ind1 sam7 nin5]) - (Studier & Moffatt, 1986)-
E. coli Lemo21 (DE3)	huA2 (lon] ompT gal (λ DE3) (dcm] ΔhsdS/ pLemo(Cam^R) λ DE3 = λ sBamHIo ΔEcoRI-B int::(lacI::PlacUV5::T7 gene1) i21 Δnin5; pLemo = pACYC184-PrhaBAD-lysY - (NEB) -
E. coli C41 (DE3)	Derivative of *E. coli* BL21, with spontaneous double mutation - (Miroux & Walker, 1996)-
E. coli TOP10	F- *mcr*A Δ(*mrr-hsd*RMS-*mcr*BC) φ80*lac*ZΔM15 Δ*lac*X74 *deo*R *rec*A1 *ara*D139 Δ(*ara*A- *leu*)7697 *gal*U *gal*K *rps*L *end*A1 *nup*G - (Invitrogen) -
E. coli MC1061	F– *araD139* Δ*(ara-leu)7696 galE15 galK16* Δ*(lac)X74 rpsL* (Strr) *hsdR2* (rK^-mK^+) *mcrA mcrB1* - (Sigma-Aldrich) -
B. pseudomallei K96243	Wildtype - (Whitmore, 1913)-
B. thailandensis E264	Wildtype - (Brett *et al*, 1998)-

Table 8. Plasmids used for cloning and protein expression

Plasmid maps for vectors generated in this work (pt7c_BP, $pBAD_{HisB}$_atpBP and pHERD28T_atpBP) can be found in the Appendix.

Plasmid	Description
pITtr5His	based on ptrc99A expression vector, *atp*-operon of. *I. tartaricus* for heterologous overexpression of ATP synthase in *E. coli*; *bla* coding sequence, *trc* promotor, β N-His_{10}, - (Oberfeld *et al*, 2006)-
pITtr5His_atpFN	based on pITtr5His vector, *atp*-operon of. *I. tartaricus* with *atpE* of *F. nucleatum* for heterologous overexpression of hybrid ATP synthase in *E. coli*; *bla* coding sequence, *trc* promotor, β N-His_{10}, - (this work) -
pt7-7	expression vector, T7 promotor, *bla* coding sequence, strong *rbs* and start codon - (Tabor & Richardson, 1985)-
pt7c_BP	based on pt7-7, insertion of *atpE* of *B. pseudomallei* - (this work) -
$pBAD_{HisB}$	pBR333-derived expression vector , *ara*BAD promotor, *ara*C gene, N-His_{10}, *bla* coding sequence, MCS - (Invitrogen) -
$pBAD_{HisB}$_atpBP	based on $pBAD_{HisB}$, insertion of N-*atp* Operon of *B. pseudomallei* - (this work) -
pHERD28T	pUCP28T P_{lac} replaced with 2.4-kb *Adh*I-*Eco*RI fragment of araC-P_{BAD} cassette (kind gift from Prof. Herbert P. Schweizer, Colorade State University, Fort Collins, Colorado) - (Qiu *et al*, 2008)-
pHERD28T_atpBP	based on pHERD28T, insertion of N-*atp* Operon of *B. pseudomallei* - (this work) -
pJET1.2	cloning vector, *bla* gene, MCS, forward and reverse primer binding sites, for direct ligation of blunt-end PCR products - (Thermo Scientific) -

2.1.6 Oligonucleotide primer

Table 9. Primer for cloning of pITtr5His_atpE_FN

The restriction sites for cloning inserted by PCR are highlighted in blue in the following primer sequences.

Name	Sequence
pt7c_FN_for	5` - CTTTAAGAAGGAGATGAGCTCATGGATCTGC - 3`
pt7c_FN_rev	5` - CGATAAGCTTCCTCCATCGATTTAGCCC - 3`

Table 10. Primer for native expression analysis of the N-*atp* operon

Name	Sequence
BT_β51_fwd	5`- GCAAGCGAAGCACGGCGTGAGCGAC -3`
BT_β1031_rev	5`- ATGCTGTCGACGTGCGCGGCGATCG - 3`
BT_β1007_fwd	5`- CGATCGCCGCGCACGTCGACAGCAT - 3`
BT_ε420_rev	5`- CTCCGGCTTCATCGGCGCGAGCATG - 3`
BT_ ε444_fwd	5`- CATGCTCGCGCCGATGAAGCCGGAG - 3`
BT_a661_rev	5`- CTTTGCAGCCGCGACGGCGCTTCGA - 3`
BT_a137_fwd	5`- TCGAAGCGCCGTCGCGGCTGCAAAG - 3`
BT_b150_rev	5`- GTGCGCCGCGTCGTCGATCAGCTTG - 3`
BT_b126_fwd	5`- CAAGCTGATCGACGACGCGGCGCAC - 3
BT_α352_rev	5`- GATCGACGACGCGCCCGAGCAGTTG - 3`
BT_α328_fwd	5`- CAACTGCTCGGGCGCGTCGTCGATC - 3`
BT_α1614_rev	5`- TGTCGCATCGCCGCTCGCGTGTTCG - 3`
BT_α1590_fwd	5`- CGAACACGCGAGCGGCGATGCGACA - 3`
BT_γ834_rev	5`- CGCAAGCTCGACGATGTCCGCCGTG - 3`
BT_GAPDH_fwd	5`- GTTACGGCCGCATCGGCCGCAACAC - 3`
BT_GAPDH_rev	5`- GTTCGCGAGCGCGATCGCCGTATCC - 3`

Table 11. Primer for cloning of $pBAD_{His}$_atpBP

The restriction sites for cloning inserted by PCR are highlighted in blue in the following primer sequences.

Name	Sequence
Bp_20-β_Bgl_F	5` - CGTGGGCGATGTGAGATCTGTGGGCGATGCGCG - 3`
Bp_Q15_Nde_R	5` - CGCCTCGCGCTTCATATGGGGCGGCC - 3`
Bp_12-Q_Nde_F	5` - GGCCGCCCCATATGAAGCGCGAGGCG - 3`
Bp_b10_Apa_R	5` - CGATTCGCATCGGGCCCTCCGCGTCAC - 3`
Bp_c241_Apa_F	5` - GTCAAGTGACGCGGAGGGCCCGATGCGAATC - 3`
Bp_α806_Ssp_R	5` - CGTGTTGGCCGCGGTCGCGGAAATATTCGG - 3`
Bp_α776_Ssp_F	5` - CCGAATATTTCCGCGACCGCGGCCAACACG - 3`
Bp_γ+29_Hind_R	5` - GCCGCACCGAAGCTTCGATGCGCCCGG - 3`

Table 12. Primer for sequencing of $pBAD_{His}$_atpBP

Name	Sequence
pBAD_fwd	5`- ATGCCATAGCATTATCC - 3`
pBAD_rev	5`- CTGATTTAATCTGTATCAGGCTG - 3`
Bp_β867_fwd	5`- GGAGCGGATCGCCTCGGTCGAGGGC - 3`
Bp_ε273_fwd	5`- GCTCGCCGAGCTCGAGGCGGTGGTG - 3`
Bp_r236_fwd	5`- GGTTTTTCGCCGCGCGGGCGATCGC - 3`
Bp_r275_fwd	5`- CCGCGTTGACGGGAGCGCGGCGATG - 3`
Bp_c189_fwd	5`- GGCGATCTACTGCCTCGTCGTCGCG - 3`
Bp_α116_fwd	5`- AGGCGATCGGGCGGGTCGAGCGCG - 3`
Bp_α1056_fwd	5`- CGGGCAGATCGTGCTCGATTCGGCG - 3

Table 13. Primer for deletion of point mutations in $pBAD_{His}$_atpBP

Mutations deleted by PCR are highlighted in blue in the following primer sequences.

Name	Sequence
pET24a_Bgl_fwd	5`- CGGGATCGAGATCTATGGGCGATGC - 3`
pET24a_R260_rev	5`- GACCGCGATCGCCCGCGCGGCGAAAAAC - 3`

Table 14. Primer for cloning of pHERD28T_atpBP

The restriction sites for cloning inserted by PCR are highlighted in blue in the following primer sequences.

Name	Sequence
pHERD28T_NcoI_2741_F	5`- GAATTCGCAATCGCCATGGTTTCACTCCATC - 3`
pHERD28T_NcoI_2741_R	5`- GATGGAGTGAAACCATGGCGATTGCGAATTC - 3`

Table 15. Primer for cloning of pt7c_BP

The restriction sites for cloning inserted by PCR are highlighted in blue in the following primer sequences.

Name	Sequence
Bp_a685_Nde_F	5`- GCAGGAGAACATATGAACAATCTCATCG - 3`
Bp_b3_HindIII_R	5`- CCAGTCGATTCGCAAAGCTTCCTCCGCGTCAC -3

Table 16. Primer for point mutations in pt7c_BP

Mutations deleted by PCR are highlighted in blue in the following primer sequences.

Name	Sequence
BP_cM63T_fwd	5`- GGCAGTAGATCGCCGTCGTCTCGAT - 3`
BP_cM63T_rev	5`- ATCGAGACGACGGCGATCTACTGCC - 3`
BP_cM63TM59V_fwd	5`- GATCGCCGTCGTCTCGATCACCGCGAG - 3`
BP_cM63TM59V_rev	5`- CTCGCGGTGATCGAGACGACGGCGATC - 3`
BP_cM63TM59VT62SI60A_fwd	5`- GATCGCCGTCGACTCCGCCACCGCGAG - 3`
BP_cM63TM59VT62SI60A_rev	5`- CTCGCGGTGGCGGAGTCGACGGCGATC - 3`

2.2 Molecular biological methods

2.2.1 Polymerase chain reaction

The polymerase chain reaction (PCR) is a method for the *in vitro* amplification of specific DNA fragments (Mullis & Faloona, 1987). Plasmid or genomic DNA was used as a template to be amplified in a repetitive cycle of three steps (denaturation, hybridization and elongation). The hybridization temperature depends on the composition and length of the respective oligonucleotide primer and the elongation time relies on the DNA polymerase activity and the length of the DNA region to be amplified.

Phusion-Polymerase (Finnzymes) was used to add specific restriction sites on the *atpE* gene of *F. nucleatum* for ligating it into pITtr5His to obtain the pITtr5His_atpE_FN construct. Extender-polymerase (5 Prime) was used for amplification of N-*atp* genes from genomic DNA of *B. pseudomallei* to clone the whole N-*atp* operon in $pBAD_{HisB}$ ($pBAD_{HisB}$_atpBP) and pHERD28T (pHERD28T_atpBP) as well as for expression analysis of the N-*atp* operon in native *B. thailandensis* cells. The PCR mixture including the Extender-Polymerase was further supplemented by an PCR combinatorial enhancer solution (CES; Ralser *et al.*, 2006) for the amplification of GC rich DNA sequences. Turbo-*Pfu* Polymerase (Stratagene) was used to create pt7c_BP mutants.

Table 17. PCR mixture for Phusion-polymerase

Component	Volume
Phusion-Polymerase (2 U/µl)	0.5 µl
HF buffer (5x)	10 µl
DNA template (100-200 ng/µl)	1 µl
sense primer (10 pmol/µl)	4 µl
anti-sense primer (10 pmol/µl)	4 µl
dNTP mix (2 mM each)	7.5 µl
H_2O	to 50 µl

Table 18. Thermocycler programme for Phusion-polymerase

Step	Parameter
Initial denaturation	95°C
Denaturation	95°C
Annealing	primer melting temperature - 5°C 10 s
Elongation	72°C 30 s/kb
Final elongation	72°C 10 min

Table 19. PCR mixture for Extender-polyermase

Component	Volume
Extender-Polymerase (5 U/µl)	0.4 µl
Tuning buffer (10x)	5 µl
template genomic DNA (60 ng/µl)	0.5 µl
sense primer (10 pmol/µl)	4 µl
anti-sense primer (10 pmol/µl)	4 µl
dNTP mix (2mM each)	7.5 µl
CES (5x) (Ralser *et al*, 2006)	10 µl
H_2O	to 50 µl

Table 20. Thermocycler programm for Extender-polymerase

Step	Parameter
Initial denaturation	98°C 5 min
Denaturation	98°C 20 s
Annealing	primer melting temperature - 5°C 10 s
Elongation	72°C 45 s/kb (30 cycles)
Final elongation	72°C 10 min

Table 21. PCR mixture for Turbo-*Pfu*-polymerase

Component	Volume
Turbo *Pfu*-Polymerase (2.5 U/µl)	1 µl
Tuning buffer (10x)	5 µl
template: plasmid DNA (50-100 ng/µl)	1 µl
sense primer (10 pmol/µl)	1 µl
anti-sense primer (10 pmol/µl)	1 µl
dNTP mix (2mM each)	2 µl
DMSO (100 % (v/v))	2.5 µl
H_2O	to 50 µl

Table 22. Thermocycler programm for Turbo *Pfu*-polymerase

Step	Parameter
Initial denaturation	95°C 1 min
Denaturation	95°C 50 s
Annealing	primer melting temperature - 5°C 10 s
Elongation	68°C 60 s/kb (25 cycles)
Final elongation	68°C 20 min

2.2.2 Purification of PCR products

Purification of amplified DNA was performed using the PCR Purification Kit (Seqlab) according to manufacturer's instructions. The DNA concentration and quality was spectroscopically determined using a Nanodrop 1000 spectrophotometer (Peqlab).

2.2.3 Agarose gel electrophoresis

Analysis of PCR and restriction products was performed by agarose gel electrophoresis. To visualize DNA fragments by the use of UV-light ethidium bromide was added as an organic fluorescent compound which intercalates double-

stranded DNA. DNA samples were mixed with 6x DNA loading dye and loaded onto a 1 % (w/v) agarose gel. 1 kb DNA ladder (NEB) and supercoiled DNA ladder (NEB) were used as molecular weight standards. Separation of DNA fragments was carried out in in 1x Tris-Acetat-EDTA (TAE-) buffer for 1 hour at 100 V.

Table 23. 1x TAE buffer

Component	Concentration
Tris HCl	40 mM
EDTA	4 mM
Acetic acid	40 mM

Table 24. 6x DNA loading dye

Component	Concentration
Tris HCl pH 7.6	10 mM
Glycerol	60 % (v/v)
Bromphenol blue	0.03 % (w/v)
Xylene cyanol blue	0.03 % (w/v)
EDTA	60 mM

2.2.4 Gelextraction of DNA

For further usage of DNA after gel electrophoresis, fragments were cut out of the gel with a scalpel and extracted by using the QIAEX II Gel Extraction Kit (Qiagen) according to manufacturer`s instructions.

2.2.5 Isolation of plasmid DNA

Transformed cells from a single colony were grown in LB medium with the respective antibiotic for 16 hours at 37°C and 220 rpm. Cells were harvested at 4°C by centrifugation for 10 min at 5.000 rpm (Sigma 3-16k centrifuge, rotor 11133) and plasmids were isolated using the QIAprep Spin Miniprep Kit (Qiagen) according to manufacturer`s instructions.

2.2.6 DNA cleavage by restriction enzymes

Restriction endonucleases were used to excise DNA regions sequence-specifically from vector DNA or to analyze produced plasmids. Enzymes were either used from New England Biolabs (NEB) or Fermentas according to manufacturer`s instructions. Digested vectors destined for ligation reactions with PCR products were treated with antarctic phosphatase (NEB) catalyzing the removal of the 5` phosphate from DNA to prevent religation of the vector. Digested DNA fragments were analyzed by agarose gel electrophoresis.

2.2.7 Ligation of DNA fragments

Ligation of purified restriction products (inserts) with digested plasmid DNA (vector) was carried out in a molar vector to insert ratio of 1:3 in a total volume of 20 µl. T4 Ligase (Fermentas or NEB) was used for ligation for six hours at 20°C or over night at 18°C. The *F. nucleatum atpE* gene was ligated in pITtr5His, the *B. pseudomallei* N-*atp* operon in $pBAD_{HisB}$ and pHERD28T and the N-*atpE* gene in pt7-7.

2.2.8 Sequencing of plasmid DNA

Sequencing of DNA regions from constructed plasmids was performed by Seqlab or SRD using specific oligonucleotide primer.

2.2.9 Gene synthesis

The *atpE* gene of *F. nucleatum* was codon-optimized for expression in *E. coli*, flanked with the restriction sites *Nde*I and *Hind*III, ligated blunt (*Eco*RV) in a pUC57 vector and purchased by GenScript Incorporation.

2.2.10 Primer synthesis

Oligonucleotide primer used for PCR and sequencing were ordered from Microsynth AG (Balgach, CH).

2.2.11 Preparation of glycerol-stocks

To prepare a permanent bacteria stock to be stored for long-term, a single colony grown on a LB-agar-plate (with the respective antibiotic) was used for inoculation of 5 ml LB medium (with antibiotic). After 16 hours at 37°C and 220 rpm, cells were harvested by centrifugation at 4°C (10 minutes at 5.000 rpm, Sigma 3-16k centrifuge, rotor 11133) and resuspended in 1 ml fresh LB medium. 0.1 ml of these cells were transferred into 1 ml 60 % (v/v) glycerol-LB and flash-frozen in liquid nitrogen. Glycerol stocks were stored at -80°C.

2.2.12 Preparation of $CaCl_2$- competent *E. coli* cells

A preculture of *E. coli* DH5α cells was grown over night in 10 ml LB medium at 37°C. The next morning, 200 ml LB medium were inoculated with OD_{600} 0.02 from the preculture and incubated at 37°C and 220 rpm until OD_{600} 0.6 was reached. Cells were then incubated for 10 minutes on ice and centrifuged for 20 minutes at 3.500 rpm at 4°C. Sedimented cells were resuspended carefully in 10 ml pre-cooled 100 mM $MgCl_2$ and subsequently centrifuged for 20 minutes at 3.500 rpm at 4°C. The cell pellet was resuspended carefully in pre-cooled $CaCl_2$ and incubated for 30 minutes on ice. Cells were centrifuged for 15 minutes at 3.500 rpm at 4°C and the pellet was again resuspended carefully in 20 ml pre-cooled $CaCl_2$. Aliquots of 0.2 ml of cells were flash-frozen in liquid nitrogen and stored at -80°C. All centrifugation steps were carried out with a Sigma 3-16k centrifuge using the rotor 11133.

2.2.13 Transformation of $CaCl_2$- competent *E. coli* cells by heat shock

The transformation reaction was performed using 0.2 ml of $CaCl_2$- competent *E. coli* cells (DH5α, BL21, Lemo21, C41, TOP10, MC1061) and 20 µl of ligation reaction or 100 ng of plasmid DNA. Competent cells were thawed on ice for 10 minutes before DNA was added. Cells were incubated for 30 minutes on ice followed by a heat-shock for 45 seconds at 42°C facilitating DNA uptake. Cells were incubated for 5 minutes on ice and after the addition of 0.8 ml LB medium incubated at 37°C and 600 rpm for 1 hour. Positive transformants were selected on LB-agar-plates containing the respective antibiotic for which a resistance gene is encoded on the plasmid.

2.2.14 Preparation of electrocompetent *B. thailandensis* cells and electroporation

B. thailandensis cells were made competent on the basis of the protocol described in (Choi *et al*, 2006). A preculture of cells was grown over night in 10 ml LB medium at 37°C. The next day, cells were distributed into six Eppendorf-tubes and harvested by centrifugation for 2 minutes at 14.000*x*g at room temperature. Cell pellets were washed thrice with 1ml of room temperature 0.3 M sucrose. Three tubes each were combined in 0.1ml 0.3 M sucrose and directly used for electroporation. 400-800 ng of plasmid DNA were mixed with 300 µl electrocompetent cells and transferred into a electroporation cuvette (2 mm gap width). A pulse (2.5 kV, 25Ω, 25µF) was applied with a Bio-RAD GenePulser (Bio-Rad). Cells were supplemented with 1 ml of room temperature LB medium, transferred into a 15 ml falcon tube and incubated for one hour at 37°C and 200 rpm, before plating on selecting agar and incubation at 37°C.

2.3 Biochemical methods

2.3.1 Protein production in *E. coli*

For the heterologous expressions 100 ml LB medium with 200 µg/ ml Ampicillin or 50 µg/ ml Trimethoprim were inoculated with 50 µl cells from a glycerol stock and incubated for 16 hours at 37°C and 220 rpm. 2 l TB medium containing 200 µg/ ml Ampicillin (hybrid ATPase) or 2 l LB medium containing 200 µg/ ml Ampicillin (c-ring and N-ATPase) were then inoculated from this preculture with OD_{600} 0.02 and incubated at 37°C and 220 rpm until OD_{600} 0.6-0.8 was reached. Expression was induced by 0.5 mM IPTG (pt7c_BP) or 0.02 % (w/v) arabinose ($pBAD_{HisB}$_atpBP and pHERD28T_atpBP). After 4 hours of expression at 37°C cells were harvested by centrifugation (35 minutes at 4°C and 4.200 rpm with a Sigma 3-16k centrifuge, rotor 11133), the cell pellet of 1 l culture with OD_{600} 1 was resuspended in 10 ml buffer and flash-frozen in liquid nitrogen. Cells were stored at -80°C.

2.3.1.1 Production *of I. tartaricus* hybrid ATPase with *F. nucleatum* c_n in *E. coli*

To produce a hybrid ATP synthase in *E. coli* a plasmid containing the F-*atp* operon of *I. tartarcicus* (pITtr5His) was used and the *atpE* gene encoding for the c-subunit was replaced by the corresponding *F. nucleatum* gene resulting in a new construct

(pITtr5His_atpE_FN). The Δ*atp E. coli* strain DK8 was transformed with this plasmid where the *atp* operon is under control of a trc (*trp-lac*) promotor. After harvesting cells were resuspended in 50 mM KPP pH 8.0 (Schulz, 2010).

2.3.1.2 Production of the *B. pseudomallei* c-ring in *E. coli*

For the production of wildtype and mutant c-rings from *B. pseudomallei* a plasmid encoding for the (modified) *atpE* gene was used (pt7c_BP) which is under control of a T7 promotor. The *E. coli* strain BL21 was transformed with the corresponding plasmid and used for expression. After centrifugation cells were resuspended in 20 mM Tris/HCl pH 8.0.

2.3.1.3 Production of the *B. pseudomallei* N-ATPase in *E. coli*

To produce the N-ATPase from *B. pseudomallei* in *E. coli*, different strains were tested and transformed with the $pBAD_{HisB}$_atpBP plasmid. Expression was induced at OD_{600} 0.5-1.0 with 0.002-0.2 % (w/v) arabinose and cells were incubated at different temperatures for several hours. After expression cells were resuspended in 20 mM Tris/HCl pH 8.0 or 50 mM KPP pH 8.0.

2.3.2 Production of endogenous ATPases in *B. thailandensis*

A glycerol stock of native *B. thailandensis* cells was used for inoculation of 100 ml preculture. After 16 hours at 37°C and 200 rpm, 2l LB medium (kanamycin) were then inoculated with OD_{600} 0.02 from the preculture and grown at 37°C and 120 rpm until OD_{600} 1.3-1.6 was reached. After harvesting cells were resuspended in 20 mM Tris HCl pH 8.0 and flash-frozen in liquid nitrogen. Under aerobic culture conditions at 37°C native *B. thailandensis* cells express both, an F-and N-ATP (synth)ase.

2.3.3 Production of the *B. pseudomallei* N-ATPase in *B. thailandensis*

To produce the N-ATPase from *B. pseudomallei* in *B. thailandensis*, strain E264 was transformed with the pHERD28T_atpBP plasmid. Expression was induced at OD_{600} 0.5-1.0 with 0.002-0.2 % (w/v) arabinose and cells were incubated at different temperatures for several hours. After expression cells were resuspended in 20 mM Tris/HCl pH 8.0 or 50 mM KPP pH 8.0.

2.3.4 Protein purification

2.3.4.1 Disruption of *E. coli* and *B. thailandensis* cells

Resuspended cells stored at -80°C were thawed in a water bath at room temperature and supplied with 1 mM DTT, traces of DNase and 1 mM Pefabloc. Disruption of cells was carried out using either a microfluidizer (for *E. coli* cells with constructs pITtr5His_atpE_FN and pt7c_BP) at 4°C and 1200 bar or using a French press (for *E. coli* cells with construct $pBAD_{HisB}$_ atpBP and *B. thailandensis* cells with or without (native expression of N-ATPase) construct pHERD28T_atpBP) at 4°C and 1000 bar, three passages in each case.

2.3.4.2 Preparation of *E. coli* and *B. thailandensis* membranes

Disrupted cells were separated from inclusion bodies and not properly disrupted cells by centrifugation for 35 minutes at 4°C and 12.500 rpm (rotor JLA16.250, Beckmann). The supernatant was then applied to ultracentrifugation for 1 hour at 4°C and 45.000 rpm (rotor Ti45, Beckmann) to sediment membranes. *E. coli* and *B. thailandensis* membrane pellets with the different constructs (pITtr5His_atpE_FN, pt7c_BP, $pBAD_{HisB}$_ atpBP and pHERD28T_atpBP; see chapter 2.3.4.1) were resuspended in 5 ml buffer per 1 l cell culture and either directly used for protein solubilization and purification or flash-frozen in liquid nitrogen and stored at -80°C.

Table 25. Membrane buffer for construct pITtr5His_atpBP

Component	Concentration
KPP pH 8.0	50 mM
NaCl	300 mM
Glycerol	10 % (v/v)
$MgCl_2$	2 mM
pefabloc	0.1 mM

Table 26. Membrane buffer for construct pt7c-BP

Component	Concentration
KPP pH 8.0	50 mM
NaCl	100 mM
Glycerol	10 % (v/v)

Table 27. Membrane buffer for *B. thailandensis*

Component	Concentration
Tris/HCl pH 8.0	20 mM
NaCl	100 mM
Glycerol	5 % (v/v)

Table 28. Membrane buffer for constructs $pBAD_{HisB}$_atpBP and pHERD28T_atpBP

Component	Concentration
Tris/HCl pH 8.0	20 mM
NaCl	100 mM
Glycerol	5 % (v/v)
$MgCl_2$	5 mM
pefabloc	0.1 mM

2.3.4.3 Solubilization of membrane proteins

The concentration of total protein was adjusted with membrane buffer to 10-15 mg/ml membranes and 1-2 % (w/v) of detergent was added for a defined time to solubilize the membrane proteins. After ultracentrifugation for 1 hour at 4°C and 50.000 rpm (rotor Ti70, Beckmann), detergent-solubilized proteins are in the supernatant whereas lipids and non-solubilized proteins are sedimented.

2.3.4.4 Immobilized metal ion affinity chromatography (IMAC)

To separate proteins with an affinity for metal ions, like Ni^{2+} or Co^{2+}, from other proteins in the supernatant, IMAC was performed using nitrilotriacetic acid material

(NTA; Chelating Sepharose Fast Flow, GE Healthcare) loaded with $NiSO_4$ according to manufacturer`s instructions. Genetically modified histidine-tagged (His_{10}) proteins bind to the Ni^{2+}NTA complex. The Ni^{2+}NTA column was equilibrated with 2 column volumes of buffer before the supernatant was loaded and incubated with the material over night at 4°C. The column was washed with 2-3 column volumes of buffer containing increasing concentrations of imidazol and the histidine-tagged proteins were eluted with a high imidazol-concentration in 2-3 column volumes. Fractions were then analyzed by silver-stained SDS-PAGE. The whole procedure was performed at 4°C.

Table 29. Buffer used for Ni^{2+} NTA-affinity chromatography

Step	Component	Concentration
basic buffer	KPP pH 8.0	50 mM
	NaCl	300 mM
	Glycerol	10 % (v/v)
	$MgCl_2$	2 mM
	DDM	0.05 % (w/v)
	pefabloc	0.1 mM
Equilibration / Wash 1	+ Imidazol pH 8.0	5 mM
Wash 2	+ Imidazol pH 8.0	20 mM
Wash 3	+ Imidazol pH 8.0	40 mM
Elution	+ Imidazol pH 8.0	400 mM

2.3.4.5 $(NH_4)_2$ SO_4 precipitation

A saturated $(NH_4)_2$ SO_4 solution in 50 mM KPP pH 8.0 was added dropwise to a protein sample until the desired final concentration was reached. The solution was incubated for 30 minutes at 20°C and then centrifuged for 35 minutes at 8.000 rpm using a Sorvall RC5B centrifuge (Dupont Instruments, Inc.) with a Fiberlite F13-14x50cy fixed-angle rotor (Piramoon Technologies, Inc.) at 20°C. The supernatant containing the protein of interest was separated from proteins which were salted out and was filtered using a 0.22 µm sterile PVDF-filter.

2.3.4.6 Dialysis

To exchange the buffer of a sample it was transferred into a dialysis tube (Spectra/Por, MWCO 6-8.000 kDa) and incubated overnight in 20 mM Tris/HCl pH 8.0 containing the corresponding detergent.

2.3.4.7 Sucrose density gradient centrifugation

For further purification of proteins density gradient centrifugation was performed using 5-35 % (w/v) sucrose in 20 mM Tris/HCl pH 8.0, 100 mM NaCl and the corresponding detergent. Proteins were separated according to their size by ultracentrifugation for 20 hours at 10°C and 40.000 rpm (rotor Ti70, Beckmann). The gradient was separated in 9-11 fractions of equal volume and analyzed by SDS-PAGE.

2.3.4.8 Hydroxylapatite chromatography

For final purification and concentration of protein samples a chromatography was carried out using hydroxylapatit ($Ca_{10}(PO_4)_6(OH)_2$) which was equilibrated with 10 column volumes of phosphate-buffer. The protein was eluted by increasing the phosphate concentration competing with the negatively charged carboxylate groups of the protein for binding to the material. The whole procedure was carried out by gravity flow on the laboratory bench at 20-22°C.

Table 30. Buffer used for hydroxylapatite chromatography

Step	Component	Concentration
Equilibration / Wash 1	KPP pH 7.0 $CaCl_2$	10 mM 0.3 % (w/v)
Wash 2	KPP pH 7.0 $CaCl_2$	50 mM 0.06 % (w/v)
Wash 3	KPP pH 7.0 $CaCl_2$	100 mM 0.03 % (w/v)
Elution	KPP pH 7.0	1000 mM

2.3.4.9 Organic extraction of the c-subunit by chloroform-methanol

Due to its hydrophobicity the c-monomer can be extracted organically by a solution of chloroform-methanol. A protein sample, membranes or cells were mixed with 10 volumes of chloroform-methanol (1:1) and mixed thoroughly for one minute. In case of cells, the sample was incubated for half an hour at room temperature and 600 rpm prior to centrifugation (five minutes at 13.000 rpm using an Himac CT15RE centrifuge (Hitachi) with a T15A61 rotor and 20°C), otherwise (protein sample or membranes) the sample was directly centrifuged. The supernatant was transferred into a fresh reaction tube and supplemented with 2.5 x volumes of buffer (20 mM Tris/HCl pH 8.0). After mixing, the sample was centrifuged for another five minutes at 13.000 rpm (Himac CT15RE centrifuge (Hitachi) with a T15A61 rotor) and 20°C leading to phase separation. The protein in the chloroform-phase was dried at 50°C and resuspended in 15 µl 2 x SDS loading dye prior to loading on a SDS-PAGE.

2.3.4.10 Polyethylene-glycol (PEG) precipitation

For purification and concentration of ATP (synth)ase samples 50 % (v/v) $Polyethyleneglycol_{6000}$ was added gradually under constant stirring at 4°C to the sample until a final concentration of 12 % (v/v). After incubation for 30 minutes at 4°C with constant stirring the sample was centrifuged for 30 minutes at 15.000 rpm (Himac CT15RE centrifuge (Hitachi) with a T15A61 rotor) and 4°C. The protein pellet was then resuspended in buffer containing the corresponding detergent.

2.3.4.11 Concentration of protein samples

Protein samples were concentrated stepwise using Amicon Ultra centrifugal filter units with molecular weight cut-offs of 10.000-100.000 kDa at 2.500-3.000 rpm (Sigma 3-16k centrifuge, rotor 11133) and 4-20°C. To prevent aggregation of the protein due to local high concentrations the samples were mixed by pipetting regularly in between.

2.3.4.12 Anion exchange chromatography (AEX)

For purification of protein (complexes) anion exchange chromatography was performed using a Mono Q 5/50 GL column (GE Healthcare) on an Äkta Purifier or

Äkta Explorer System (GE Healthcare). The column was equilibrated with buffer 1 before 0.5-2.5 ml protein sample was loaded with a flow rate of 0.3 ml/min. The protein was eluted with a continuous NaCl-gradient during 20 column volumes using buffer 1 and 2 (table 31 and 32). All buffers were filtered and degased before usage.

Table 31. Buffer 1 used for anion exchange chromatography (MonoQ)

Component	Concentration
Tris/HCl pH 8.0	20 mM
Glycerol	5 % (v/v)
$MgCl_2$	5 mM
DDM	0.1 % (w/v)

Table 32. Buffer 2 used for anion exchange chromatography (MonoQ)

Component	Concentration
Tris/HCl pH 8.0	20 mM
NaCl	1000 mM
Glycerol	5 % (v/v)
$MgCl_2$	5 mM
DDM	0.1 % (w/v)

2.3.4.13 Size exclusion chromatography (SEC)

To analyze the quality (monodispersity) of a protein sample or to determine the size of a protein complex, size exclusion chromatography was applied using a Superose 6 10/300 column (GE Healthcare) on an Äkta Purifier or Äkta Explorer System. The column was equilibrated with buffer (table 33) and 0.5 ml protein sample was loaded with a flow rate of 0.4 ml/min. The SEC buffer was filtered and degased prior to use.

Table 33. Buffer used for size exclusion chromatography (Superose 6) for F-type ATP synthase

Component	Concentration
Tris/HCl pH 8.0	20 mM
Glycerol	5 % (v/v)
$MgCl_2$	5 mM
DDM	0.1 % (w/v)

Table 34. Buffer used for size exclusion chromatography (Superose 6) for N-type c-ring

Component	Concentration
Tris/HCl pH 8.0	20 mM
NaCl	150 mM
DDM	0.05 % (w/v)

2.3.5 Protein analysis

2.3.5.1 Determination of protein concentration (BCA)

The protein concentration of a sample was measured photometrically using the bicinchoninic assay (BCA) with bovine serum albumin (BSA) as a standard. The protein sample was supplemented with buffer to a total volume of 50 µl and mixed with 1 ml BCA-solution and 20 µl 4 % (w/v) $CuSO_4$. After 30 minutes of incubation at 60°C, the sample was cooled down to room temperature for 15 minutes before absorption was measured photometrically at λ = 562 nm.

2.3.5.2 Determination of maltoside concentration

The determination of the maltoside concentration was used to assign the concentration of DM and DDM in a given protein sample. 1 µl of sample in 250 µl 2 % (v/v) phenol was supplemented with 1 ml of concentrated H_2SO_4 leading to heating and yellow(ish) colouring of the mixture. After 20 minutes of incubation at room temperature, it was centrifuged for 5 minutes at 2.000 rpm (Sigma 3-16k centrifuge, rotor 11133) and the supernatant was measured photometrically at λ = 480 nm.

2.3.5.3 Trichloroacetic acid (TCA) precipitation of c-rings

Precipitation with trichloroacetic acid was used for the identification of c-ring in a protein sample as it precipitates into its subunits upon addition. The protein sample was incubated with 15 % (w/v) TCA for five minutes on ice and then centrifuged for five minutes at 13.000 rpm (Sigma 3-16k centrifuge, rotor 1113) and 4°C. The protein pellet was resuspended in 15 µl 2 x SDS loading dye and neutralized by the addition of 0.5 µl 0.5 M NaOH. Analysis of the sample was performed by SDS-PAGE.

2.3.5.4 Sodium dodecyl sulfate polyacrylamide gelelectrophoresis (SDS-PAGE)

Analysis of protein samples was performed electrophoretically according to (Schagger & von Jagow, 1987). The percentage of polyacrylamide in the stacking gel was 3.8 % (v/v) and in the separating gel 13.2 % (v/v). Protein samples were supplemented with 1x SDS-loading buffer and separated according to their molecular weight for two hours at 45 mA and 18°C. Page Ruler Unstained protein marker (Fermentas) was used as a molecular weight marker. All buffers used are listed in table 35-39.

Table 35. 1x SDS-loading dye

Component	Final concentration
Tris/HCl pH 6.8	50 mM
SDS	2 % (w/v)
Glycerol	12 % (v/v)
Serva Blue	0.01 % (w/v)
Bromphenol blue	0.01 % (w/v)

Table 36. 1x Cathode buffer for SDS-PAGE

Component	Concentration
Tris/HCl pH 8.25	100 mM
Tricine	100 mM
SDS	0.1 % (w/v)

Table 37. 1x Anode buffer for SDS-PAGE

Component	Concentration
Tris/HCl pH 8.9	200 mM

Table 38. Stacking gel buffer for SDS-PAGE

Component	Final concentration
Tris/HCl pH 8.45	1 M
Acrylamide	13.2 % (v/v)
Glycerol	13 % (v/v)
SDS	0.1 % (w/v)
APS	0.05 % (v/v)
TEMED	0.05 % (v/v)

Table 39. Separating gel buffer for SDS-PAGE

Component	Final concentration
Tris/HCl pH 8.45	0.74 M
Water	60.5 % (v/v)
Acrylamide	3.8 % (v/v)
SDS	0.074 % (w/v)
APS	0.12 % (v/v)
TEMED	0.14 % (v/v)

2.3.5.5 Silver-staining of sodium dodecyl sulfate polyacrylamide gels

SDS-gels were stained with silver according to (Nesterenko *et al*, 1994).

2.3.5.6 Blue native polyacrylamide gelelectrophoresis (BN-PAGE)

Native conformation of protein complexes was analyzed by non-denaturing PAGE using 4-16 % NativePAGE Novex Bis-Tris gels (Life technologies). Protein samples were diluted with 1xBN-loading buffer and separated for 1 hour at 4°C and 100 V and

another hour at 400 V. Gels were destained in 10 % (v/v) Methanol and 10 (v/v) % glacial acetic acid. NativeMARK Unstained Protein Standard (Life technologies) was used as a molecular weight marker. All buffers used are listed in table 40-42.

Table 40. 1x Anode buffer for BN-PAGE

Component	Final concentration
Bis Tris pH 7.0	50 mM

Table 41. 1x Cathode buffer for BN-PAGE

Component	Final concentration
Bis Tris pH 7.0	15 mM
Tricine	50 mM
Coomassie G-250	0.02 % (w/v)

Table 42. 1x BN-loading dye

Component	Final concentration
Bis Tris pH 7.2	50 mM
HCl	6 N
NaCl	50 mM
Glycerol	10 % (w/v)
Ponceau S	0.001 %

2.3.5.7 Western Blot analysis

To detect heterologously expressed proteins Western Blot analysis was performed. Proteins were separated by SDS-PAGE before the gel was soaked in transfer buffer. A PVDF-membrane (Merck Millipore) was first soaked in 100 % (v/v) Methanol, rinsed with water and then soaked in transfer buffer. Proteins from the gel were blotted on the membrane for 45 minutes at 15 V. The membrane was incubated for one hour with blocking buffer and afterwards over night with the primary antibody. After washing the membrane 3 times with 1x TBS buffer it was incubated with the

secondary antibody for two hours. Then the membrane was again washed 3 times with 1x TBS buffer and protein bands were detected using BCIP/NBT (Sigma-Aldrich). The reaction was stopped by the addition of water. Page Ruler Prestained protein marker (Fermentas) was used as a molecular weight marker. All steps were carried out at 18-22°C. All buffers and antibodies used in this work are listed in table 43.

Table 43. Buffers and antibodies used for Western Blot

Buffer	Components	Concentration
Transfer buffer	Tris/HCl	25 mM
	Glycine	10 mM
	Methanol	10 % (w/v)
	DTT	0.25 mM
1x TBS buffer	Tris/HCl pH 7.5	20 mM
	NaCl	150 mM
Blocking buffer	TBS buffer	1x
	BSA	3 % (w/v)
primary anti-His antibody	TBS buffer	1x
	BSA	3 % (w/v)
	Monoclonal Anti-poly-histidine, produced in mouse (Sigma-Aldrich)	1:1000
secondary anti-mouse antibody	TBS buffer	1x
	BSA	3 % (w/v)
	Anti-mouse IgG (whole-molecule)-Alkaline Phosphatase, produced in rabbit (Sigma-Aldrich)	1:2000
primary anti-c antibody	TBS buffer	1x
	BSA	3 % (w/v)
	Polyclonal anti-c of *A. thaliana,* produced in rabbit (Agrisera)	1:5000

	TBS buffer	1x
	BSA	3 % (w/v)
secondary anti-rabbit	Anti-rabbit IgG	
antibody	Alkaline-phosphatase	1:2000
	produced in mouse	
developer	BCIP/NBT	1 tablet

2.3.6 Protein function

2.3.6.1 ATP hydrolysis assay (coupled assay)

To determine the ATP hydrolysis activity of ATP synthases a coupled enzyme assay was performed according to (Cook *et al*, 2003). Hereby the ATP hydrolysis is determined indirectly by measuring the decrease of absorption of NADH at λ = 340 nm. After hydrolysis of ATP to ADP and P_i by the ATP synthase, the enzyme pyruvate-kinase catalyzes the reaction of ADP and PEP to ATP and pyruvate. Pyruvate is then reduced with NADH + H^+ to lactate and NAD^+ leading to a decrease in the NADH concentration and thereby the absorption. A typical reaction mixture contained 980 µl of hydrolysis buffer, 10 µl 250 mM ATP and up to 10 µl sample, which was mixed thoroughly in a cuvette (Sarstedt). ATP hydrolysis activity was calculated by using the following equation:

$$\text{activity [U/ml]} = (\Delta E \cdot V_{ges}) / (\varepsilon NADH \cdot V_p)$$

ΔE : change of extinction per minutes at λ = 340 nm

V_{ges}: total volume of reaction mixture [µl]

εNADH: 6.22 $mM^{-1} \cdot cm^{-1}$ (extinction coefficient of NADH at λ = 340 nm)

$V_{p:}$ volume of sample [µl]

2.3.6.2 NCD-4 modification reaction

The ion specificity of a rotor ring was analyzed with a fluorescent analogue of the ATP synthase inhibitor dicyclohexylcarbodiimide (DCCD). To perform the modification reaction, a 60 µl-sample containing 0.45 mg/ml c-ring in 20 mM Tris/HCl pH 8.0 and 1.5 % (w/v) n-octyl-β-D-glucoside (OG; *F. nucleatum* c-ring) or n-dodecyl-β-D-maltoside (DDM; *B. pseudomallei* c-ring) was adjusted to pH 5.7-6.0 by the addition of 0.5 M MES/HCl pH 5.0. The reaction was started with 100 µM N-cyclohexyl-N`-[4(dimethylamino)-α-naphtyl]carbodiimide (NCD-4) (Invitrogen) in 10 % (w/v) DDM or dimethyl sulfoxide (DMSO). The continuous increase of fluorescence was monitored with an F-450 Hitachi Fluorescence Spectrophotometer ((λ_{ex}= 324 nm, (λ_{em}= 324 nm) at 25-35°C. The binding reaction was stopped either by the addition of 15 mM NaCl (final concentration) or by increasing the pH to 9.0 by the addition of 2.5 M Tris base.

2.3.6.3 DCCD-modification reaction

The ion specificity of the *B. pseudomallei* rotor ring was determined by a DCCD-modification reaction. A 20 µl-sample containing 0.3 mg/ml c-ring in 20 mM TrisHCl pH 8.0 and 0.05 % DDM was incubated in the absence or presence (5 and 50 mM) of NaCl with 500 µM DCCD (10 mM stock in 100 % DMSO). 1 µl aliquots were taken 0, 15, 30, 45 and 60 minutes after starting the DCCD-modification reaction of the c-ring and applied on a MADLI targed together with a DHB-matrix (1:1).

2.4 Biophysical methods

2.4.1 Matrix-assisted laser desorption/ionization mass spectrometry (MALDI-MS) and electrospray ionization mass spectrometry (ESI-MS)

For the determination of the molecular weight of a protein or to analyze DCCD-modified c-ring samples MALDI-MS was performed while identification of single proteins was done by ESI-MS by Dr. J. Langer (Max Planck Institute of Biophysics, Molecular Membrane Biology). Organically extracted c-subunits were dried and directly used for MALDI-MS. Purified protein samples were either used directly for

in-solution digestion or cut out from SDS-gels and digested in gel with proteases for ESI-MS.

2.4.2 X-ray crystallography of the *F. nucleatum* and *B. pseudomallei* c-rings

Purified c-rings of *F. nucleatum* and *B. pseudomallei* were used for 3D crystallization by vapor diffusion in hanging drops. A complete dataset collected of the c-ring of *F. nucleatum* was used for structure determination of it.

2.4.2.1 3D crystallization

Crystals of the *F. nucleatum* c-ring were set up in 24-well plates. A sample containing 2 mg/ml c-ring in 2 % (w/v) DDM was mixed with an equal volume of crystallization buffer for 1-2 µl hanging drops. The same buffer was used for the reservoir solution (500 µl). After three to four months of incubation at 18°C, crystals were fished using a nylon loop and flash-frozen in liquid nitrogen.
Crystallization of the *B. pseudomallei* c-ring was performed in 96- or 24-well plates. Crystallization trials in 96-well plates were set up with 300 nl of sample containing 2-4 mg/ml c-ring in 2-4 % DDM using a Mosquito pipetting robot. Reservoirs were filled with crystallization buffer from the following commercial screens: JBScreen classic 1-8 (Jena Bioscience), JBScreen Membrane 1-3 (Jena Bioscience), MemGold HT-96 Green Screen (Molecular Dimensions), Crystal Screen 1 and 2 (Hampton), Nextal Classics Suite 1 (Qiagen) and MIDAS MD1-59 Screen (Molecular Dimensions). Crystallization in 24-well plates was performed with the same protein sample as for 96-well plates with 1-2 µl hanging drops and 500 µl reservoir solution. Crystals were fished with nylon loops after 1-12 weeks of incubation at 18°C and flash-frozen in liquid nitrogen.

2.4.2.2 Data collection

Data of *F. nucleatum* c-ring crystals were collected at the Max-Planck/Novartis beamline X10SA (PXII) of the Swiss Light Source (SLS, Villigen, Switzerland) and the beamline ID23.2 of the European Synchrotron Radiation Facility (ESRF, Grenoble, France). To prove crystal quality three test images at three different angles (0°C, 45°C, 90°C) were taken from each crystal before data collection. These images

were autoindexed and data collection strategy was assigned using Mosflm. Crystals showing high resolution were used for complete data collection.

Crystals of *B. pseudomallei* c-rings were measured at the Max-Planck/Novartis beamline X10SA (PXII) of the Swiss Light Source (SLS, Villigen, Switzerland).

2.4.2.3 Data processing and molecular replacement

Data processing including data reduction (XDS), scaling (XSCALE) and converting (XDSCONV) were performed using the XDS package (Kabsch, 1993). Quality of data sets was judged by the completeness of the data (%), the intensity signal-to-noise ratio (I/σI) and $R_{merged\text{-}F}$ and R_{meas} factors (formula below).

During data collection using X-rays only indices and intensities of each diffracted beam are measured. To determine the phase angles, molecular replacement was applied using the c-ring of *I. tartaricus* (pdb: 1yce) as a search model.

2.4.2.4 Model building and structure refinement

The 3D model was build by iterating processes of fitting the model into the actual electron densities using Coot (Emsley & Cowtan, 2004) and refinement of the atoms at their positions using Phenix (Zwart *et al*, 2008) and Refmac (Murshudov *et al*, 1997). The quality of the final model was judged by the R_{work} and the R_{free} factors (formula below). Figures were rendered using PyMOL (DeLano, 2002).

$$R_{meas} = \frac{\sum_{hkl} \sqrt{\frac{n}{n-1}} \sum_{j=1}^{n} \left| I_{hkl,j} - \langle I_{hkl} \rangle \right|}{\sum_{hkl} \sum_{j} I_{hkl,j}}$$

$$R_{mergd-F} = \frac{\sum_{hkl} \sqrt{\frac{n}{n-1}} \sum_{j=1}^{n} \left| F_{hkl,j} - \langle F_{hkl} \rangle \right|}{\sum_{hkl} \sum_{j} F_{hkl,j}}$$

$$R_{work} = \frac{\sum_{hkl} \left| F_{hkl}^{obs} - F_{hkl}^{calc} \right|}{\sum_{hkl} F_{hkl}^{obs}}$$

$$R_{free} = \frac{\sum_{hkl \subset T} \left\| F_{obs} \right| - k \left| F_{calc} \right\|}{\sum_{hkl \subset T} \left| F_{obs} \right|}$$

2.4.3 Single-particle electron microscopy of the *B. pseudomallei* N-type c-ring

The purified c-ring of *B. pseudomallei* was investigated by single-particle negative stain and Cryo-EM. The stoichiometry of the complex was determined by 2D classification of single c-ring particles in RELION 1.3 (Scheres, 2012).

2.4.3.1 Negative staining

Negative staining was performed with 0.05-0.1 mg/ml *B. pseudomallei* c-ring in amphipol (A8-35) or detergent (DDM). 3 µl of the sample were loaded on a glow-discharged carbon-coated copper grid and incubated for 1 minute. The grid was then washed twice with water and once with 1 % (w/v) uranyl acetate before it was stained for 1 minute with 1 % (w/v) uranyl acetate.

2.4.3.2 EM data collection of negatively stained c-rings

Micrographs of the negatively stained c-ring were taken on a Phillips CM120 electron microscope operating at 120 kV with a 2k x 2k CCD camera, a magnification of 59 k and a defocus range from 1.1 µm to 1.5 µm.

2.4.3.3 Cryo-EM specimen preparation

Cryo-EM was performed with 2.5 mg/ml *B. pseudomallei* c-ring in amphipol (A8-35) or detergent (DDM and LDAO). 3 µl of the sample were loaded on a glow-discharged Quantifoil holey carbon grid and blotted for 7-11 seconds with 70 % humidiy at 10° C, plunge-frozen in liquid ethane using a FEI Vitrobot Mark III (FEI Company) and transferred into liquid nitrogen.
Cryo-grids were prepared by Martin Wilkes (Structural Biology, Max-Planck-Institute of Biophysics, Frankfurt).

2.4.3.4 Cryo-EM data collection

Cryo-EM data of the c-ring were collected on a JEOL 3200 FSC electron microscope operating at 300 kV with an in-column energy filter and a K2 Summit direct electron detector camera (Gatan). All micrographs were recorded with a defocus ranging from 0.5 µm to 3.7 µm at a nominal magnification of 30.000 x resulting in a pixel size of 1.14 Å on the specimen. The total exposure time of five (amphipol A8-35 and DDM) or seven (LDAO) seconds was leading to a total accumulated electron dose of about 45 to 70 $e^-/Å^2$ on the specimen.
Data were collected together with Martin Wilkes (Structural Biology, Max-Planck-Institute of Biophysics, Frankfurt).

2.4.3.5 Cryo-EM data processing

Every image was motion-corrected (Li *et al*, 2013) and CTF-corrected using CTFFIND3 (Mindell & Grigorieff, 2003) in the RELION 1.3 (**RE**gularized **LI**kelihood **O**ptimizatio**N**) workflow (Scheres, 2012). First, particles were picked manually using the EMAN programm Boxer after images were 3x3 binned in EMAN2 (Ludtke *et al*, 1999; Tang *et al*, 2007). Further particles were picked automatically in RELION 1.3 from unbinned images, whereby each micrograph was edited manually afterwards to guaranty good particle quality. 2D class averages with these particles were performed in RELION 1.3.
Particles were picked together with and data processing was performed by Martin Wilkes (Structural Biology, Max-Planck-Institute of Biophysics, Frankfurt).

2.4.4 Alignments

Alignments of amino acid and nucleotide sequences were performed with ClustalW included in BioEdit (http://www.mbio.ncsu.edu/bioedit/bioedit.html). Alignments of amino acid sequences with public databases were done with the BLAST programs (http://blast.ncbi.nlm.nih.gov/Blast.cgi).

2.4.5 Design of vector maps

Vector maps of nucleotide sequences were created with PlasMapper (http://wishart.biology.ualberta.ca/PlasMapper/index.html, (Dong *et al*, 2004)).

2.4.6 Computation of a homology model of the *B. pseudomallei* c-ring

A homology model of the N-type c-ring was generated with the WHATIF server (http://swift.cmbi.ru.nl/servers/html/index.html (Rodriguez *et al*, 1998)) using the *F. nucleatum* c-ring structure as a template.

2.4.7 Generation of structural models of c-rings with different stoichiometries

The structural models of c-rings with different stoichiometries were generated using a Fortran language-based software written by Prof. Kay Diederichs, University of Konstanz, Germany.

2.4.8 Generation of protein structure figures

The 3D structure figures were created with Pymol (DeLano, 2002) and further edited in Photoshop CS5.

3 Results

3.1 The hybrid F_1F_o ATP synthase and the c-ring of *F. nucleatum*

In the first part of this thesis the F_1F_o ATP synthase rotor ring of the anaerobic, opportunistic pathogenic bacterium *Fusobacterium nucleatum* was investigated with the ultimate goal to determine this c-ring structure by X-ray crystallography. The c-subunit sequence of *F. nucleatum* shows an altered Na^+-binding signature if compared with the Na^+-specific *I. tartaricus* c-subunit harboring a "two-carboxylate-motif" as previously introduced (chapter 1.3.4.1). This makes it an attracting object for structural and functional studies with respect to the ion specificity of this c-ring and the exact contribution to ion-coordination by the residues within the ion-binding sites. Besides that, the stoichiometry of the oligomeric protein complex was set to be elucidated in this work.

Previous experiments showed that the heterologous expression of the *F. nucleatum* c-ring in *E. coli* using a pt7-7 vector system did not yield any oligomeric complex, which could be isolated (Schulz, 2010). We hence set out to look for an alternative expression method. The heterologous expression of the entire *I. tartaricus atp* operon in *E. coli* could successfully be performed by using a pTrc99A expression plasmid (Oberfeld, 2006). Therefore we decided to use this expression system but try to exchange the *I. tartaricus atpE* gene with the *F. nucleatum atpE* gene and use it to express a hybrid F_1F_o ATP synthase in *E. coli*, consisting of F_1ab_2 of *I. tartaricus* and the c-ring of *F. nucleatum*. The expression and purification of this hybrid enzyme was already described previously (Schulz, 2010). Optimizing steps of the procedure, however, which were carried out in this work, are described in the following part.

3.1.1 Expression and purification of the hybrid ATP synthase

Plasmid pITtr5His_atpE.FN encoding for the water-soluble F_1 headgroup and the membrane-incorporated parts ab_2 of *I. tartaricus* and c_n (c-ring with yet unknown stoichiometry) of *F. nucleatum* was expressed in the Δ*atp E. coli* strain DK8. Initially the expression was performed in 2xYTG medium at 37°C (Schulz, 2010) but the yield of the ATP synthase could be increased when expressing the plasmid in TB medium

at 37°C. The cells reached an OD_{600} of only 1.5 to 2.0. However, longer incubation times decreased the yield of the ATP synthase obtained after purification.

E. coli membranes with the heterologously expressed protein were prepared and the enzyme was solubilized with 1 % (w/v) n-dodecyl-β-D-maltoside (DDM) for 1 hour at 4°C under constant mixing. The use of DDM instead of Triton-X-100 (Schulz, 2010) increased the amount of enzyme solubilized from *E. coli* membranes.

The hybrid ATP synthase was isolated by Ni^{2+} NTA affinity chromatography due to the hexameric His-tag at the ß-subunit of the enzyme. Less contaminations were obtained in the Ni^{2+}NTA elutions, if 5 mM (final concentration) imidazol was added to the solubilized fraction preventing low affinity binding of *E. coli* proteins to the resin. Furthermore, incubation of the solubilizate with the sepharose Ni^{2+} NTA material overnight at 4°C significantly increased the amount of enzyme binding to the resin. Washing of the column was performed with 5, 20 and 40 mM imidazol containing buffers before the ATP synthase was eluted with 400 mM imidazol buffer (figure 19 A).

The migration levels of the *I. tartaricus* ATP synthase subunits on a SDS-gel are already known from previous studies (Neumann *et al*, 1998). To compare the purification of the *I. tartaricus* ATP synthase with the new hybrid enzyme, both purified enzymes were analyzed by SDS-PAGE side by side. The analysis shows that the eluted hybrid ATP synthase contained severel contaminating proteins which do not occur in the eluted *I. tartaricus* enzyme (figure 19 A and C), However, these contaminations (marked with an x in figure 19) were not further analyzed as we aimed to obtain a highly pure rotor ring by using the hybrid ATP synthase just as a heterologous expression system in *E. coli*.

Applying imidazol concentrations higher than 40 mM in the washing steps caused detachment of single subunits from the enzyme (not shown), in particular the c-ring. This suggests that the hybrid ATP synthase is either not as tightly assembled as the wildtype enzyme, which can be washed using higher imidazol concentrations, or that it is more aggregated in the solution. In line with this, the solubilized hybrid ATP synthase showed lower ATP hydrolytic activity (1.5 U/l cells), as determined by the NADH regeneration assay, than the *I. tartaricus* enzyme (4.4 U/l) (Schulz, 2010). However, in both cases, the activity was significantly reduced after solubilization of the enzyme as the membrane ATPase activity was determined to be 37 and 35 U/l

cells for the wildtype and the hybrid enzyme, respectively. This might reflect a high background ATPase activity in *E. coli* membranes resulting from other enzymes localized in there.

Nevertheless, the *F. nucleatum* c-ring was SDS-stable and migrated as a thin, black band directly beneath the α and ß-subunits on the SDS polyacrylamide gel. Despite the amount of c-ring was very low, it turned out that after further purification and concentration (3.1.2) it was enough protein to perform biochemical and structural investigations of the c-ring.

A

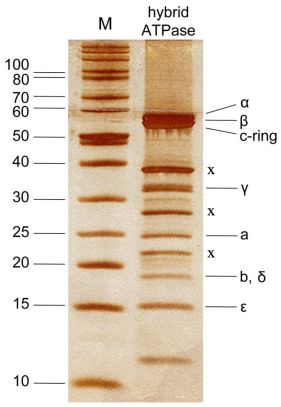

B

subunits of the hybrid ATP synthase	theoretical molecular masses of the subunits
α (*I. tartaricus*)	51.0 kDa
β (*I. tartaricus*)	50.6 kDa
γ (*I. tartaricus*)	31.7 kDa
δ (*I. tartaricus*)	20.0 kDa
ε (*I. tartaricus*)	15.1 kDa
a (*I. tartaricus*)	32.3 kDa
i (*I. tartaricus*)	14.2 kDa
b (*I. tartaricus*)	18.7 kDa
c_{i} (*F. nucleatum*)	8.8 kDa
c_{11} (*F. nucleatum*)	97.5 kDa*

C

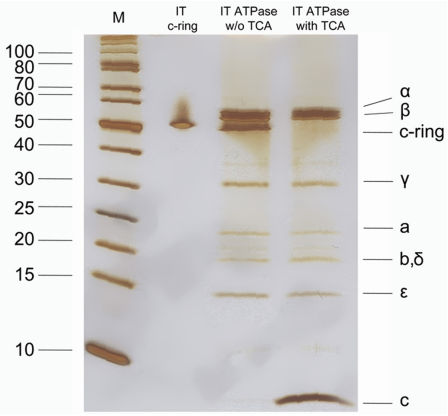

Figure 19. SDS-PAGE of the purified hybrid ATP synthase.

(A) The hybrid enzyme was isolated by Ni^{2+} NTA affinity chromatography and eluted from the column with 400 mM imidazol buffer. All subunits of the ATP synthase are indicated on the right side in the gel. Remaining contaminating proteins are marked with an x. **(B)** The theoretical molecular masses of the corresponding ATP synthase subunits are listed in kilo Daltons [kDa]. *The molecular mass of the c-ring of *F. nucleatum* was calculated assuming it has the same undecameric stoichiometry as the *I. tartaricus* c-ring has. **(C)** The *I. tartaricus* ATP synthase purified by Ni^{2+}NTA affinity chromatography without any contaminating proteins.

3.1.2 Purification of the *F. nucleatum* c-ring

As in previous experiments established, the c-ring was solubilized from the hybrid ATP synthase by heat incubation using 1 % N-lauroyl-sarcosine, precipitation with ammonium sulfate and sucrose gradient density centrifugation (Schulz, 2010).

To improve the purity of the protein and to concentrate the sample, additional steps were developed in this work. The sample in sucrose buffer was further purified by

hydroxy-apatite chromatography and desalted with PD-10 columns. The detergent used during these purification steps was dependent on the purpose of the corresponding protein sample; n-octyl-β-D-glucoside (OG) was used for labeling experiments (3.1.3) and n-decyl-β-D-maltoside (DM) for crystallization (3.1.4). Final protein concentration was performed using Amicon Ultra centrifugal filter units or Microcon centrifugal filters (MWCO 100.000 kDa). By applying the purification procedure described, 0.4 mg pure c-ring (200 µl of 2 mg/ml) could be obtained from 12 l *E. coli* cells. This low yield originates from the fact that the expression of the hybrid ATP synthase already does not yield as much enzyme as when expressing the *I. tartaricus* ATP synthase. Further, losing of the protein occurs due to several consecutive purification steps necessary to gain the required high purity of the c-ring for subsequent 3D crystallization.

The final protein quality was analyzed by SDS-PAGE (figure 20 A) and the exact molecular mass of one c-subunit was determined by MALDI-MS (figure 20 B), which was performed by Dr. Julian Langer (Molecular Membrane Biology, Max-Planck-Institute of Biophysics).

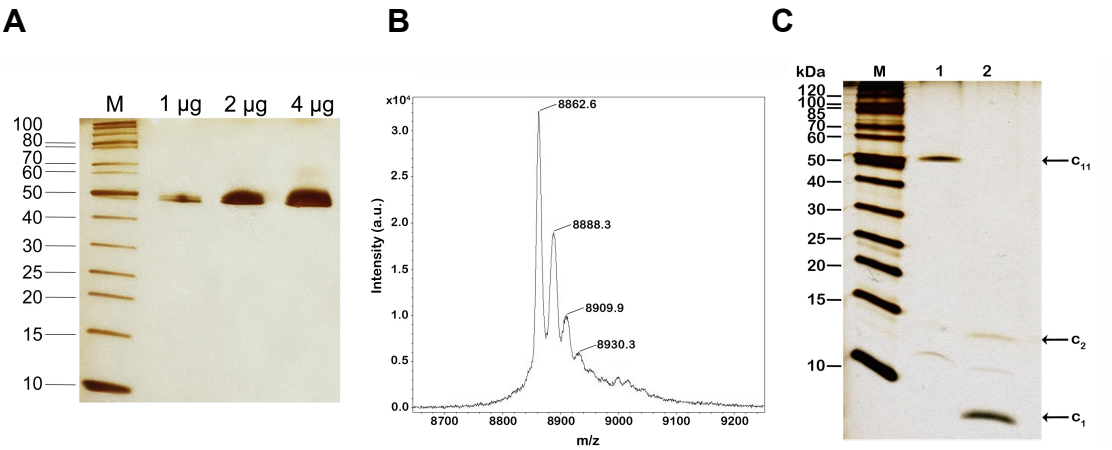

Figure 20. Silver-stained SDS-PAGE of the purified *F. nucleatum* c-ring and MALDI-MS spectrum of the c-subunit.

(A) 1-4 µg of highly pure c-ring migrating as an SDS-stable oligomeric complex on a level of 50 kDa. **(B)** The spectrum of the c-ring sample shows the intensities for four different molecular masses including the unmodified c-subunit (8862.94 Da), the formulated protein (8890.94) as well as the formylated, single oxidized (8906.94 Da) and double oxidized c-subunit (8922.94 Da). **(C)** 1 µg of *F. nucleatum* c-ring before (1) and after the treatment with 15 % (w/v) trichloroacetic acid (TCA) (2), disassembling the complex into c-monomers (c_1) and c-dimers (c_2).

The c-ring is migrating at about 50 kDa on a SDS gel just at the same level as the *I. tartaricus* rotor ring does indicating that the two rings have the same or at least a similar stoichiometry. The complex could be disassembled into its c-subunits by trichloroacetic acid (figure 20 C).

3.1.3 The ion specificity of the *F. nucleatum* c-ring

The biochemical evidence for the ion specificity of the *F. nucleatum* c-ring was provided by performing labeling experiments using a derivative of the ATP synthase inhibitor dicyclohexylcarbodiimide (DCCD), named N-cyclohexyl-N`-[4(dimethylamino)-α-naphtyl]carbodiimide (NCD-4) (Chadwick and Thomas, 1983). While NCD-4 itself is nonfluorescent, the protein product is fluorescent, which enables monitoring of the binding reaction between the fluorophore and a protein. In this case NCD-4 binds to the protonated glutamate residues (E65) of the ion-binding sites of the c-ring. Upon addition of the fluorophore NCD-4 to 27 μg c-ring solubilized in 1.5 % n-octyl-β-D-glucoside (OG) at pH 5.7 the continuous increase of fluorescence was monitored for 900 seconds when NCD-4 was binding to the protein (figure 21 A). Further binding of NCD-4 could be precluded by adding NaCl to a final concentration of 15 mM to the sample. This indicates a high affinity of Na^+ for the ion-binding site thereby competing with protons even at low pH (5.7).
Besides, the corresponding control experiment was carried out (figure 21 B), where the NCD-4 binding reaction of the isolated c-ring was monitored for a time span of 140 minutes without the addition of NaCl to the sample showing that the termination of the reaction was specifically caused by Na^+.

A sample of the NCD-4 modified c-ring was treated with trichloroacetic acid (TCA) and subsequently loaded on a SDS-gel to check if the modified protein can also be disassembled by this strong acid. A clear shift in the molecular mass of the modified complex (c_{11}) as well as of the modified single c-subunits (c_1) and c dimers (c_2) can be detected when comparing with the unmodified c-ring with and without TCA (figure 22 A). Besides, a sample of NCD-4 modified c-ring was loaded on a SDS gel which was exposed with UV light visualizing the fluorecent NCD-4 bound protein (figure 22 B).

A

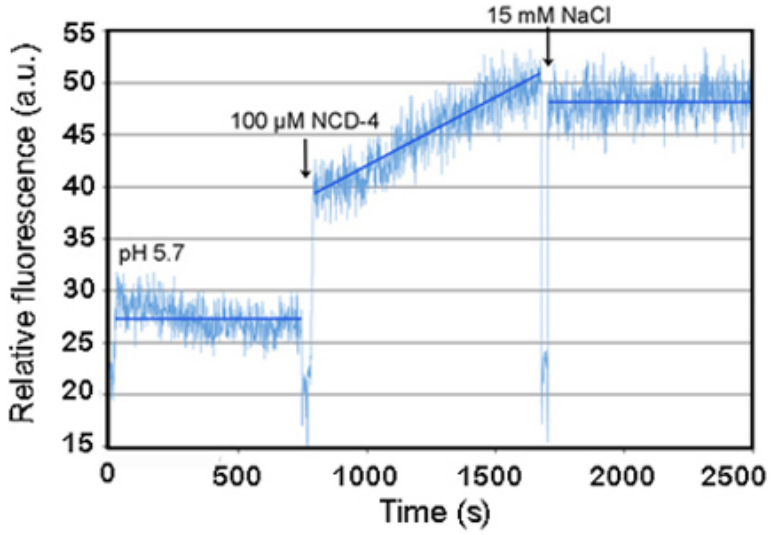

B

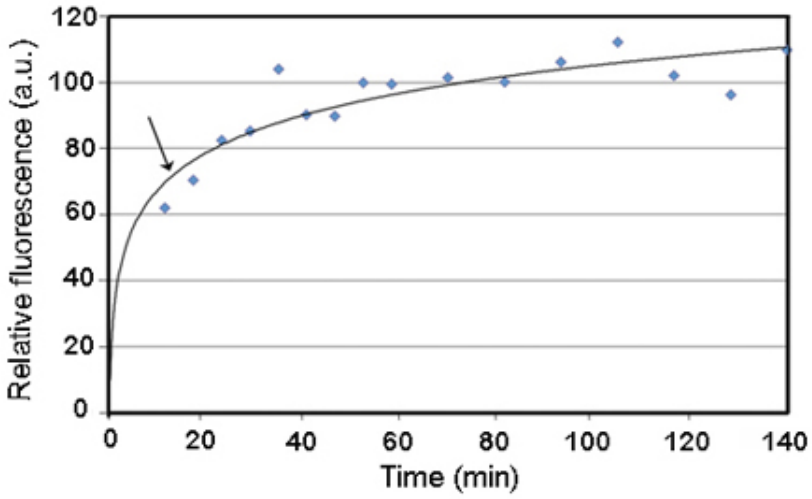

Figure 21. Kinetics of the NCD-4 modification reaction of the detergent-solubilized *F. nucleatum* c-ring.

The reactions of NCD-4 with the c-ring were performed at pH 5.7 in MES buffer and 1.5 % OG, where the glutamates of the ion-binding sites (E65) are protonated. The continuous increase of fluorescence was monitored (λ_{ex} = 324 nm, λ_{em} = 452 nm) upon addition of 100 µM NCD-4 to 27 µg c-ring. **(A)** After adding 15 mM NaCl to the sample, further binding of NCD-4 to the protein and thereby further increase of fluorescence was precluded. **(B)** Fluorescence was determined in regular intervals for a time period of 140 minutes without adding NaCl to the sample. Here, the reaction continues above the time point where it was specifically stopped in the previous short-term experiment.

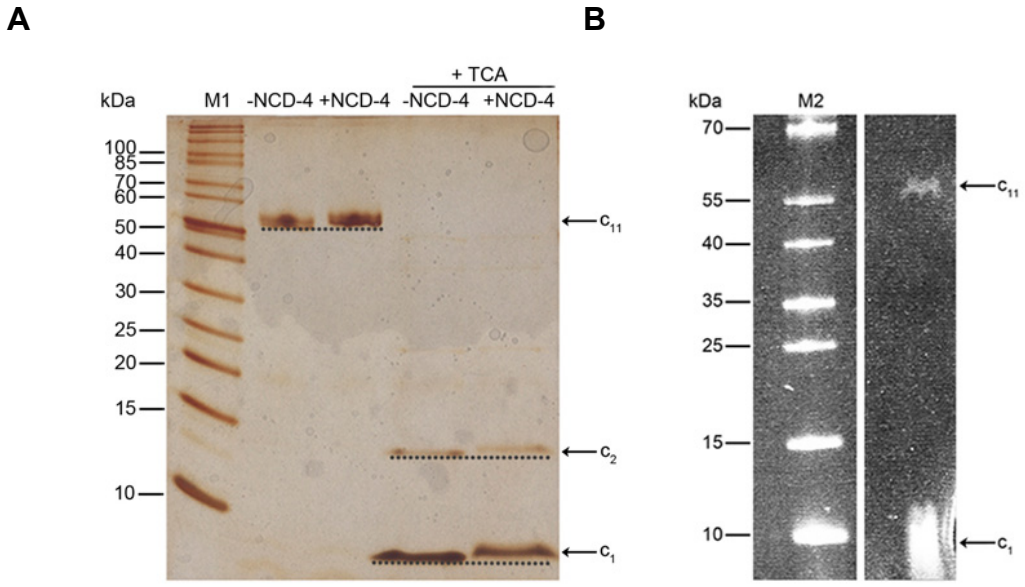

Figure 22. SDS-PAGE of the NCD-4 modified *F. nucleatum* c-ring and the c-monomers.
(A) Silver-stained SDS gel of the c-ring after binding of NCD-4. The modified complex (c_{11}), the c-monomers (c_1) and c-dimers (c_2) migrated sligtly slower on the gel in comparison to the unmodified samples (dahed lines). **(B)** UV-light exposed SDS-gel visualizing the NCD-4 bound c-ring and c-monomers. M1: PageRuler Unstained Protein Ladder (Fermentas), M2: PageRuler Prestained Protein Ladder (Fermentas). The figure was taken from (Schulz *et al*, 2013).

In order to determine if the ion specificity of the isolated *F. nucleatum* rotor ring is resembling the actual ion specificity of the protein complex in the assembled ATP synthase, complementing experiments were performed in collaboration with the group of Prof. Dr. Gregory M. Cook and carried out by Dr. Marina Iglesias-Cans (Otago School of Medical Science, Dunedin, New Zealand). They could show that Na^+ is stimulating the ATP hydrolysis activity of the *F. nucleatum* enzyme when prepared from native cells (figure 23). A similar stimulation is seen by the addition of Li^+, but not of K^+; aside with this, Na^+ prevents blocking of hydrolysis activity by the ATP synthase inhibitor DCCD, which is in good agreement with the Na^+-protective effect seen in the NCD-4 labeling experiment with the solubilized c-ring. Furthermore, it becomes apparent that there is no difference in Na^+-specificity irrespective of whether the whole ATP synthase from native membranes is investigated or if the heterologously expressed, detergent-solubilized c-ring is used for analysis.

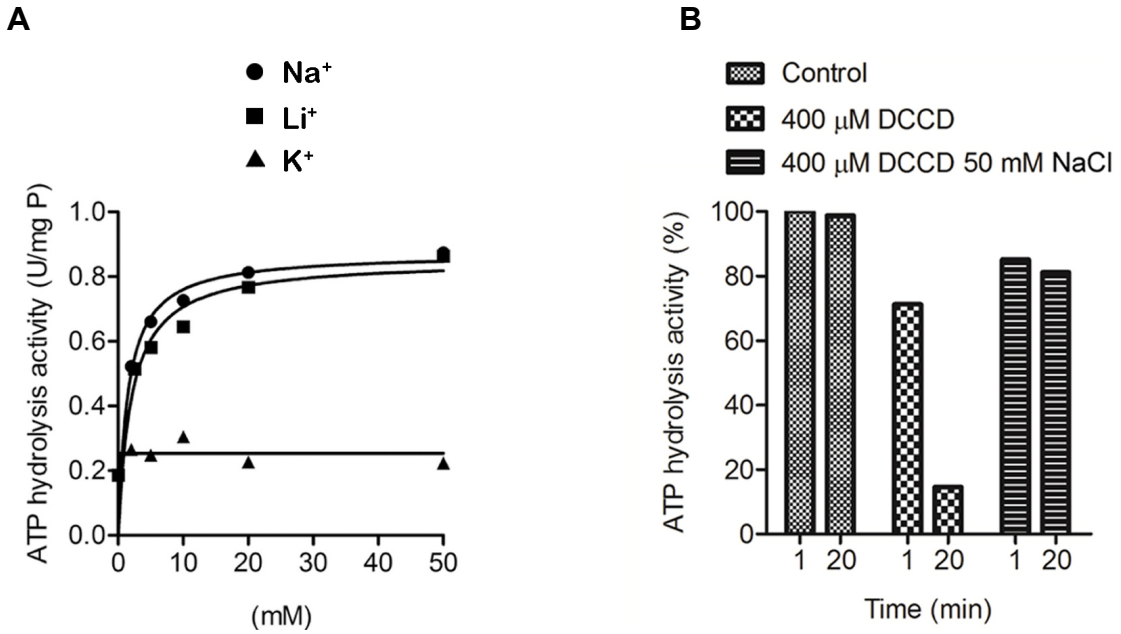

Figure 23. Hydrolysis activity and DCCD inhibition of the *F. nucleatum* ATP synthase purified from native membranes.

(A) The ATP hydrolysis activity of 120-140 µg isolated enzyme in 50 mM MOPS pH 7.5, 2 mM $MgCl_2$ was stimulated by Na^+, Li^+, but not by K^+. Measurements were performed at 37°C using the ATP-regeneration assay. **(B)** Inhibition of the hydrolysis activity by 400 µM DCCD could be protected by the addition of 50 mM NaCl. Measurements were carried out as in (A) after incubating the purified protein (120-140 µg) for 20 minutes at 25°C with DCCD in the presence or absence of NaCl. 100 % activity refers to 1-2 U/mg of protein. (These experiments were carried out by Dr. Marina Iglesias-Cans in the group of Prof. Dr. Gregory M. Cook, Dunedin, New Zealand.)

To confirm the biochemically determined ion specificity as well as to determine the stoichiometry of the c-ring, a high-resolution X-ray structure of the protein complex is indispensable. A highly pure and stable protein sample is essential for high quality three-dimensional crystal growth. To investigate - besides SDS-stability - also thermal stability of the protein complex, the isolated c-ring (in 20 mM Tris/HCl pH 8.0, 1.5 % OG and 4°C) was incubated for different time spans at 95°C and subsequently loaded on a SDS gel. It was shown in a previous study that the remarkable stability of the Na^+ binding c-ring of *I. tartaricus* is due to intersubunit crossbridging by Na^+ or Li^+ ions (Meier and Dimroth, 2002). Therefore, the influence of Na^+ on the thermal stability of the *F. nucleatum* c-ring was assigned by comparing samples with and without NaCl added prior to heat incubation. The Na^+-background concentration in the Tris/HCl buffer was determined by flame atomic absorption spectroscopy to be very low (3.3 mM Na^+) (figure 24).

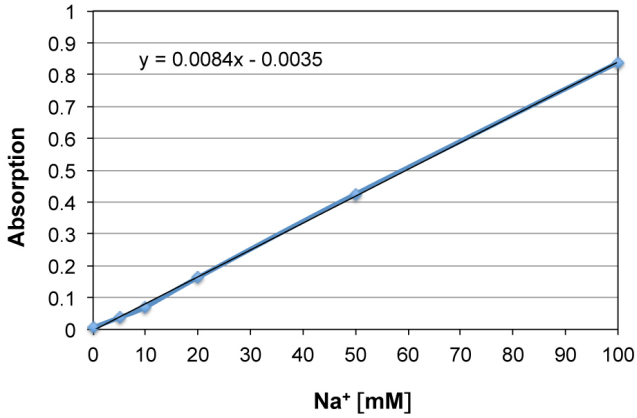

Figure 24. Determination of the Na^+-concentration in Tris/HCl buffer by flame absorption spectroscopy.

The linear regression line was made using calibration solutions containing 0, 5, 10, 20, 50 and 100 mM Na^+. The absorption of 20 mM Tris/HCl buffer was 0.024 corresponding to 3.3 mM Na^+.

The SDS gel revealed that the c-ring was also remarkably heat-stable, resisting boiling even for 30 minutes at 95°C. Under the particular conditions, which were tested here, the complex was stable irrespective of prior NaCl addition to the sample (figure 25). This tremendous stability of the c-ring can have positive effects on the subsequent crystallization of the protein.

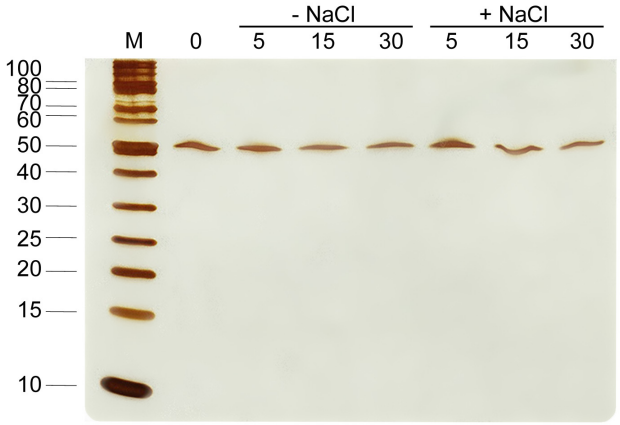

Figure 25. Temperature stability of the isolated *F. nucleatum* c-ring analyzed by silver-stained SDS-PAGE.

The protein in 20 mM Tris/HCl pH 8.0 and 1.5 % OG was incubated in the presence or absence of NaCl for 5-30 minutes at 95°C. The c-ring remained stable over the whole time span irrespective of the additional NaCl in the sample.

3.1.4 High resolution X-ray structure of the *F. nucleatum* c-ring

To obtain high-resolution structural data from the *F. nucleatum* c-ring, the purified protein in 2 % n-decyl-β-D-maltoside (DM) was used for 3D crystallization by the hanging drop vapor diffusion method. Crystal drops were set up with a protein concentration of 2 mg/ml and a protein-to-reservoir ratio of 2:1 in 24 well plates with a reservoir volume of 500 µl. First crystals of different shapes became visible within two weeks of incubation at 18°C. The most promising crystallization condition (0.1M NaAc pH 4.5 and PEG_{300} as a precipitant) as judged by the outside appearance of the individual crystals, was used as a basis for further optimization. Remarkably, very small changes in the PEG concentration (1-2 %) induced formation of differently-shaped crystals. The crystal size increased with longer incubation times and crystals were stable within the drop once no further increment was observed. Figure 26 shows exemplary c-ring crystals in DM grown at acidic pH with varying concentrations of PEG_{300} and PEG_{600}.

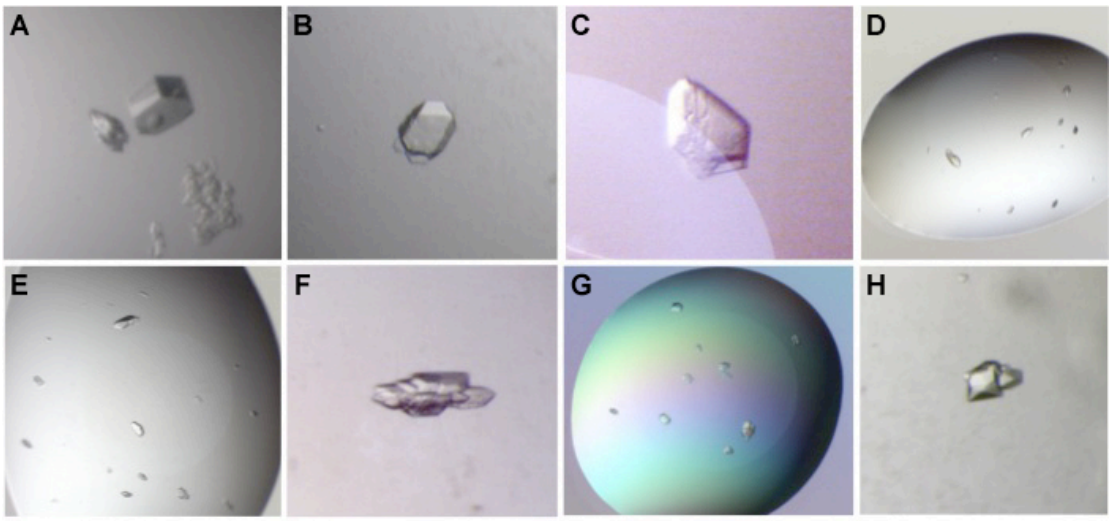

Figure 26. Three-dimensional crystals of the *F. nucleatum* c-ring grown at acidic pH.
Crystals were grown after two to three months at 18°C in 0.1M NaAc pH 4.5 and 25 % PEG_{300} **(A)**, 29 % PEG_{300} **(B)**, 28.57 % PEG_{300} **(C-F)**, 17.14 % PEG_{600} **(D)** or 28.25 % PEG_{300} **(G and H)**. The best crystal **(F)** diffracted isotropically and a complete dataset to a resolution of 2.2 Å could be collected for structure determination.

Some of these crystals were used to exclude the possibility that protein impurities, co-purified along with the *F. nucleatum* c-ring have been crystallized. Therefore, single

crystals were fished using a nylon loop, dissolved in reservoir solution and subsequently loaded on an SDS gel. The result of this investigation was that the crystallized material was just c-ring, as it was migrating at the same size as the purified protein itself with no further proteins visible aside (figure 27).

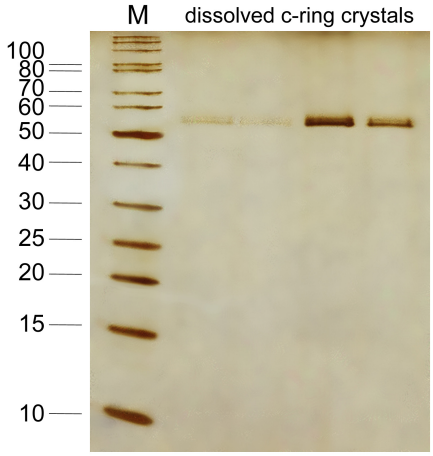

Figure 27. Silver-stained SDS-PAGE of dissolved three-dimensional *F. nucleatum* c-ring crystals grown at acidic pH.

Crystals were fished from the crystallization drops, dissolved in reservoir solution and subsequently analyzed by SDS-PAGE. The silver-stained PA-gel shows that the crystallized protein co-migrated with the purified *F. nucleatum* c-ring. The experiment confirms that the crystallized material consisted only of *F. nucleatum* c-ring.

The best diffracting crystal at low pH was obtained when the c-ring was solubilized in 1 % DM in 20 mM Tris/HCl buffer pH 8.0 and grown in crystallization buffer containing 0.1 M NaAc pH 4.5 (HCl) and 28 % (v/v) PEG_{300} (figure 28 F) so that the final pH of the drop was 5.3. The crystal was fished with a nylon loop after three month of incubation at 18°C and directly flash-frozen in liquid nitrogen. It was apparently very inhomogenous being the outcome of many single crystals grown together. Nevertheless it diffracted X-rays to high-resolution and a complete dataset to 2.2 Å resolution could be collected, although it contained diffraction spots from a second crystal lattice originating from the assembly of multiple crystals (figure 28 A).

To investigate the influence of pH on the conformation and protonation state of single residues within the ion-binding site of the c-ring, the protein was also crystallized in buffers of high pH. Several buffers were tested and crystals were obtained with CAPS, Tris, Tricin, Glycin and CHES.

The best diffracting crystal obtained at high pH was grown in crystallization buffer containing 0.1 M CHES pH 9.6 (NaOH), 5 mM $MgCl_2$ and 27 % (v/v) PEG_{300}. The protein was also solubilized in 1 % DM in 20 mM Tris/HCl buffer pH 8.0 resulting in a final pH of the drop of 8.7. The crystal was fished after four month of incubation at 18°C with a nylon loop and directly flash-frozen in liquid nitrogen. In this case a complete dataset to 2.64 Å resolution was collected (figure 28 B).

3.1.4.1 Data collection and structure determination

Crystal diffraction data to 2.2 Å (pH 5.3) and 2.64 Å (pH 8.7) were collected at the Max-Planck/Novartis beamline X10SA (PXII) of the Swiss Light Source (SLS, Villigen, Switzerland) and the beamline ID23.2 of the European Synchrotron Radiation Facility (ESRF, Grenoble, France), respectively.
Initially three images were collected from a single crystal at three different angles, usually at 0, 45 and 90°C. Crystals diffracting isotropically to less than 3 Å were used for data collection. The ideal way of collecting was assigned using the software STRATEGY within the processing package MOSFLM.
Data reduction was performed using XDS thereby determining the space group and cell parameters of the crystals at pH 5.3 and pH 8.7. The c-ring crystallized each time in space group $P2_1$ and with two rings in the asymmetric unit, two of them building the unit cell. The cell paramaters of the c-ring crystal at pH 5.3 (a 135.8 Å, b 84.0 Å, c 151.1 Å; α 90°, β 112.8°, γ 90°) are very similar to these of the crystal at pH 8.7 (a 136.5 Å, b 84.1 Å, c 152.1 Å; α 90°, β 112.9°, γ 90°). The data collection statistics of both structures are summarized in table 47.

A

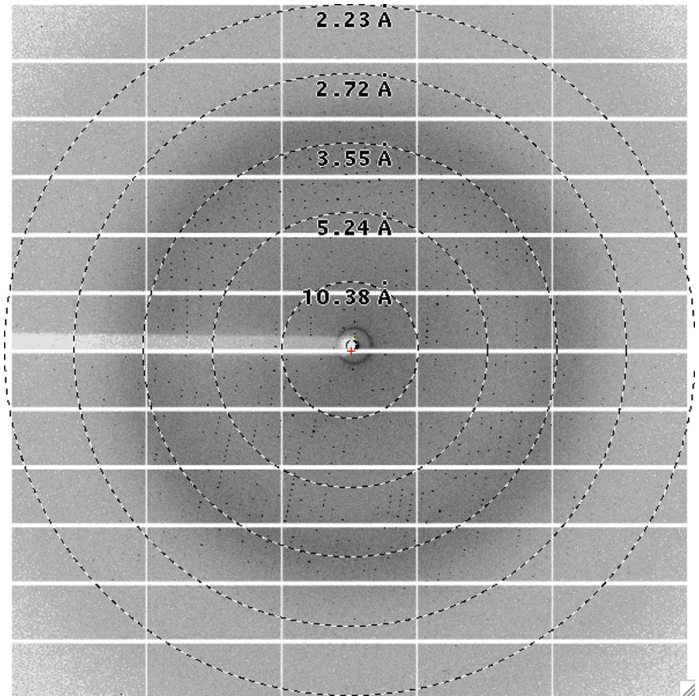

B

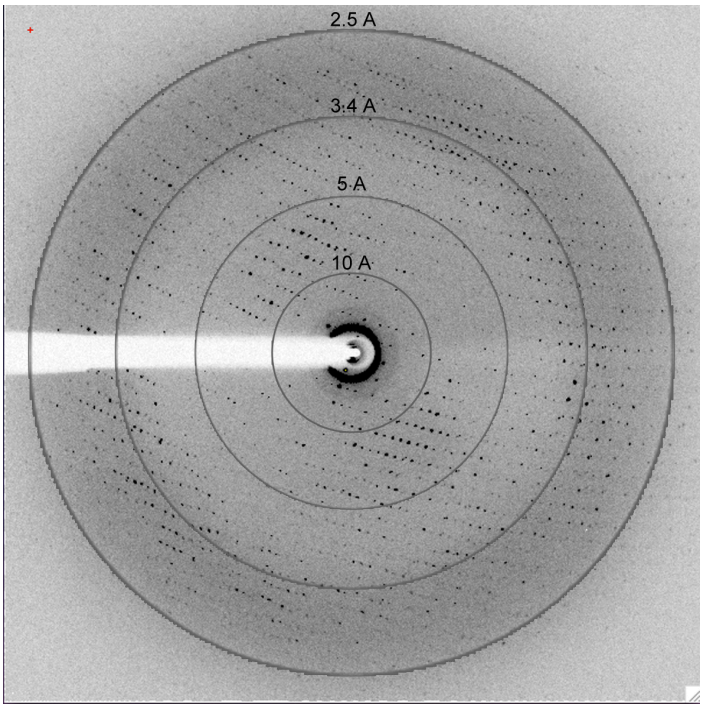

Figure 28. Diffraction pattern of the c-ring crystals at pH 5.3 and pH 8.7.

The first data set **(A)** was collected to a resolution of 2.2 Å at the X10SA beamline (SLS) from a crystal at pH 5.3, shown in figure 23 F. The second data set **(B)** was collected at the ID23.2 beamline (ESRF) from a crystal grown at pH 8.7. These data sets were used for structure determination of the c-ring at low and high pH.

Table 44. X-ray diffraction data collection statistics of the *F. nucleatum* c-ring crystals

Data collection	c_{11}, pH 5.3	c_{11}, pH 8.7
Beamline	X10SA (PXII), SLS	ID23.2, ESRF
Space group	$P2_1$	$P2_1$
Cell dimensions		
a, *b*, *c* (Å)	135.8, 84.0, 151.1	136.5, 84.1, 152.1
α, β, γ (°)	90.0, 112.8, 90.0	90.0, 112.9, 90.0
Resolution (Å)[a]	20-2.22 (2.36-2.22)*	50-2.64 (2.80-2.64)*
R_{meas} #	13.6 (100.8)	24.0 (117.4)
$R_{mergd\text{-}F}$ #	20.2 (96.9)	28.0 (112.6)
$I / \sigma I$	8.92 (1.56)	7.10 (1.57)
Completeness (%)	99.1 (97.3)	99.0 (95.4)
Redundancy	4.54 (4.52)	4.21 (3.97)

*Values in parentheses are for the highest-resolution shell. Inclusion of data to 2.22 Å resolution, despite the high R_{meas}, $R_{mergd\text{-}F}$ and $I/\sigma I$ values, resulted in e noticeable improvements in the electron densities of the map.

At first, the structure of the c-ring at pH 5.3 was solved by molecular replacement (MR) using the *I. tartaricus* c-ring structure (pdb 1yce) as a search model. To prevent model bias regarding the coupling ion, the bound Na^+ and water molecules were omitted from the template structure. The c-subunits of *F. nucleatum* and *I. tartaricus* have a high sequence identity of 83 % what made 1yce a suitable template for MR. Indeed, the resulting MR solution showed a c-ring model of eleven subunits with no clashes of amino acid side chains within the molecule. Nevertheless, to prove the stoichiometry of the *F. nucleatum* c-ring, i.e. to determine if it is actually undecameric or rather composed of more or less than eleven subunits, search models of the *I. tartaricus* c-ring were build having stoichiometries of ten and twelve subunits. Indeed the MR solutions obtained with either a decameric or a dodecameric c-ring as a template turned out to be less reasonable due to their overall shape (figure 29). These results confirm a stoichiometry of eleven subunits for the *F. nucleatum* c-ring.

The structure of the c-ring at pH 8.7 was solved in almost the same manner besides using the previously determined *F. nucleatum* c-ring structure at pH 5.3 as a search model for MR. The MR solution was a structural model for the c-ring at pH 8.7 having a very similar overall shape as the one resembling the ring at pH 5.3.

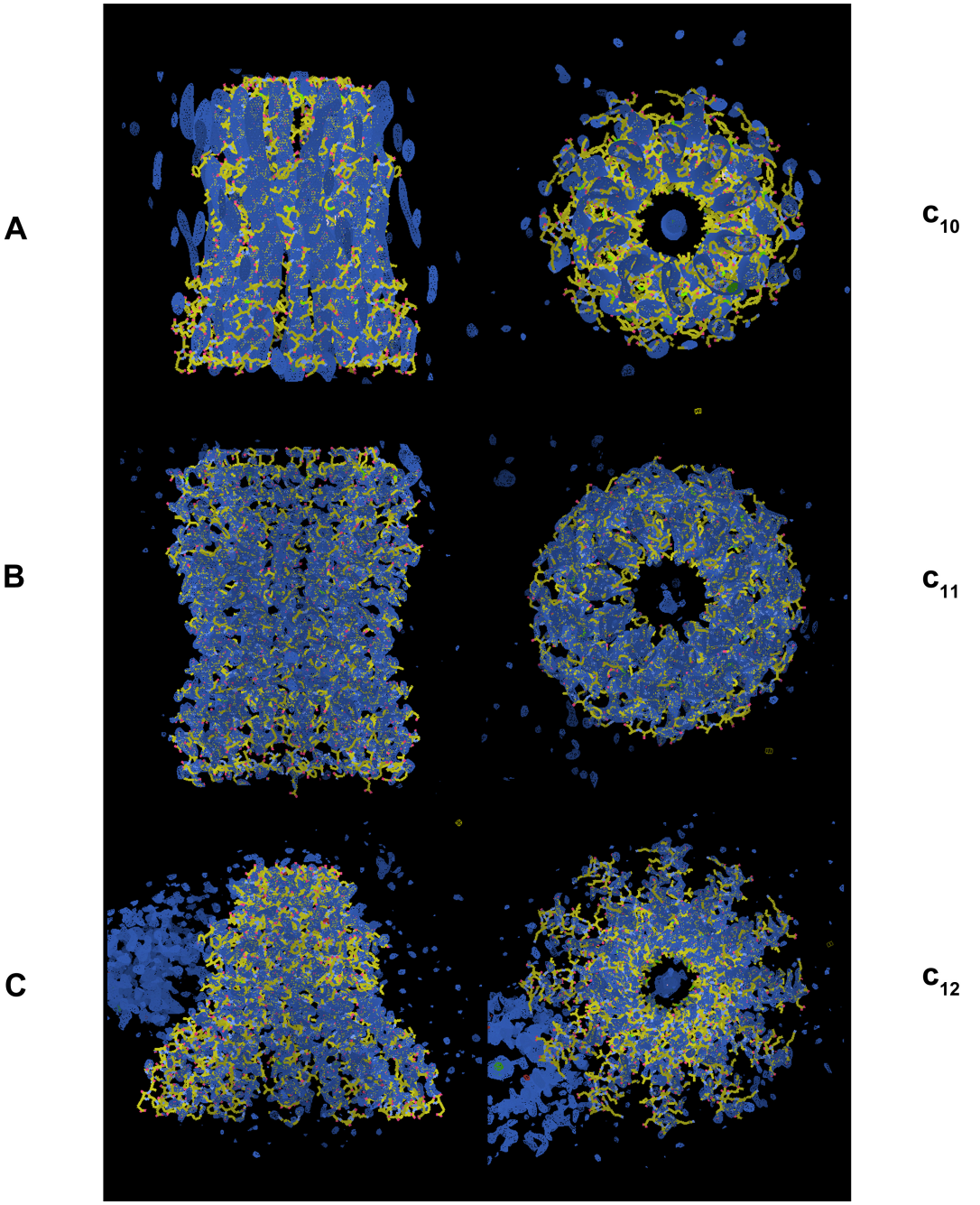

Figure 29. Molecular replacement solutions for the *F. nucleatum* c-ring based on a decameric, undecameric and dodecameric *I. tartaricus* c-ring.

The $2F_{obs}$-F_{calc} densities of side and top views of MR solutions using either a c_{10} **(A)**, c_{11} **(B)** or c_{12} **(C)** ring based on the *I. tartaricus* c-ring structure (pdb 1yce). The original X-ray data were obtained from a c-ring crystal at pH 5.3. Densities fit best into the undecameric c-ring model suggesting that the *F. nucleatum* ring is likewise composed of eleven identical c-subunits.

To improve the initial model of the *F. nucleatum* c-ring structure after MR, iterative cycles of manual model building with Coot and refinement using Phenix were performed. First, the structure was refined without any kind of ion in the binding sites. After several cycles of model building and refining, the *F. nucleatum* c-ring model fits increasingly better with the experimental X-ray diffraction data of the protein, including the two distinct electron densities within the ion-binding sites, which may well indicate the presence of a Na^+ and a structural water molecule at these positions. Thus, sodium ions as well as the structural water molecules were modeled in all the eleven binding sites likewise in the c-ring of *I. tartaricus*. Further refinement was carried out using Refmac and resulted in a model structure exhibiting further improved overall quality in respect to the prior model without heteroatoms. This way, it was assured that the Na^+ as well as the water molecules indeed resulted from real electrons densities measured in the X-ray diffraction experiment but not from the crystallographic search model which was applied. In the end the solvent water and the detergent molecules were fitted in the remaining, until then unassigned densities, to complete the structure. Furthermore, the structure of the c-ring at pH 8.7 was built and refined as just described.

The quality of the two structures was assessed from their Ramachandran plots (figure 30) and R factors (R_{work} and R_{free}; table 45). A Ramachandran plot shows the distribution of the torsion angles φ and ϕ of all residues within a structure. A reliable structure model needs to have a very large part of residues within the preferred regions and only few in disallowed regions building the outliers (Kleywegt & Jones, 1996). The R factors indicate how well a final structure model actually fits to the initial experimental data obtained from the X-ray diffraction experiment. At high resolution a conventional R factor (R_{work}) below 0.25 generally indicates that a structure model is essentially correct (Branden & Jones, 1990). Besides, the R_{free} factor serves for cross-validation of the structural model measuring how well the model describes the experimental data which were not used to fit the model (Brunger, 1992). The difference between the two R factors should be quite small, i.e. it should not exceed 7 % (Kleywegt & Jones, 1995).

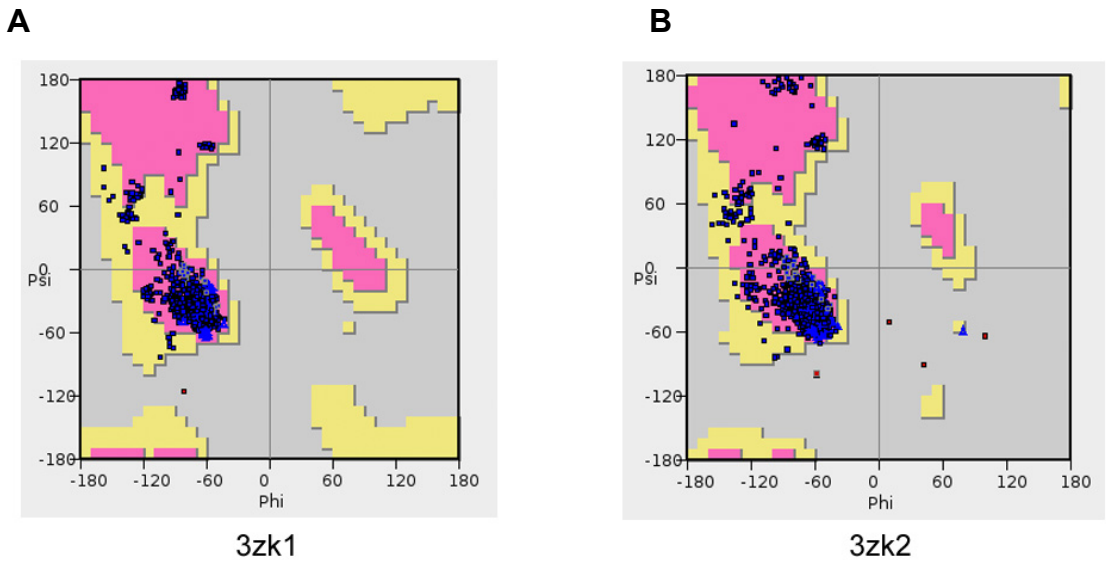

Figure 30. Ramachandran plots of the *F. nucleatum* c-ring structures.

(A) The plot shows that the structure solved at pH 5.3 (3zk1) has 98.17 % of the residues (1879 residues) in the most favoured regions, 1.78 % (34 residues) within the allowed regions and only 0.05 % (1 residue) outliers. **(B)** In the structure solved at pH 8.7 (3zk2) 97.34 % of the residues (1863 residues) are found in the most favoured regions, 2.5 % (46 residues) within the allowed regions and only 0.26 % (5 residues) are outliers in the plot.

Table 45. X-ray refinement statistics of the *F. nucleatum* c-ring structures

Refinement	c_{11}, pH 5.3	c_{11}, pH 8.7
Resolution (Å)	29.75-2.22	47.37-2.64
No. reflections	158181	92184
$^{\#}R_{work}$ / $^{\#}R_{free}$	19.93 / 23.08	18.46 / 23.64
No. atoms	14836	14537
Protein	13640	13639
Ligand	853	759
Water	321	117
B-factors	40.35	39.87
Protein	36.74	36.21
Ligand	96.20	106.34
Water	46.09	35.84
R.m.s. deviations		
Bond lengths (Å)	0.004	0.007
Bond angles (°)	0.854	1.038
Ligands^{+}	22 DMU, 3 LMT, 2 TAM, 22 Na^{+}	23 DMU, 22 Na^{+}

$^{+}$DMU: β-decyl-maltoside, LMT: β-dodecyl-maltoside, TAM: tris(hydroxymethyl)aminomethane.

The atomic coordinates and structure factors of the final *F. nucleatum* c_{11} rings were deposited in the Protein Data Bank (PDB) with the accession codes 3zk1 (pH 5.3) and 3zk2 (pH 8.7)

3.1.4.2 Overall structure of the *F. nucleatum* c-ring

The high-resolution X-ray structure of the *F. nucleatum* c-ring reveals that the complex consists of eleven identical c-subunits. Each subunit comprises two transmembrane α-helices connected by a short cytoplasmic loop. The shape of the ring resembles an hour glass with a hight of 68 Å being wider at the periplasmic termini and the cytoplasmic loop (52 Å) while the narrowest part is approximately in the middle of the membrane (40 Å), where the ion-binding sites are localized.
A structural model of the c-ring with the sodium ions and the water molecules bound at each interface of two adjacent c-subunits is shown as a cartoon in figure 31. This model describes the c-ring crystallized at pH 5.3 as well as at pH 8.7 since there was no difference in the outside appearance of the protein complex.

A

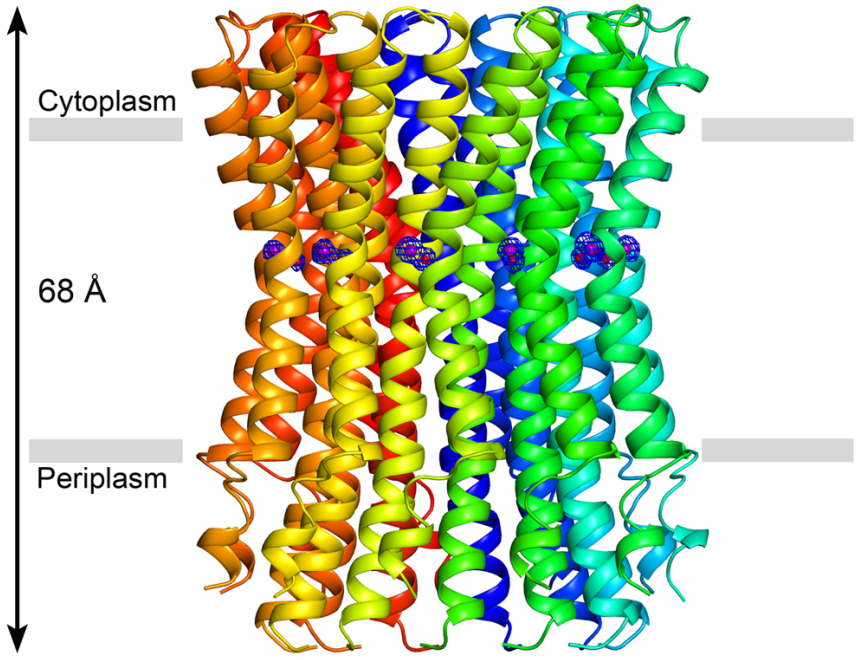

B

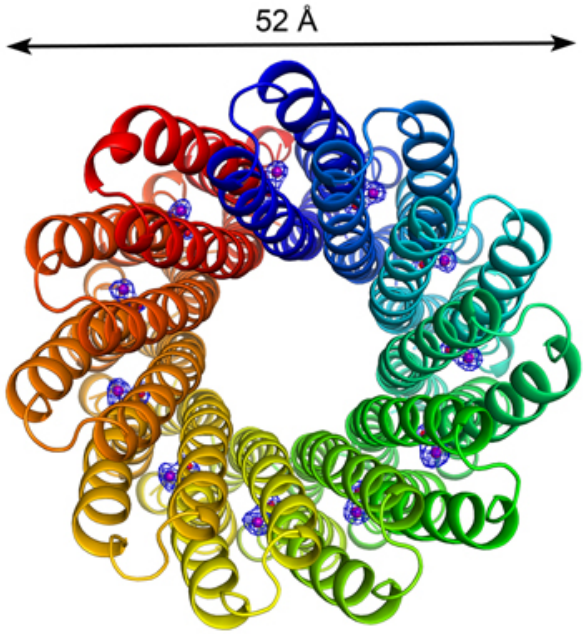

Figure 31. Crystal structure of the *F. nucleatum* c_{11} ring at 2.2 Å resolution.
(A) Side view of the c-ring, parallel to the membrane. Each c-subunit is shown in a different colour in ribbon representation. The eleven sodium ions and structural water molecules are shown as purple and red spheres, respectively and the membrane borders are drawn in grey bars. **(B)** View of the c-ring from the cytoplasmic side of the membrane. The F_{obs}-F_{calc} omit electron density maps for the Na^+ and H_2O within each binding site are given at 3.2σ (blue meshes). The figure was taken from (Schulz *et al*, 2013).

The transmembrane part of the protein, reaching from Y80 on the periplasmic side to S55 on the cytoplasmic side, is mainly build by hydrophobic residues whereas polar and charged residues can rather be found at the loop and the termini regions, which can be demonstrated by an electrostatic surface representation of the ring (figure 32).

A section through the c-ring shows the hydrophobic inner protein pore. At the periplasmic side, detergent molecules i.e. DDM molecules used during purification and DM molecules used for crystallization of the protein, are bound to the ring as *in vivo* a lipid plug presumably locks this inner-protein hole (figure 32 B). This observation is in line with previous studies showing that the inner pore of the c-ring is occupied by lipids forming a periplasmic plug (Meier *et al*, 2001).

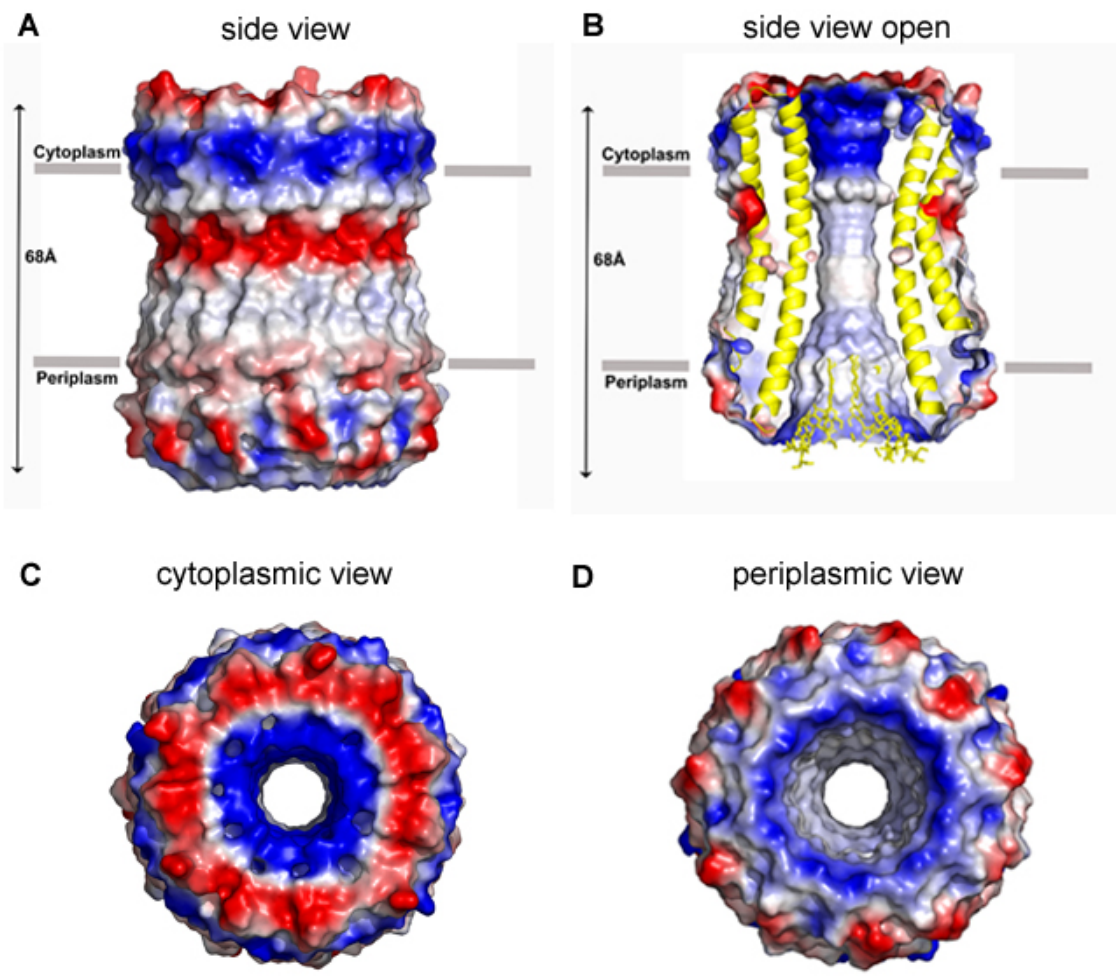

Figure 32. Electrostatic surface potential distribution of the *F. nucleatum* c-ring.
(A) Side view of the ring perpendicular to the membrane and **(B)** a section of it showing the hydrophobic inner pore and the detergent molecules (yellow) bound at the periplasmic entrance of the ring. Charged regions are mainly found in the cytoplasmic loop region and the periplasmic termini as indicated in red (negative) and blue (positive). The transmembrane region is mostly hydrophobic and uncharged as displayed in white between the membrane borders shown as grey bars. **(C)** Periplasmic and **(D)** cytoplasmic view of the c-ring. The figure was created with PyMol (DeLano, 2002).

To confirm that the two electron densities in all the ion-binding sites which have been assigned to be a sodium ion and a structural water molecule are not biased by the model applied for structure determination, an F_{obs}-F_{calc} omit electron density map was calculated. The map shows unambiguously that these distinct densities are originated from actual experimental data and are therefore unbiased (figure 33).

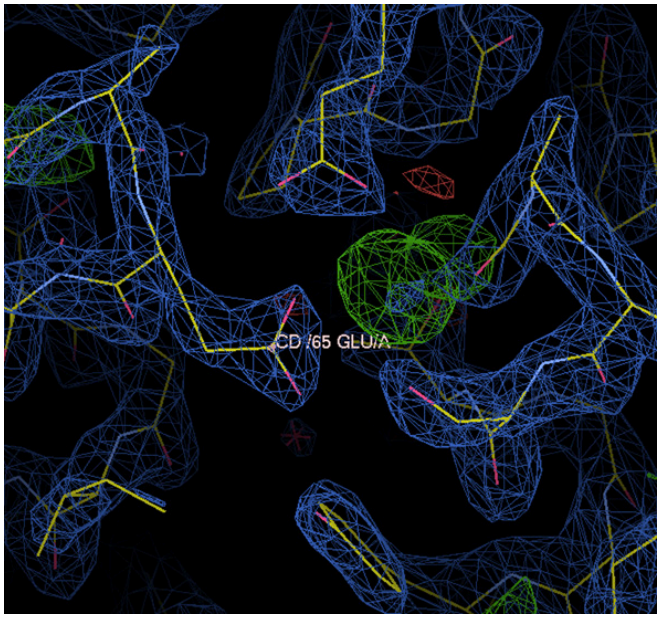

Figure 33. F_{obs}-F_{calc} omit electron density map for the Na^+ and H_2O of the *F. nucleatum* c-ring ion-binding site.

The Na^+ and H_2O in the binding site were withdrawn from the structural model and an omit map was calculated showing clear densities emerging at the same position. Glutamate 65 of chain A is shown representative for all binding sites in the c-ring.

3.1.4.3 The ion-binding site of the *F. nucleatum* c-ring

The actual arrangement of all residues building the ion-binding site and the particular involvement of each of them in ion-coordination was of main interest. The binding sites are localized approximately in the middle of the membrane where the helices sharply kink outwards (figure 31). Each of the eleven binding sites is formed by the N- and C-terminal helix of one subunit (green in figure 34) and the C-terminal helix of the adjacent c-subunit (yellow in figure 34).

A close up of the site at pH 5.3 shows the tight coordination of the Na^+ by five ligands including a structural water molecule (figure 35 A). A highly conserved acidic residue (E or D, E65 here) in the C-terminal helix is part of the binding site in all c-rings described so far. In case of the *F. nucleatum* c-ring, a second glutamate (E32) is present in the N-teminal helix of the same c-subunit coming in close spatial proximity to the conserved one (E65) as the two helices are forming a hairpin in the ring. While one side chain oxygen of E32 (Oε1) is coordinating the Na^+, the other one (Oε2) is building a hydrogen network to one side chain oxygen of E65 (Oε1) which in turn is

also coordinating the Na^+. This key glutamate residue further hydrogen bonds with S66 and T70 of the neighbouring c-subunit creating a very tight coordination network. Further, the backbone carbonyl oxygen of V63 and the side chain oxygen of S66 in the C-terminal helix of the adjacent c-subunit are involved in Na^+-binding. As a fifth ligand, a structural water molecule is binding the Na^+, while itself being coordinated by the side chain oxygen of T67 and the backbone oxygen of A64 of the neighbouring c-subunit. The distance between the two side chain oxygens of the glutamate residues which build a hydrogen bond with each other is ~ 2.7 Å. Thus, a proton is supposed to be bound between the two glutamate side chains which means that a second ion is present within the binding site. This is further supported by free-energy calculations performed with the c-ring (Schulz *et al*, 2013). The constellation described here represents the stable, ion-locked conformation of the binding site, as it occurs in the hydrophobic core of the membrane during Na^+-translocation.

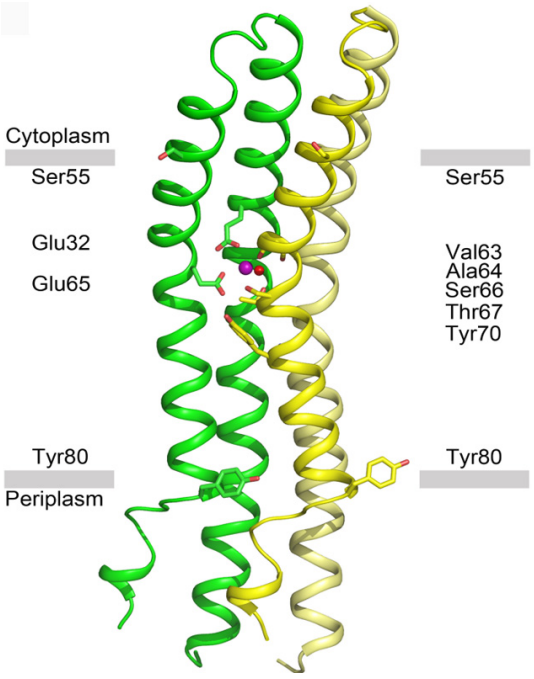

Figure 34. Overview of the ion-binding unit of the *F. nucleatum* c-ring.

The N- (inner) and C- (outer) terminal helices forming one c-subunit (green) as well as the C-terminal helix of the adjacent subunit (yellow) are building the ion-binding site. All residues involved in Na^+ binding are displayed as sticks and labeled on the left and right side at the corresponding height of the helices. The Na^+ and the structural water molecule are shown as purple and red spheres, respectively. The membrane borders are displayed as grey bars. The figure was taken from (Schulz *et al*, 2013).

To investigate the influence of the external pH on the protonation and conformational state of the ion-binding site, the c-ring was also crystallized at pH 8.7. A comparison of the binding sites in both structures (pH 5.3 and 8.7) reveals that there are neither prominent conformational changes nor alterations in the protonation state induced by the pH shift (figure 35 B). This is in good agreement with previous studies showing that the detergents used for crystallization uncouple the binding sites from the pH and Na^+-concentration just like the lipid membrane does under native conditions during c-ring rotation to allow protonation and deprotonation events only in a more hydrohpilic environment like in the a/c-ring interface (Pogoryelov *et al*, 2010; Preiss *et al*, 2013; Symersky *et al*, 2012). The results obtained here confirm that this is a quite general feature of c-rings. Thus, the structure solved at pH 8.7 represents likewise the c-ring in the ion-locked conformation of E65 while two ions, a Na^+ and a proton are concurrently bound within the same binding site (figure 35 B).

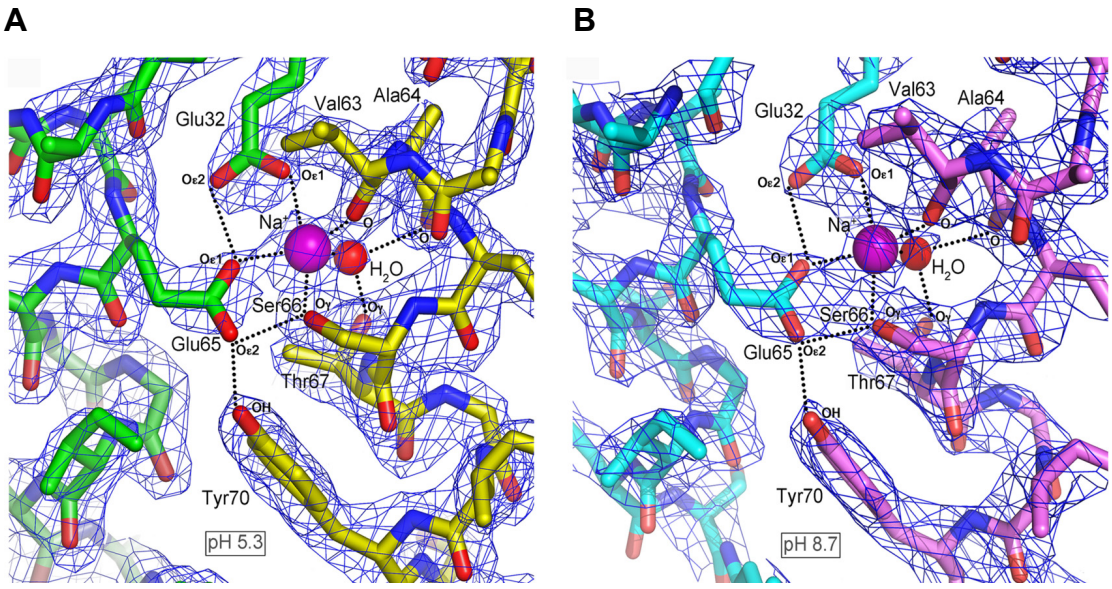

Figure 35. Close-up of the Na^+-binding site of the *F. nucleatum* c-ring at pH 5.3 and pH 8.7.
The binding sites at 2.2 Å (pH 5.3) and 2.64 Å (pH 8.7) are displayed from the membrane plane showing the Na^+ and structural water molecule as purple and red spheres, respectively, bound in a tight coordination network. All residues involved in Na^+-coordination are labeled. Hydrogen bonds and ion-protein interactions are indicated with dashed lines. The conserved key glutamate (E65) side chain is shown in the stable, ion-locked conformation whereas the second glutamate (E32) is protonated at both pH. The $2F_{obs}$-F_{calc} electron density maps are given at 1.9 σ. The figure was taken from (Schulz *et al*, 2013).

The structure of the *F. nucleatum* c-ring shows the precise coordination of the Na^+ in the ion-binding site as well as the presence of an additional proton being present. The exact position of the proton, i.e. if it is bound at E65, E32 or shared between both, however, can not be determined from the X-ray data. Nevertheless, MD simulations and free energy calculations revealed that most probably the proton is bound to E32 (Schulz *et al*, 2013). All inter-atomic distances in the ion-binding sites of the solved structures as well as in the model created for simulations and free energy calculations are listed in table 49. Apparently the respective distances do not differ considerably.

Table 46. Inter-atomic distances in the Na^+-binding sites of the *F. nucleatum* c-ring at pH 5.3 and pH 8.7 and in the MD simulation

From	To	Distance (Å] pH 5.3	Distance (Å] pH 8.7	Distance (Å] simulation
Na^+	Glu^{32} Oε1	2.35 +/- 0.07	2.40 +/- 0.13	2.33 +/- 0.14
Na^+	Val^{63} O	2.33 +/- 0.08	2.36 +/- 0.09	2.33 +/- 0.13
Na^+	Glu^{65} Oε1	2.37 +/- 0.06	2.43 +/- 0.07	2.19 +/- 0.08
Na^+	Ser^{66} Oβ	2.32 +/- 0.07	2.30 +/- 0.08	2.32 +/- 0.09
Na^+	HOH	2.44 +/- 0.10	2.46 +/- 0.09	2.31 +/- 0.10
HOH	Ala^{64} O	2.61 +/- 0.12	2.65 +/- 0.17	2.27 +/- 0.12
HOH	Thr^{67} Og	2.69 +/- 0.15	2.77 +/- 0.19	2.82 +/- 0.13
Glu^{65} Oε1	Glu^{32} Oε2	2.66 +/- 0.06	2.67 +/- 0.09	2.60 +/- 0.08
Glu^{65} Oε2	Tyr^{70} OH	2.72 +/- 0.10	2.81 +/- 0.10	2.74 +/- 0.19
Glu^{65} Oε2	Ser^{66} Oβ	2.52 +/- 0.09	2.55 +/- 0.14	2.73 +/- 0.18

3.1.4.4 Ion translocation in the *F. nucleatum* ATP synthase

At this point it is not clear whether the second ion in the bindings site, the proton at E32, can also be transported during enzyme operation (two-carboxylate-motif, see chapter 1.3.4.1). As seen in previous studies (Pogoryelov *et al*, 2010; Symersky *et al*, 2012) the conformational change of the key glutamate going along with ion release is

induced by the direct environment of the binding site, i.e. upon reaching a more hydrophilic region as in the a/c-ring interface.

To investigate the probability of the proton to be released from E32 in the a/c-ring interface, an idealized structural model of the c-ring in this hydrohpilic environment was created and the pKa of E32 was re-calculated in this open conformation of E65. The results revealed that deprotonation of E32 remains very unlikely even when the environment has changed (Schulz *et al*, 2013).

Besides, ACMA-quenching experiments with the *F. nucleatum* ATP synthase in native membranes were performed in collaboration with the group of Prof. Dr. Gregory M. Cook and carried out by Dr. Marina Iglesias-Cans (Otago School of Medical Science, Dunedin, New Zealand). The results showed no proton co-transport under conditions where the enzyme is active in ATP hydrolysis mode, i.e. in the presence of up to 10 mM NaCl (Schulz *et al*, 2013).

In the first part of this PhD thesis, the rotor ring of the *F. nucleatum* F_1F_o ATP synthase was biochemically and structurally investigated. The c-ring was expressed heterologously within a hybrid ATP synthase and successfully purified from the enzyme in crystallization quality. It could be shown that the detergent-solubilized protein complex is Na^+-specific as NaCl prevents modification of the ring with the fluorescent ATP synthase inhibitor NCD-4. These results are in good agreement to which was previously expected as the *F. nucleatum* c-subunit carries a full set of Na^+-binding ligands. Two high resolution structures of the c-ring, solved at low and high pH, confirmed the Na^+-specificity. The Na^+-binding signature of the *F. nucleatum* c-subunit has not been structurally described before. Our results present the exact Na^+-coordination which involves the two-carboxylate-motif including residues E32 and E65. We conclude that one of these glutamate residues (E32) has to be constitutively protonated for tight Na^+-coordination in the amino acid network. In addition, MD simulations (see figure 80, 4.1.4) confirmed our findings that the Na^+ is the only translocated ion during enzyme operation, whereas the H^+ bound to E32 is a structural feature of the c-ring ion-binding site (Schulz *et al*, 2013).

3.2 The N-type ATPases of *Burkholderia* species

3.2.1 mRNA transcription analysis of the N-*atp* operon in *B. thailandensis* cells

As introduced in chapter 1.2, a new (N-) type of rotary ATPase was proposed based on an *in silico* study, which showed the genotypic existence of the N-*atp* operon in different, phylogenetically diverse bacteria (Dibrova *et al*, 2010). Nevertheless, the physiological function or even its phenotypic existence still remains to be elucidated. In order to prove the latter for the N-ATPase in *B. thailandensis* cells, the first goal in this part of the work was to check whether the transcription of the N-*atp* operon could be identified by R(everse)T(ranscription)-PCR in isolated total-RNA from the corresponding organism. More specifically, primer pairs were designed to amplify all the genes encoding for the N-ATPase subunits (figure 36).

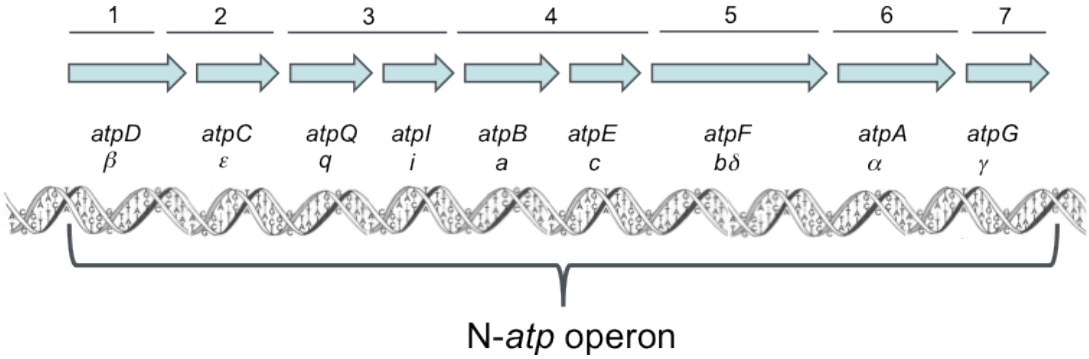

Figure 36. Schematic representation of the N-*atp* operon of *B. thailandensis* and regions amplified by R(everse)-T(ranscription)-PCR.

All *atp* genes are displayed by arrows with the particular lengths reflecting the actual lengths of the corresponding genes. The gene names (*atpD-atpG*) and the proteins they are encoding for (β-γ), are annotated below the respective arrows. The operon (6974 bp) was amplified in seven fragments (1-7), as indicated by the lines and numbers above the arrows, whereby specific primer pairs were designed for each amplification reaction.

Prior to use the designed primer pairs for the RT-PCR, their specificity was tested by performing PCR using isolated genomic DNA from *B. thailandensis* as a template. In addition, different PCR conditions were tested as the GC-content of the *B. thailandensis* genome and the N-*atp* operon (70 %) is very high. The reaction could be successfully perfomed by using a polymerase (Extender polymerase, 5 Prime) designed for the amplification of long and GC-rich nucleotide sequences and the

addition of an PCR combinatorial enhancer solution (CES (Ralser *et al*, 2006); see chapter 2.2.1).

Three primer pairs were chosen for the specific amplification of parts of the N-*atp* operon as well as to amplify the gene encoding for the glyceraldehyde-3-phosphate-dehydrogenase (GAPDH) which was frequently used as a control in previous gene expression studies (Fujisaki *et al*, 1995; Sheng *et al*, 1997; Wollert *et al*, 1996) although other investigations showed that its usage as a normaliser is critical because GAPDH mRNA levels are not always constant in a cell (Zhu *et al*, 2001). However, in our case, the amplification of the GAPDH gene served only to assess functionality of the RT-PCR and not to normalize patterns of gene expression. This approach is suitable here as the RNA encoding GAPDH is ubiquitously expressed and moderately abundant in different cells (Bustin, 2000a; Winer *et al*, 1999).

All the PCR products were analyzed by agarose gelelectrophoresis and showed the correct fragment sizes (figure 37). This result confirmed that the designed primer pairs meet the requirements for the specific amplification reactions.

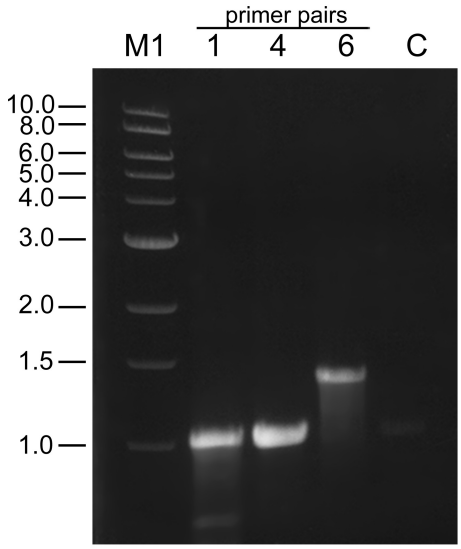

Figure 37. PCR to test primer pairs for the amplification of the N-*atp* operon of *B. thailandensis* from genomic DNA.

Isolated genomic DNA of *B. thailandensis* was used as a template and three primer pairs (1, 4, 6) were chosen for PCR. Specific products were obtained in each case showing the correct fragments (1: 981 bp, 4: 974 bp, 6: 1287 bp) by agarose-gelelectrophoresis. A primer pair for the amplification of the gene encoding for the glyceraldehyde-3-phosphate dehydrogenase (GAPDH) was used as a positive control (C: 977 bp). M1: 1 kb marker, NEB.

As in bacteria transcription and translation is not spatially separated in different compartments, both processes often occur simultaneously (Miller *et al*, 1970). This indicates that the existence of a certain transcript often implies biosynthesis of the corresponding protein. Figure 38 shows the result of the RT-PCR. Six out of seven products could be obtained with the synthesized cDNA as a template, indicating that the N-*atp* operon is actually transcribed. Besides, as all genes within an operon are controlled by the same promotor and terminator, only one polycistronic mRNA is transcribed. One can conclude from this experiment that, presumably, the presence of this polycistronic mRNA leads to a constitutive production of the N-ATPase in these bacterial cells.

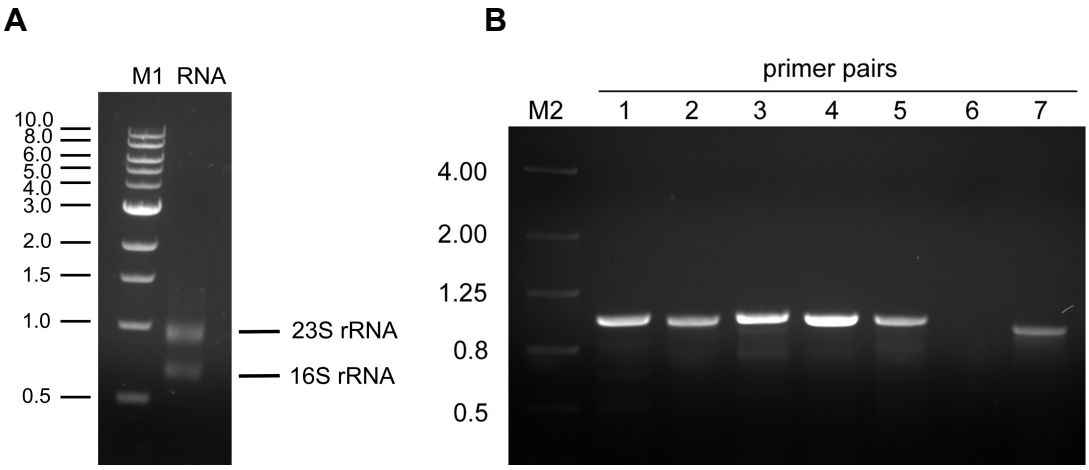

Figure 38. Isolated total-RNA and RT-PCR of the entire N-*atp* operon of *B. thailandensis.*
(A) The quality of the isolated total-RNA was analyzed and judged by agarose gelelectrophoresis. The gel shows the 23S rRNA and the 16S rRNA while the 5S rRNA is not visible. **(B)** Products of RT-PCR using cDNA as a template and primer pairs to amplify all seven fragments forming together the complete N-*atp* operon. Six out of seven products were obtained (1: 981 bp, 2: 966 bp, 3: 980 bp, 4: 974 bp, 5: 960 bp, 7: 912 bp). M1: 1 kb marker, NEB, M2: 4 kb marker, Lonza.

3.2.2 Purification of the N-type ATPase from *B. thailandensis* cells

The result obtained from the RT-PCR experiment (figure 38) showed the transcription of the N-*atp* operon and with it, presumably, the production of the N-ATPase in *B. thailandensis* cells under aerobic growth conditions. The next point to be adressed was to isolate this enzyme for its characterization.

Cells were again grown under the same conditions in order to try to isolate the N-ATPase from these cells. So far, an isolation protocol for such an ATPase is not available but the past decades of ATP synthase research yielded a variety of protocols for the isolation and purification of F-type ATP synthases. A selection of these protocols was taken as a basis for purification trials of the yet uncharacterized N-type complex. Following the purification of the N-ATPase was not straightforward as there was no activity of the enzyme detectable (not shown). Often protein purification is followed by the use of either a specific antibody against the protein itself or against an affinity-tag which has been genetically fused to the corresponding gene. However, there was neither a specific antibody available for the detection of the N-ATPase nor has the corresponding *atp* operon been genetically modified. Thus, protein purification steps as previously successfully performed for the isolation of F- ATP synthases were carried out and the obtained proteins were subsequently analyzed by SDS-PAGE. The molecular masses of the proteins detected on the gel were compared to the expected molecular masses of both, the N- and the F-type ATPases (figure 39).

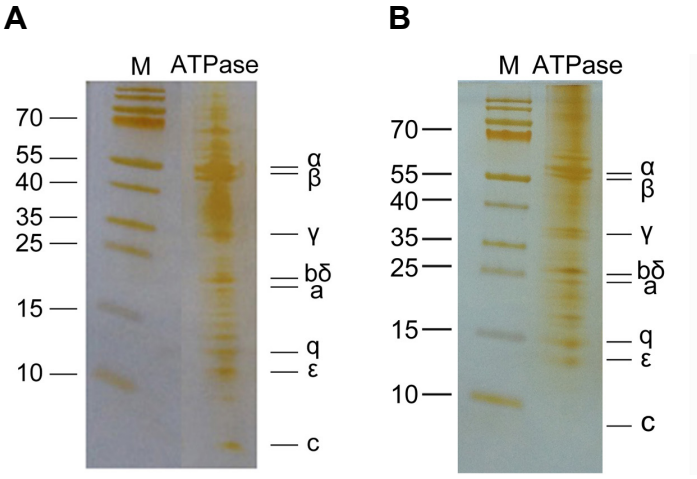

C

ATPase subunits	N-ATPase	F-ATPase
α	58.5 kDa	55.9 kDa
β	53.3 kDa	50.6 kDa
γ	29.9 kDa	31.9 kDa
bδ	26.6 kDa	-
b	-	17.1 kDa
δ	-	18.9 kDa
a	24.5 kDa	30.8 kDa
q	17.3 kDa	-
ε	16.6 kDa	14.9 kDa
r	9.9 kDa	-
c	8.5 kDa	9.1 kDa

Figure 39. Purification trial of the *B. thailandensis* N-ATPase and the theoretical molecular masses of its N-and F-type ATPase subunits.

(A) Membranes after DDM-solubilization and $(NH_4)_2SO_4$ precipitation. **(B)** Pellet after PEG_{6000} precipitation. Distinct ATPase subunits are labeled on the right side of the gel according to the expected molecular masses of the N-*atp* subunits. Subunit r is not marked as it is ambiguous whether it is a structural subunit of the enzyme. **(C)** The calculated theoretical molecular masses of the *B. thailandensis* N- and F-ATPase subunits. It needs to be noted at this point that it can not be stated whether the isolated complex resembles the N- or the F-type ATPase as protein bands visibile could be attributed to both types of enzymes.

The expression and purification procedure yielding all putative ATP (synth)ase subunits as shown by SDS-PAGE, is summarized in the following: *B. thailandensis* cells were grown (2.3.2), disrupted (2.3.4.1) and membranes were prepared (2.3.4.2). Afer solubilization (2.3.4.3), contaminating proteins were first precipitated with 30 % $(NH4)_2$ SO_4 before the ATPase was precipitated with 65 % $(NH4)_2$ SO_4 (2.3.4.5) (figure 39 A).The protein was further purified and concentrated by precipitation with 12 % PEG_{6000} (2.3.4.10) (figure 39 B).

The sample was then loaded on a MonoQ anion exchange chromatography column using an Äkta Purifier System. The sample was loaded with a flow rate of 0.3 ml/min on the equilibrated column. It was washed with two column volumes of buffer before proteins were eluted with a continuous gradient from 0 to 1 M NaCl over 20 column volumes. ATP synthase started eluting with 280 mM NaCl and the corresponding fractions, as identified by SDS-PAGE, were pooled (figure 40).

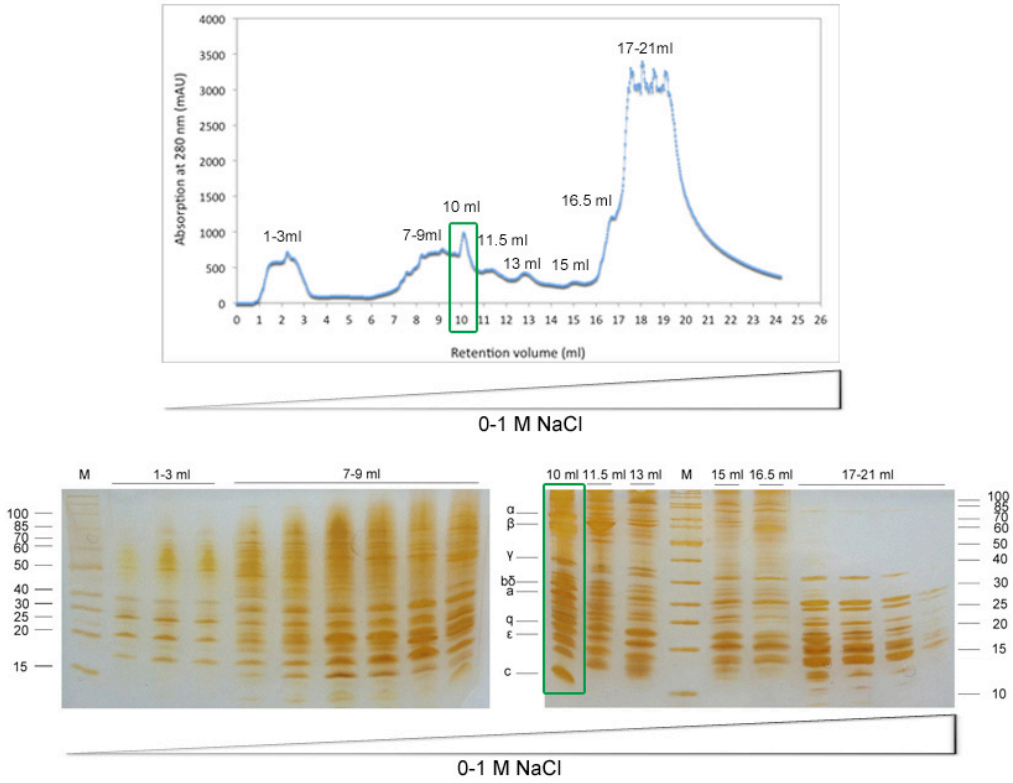

Figure 40. Anion exchange chromatography (MonoQ) of the precipitated *B. thailandendensis* ATPase and SDS-PAGE of the corresponding MonoQ-fractions.

The ATPase sample after $(NH_4)_2SO_4$ and PEG_{6000} precipitation was loaded on a MonoQ column and proteins were separated within a continuous NaCl-gradient (0-1M NaCl) over 20 CV. The ATPase eluted with 280 mM NaCl concentration (10 ml peak).

ATPase containing MonoQ fractions (boxed in figure 36) were further loaded on a Superose 6 column performing size exclusion chromatography (SEC) using an Äkta Purifier System with a constant flow rate of 0.3 ml/min. The 2 ml fraction of ATPase eluted at 11-13 ml corresponding to a protein complex between 550 and 780 kDa (figure 41), which was confirmed by SDS-PAGE. Besides, the SDS gel revealed that the elutions at 14-17 ml as well as at 19-23 ml did not contain ATPase subunits but co-purified *B. thailandensis* proteins (not shown), which were not further analyzed.

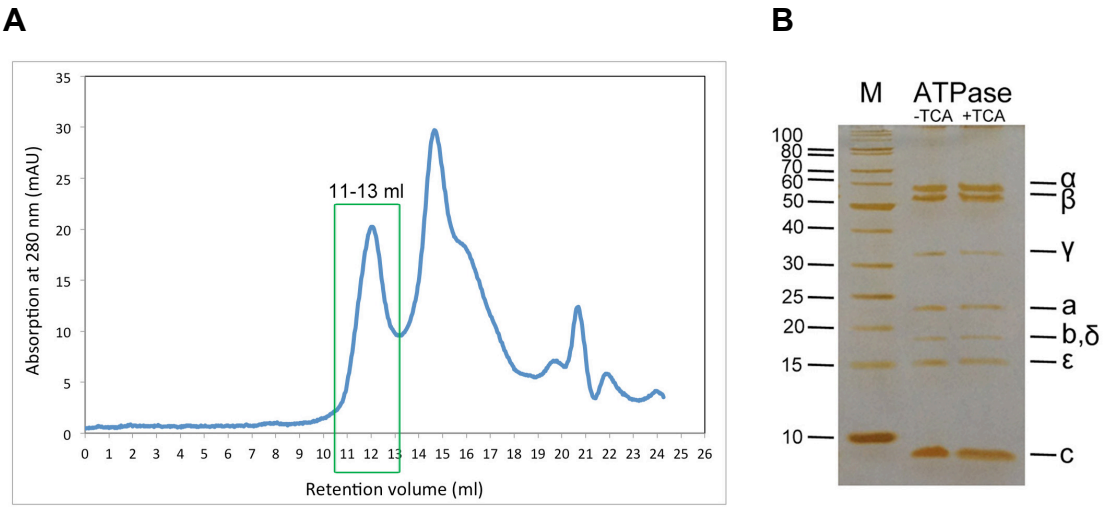

Figure 41. Size exclusion chromatography of the *B. thailandensis* ATPase and silver-stained SDS-PAGE of the ATPase containing fractions.

(A) The SEC-profile indicates that the ATPase sample loaded on a Superose 6 10/300 column was not pure, although some residual contaminations could be separated from other proteins. The ATPase eluted with a retention volume of 11-13 ml. This was confirmed by SDS-PAGE **(B)** showing the presence of all ATPase subunits as indicated on the right side. A protein band at the expected molecular mass of a c-subunit (N-type: 8.5 kDa, F-type: 9.1 kDa) is visible on the gel independent of the addition of trichloroacetid acid (TCA) to the enzyme, which precipitates a c ring into its subunits, indicating that the c-ring of the purified ATPase is SDS-unstable.

3.2.3 Identification of ATPase-subunits by ESI-MS peptide mass fingerprint

To identify the purified proteins, the sample was loaded on a SDS-gel, stained with Coomassie Brilliant Blue and all seven protein bands visible in figure 41 were cut out for tryptic digestion (with trypsin or chymotrypsin). ESI-MS peptide mass fingerprint identified subunits α, β, γ and ε of the F-ATP synthase of *B. thailandensis* (figure 42).

F-type ATPase α-subunit (513 aa, 55911.81 Da) : 77 % sequence matched

```
  1 MQLNPSEISELIKSRIQGLEASADVRNQGTVISVTDGIVRIHGLSDVMQG
 51 EMLEFPGNTFGLALNLERDSVGAVILGEYEHISEGDIVKTTGRILEVPVG
101 PELVGRVVDALGNPIDGKGPVNAKLTDAIEKIAPGVIWRKSVSQPVQTGL
151 KSIDSMVPIGRGQRELIIGDRQCGKTAVAIDTIINQKGKDLICIYVAIGQ
201 KASSIMNVVRKLEETGALEYTIVVAASASESAAMQYLAPYAGCTMGEYFR
251 DRGQDALIIYDDLTKQAWAYRQISLLLRRPPGREAYPGDVFYLHSRLLER
301 AARVSEEYVEKFTNGEVKGKSGSLTALPVIETQAGDVTAFVPTNVISITD
351 GQIFLETDLFNAGIRPAINAGVSVSRVGGAAQTKVVKKLSGGIRTDLAQY
401 RELAAFAQFASDLDEATRKQLERGRRVTELLKQPQYQPLQVWELAVSLFS
451 ANNGYLDDLDVKDVLPFEKGLREYLKTSHADLIKRIEDTKDLSKDDESAL
501 HAALKDFKKSGAY
```

F-type ATPase β-subunit (464 aa, 50623.01 Da) : 91 % sequence matched

```
  1 MSTAALVEGKIVQCIGAVIDVEFPRESMPKIYDALILEGSELTLEVQQQL
 51 GDGVVRTICLGASDGLRRGVVVKNTGNPISVPVGKPTLGRIMDVLGRPID
101 EAGPIESENKRSIHQKAPAFDELSPSTELLETGIKVIDLICPFAKGGKVG
151 LFGGAGVGKTVNMMELINNIAKEHGGYSVFAGVGERTREGNDFYHEMKDS
201 NVLDKVALVYGQMNEPPGNRLRVALTGLTMAEHFRDEGLDVLFFVDNIYR
251 FTLAGTEVSALLGRMPSAVGYQPTLAEEMGKLQERITSTKKGSITSVQAV
301 YVPADDLTDPSPATTFGHLDATVVLSRDIASLGIYPAVDPLDSTSRQIDP
351 NVIGEEHYSITRRVQQTLQRYKELRDIIAILGMDELSPEDKLSVARARKI
401 QRFLSQPFHVAEVFTGSPGKYVPLKETIRGFKMIVDGECDHLPEQAFYMV
451 GTIDEAFEKAKKIQ
```

F-type ATPase γ-subunit (291 aa, 31899.78 Da) : 63 % sequence matched

```
  1 MAGMKEIRGKIKSVQNTRKITKAMEMVAASKMRRAQERMRAARPYAEKVR
 51 AIAAHMSRANPEYRHPFMVANEGVKTAGMILVTTDKGLCGGLNTNVLRAS
101 LQKFKELEEKGQKVEATAIGGKGLGFLNRFGAKVISQVVHLGDTPHLDKL
151 IGAVKTQLDLYSEGRLSAVYLAYTRFVNTMKQETVIEQLLPLSSEHFDAN
201 DGTPATSWDYIYEPDAQAVVDELLVRYVEALVYQAVAENMASEQSARMVA
251 MKAASDNAKTVISELQLSYNKSRQAAITKELSEIVGGAAAV
```

F-type ATPase ε-subunit (141 aa, 14926.09 Da) : 51 % sequence matched

```
  1 MATIKVDVVSAEEQIFSGLAKFVALPGEAGELGILPGHTPLITRIRPGAV
 51 RIEAESGDEEFVFVAGGILEVQPGAVTVLADTAIRGKDLDAAKAEEARKR
101 AEETLQNAKSDIDLAKAQSELATAMAQLEAIQRLAKIRGRH
```

Figure 42. ESI-MS peptide mass fingerprint of the purified ATPase complex identifying subunits α, β, γ and ε of the F-type ATP synthase of *B. thailandensis*.

Proteins extracted from the SDS-polyacrylamide gel (figure 37) were digested with trypsin and chymotrypsin. Amino acid residues matching to the sequences of the corresponding *B. thailandensis* F-type ATP synthase subunits (www.ncbi.nlm.nih.gov/protein) are highlighted in green. The measurement was carried out by Dr. Julian Langer (Molecular Membrane Biology, Max-Planck-Institute of Biophysics, Frankfurt).

Subunits a, b, δ and c could not be identified. This might be due to a lower abundance of these proteins in the sampe or because of a lower stability of these subunits.

3.2.4 ATP hydrolysis activity

To determine whether the purified F-type ATP synthase of *B. thailandensis* is active, the hydrolytic activity of the enzyme was determined indirectly by measuring photometrically the decreasing absorption of NADH at 40°C which is oxidized upon ATP hydrolyis. 2.5 µg of purified F_1F_o ATP synthase in 20 mM Tris/HCl pH 8.0 and 1 % DDM were used for measurements.

Initial measurements revealed only low activity of the enzyme (0.14-0.18 U/mg) in comparison to previously reported ATPase activities, as for example of the *Ilyobacter tartaricus* enzyme (1.28 U/mg) (Neumann *et al*, 1998) or the *E. coli* ATP synthase (1.9 U/mg) (Ishmukhametov *et al*, 2005). Former studies have also shown that different chemical compounds can influence the ATPase activity. Trypsin and methanol have a stimulating effect on the mycobacterial ATPase activity (Haagsma *et al*, 2010; Nakagawa *et al*, 1977), LDAO was used for activating the *Caldalkalibacillus thermarum* sp. strain TA2.A1 enzyme (Cook *et al*, 2003) while $NaSO_3$ and $CaCl_2$ stimulate the hydrolytic ATPase activity of the *Thermus thermophilus* (Yokoyama *et al*, 1990) and *Strepococcus lividans* ATPase (Hensel *et al*, 1991).

To investigate the potential impact of these components on the *B. thailandensis* ATPase activity, the chemicals were either preincubated with the enzyme or added during the measurement. The addition of 0.5-1.0 mg trypsin (from a 10 mg/ml stock solution in water) was found to have an immediate stimulating effect on the ATPase activity (1.36-1.61 U/mg).

Dicyclohexylcarbodiimide (DCCD) has been described to specifically react with the conserved carboxylic residue (glutamate or aspartate) within the ion-binding site of the F_o rotor ring thereby inhibiting the ion translocation (Hoppe & Sebald, 1980; Sebald *et al*, 1980). ATP hydrolysis in the F_1-subcomplex of the enzyme, however, is only effected if both parts of the enzyme are tightly coupled. In a further experiment,

500 µM DCCD (from a 10 mM stock solution in 100 % ethanol) were preincubated with the *B. thailandensis* ATP synthase sample leading to an inhibition of ATPase activity by 30-50 % (0.09 U/mg instead of 0.14-0.18 U/mg).

Besides, the F_1 ATPase inhibitor tributylin chloride (TBT-Cl) (von Ballmoos *et al*, 2004) was tested for its inhibitory effect on the *B. thailandensis* enzyme. Therfore, 2 µM TBT-Cl (from a 2 mg/ml stock solution in 100 % Ethanol) were added to the ATP synthase sample. TBT-Cl caused an inhibition of the ATPase activity by 50 % (0.41 U/mg instead of 0.81 U/mg after trypsin activation).
All results are summarized in figure 43 and table 50.

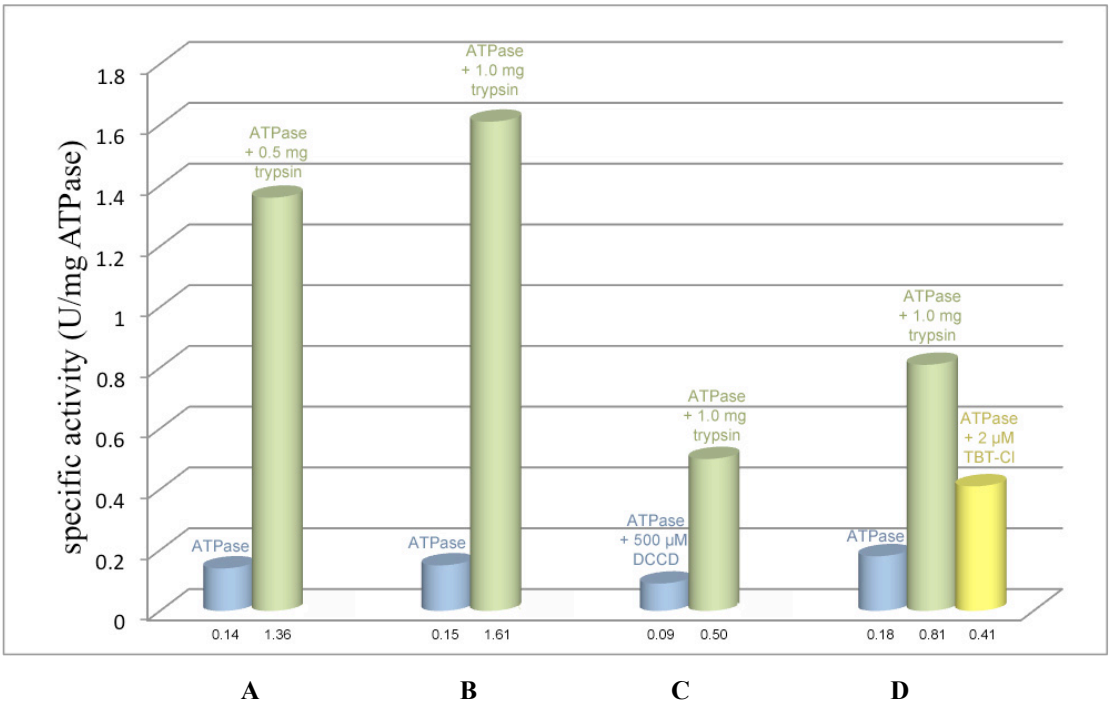

Figure 43. ATP hydrolysis activity of the *B. thailandensis* F_1F_o ATP synthase in dependency of the activator trypsin and the inhibitors DCCD and TBT-Cl.
(A) The ATPase activity without the addition of any chemical compound (blue) and with 0.5 mg trypsin (green). **(B)** The activity of the enzyme without the addition of any chemical compound (blue) and with 1.0 mg trypsin (green). **(C)** The ATPase activity preincubated with 500 µM DCCD (blue) and with 1.0 mg trypsin (green). **(D)** The activity of the enzyme without the addition of any chemical compound (blue), with 1.0 mg trypsin (green) and with 2 µM TBT-Cl (yellow). The activities are given in U/mg below the corresponding bars.

Table 47. ATP hydrolysis activity of the purified *B. thailandensis* F_1F_o ATP synthase

Activity (U/mg) w/o trypsin	Activity (U/mg) with trypsin	Activation by trypsin
0.14	+ 0.5 mg trypsin: **1.36**	9.7 x
0.15	+ 1.0 mg trypsin: **1.61**	10.7 x
preincubated with 500 µM DCCD: **0.09**	+ 1.0 mg trypsin: **0.50**	5.5 x
0.18	1.0 mg trypsin: **0.81** +2 µM TBT-Cl: **0.41**	4.5 x (50 %)

The first experiments (chapters 3.2.1-3.2.4) carried out to investigate the not yet characterized N-type ATPase revealed that the corresponding N-*atp* operon is actually transcribed in *B. thailandensis* cells. Purification of the N-type complex from these cells was not successful when a selection of protocols established for the purification of F-type ATP synthases was applied. However, a protocol was developed for the isolation of the F_1F_o ATP synthase of *B. thailandenis.* ATP hydrolysis activity measurements showed a low basis activity of the purified enzyme which could be further stimulated by the addition of 0.5-1.0 mg trypsin.

In order to also analyze the N-type ATPase of *Burkholderia,* the complete *atp* operon of *B. pseudomallei* was subsequently cloned into a vector for the heterologous over-expression of this enzyme (see chapter 3.2.5).

3.2.5 Heterologous expression of the *B. pseudomallei* N-ATPase in *E. coli*

For the heterologous expression of the complete N-*atp* operon (figure 36) of *B. pseudomallei* in *E. coli*, it was amplified by PCR using its genomic DNA as a template. As the operon has a large size of about 7.3 kb the likelihood of the occurrences of unwanted mutations during natural replication is increased. Furthermore, the operon has a very high GC-content of 74 %, which further enhances the probability of the incorporation of unwanted mutations during PCR procedures. Therefore, four reactions were carried out to obtain smaller fragments of 1.5 to 2.1 kb, which were initially cloned blunt into a pJET1.2 vector. In addition, PCR was performed with an Extender polymerase (5Prime) designed for the amplification of long and GC-rich nucleotide sequences and the reaction mixture was supplemented by

a PCR combinatorial enhancer solution (CES) (Ralser *et al*, 2006). Afterwards, each two of the four fragments were first ligated together. Finally, the resulting larger two fragments were ligated into a $pBAD_{HisB}$ expression vector to rebuild the complete N-*atp* operon. The vector created thereby has a size of about 11.4 kb and carries an N-terminal His_6-tag which, after expression, is then fused to the β-subunit of the enzyme, being encoded by the first gene (*atpD)* of the operon (see Appendix for a plamid map).

To clarify whether the N-*atp* operon can be heterologously expressed in *E. coli* and if so, which expression conditions are most successful, different *E. coli* strains, media and expression conditions were tested, including growth temperature, induction times as well as the amount of arabinose used for induction. Western Blot analysis with *E. coli* cell extracts was performed using an anti-His antibody to detect the His-tagged β-subunit of the enzyme after successful expression of the N-*atp* operon. A representative Western Blot analysis of *E. coli* TOP 10 cells before and after protein induction in different media (2YT, TB and LB) is shown in figure 40 A. A protein band migrating on the expected level of the His-tagged β-subunit (54.1 kDa) is visible on the blot after induction whereas it can not be found before inducing the expression. The purified F_1F_o ATP synthase of *I. tartaricus* also containing a His-Tag on the β-subunit (51.6 kDa) was used as a control (Oberfeld, 2006). The N-type β-subunit of *B. pseudomallei* is migrating slightly higher on the SDS-gel as the F-type β-subunit of *I. tartaricus*, just as expected from their molecular masses. However, there are additional slower migrating protein bands detectable, indicating that the N-type β-subunit is presumably degraded in *E. coli* resulting in smaller protein fragments still carrying the His-tag.

To isolate the N-ATPase from *E. coli* membranes, solubilization tests were performed using different detergents in different concentrations to extract the enzyme. Figure 44 B shows a Western Blot analysis of the extraction with four selected detergents (1 % of DDM, Triton-X-100, DM or OG).

There was no difference in efficiency of extracting the enzyme from membranes, but in all cases, the detection of smaller tagged fragments again indicated the possible degradation of the ATPase β-subunit (arrows in figure 44).

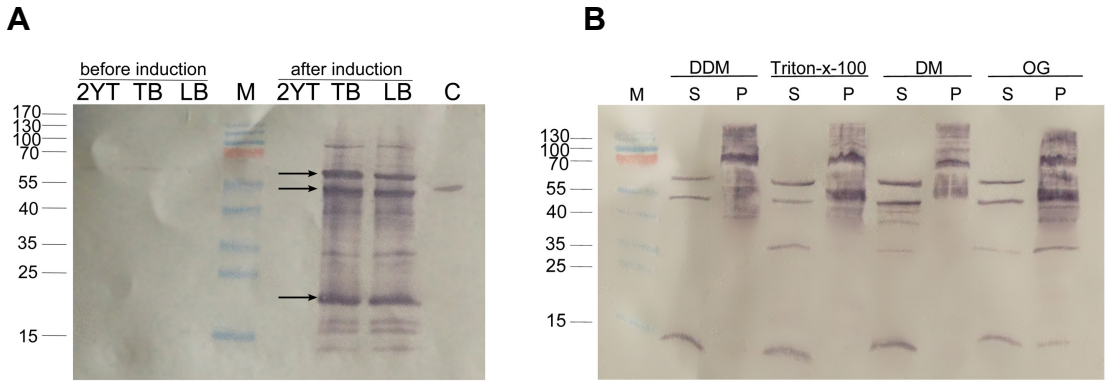

Figure 44. Heterologous expression of the *B. pseudomallei* N-*atp* operon in *E. coli* TOP10 cells and solubilization of the N-ATPase.

(A) The His-tagged β-subunit (54.1 kDa) could be detected using an anti-His antibody (sigma) after inducing the expression in TB and LB medium, but not in 2YT medium. Besides, smaller His-tagged protein bands indicate degradation of the ATPase β-subunit (arrows). C: Control: His-tagged β-subunit of the *I. tartaricus* F_1F_o ATP synthase (51.6 kDa). **(B)** The His-tagged β-subunit could be extracted from *E. coli* membranes using either 1.0 % DDM, 1.0 % Triton-X-100, 1.0 % DM or 1.0 % OG. Additional smaller tagged proteins are again visible on the blot, whereas there were no differences between the selected detergents regarding the solubilization process. S: Solubilized proteins from the membrane; P: Unsolubilized proteins (Pellet); M: PageRuler Prestained Protein Ladder (Fermentas).

Due to the His-tagged β-subunit of the enzyme, purification of the N-ATPase was performed by Ni^{2+}NTA-affinity chromatography thereby trying to isolate the enzyme from *E. coli* membrane proteins having also been extracted by the abovementioned detergents. However, Western Blot analysis of the expression and solubilization tests of the enzyme already indicated that the His-tagged β-subunit might be degraded in *E. coli* cells. This observation could be ascertained by performing ESI-MS peptide mass fingerprint of all the distinct protein bands in the elutions from the affinity chromatography revealing that most of the bands contained a fragment of the β-subunit (figure 45). Further, subunits α, γ, bδ and ε of the enzyme were identified in the Ni^{2+}NTA-elution, whereas subunits a, c, q and r could not be detected.

A

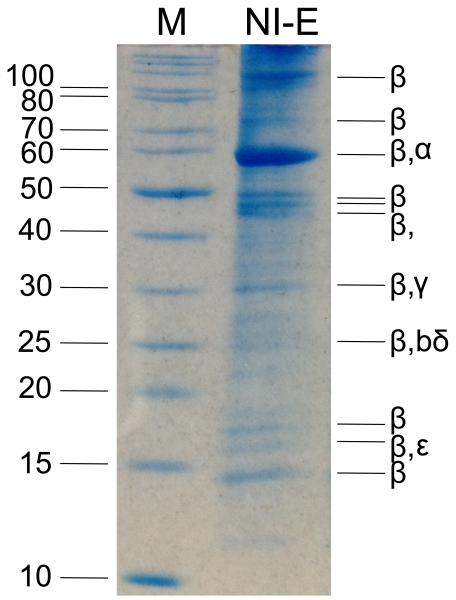

B

N-ATPase-subunits	molecular masses
α	69.8 kDa
β	53.1 kDa
γ	29.5 kDa
bδ	26.6 kDa
a	24.6 kDa
q	16.7 kDa
ε	16.5 kDa
r	9.8 kDa
c	8.2 kDa

Figure 45. Ni^{2+}NTA-affinity chromatography of the His-tagged N-ATPase of *B. pseudomallei* purified from *E. coli* membranes and the molecular masses of the N-ATPase subunits.
(A) The fraction eluted from the Ni^{2+}-column with 200 mM imidazol was analyzed by Coomassie-stained SDS-PAGE. All proteins present in the elution were cut out from the gel and analyzed by ESI-MS peptide mass fingerprint disclosing that the His-tagged β-subunit of the enzyme is degraded and distributed within the entire sample. Besides, subunits α, γ, bδ and ε were identified as indicated on the right side of the gel at the respective protein bands. Subunits a, c, q and r were not detected in the elution fractions. **(B)** The calculated theoretical molecular masses of the single N-ATPase subunits are listed in a table.

These results denote that the N-ATPase of *B. pseudomallei* is either not fully assembled in *E. coli* cells or not stable when extracted and purified from the membranes. However, due to the fact that fragments of the His-tagged β-subunit have already been detected by performing Western Blot analysis with *E. coli* cells and likewise after extracting the enzyme from its membranes it is more likely that the enzyme is not properly assembled in *E. coli* cells.

Different purification steps were tested including IMAC using several metal ions (Cu^{2+}, Zn^{2+} and Co^{2+}) and different buffer conditions including diverse detergents for extraction as well as during IMAC. Besides, isolation of the heterologously expressed enzyme by applying purification procedures independent of the His-tag was tried, e.g. precipitation of the enzyme with $(NH_4)_2SO_4$ and PEG_{6000} or sucrose density gradient

centrifugation. Nevertheless, a fully assembled N-type ATPase could not be purified from *E. coli* cells. For this reason, another strategy was chosen to express and purify the *B. pseudomallei* N-ATPase which is described in the following chapter.

3.2.6 Heterologous expression of the *B. pseudomallei* N-ATPase in *B. thailandensis*

The experiments in chapter 3.2.5 showed that *E. coli* seemed to be not the adequate host for expressing the complete N-ATPase of *B. pseudomallei*. Therefore, a different host strain for expression was looked for. Due to the fact that a vector for heterologous protein expression in *Burkholderia* strains was constructed by another group (Prof. Herbert P. Schweizer, Colorado State University, Fort Collins, Colorado) and available upon request, the choice has been made in favor of *B. thailandensis*, a non-pathogenic *Burkholderia* strain, having already been used for previous experiments (chapter 3.2.1). The expression vector (pHERD28T) holds an *ori* for replication in *Burkholderia* and an *ORF* conferring resistance to the antibiotic trimethoprim, as *Burkholderia* strains are intrinsically resistant to most antibiotics commonly used for genetic selection (see 1.4.3).

The complete N-*atp* operon was hence cloned into pHERD28T and *B. thailandensis* cells were transformed with the plasmid by electroporation (chapter 2.2.14). Initial expression experiments as well as solubilization tests of the enzyme were performed likewise and analyzed by Western Blot (figure 46). The ATPase could be extracted from membranes using 0.1, 0.5 and 1.0 % DDM as well as 1.0 % DM, 1.0 % Triton-X-100 and 1.0 % Cymal-5. In each case, residual amounts of His-tagged β-subunit could also be detected in the unsolubilized membrane fractions. This Western Blot analysis indicated that most of the enzyme could be extracted using 1.0 % Triton-X-100.

These initial expression tests of the N-ATPase in *B. thailandensis* showed that the enzyme is more stable in these cells than in *E. coli*, even if extracted from membranes. There were no additional protein bands detectable on the blot which could be assigned to be degradation products of the His-tagged β-subunit.

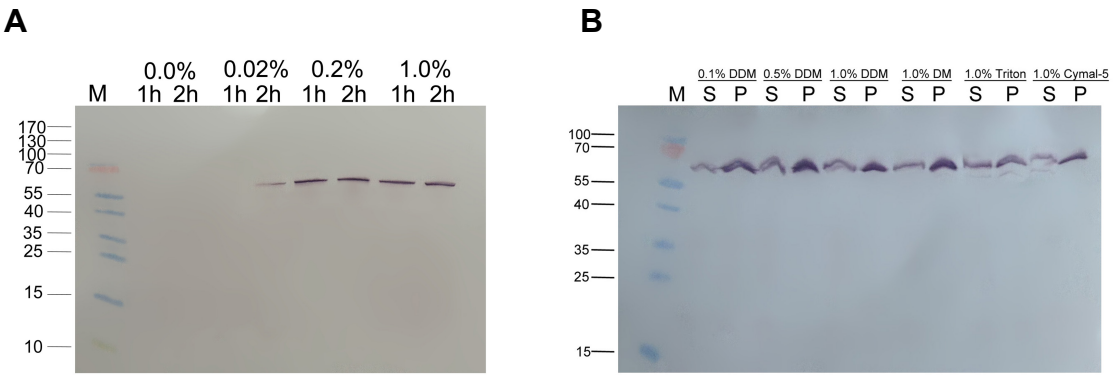

Figure 46. Heterologous expression of the *B. pseudomallei* N-*at*p operon in *B. thailandensis* cells using pHERD28T_atpBP and solubilization of the N-ATPase.

(A) The His-tagged β-subunit (54.1 kDa) could be detected using the anti-His antibody after inducing the expression with 0.02, 0.2 and 1.0 % arabinose, whereby the best signal was detected 2 h after induction with 0.2 and 1.0 % arabinose. **(B)** Membrane solubilization experiments. The His-tagged β-subunit of the enzyme was extracted from *B. thailandensis* membranes with 0.1, 0.5 and 1.0 % DDM as well as with 1.0 % DM, 1.0 % Triton-X-100 and 1.0 % Cymal-5. In each case a considerable amount of tagged protein could be detected in unsolubilized membrane fractions. The least amount of unsolubilized enzyme was revealed by the use of 1.0 % Triton-X-100. No degradation of the β-subunit is visible on either blot. S: Solubilized proteins from the membrane; P: Unsolubilized proteins (Pellet); M: PageRuler Prestained Protein Ladder (Fermentas).

To localize the heterologously expressed N-ATPase in inverted membrane vesicles made from *B. thailandensis* cells, the enzyme was labeled with a specific antibody against the His-tag and a second antibody against the first one carrying an 8 nm gold particle. After fixing the labeled vesicles on a carbon-coated grid, the gold particles can be visualized by negative stain EM (figure 47).

The sample contained membrane vesicles of different sizes. Gold particles can be found attached to the smaller vesicles, whereas there was no gold visible in the environmental solution of the sample. A negative control containing fixed membrane vesicles, in which expression of the N-ATPase was not induced, shows no gold particles at all. This result implicates that the labeling occurred specifically at the His-tagged β-subunit of the *B. pseudomallei* N-ATPase. As the gold particles are localized at the vesicles, thus it can be assumed that the soluble F_1-part of the enzyme which carries the His-tag and the gold particles is assembled with the membrane-bound F_o part of the enzyme.

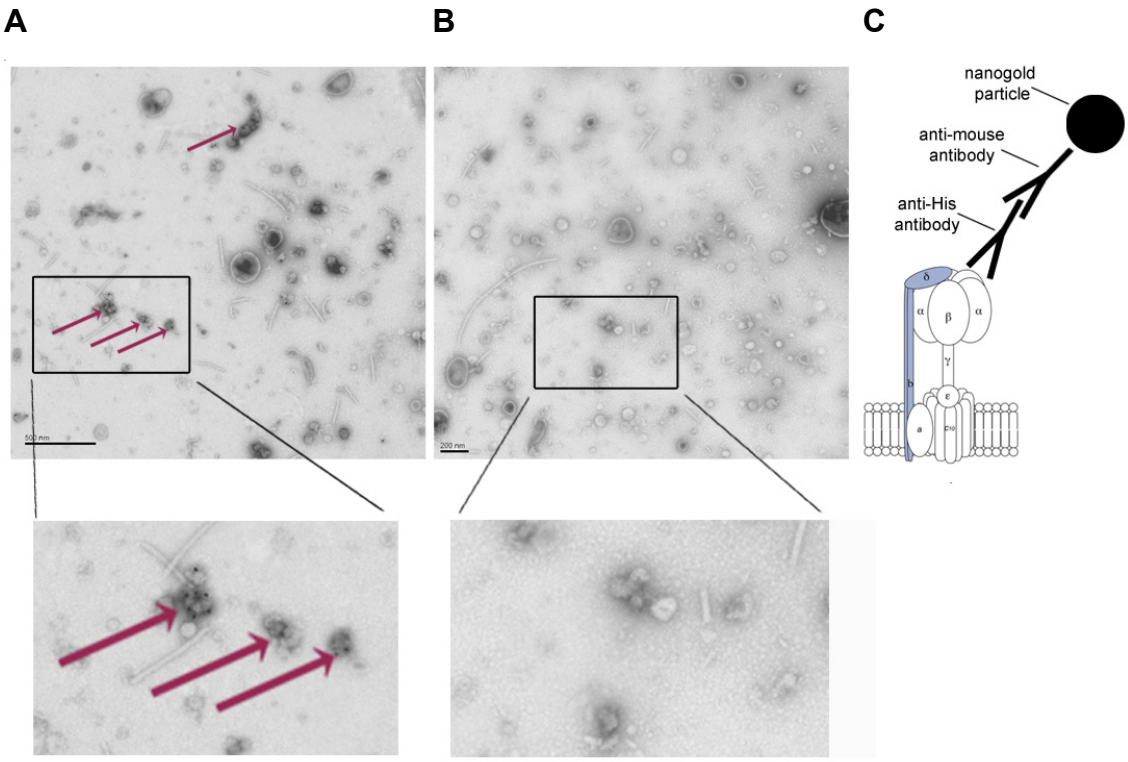

Figure 47. Immunogold-labeling and negative staining of inverted *B. thailandensis* membrane vesicles with the pHERD28T_atpBP expression vector.

B. thailandensis cells were disrupted by French press and inverted membrane vesicles were sedimented by ultracentrifugation. After immunogold-labeling, vesicles were loaded on a carbon-coated grid, negatively stained with uranyl acetate and micrographs were taken in a CM120 electron microscope (Phillips) by Friederike Joos (Structural Biology, Max-Planck-Institute of Biophysics, Frankfurt). **(A)** Vesicles imaged after inducing expression of the *B. pseudomallei* N-ATPase. Gold particles of 8 nm were observed at some small vesicles (purple arrows), whereas no diffuse particles were present in the sample. A scale bar is given in the lower left-hand corner (500 nm). **(B)** Vesicles imaged without preceding induction of protein expression showed no bound gold particles. A scale bar is given in the lower left-hand corner (200 nm). **(C)** Principle of immunogold-labeling of the F-type ATP synthase (enzyme adapted from (Oot *et al*, 2012)).

Based on the knowledge that the N-type ATPase is assembled in the membranes of *B. thailandensis*, the enzyme was isolated and purified by Ni^{2+}NTA-affinity-chromatography. The different fractions of the purification procedure, including the unbound proteins in the flow through as well as all proteins eluted by applying increasing imidazol concentrations to the Ni^{2+}NTA column, were analyzed by SDS-PAGE and Western Blot. As already indicated on the SDS gels, none of the fractions contained the fully assembled N-ATPase (figure 48).

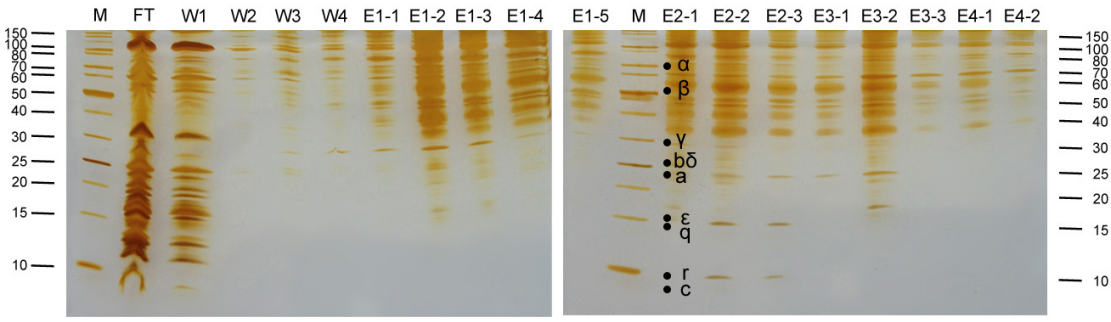

Figure 48. Ni^{2+} NTA-affinity chromatography of the His-tagged *B. pseudomallei* N-ATPase from *B. thailandensis* membranes.

Membranes solubilized using 1 % Triton-X-100 were bound over night to the Ni^{2+}NTA resin and the column was washed with increasing imidazol concentrations (W1: 0, W2: 5, W3: 10 and W4: 20 mM imidazol) before proteins were eluted with 40 (E1), 70 (E2), 100 (E3) and 200 mM imidazol (E4). None of the fractions contained the fully assembled and purified N-ATPase, which subunits are indicated according to their calculated theoretical molecular masses (figure 41).

Western Blot analysis was performed using not only an antibody against the His-tagged β-subunit, being part of the soluble head group of the enzyme, but also against the c-ring (anti-c of *A. thaliana*) of the membrane-bound part of the ATPase (figure 49).

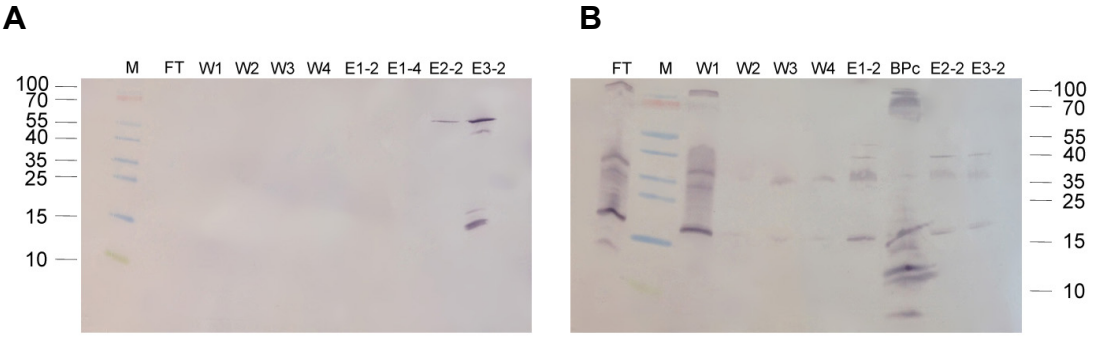

Figure 49. Ni^{2+} NTA-affinity chromatography of the His-tagged *B. pseudomallei* N-ATPase purified from *B. thailandensis* membranes.

(A) Western Blot analysis with an anti-His antibody and **(B)** an anti-c antibody (*A. thaliana)*. The His-tagged β-subunit could be detected in the Ni^{2+}NTA-elutions (E2-2: 70 mM imidazol and E3-2: 100 mM imidazol), whereas the c-ring was present in the flow through (Kramer & Crofts) and after washing the column without imidazol (W1), indicating that the F_o-part is not properly attached to F_1 and thereby not binding to the column. BPc: purified *B. pseudomallei* c-ring (control).

This approach enables to determine if both parts of the enzyme are attached to each other, thereby expecting them to elute in the same fraction. However, the results revealed that the β-subunit and thereby presumably the complete F_1-part has bound to the Ni^{2+}NTA resin whereas the c-ring did not (figure 49).

Finally, a selection of milder conditions during purification were tried, including lowering the detergent concentration and adding stabilizing agents, like glycerol and $MgCl_2$, however Western Blot analysis revealed that in each trial the c-ring was separated from the β-subunit of the enzyme. The detergents and chemicals which were used probably destabilize intramolecular interactions of the enzyme causing uncoupling of the N-ATPase. However, at this point it can not be determined whether this happens while extracting the enzyme from membranes or during the purification procedure after applying the extract to the Ni^{2+}NTA resin.

The section above (3.2.5-3.2.6) describes the heterologous expression of the N-*atp* operon of *B. pseudomallei* in *E. coli* and *B. thailandensis* cells. The experiments were carried out to produce the N-ATPase in these bacterial cells to perform structural and functional analysis of the enzyme. However, expressing the operon in *E. coli* caused strong degradation of the enzyme, as shown by SDS-PAGE, Western Blot and ESI-MS peptide mass fingerprint. *B. thailandensis* is a very closely related representative of *B. pseudomallei*. For this reason, it was assumed that gene expression and protein production mechanisms are well conserved betweeen both *Burkholderia* species, potentially improving the heterologous expression of the N-ATPase in these cells. Indeed, the enzyme seemed to be more stable than in *E. coli* cells when analyzing the expression in whole cells by SDS-PAGE and Western Blot. Nevertheless, extraction of the enzyme from *B. thailandensis* membranes has not yet been successful with the procedures described.

Further optimization of the purification steps, for example by the addition of lipids or the use of other detergents which have not yet been tested, could be done. Alternatively, the nucleotide sequence of the N-*atp* operon of *B. pseudomallei* could be genetically modified by changing codons for a more stable expression of the β-subunit, which is the most degraded subunit of the enzyme. Finally, a homologous N-ATPase from another species could be tried to be expressed and purified which is more stable upon its isolation from membranes.

3.3 The N-type c-ring of *B. pseudomallei*

Having suggested that the N-ATPase is a novel type of rotary ATPase, the question of its physiological function and its subunit organization immediately arises. According to the primary sequence of the c-subunit of these enzymes, it was assumed that at least some of these N-ATPases use Na^+ as the coupling ion for functioning. In the following part of this work, the experiments carried out with the N-ATPase rotor ring of *B. pseudomallei* are described. We aimed to determine the ion specificity of the c-ring as well as its oligomeric size to identify the ion-to-ATP ratio of this enzyme which is determined by the c-ring stoichiometry. These results provide initial information about this type of rotary ATPase.

3.3.1 Biochemical investigation of the *B. pseudomallei* c-ring

3.3.1.1 Cloning and expression of the *B. pseudomallei* c-ring

For structural and functional analysis of the N-type ATPase c-ring the protein complex needs to be produced in high quality and large amounts. Therefore, the *atpE* gene encoding for the c-subunit of *B. pseudomallei* was cloned into a pt7-7 vector for an IPTG-inducible heterologous over-expression in *E. coli*. Genomic DNA from the *B. pseudomallei* strain K96243 was used as a template for PCR to generate fragments containing *Nde*I and *Hind*III restriction sides for ligation into pt7-7, thereby obtaining p7tc_BP. To introduce point mutations in the *atpE* gene, site directed mutagenesis was performed using pt7c_BP as a template and primer pairs carrying the corresponding single, double and quadruple mutations within the amino acids presumed to be involved in ion-binding.

Next, the protein expression using this vector was tested. Several expression conditions were tried, including temperatures varying from 18°C to 37°C, different times for induction (at OD_{600} 0.4 to OD_{600} 1.0), different media (LB, TB, 2xYTG) and IPTG concentrations for induction (0.25 mM -1.0 mM IPTG). The best results were obtained expressing the *atpE* gene in *E. coli* Lemo21 in 2 L LB medium for four hours at 37°C after induction with 0.5 mM IPTG. After inducing the heterologous protein expression at OD_{600} 0.8-0.9, cell division was significantly slowed down so that a final OD_{600} of 1.2 was reached when cells were harvested (figure 50).

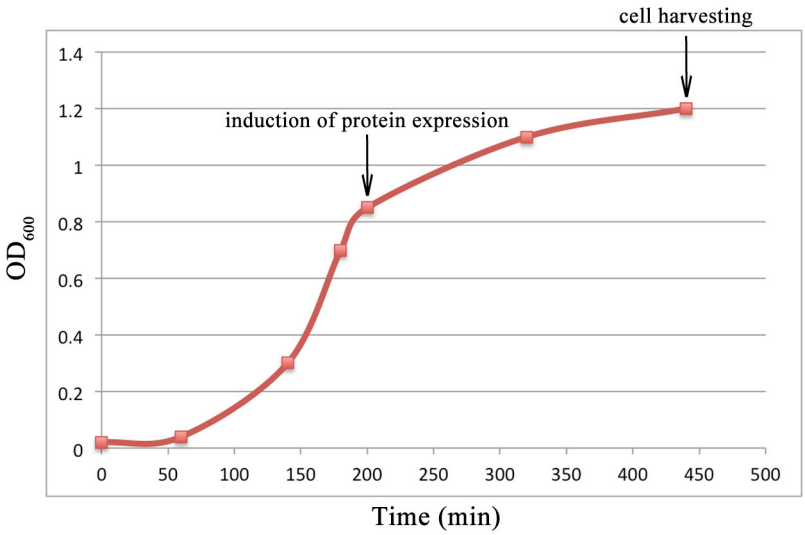

Figure 50. Growth curve of *E. coli* Lemo21 cells used for heterologous over-expression of the *B. pseudomallei* N-ATPase c-ring.

Cells were grown in a 2-l Erlenmeyer flask under constant shaking at 37° C until OD_{600} 0.8-0.9 was reached. Protein production was induced using 0.5 mM IPTG (left arrow). Cells were harvested (right arrow) after four hours of continuous shaking at 37°C after induction. The final OD_{600} of the culture was 1.2, which corresponds to approximately 1.2 g/l culture of *E. coli* wet cell weight.

3.3.1.2 Purification of the *B. pseudomallei* c-ring for biochemical investigations

Membranes of *E. coli* with the c-subunit of *B. pseudomallei* expressed were prepared and solubilization tests were performed using different detergents with the best result obtained by incubating the protein with 2 % (w/v) lauroylsarcosine for twelve minutes at 66°C. After centrifugation of the sample nearly all proteins being in the supernatant could be precipitated with 70 % $(NH_4)_2$ SO_4 whereas the soluble fraction contained only one dominant protein migrating at a level of 90 kDa on a SDS gel and some stacked, probably aggregated protein above (figure 51 A).

Likewise formerly characterized c-rings the protein at 90 kDa could be precipitated with trichloroacetic acid (TCA), disposing of the corresponding protein band on a gel thereby bringing fourth another protein band migrating at the size of 8 kDa, just as expected for the corresponding c-monomer (figure 51 A).

Several previously purified c-rings are SDS-stable migrating as a homomeric complex at a level of 40 to 60 kDa (Meier *et al*, 2006; Meier *et al*, 2001; Meier *et al*, 2003; Pogoryelov *et al*, 2007; Pogoryelov *et al*, 2005; Preiss, 2013), thus significantly lower than the putative c-ring considered here.

The exact molecular mass of the isolated, monomeric protein was determined by MALDI-MS by Dr. Julian M. Langer (Molecular Membrane Biology, Max-Planck-Institute of Biophysics). The mass spectrum obtained showed several peaks corresponding to molecular weights of 8349.6 Da and 8378.3 Da what is in good correlation with the theoretical molecular weights of 8349.96 Da for the unmodified and 8378.96 Da for the formylated c-subunit, respectively (figure 51 B).

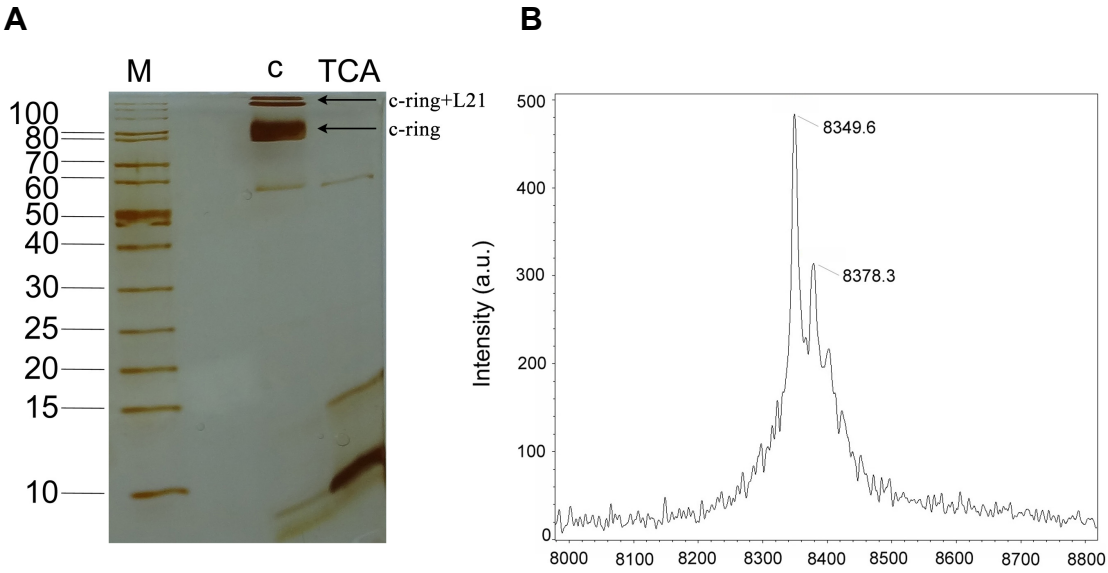

Figure 51. Isolation of the *B. pseudomallei* c-ring and determination of its correct subunit molecular mass by MALDI-MS.

(A) The heterologously expressed c-ring was extracted from *E. coli* membranes and analyzed on a silver-stained SDS-gel. The isolated c-ring (c) migrates at a very high molecular weight level (80-100 kDa), compared to previously isolated rings migrating between 40 and 60 kDa. The ribosomal *E. coli* protein L21 was co-purified with the c-ring. Treatment of the oligomeric complex with trichloroacetic acid (TCA) leads to formation of monomeric protein (8349.96 kDa). **(B)** The molecular weight of the c-subunit was confirmed by MALDI-MS (performed by Dr. Julian M. Langer, Molecular Membrane Biology, Max-Planck-Institute of Biophysics). The measured molecular weights correspond to the unmodified c-subunit (8349.6 Da) and the formylated protein (8378.3 Da).

To ascertain whether there are other proteins besides c-ring in the sample, all visible protein bands were cut out from a Coomassie-stained SDS-PAGE and analyzed by ESI-MS peptide mass fingerprint. The result showed that the lower, dominant protein band from the gel contained only c-ring from *B. pseudomallei* whereas the upper band

contained c-ring associated with the 50 S ribosomal protein L21 from *E. coli* originating from heterologous over-expression in this strain (figure 51 A).

The c-ring in 70 % $(NH_4)_2SO_4$ was dialyzed against buffer not containing any detergent to concentrate the protein by precipitation. The protein was then dissolved in 20 mM Tris /HCl pH 8.0 with 1-3 % DM or DDM. To separate pure c-rings from aggregated c-rings associated with *E. coli* L21 a sucrose density gradient centrifugation was performed. Using this procedure, two populations could be successfully separated, one containing the c-ring associated with L21 and the other comprising only purified c-ring (figure 52).

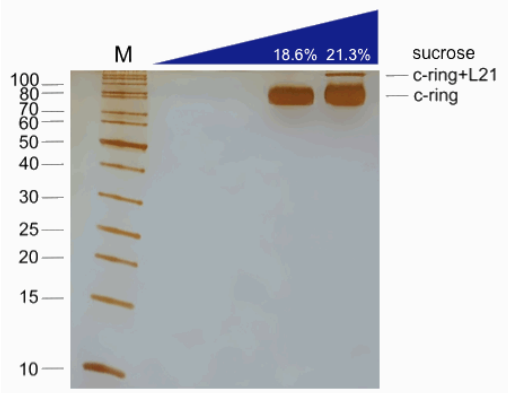

Figure 52. Purification of the *B. pseudomallei* c-ring by sucrose density gradient centrifugation.
The isolated protein complex was further purified by centrifugation for 20 hours using 5-35 % sucrose and 0.05 % DDM at 10 °C. The c-rings associated with L21 could be separated from single c-rings as the two populations sedimented in different sucrose concentrations.

To further improve the protein quality of the c-ring and to concentrate the sample, the pure c-ring containing fractions in (18.6 %) sucrose were combined, the buffer was exchanged and the sample was concentrated by centrifugation. The final protein quality was verified by SDS-PAGE (figure 53 A). Due to the unexpectedly slow migration of the complex in the SDS-polyacrylamide gel, BN-PAGE was subsequently performed. This indicated that the c-ring has a molecular weight of approximately 200-250 kDa, depending on how much Coomassie is bound to the protein during electrophoresis (figure 53 B). The second dimension SDS-PAGE of the protein band cut out from the BN-gel showed again the c-ring migrating just as in the

previous SDS-gel and some dimeric protein (c_2) was formed out of the c-ring (figure 53 C).

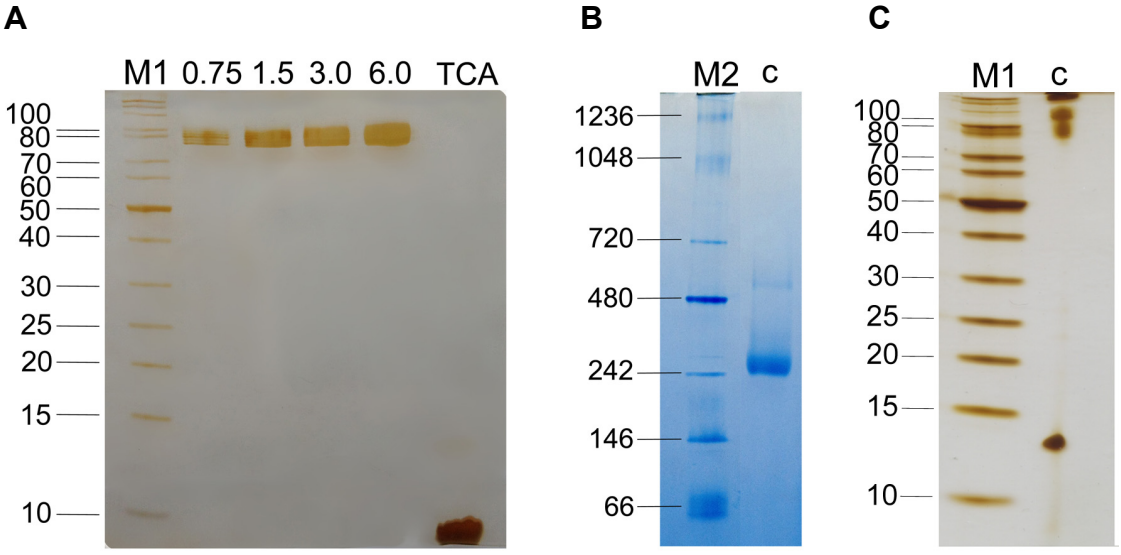

Figure 53. Biochemical investigation of the oligomeric size of the *B. pseudomallei* c-ring by SDS-PAGE, BN-PAGE and second-dimension SDS-PAGE.

(A) The SDS-polyacrylamide (PA) gel shows 0.75, 1.5, 3.0 and 6.0 µg of purified c-ring migrating at 80-100 kDa. Addition of trichloroacetic acid (TCA) precipitated the c-ring into its monomers. **(B)** The blue native (BN) gel shows the c-ring at a molecular level of 200-250 kDa. **(C)** A second dimension SDS-PA gel reveals that the protein cut out from the BN-gel shows the same migration behaviour than in the primary SDS-PA gel (A). M1: PageRuler Unstained Protein Ladder (Fermentas); M2: NativeMark Unstained Protein Standard (Life Technologies).

By applying the purification procedure described here, 1.5 mg (0.5 ml 3 mg/ml) pure c-ring could be obtained from 12 l of *E. coli* cell culture, suitable for a subsequent biochemical analysis of the protein complex to investigate the ion specificity of the rotor ring (1.3.3.2). In addition to that, expression and purification of c-rings carrying a single (M63T), double (M63T M59T) or quadruple point mutation (M63T M59T T62S I60A) in the ion-binding site was performed analogous to the protocol described above yielding a comparable amount of purified protein, besides that the mutant rings in $(NH4)_2$ SO_4 were directly used for biochemical labeling studies (2.3.6.2) as sample quality was sufficiently good for these experiments.

3.3.1.3 Ion specificity of the wildtype *B. pseudomallei* c-ring heterologously expressed in *E. coli*

Alignments of the primary sequences of various c-subunits revealed similar amino acid motifs between rings of known and unknown ion specificities suggesting an ion specificity of a biochemically uncharacterized c-ring of a given species (figure 15 in 1.3.4.1). Due to the Na^+-signatures that can be found in the primary sequences of some N-type c-subunits, it appears that the corresponding c-rings of these N-ATPases use Na^+ during their operation cycle (1.4). Consequently, such N-type ATPases would either use a Na^+-gradient for the generation of ATP or, vice versa, pump Na^+ across the membrane by consuming the energy relase of ATP hydrolysis.

To study the ion specificity of the purified wildtype c-ring of the N-ATPase of *B. pseudomallei*, the DDM-solubilized protein in 20 mM Tris HCl pH 8.0 was used for NCD-4 labeling reactions likewise previously described for the c-ring of *F. nucleatum* (chapter 3.1.3). Initial experiments were done to test whether Na^+ competes with H^+ and thereby with NCD-4 for binding to the c-ring. The resulting kinetics of the labeling reaction obtained indicated that NCD-4 binding could not be blocked by the addition of NaCl to the sample, the reaction continued even in the presence of 150 mM NaCl (figure 54A). This points out that the c-ring investigated here seems not to be Na^+-specific.

As Na^+-specific c-rings also bind Li^+, even though with a 10-times lower affinity (Kluge & Dimroth, 1993; von Ballmoos *et al*, 2002b), the experiment was subsequently carried out as before but substituting NaCl by LiCl. Kinetics of the labeling reaction were comparable in both cases, a quantification of the labeling yield is given below in table 51. This indicated that the c-ring does also not bind Li^+, even when ions are present in very high concentrations (150 mM LiCl) (figure 54 B).

Although the binding reaction could not be stopped in the presence of Na^+ or Li^+, there is a reduction in labeling efficiency observable in both cases. To determine whether this reduction is significant and due to the binding of the monovalent ions to the c-ring or rather produced by side effects, the labeling reaction was also performed adding CsCl to the c-ring sample. Cs^+ has a larger ion radius (167 pm) than Na^+ (102 pm) and Li^+ (76 pm) (Shannon, 1976) have and does therefore not fit into the ion-binding site of the c-ring. The kinetics of the NCD-4 binding reaction in the presence

of CsCl are again comparable to the kinetics seen after the addition of NaCl or LiCl (figure 54 C; table 48). These results demonstrated that the reduced NCD-4 labeling of the c-rings in all three cases could be traced back to unspecific salt effects of the reaction and is not caused specifically by the binding of Na^+ or Li^+ to the ring.

Binding of NCD-4 to the carboxyl group of the ion-binding glutamate implies protonation of the same. Hence, under conditions were this is not feasible like high pH, NCD-4 should not bind to the carboxylic residue. The control experiment performed at pH 9.0 showed that NCD-4 binding was totally abolished at this pH, reinforcing that indeed the glutamate of the ion-binding side is targeted by NCD-4 (figure 54 D). Integrating all available results (table 51) it can be assumed that the c-ring of *B. pseudomallei* is H^+-specific and not Na^+.

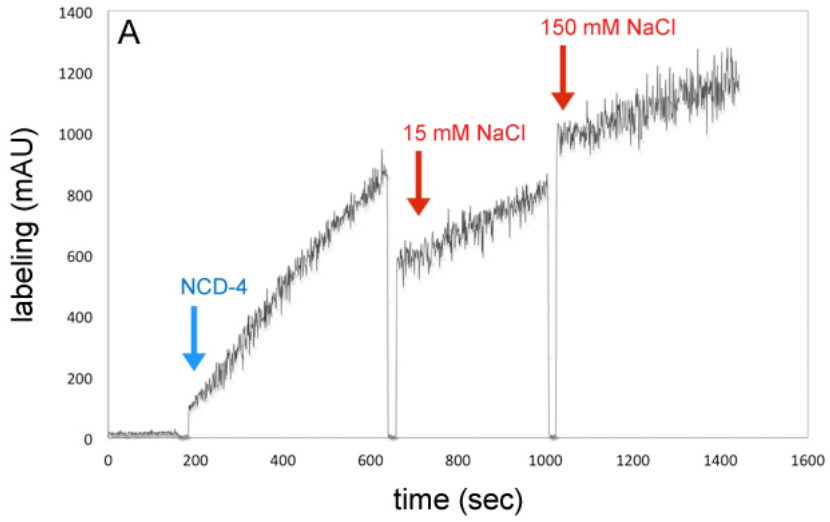

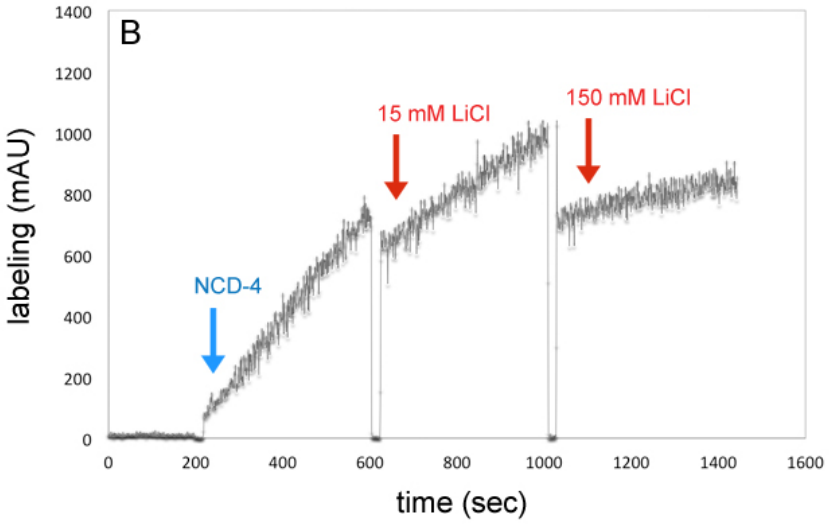

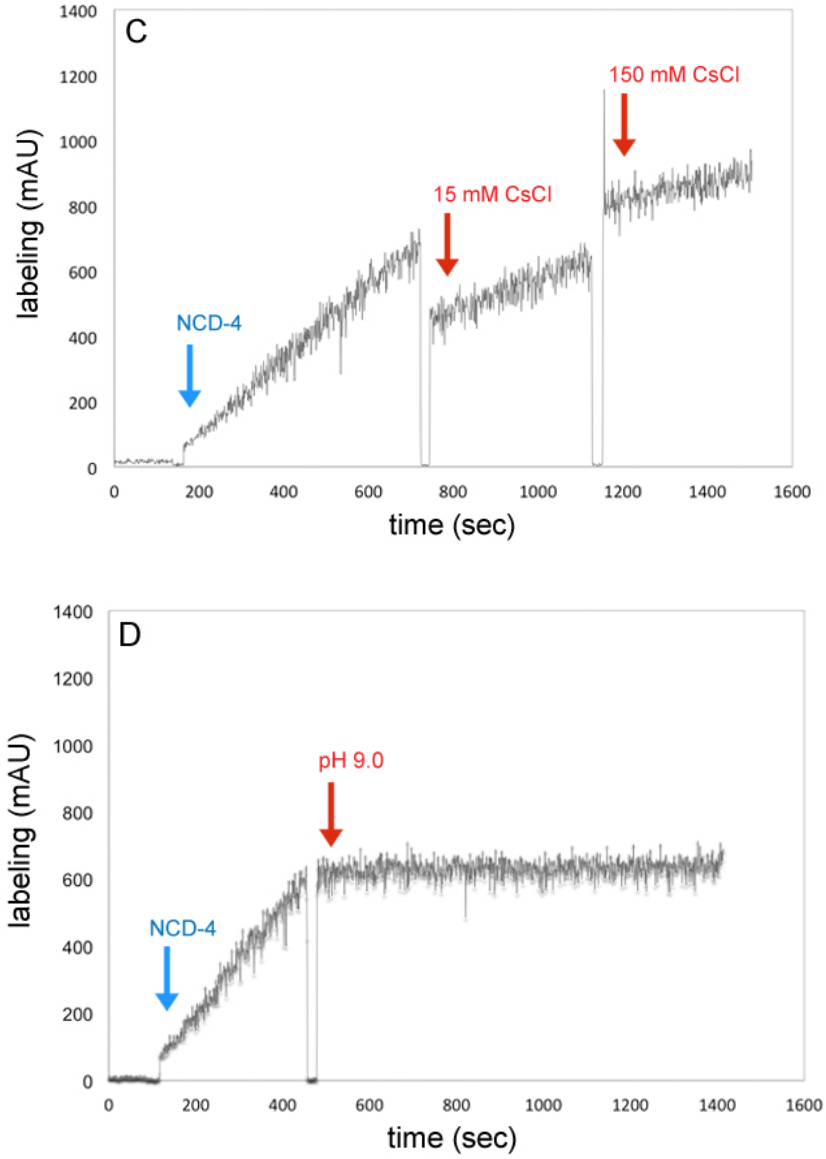

Figure 54. Effect of Na^+, Li^+, Cs^+ and high pH on the kinetics of the NCD-4 modification of the purified *B. pseudomallei* wildtype c-ring.

The reaction was started by the addition of 100 µM NCD-4 to the c-ring solubilized in 1 % DDM and MES buffer pH 6.0. The continuous increase of fluorescence was measured upon binding of NCD-4 to the protonated E61 in the ion-binding site. The addition of 15 and 150 mM NaCl **(A)**, LiCl **(B)** or CsCl **(C)** does not prevent NCD-4 from further labeling, indicating that the monovalent ions (Na^+, Li^+ and Cs^+) do not compete with H^+ and thereby NCD-4 for binding to E61. An increase of the pH to 9.0 **(D)** totally impedes NCD-4 binding to the glutamate, as the carboxyl group is then no longer protonated which is a prerequisite for the reaction.

Table 48. NCD-4-labeling efficiency of the *B. pseudomallei* c-ring in dependency of NaCl, LiCl or CsCl and the pH of the reaction

The slopes of the increasing fluorescence upon NCD-4 binding to the c-ring were calculated. The slope of the reaction with the unmodified c-ring at pH 6.0 was set to 100 % in each measurement and the relative slopes of the increasing fluorescence after the addition of NaCl, LiCl or Cs or after changing the pH from 6.0 to 9.0 are given in % in relation to this.

	NaCl, pH 6.0	LiCl, pH 6.0	CsCl, pH 6.0	pH 9.0
w/o at pH 6.0	100 %	100 %	100 %	100 %
15 mM	40.5 %	55.2 %	43.9 %	1 %
150 mM	27.5 %	16.7 %	23.7 %	1 %

To further assure the results for the ion specifictiy of the *B. pseudomallei* N-ATPase c-ring obtained by the NCD-4 modification reaction, a DCCD-labeling experiment with the purified rotor ring was performed. Therefore, the DDM-solubilized protein complex in 20 mM Tris HCl pH 8 was incubated with 500 µM DCCD either in the absence or presence of NaCl (5 and 50 mM). The binding of DCCD to the E61 of the ion-binding sites was determined by MALDI-MS by Dr. Julian M. Langer (Molecular Membrane Biology, Max-Planck-Institute of Biophysics, Frankfurt) at different time points after starting the reaction. The DCCD-labeling efficiency was not altered in the presence of NaCl indicating the Na^+ does not compete with DCCD for the ion-binding glutamate and hence confirming that the investigated c-ring is H^+-specific (figure 55).

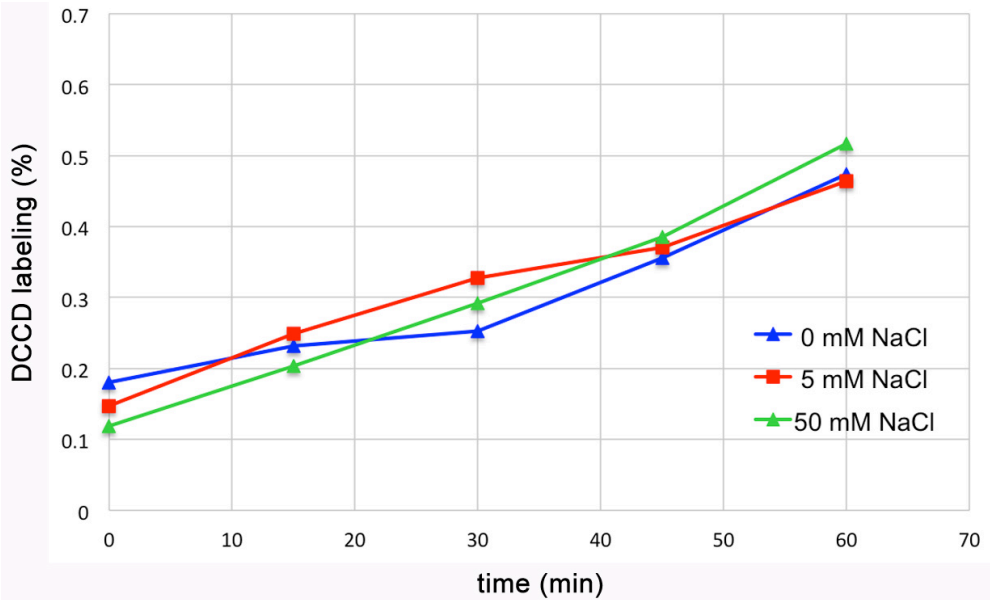

Figure 55. Effect of Na^+ on the kinetics of the DCCD modification of the purified *B. pseudomallei* wildtype c-ring.

The purified c-ring in 20 mM Tris HCl pH and 0.05 % DDM was supplemented with 0, 5 or 50 mM NaCl as indicated. After the addition of 500 µM DCCD to the sampple, the modification reaction of the E61 by DCCD was analyzed by MALDI-MS in a time-dependent manner (0, 15, 30, 45 and 60 min). The DCCD labeling efficiency (given in %) was not impeded by (5 or 50 mM) NaCl indicating that the investigated c-ring does not bind Na^+ specifically. MALDI-MS measurements were performed by Dr. Julian D. Langer (Max Planck-Institute of Biophysics, Molecular Membrane Biology).

3.3.1.4 Homology model of the *B. pseudomallei* c-ring

One of the remarkable features of the c-subunit sequence of *B. pseudomallei* is the existence of two methionine residues (M59 and M63; figure 56) within the presumed ion-binding site. These residues might contribute to a H^+-specificity in this c-ring.

Preliminary information of an unknown protein structure can be obtained by caluclating a homology model of it. The reliability of such a model depends on the percentage of sequence identity to the template which is used. High accurancy models are often received with sequence identities of around 50 % (Baker & Sali, 2001). Here, the WHATIF online server (2.4.6) was used to generate a model of the *B. pseudomallei* c-ring based on the *F. nucleatum* protein complex. The two c-subunit sequences show an identity of 46 % and a conservation of 76 % of all residues (https://blast.ncbi.nlm.nih.gov/Blast.cgi) implicating that a reliable homology model

could be obtained. As the result is only a model of the c-ring and its ion-binding sites, it does not ultimately describe the actual protein structure which might differ in reality. Errors are most often occuring in the side-chain packing and sometimes in the loop regions of the protein (Baker & Sali, 2001).

The existence of two methionine residues in the ion-binding site could minimize the space for the presence of a Na^+ and moreover a structural water molecule within the binding site of the modeled *B. pseudomallei* c-ring (figure 56). However, it is not feasible to disclose whether Na^+-coordination is sterically possible in the binding site or not as the rotameric states of the ion-binding residues can not be determined exactly based on a model.

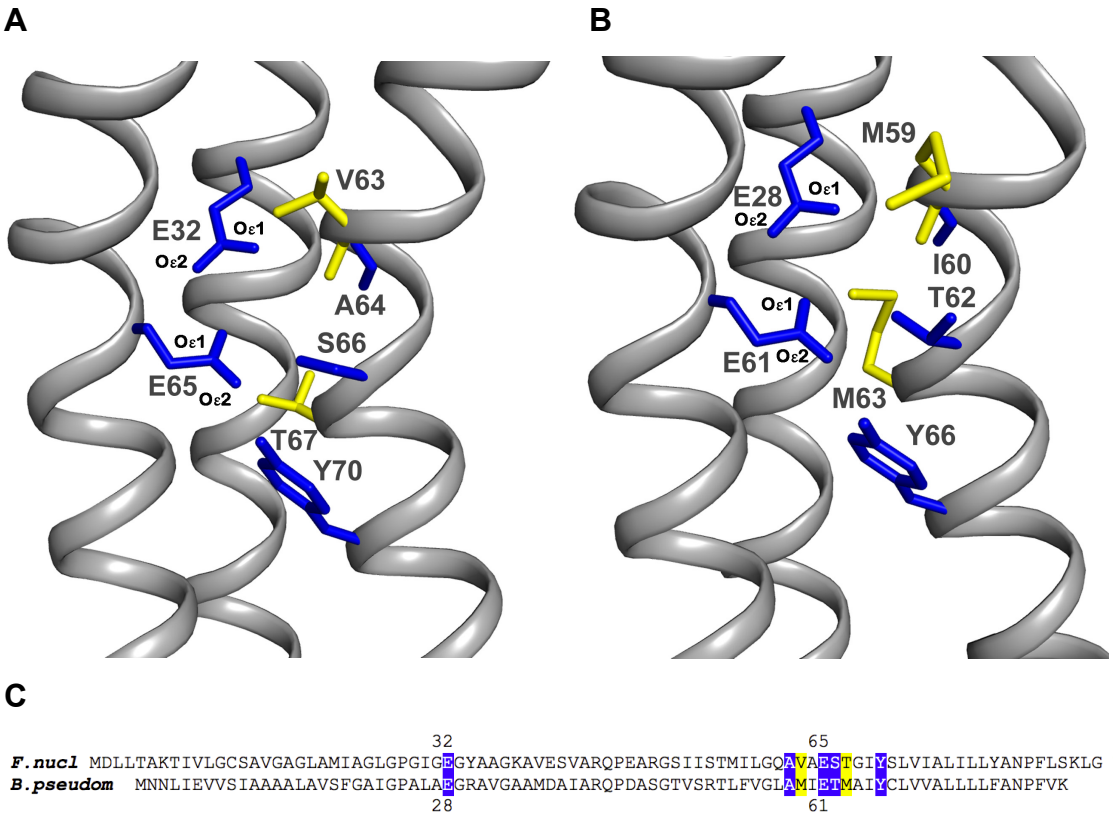

Figure 56. Comparison of the ion-binding site of the *F. nucleatum* c-ring with the putative ion-binding site of a *B. pseudomallei* c-ring homology model.

(A) Ion-binding site of the *F. nucleatum* c-ring without Na^+ and the structural H_2O. **(B)** Putative ion-binding site of the *B. pseudomallei* c-ring homology model based on the structure of the *F. nucleatum* c-ring without the coordinated ion. **(C)** Alignment of the c-subunits of *F. nucleatum* and *B. pseudomallei*. The two methionine residues in the *B. pseudomallei* c-ring model as well as the corresponding residues in the *F. nucleatum* c-ring are shown as yellow sticks whereas all other residues (presumably) involved in ion-binding are given in blue sticks, as these are either identical or conserved within the two species.

All inter-atomic distances within the ion-binding site of the *F. nucleatum* c-ring and the ion-binding site of the modeled *B. pseudomallei* c-ring were measured. A comparison of the inter-atomic distances in both binding sites reveals that the distances are shortened in the *B. pseudomallei* c-ring binding site when one or two residues are replaced by a methionine (M59 or M63) (table 49). This finding suggests that these residues might spatially exclude Na^+-coordination thereby defining a H^+-binding c-ring.

Table 49. Inter-atomic distances in the ion-binding site of the *F. nucleatum* c-ring compared to the putative ion-binding site of the *B. pseudomallei* c-ring model

The inter-atomic distances (in Å) within the ion-binding sites of the *F. nucleatum* c-ring and the *B. pseudmallei* c-ring model were measured using Pymol. The first amino acid represents the residue in the *F. nucleatum* and the second amino acid in the *B. pseudomallei* c-subunit. Distances involving methionine residues (highlighted in yellow) are shortened (bold and marked by an asterisk) in the modeled *B. pseudomallei* ring in comparison to the corresponding distances in the *F. nucleatum* c-ring. Distances between conserved residues (highlighted in blue) are not significantly altered. The colour-code is the same as in figure 56.

from residue	to residue	*F. nucleatum* structure	*B. pseudomallei* model
V63 O / M59 O	S66 Oβ / T62 Oβ	3.2 Å	**2.7 Å***
V63 O / M59 S	T67 O / M63 S	6.7 Å	**4.1 Å ***
E32 Oε1 / E28 Oε1	S66 Oβ / T62 Oβ	4.6 Å	4.2 Å
E32 Oε1 / E28 Oε1	T67 O / M63 S	6.3 Å	**3.6 Å ***
E65 Oε1 / E61 Oε1	S66 Oβ / T62 Oβ	3.1 Å	3.1 Å
E65 Oε1 / E61 Oε1	T67 O / M63 S	5.5 Å	**3.1 Å ***
T67 O / M63 S	S66 Oβ / T62 O	5.0 Å	**3.2 Å ***

***** shortened distances in the modeled *B. pseudomallei* ion-binding site involving methionine residue(s) in comparison to the corresponding distances in the *F. nucleatum* binding site

3.3.1.5 Ion specificity of mutant *B. pseudomallei* c-rings heterologously expressed in *E. coli*

To determine whether one of the methionine residues or even both are accountable for the H^+-specificity of this c-ring, mutations at the corresponding positions were introduced in the primary c-subunit sequence of *B. pseudomallei*. Thus c-ring mutants were created having changed one (M63T) or two (M63T M59T) of the methionine residues to the respective residues being present in the Na^+-binding c-ring of *F. nucleatum*. Besides, a third mutant (M59T, M63T, T62S, I60A) was generated exhibiting ion-binding residues fully identical to these in the *F. nucleatum* Na^+-binding c-ring (figure 57).

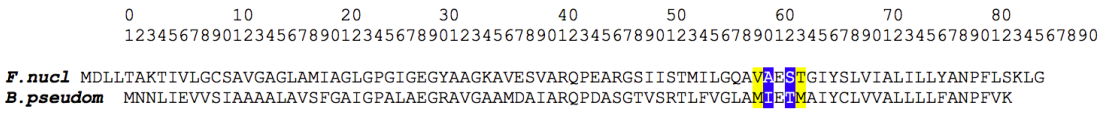

Figure 57. Alignment of the c-subunit sequences of *F. nucleatum and B. pseudomallei*.
The coloured residues of the *B. pseudomallei* c-subunit were changed according to the corresponding residues in the *F. nucleatum* c-subunit (shown in bold). A single (M63T, yellow) and a double mutant (M63T M59V, yellow) as well as a quadruple mutation (M59T, yellow; M63T, yellow; I60A, blue; T62S, blue) within the ion-binding site were introduced by site directed mutagenesis. The colour code is the same as in figure 51. The numbering corresponds to the *B. pseudomallei* c-subunit sequence.

To determine the ion specificity of the created mutants (figure 57) they were investigated using the fluorescent ATP synthase inhibitor NCD-4 analogous to the wildtype c-ring (3.3.1.3). As there was no significant difference between the labeling kinetics in the presence of NaCl, LiCl or CsCl, the results of the NCD-4 binding reactions in dependence of NaCl are shown representative for the three monovalent ions (Na^+, Li^+ and Cs^+). The measurements are similar for all of the mutants, showing further labeling after the addition of NaCl (respectively LiCl or CsCl) to the reaction sample whereas labeling was completely arrested when increasing the pH to 9.0, where the ion-binding glutamate is no longer protonated (figure 58).

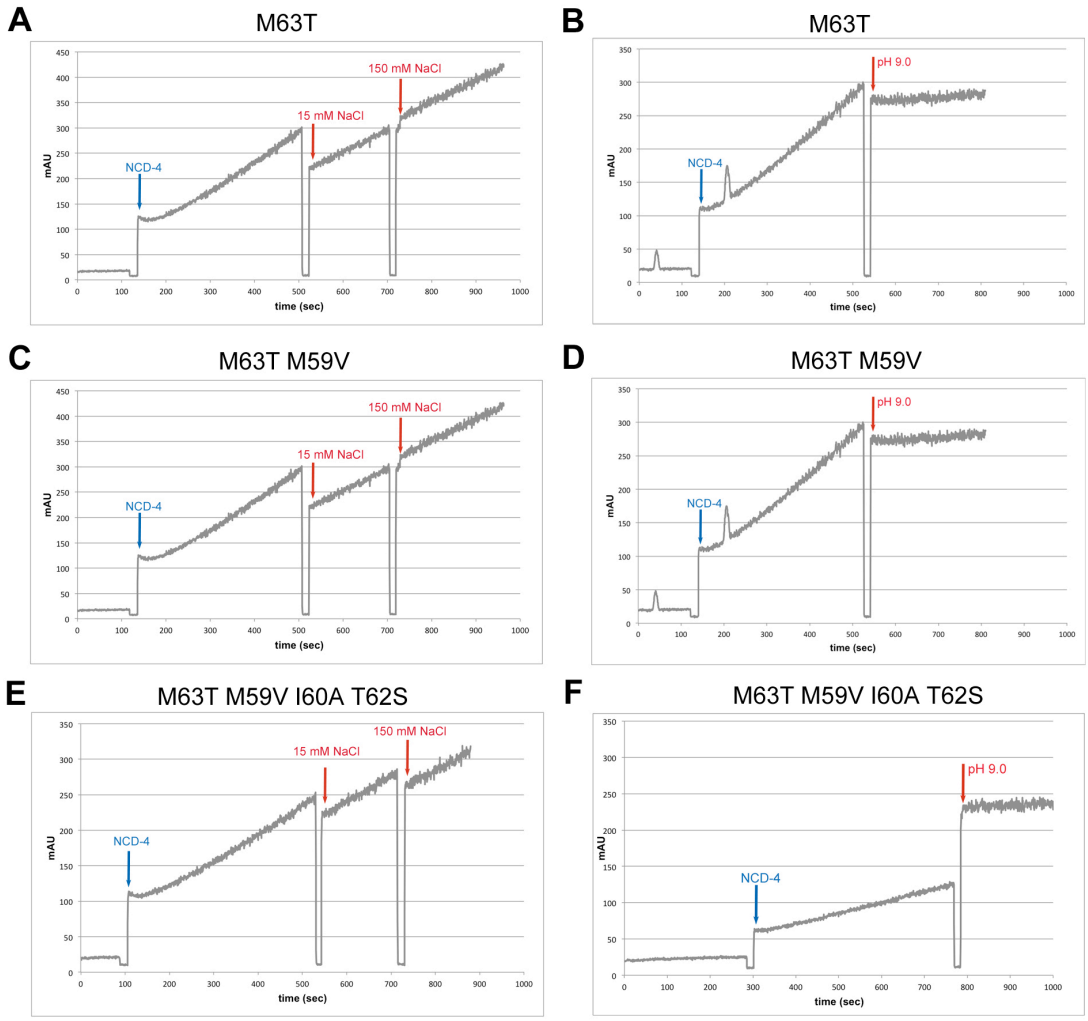

Figure 58. Effect of Na^+ and high pH on the kinetics of the NCD-4 modification reaction of the purified *B. pseudomallei* mutant c-rings.

The c-rings used in the labeling reactions carry the single mutation M63T **(A and B)**, the double mutation M63T M59T **(C and D)** or the quadruple mutation M63T M59V T62S I60A **(E and F)**. The reactions were started by the addition of 100 µM NCD-4 to the c-rings solubilized in 1 % DDM and MES buffer pH 6.0. The continuous increase of fluorescence was monitored upon binding of NCD-4 to the protonated Glu61 in the ion-binding sites. Whereas the addition of 15 and 150 mM NaCl did not prevent further labeling (**A, C, E**), increase of the pH to 9.0 totally abolished NCD-4 binding to the Glu61 in each case (**B, D, F**).

In order to experimentally determine the ion specificity of the *B. pseudomallei* c-ring, biochemical labeling reactions were performed with the isolated, detergent-solubilized wildtype protein in this work. The results indicated a H^+-specificity of the c-ring as Na^+ did not bind to the protein to prevent NCD-4 or DCCC-labeling (figures 54, 55 and 58). To find out which amino acids might be involved in the determination

of the ion specificity in this ring, some of the residues which were assumed to be involved in ion-coordination were mutated. In this step, two methionine residues (M63 and M59) were substituted by residues which can be found at this position in the Na^+-binding c-ring of *F. nucleatum* (figure 57). However, both mutants (M63T) and (M63T M59V) did not show Na^+-specificity in the NCD-4 binding reactions (figure 57). Besides, another mutant carrying all Na^+-binding residues as in the *F. nucleatum* c-ring (M63T M59V I60A S62T) was likewise shown to be H^+-specific (figure 58). The experimental results described here indicate that the *B. pseudomallei* c-ring ion specificity might not only be determined by the chemical nature of its ion-binding residues but by additional factors as the overall geometry of the binding site (4.2.5).

3.3.2 Structural investigations of the *B. pseudomallei* c-ring using X-ray crystallography

The biochemical experiments with the isolated *B. pseudomallei* c-ring indicated a H^+-specificity for the protein complex. To confirm the ion specificity on a structural level as well as to determine the stochiometry of the N-type ATPase rotor ring and the overall structure of the protein complex, the purified c-ring was further used for X-ray crystallographic experiments.

3.3.2.1 Purification of the *B. pseudomallei* c-ring for structural investigations

To obtain high resolution structural information about the c-ring 3D-crystallization of the purified protein complex was performed. As a highly pure and monodisperse solution of protein is a prerequisite for high quality protein crystal growth, the isolated c-ring was further purified by size exclusion chromatography (SEC). Two SEC steps were necessary to obtain a monodispers c-ring sample. The precipitated protein after dialysis was resuspended in 1 ml 20 mM Tris HCl pH 8.0 buffer containing 2-3 % DDM per liter *E. coli* starting culture. After concentrating the sample about 10 times by centrifugation, the protein had a concentration of 12 mg/ml. It was filtered through a 0.22 µm PVDF-filter and loaded on a Superose 6 column collecting fractions of 0.25 ml with a constant flow of 0.3 ml/min. The first SEC profile identified a polydispersity of the sample comprising several peaks with each of them merging into the proximate one (figure 59 A). All fractions of the first SEC

were subsequently analyzed by SDS-PAGE revealing different states of the isolated c-ring (figure 59 B). Some protein was present in the void volume (8 ml), which was considered to be aggregated. The protein eluting with a retention volume of 12-14 ml mainly consists of single c-rings with a minor population of two or more rings stacking together, whereas the main peak at 15 ml retention volume only contains single c-rings. Fractions of protein eluting with a retention volume of 17-19 ml comprise only monomeric c-subunits (figure 59 A).

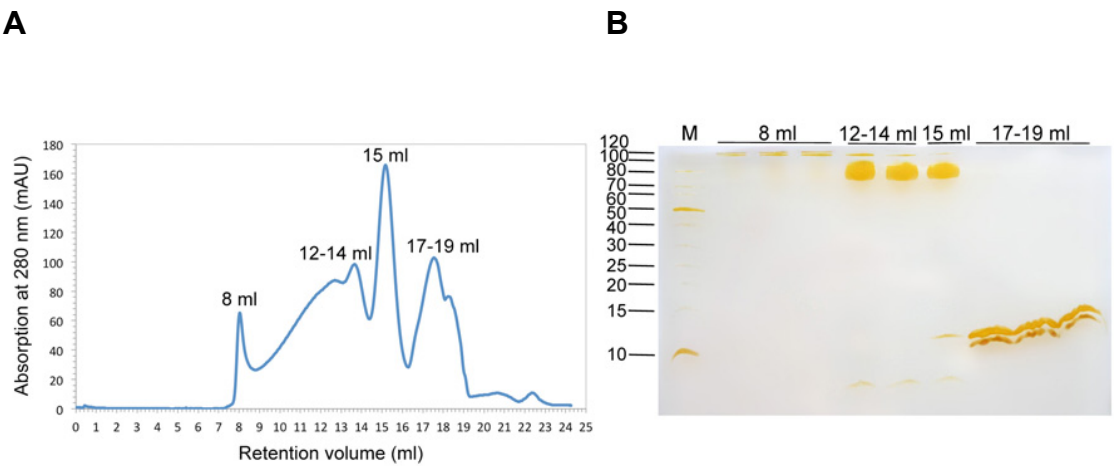

Figure 59. First size exclusion chromatography of the *B. pseudomallei* c-ring and silver-stained SDS-PAGE of the corresponding SEC-fractions.

(A) SEC was performed using a Superose 6 column with a constant flow of 0.3 ml/min and a total bed volume of 24 ml. The profile shows the polydispersity of the protein in DDM which elutes in several peaks with retention volumes of 8 to 19 ml. **(B)** Analysis of all fractions on a SDS-gel discloses the different states of the protein, including aggregated protein in the void volume (8 ml), single, dimeric and multiple c-rings eluting together at 12-14 ml, single c-rings at 15 ml and monomeric protein with a retention volume of 17-19 ml.

Fractions eluting in the peak corresponding to a retention volume of 15 ml contained 0.5 mg of single c-rings in a total volume of 1.75 ml. After combining all these fractions the protein was concentrated to 0.5 ml and subsequently loaded again on a Superose 6 column. After the second SEC the protein eluted in a single, almost monodisperse peak with a retention volume of 15 ml with just a small shoulder at 14 ml (figure 60 A). The fractions of the peak were analyzed by SDS-PAGE (figure 60 B), combined and the c-ring was concentrated for structural investigations.

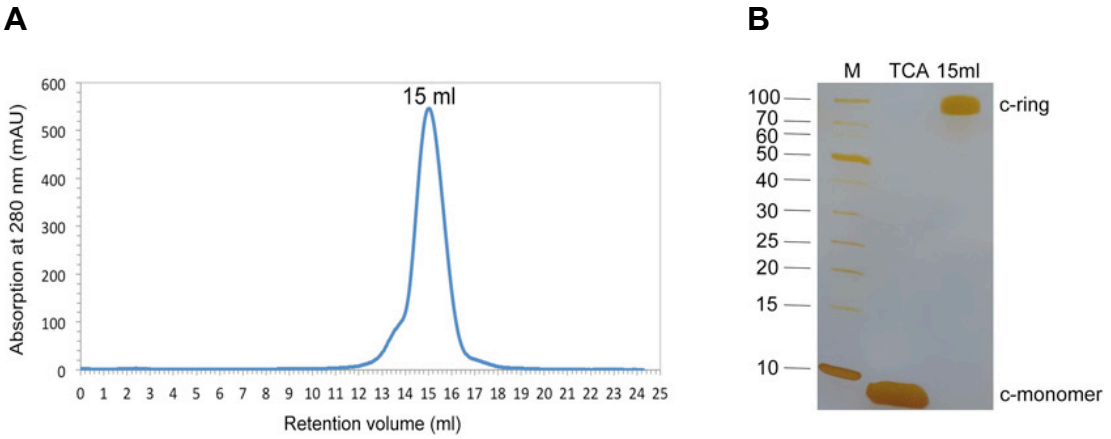

Figure 60. Second size exclusion chromatography of the *B. pseudomallei* c-ring and silver-stained SDS-PAGE of the corresponding fractions.

(A) The profile reveals that the protein was eluting in an almost monodisperse peak with a retention volume of 15 ml, alongside a small, negligible shoulder at 14 ml. **(B)** Analysis of the fractions of the peak confirmed that only single c-rings were present in the sample.

3.3.2.2 3D-crystallization of the *B. pseudomallei* c-ring

The purified, monodisperse protein after SEC was concentrated by centrifugation to a final concentration of 3 mg/ml and used for 3-dimensional crystallization. It was performed in 96-well plates using commercially available screens as well as simultaneously in 24-well plates testing different buffer and precipitants. Crystals could be grown under varying conditions. After incubation of the protein for one week at 18°C, a shower of very thin and tiny crystals could be observed (figure 61). Several modifications including increasing the protein concentration or changing the buffer or precipitant did not help to increase crystal size. However, larger crystals could be obtained under certain conditions after much longer incubation times or by shifting the incubation temperature after a certain time span.

The best diffracting crystals could be grown in 0.1 M NaCl, 0.325 M NaAc pH 7.8 and 0.1 M Tris HCl pH 8.0 using 3 mg/ml c-ring in 1 % DDM with 21 % PEG_{300} or 21 % PEG_{200} as a precipitant and in 0.2 M NaCl and 0.1 M HEPES pH 7.0 with 19 % PEG_{550MME} as a precipitant. Another condition for successful crystal growth using the same protein sample (3 mg/ml c-ring in 1 % DDM) contained 0.05 M $(NH_4)_2SO_4$, 0.1 M NaCi (and 0.1 M glycine) by using 14 % PEG_{8000} as a precipitant agent. Selected examples from early crystals appearing after one week of incubation are shown in

figure 60. Crystals of increased size obtained after at least three months of incubation in related conditions are described in figure 62.

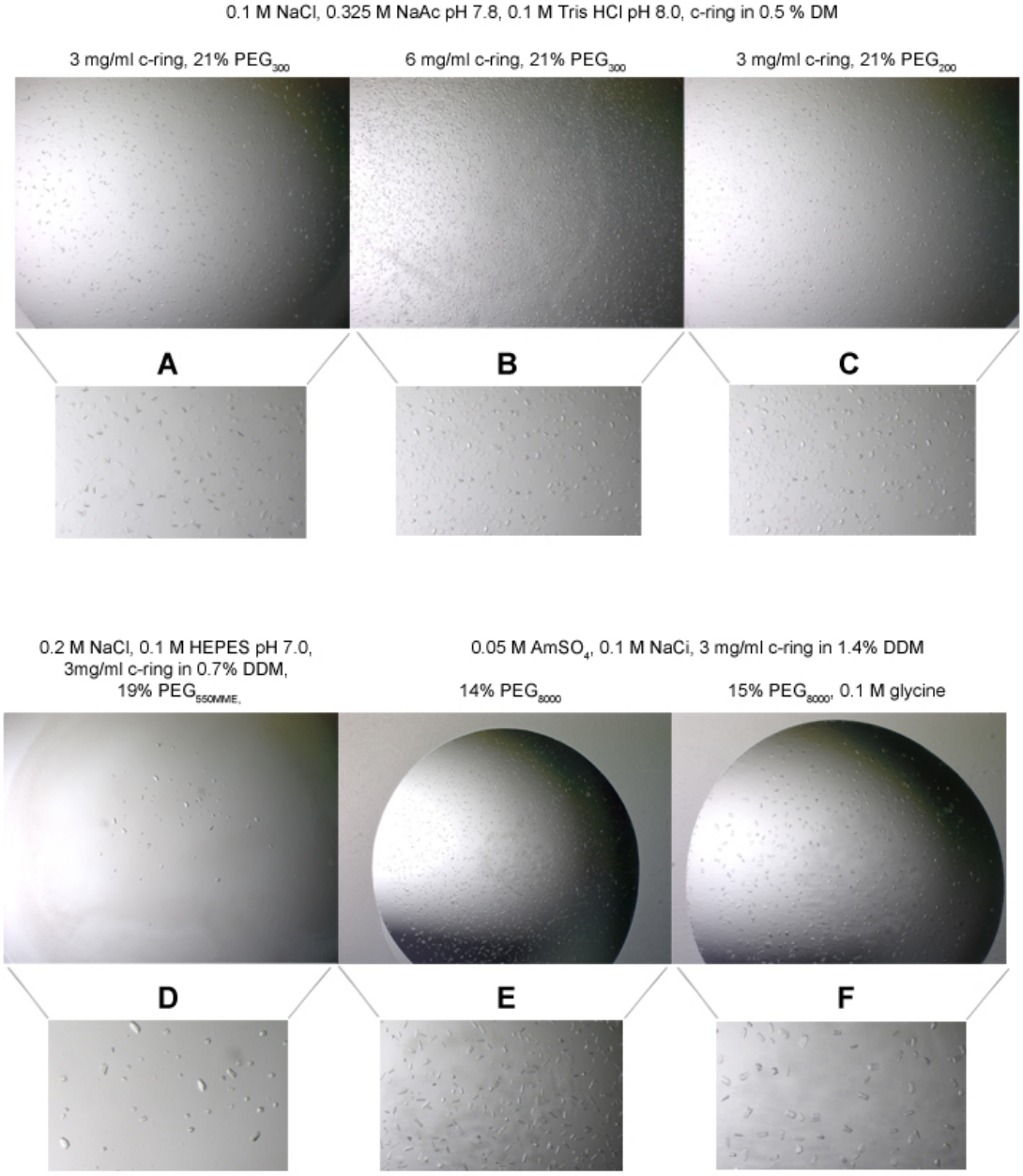

Figure 61. Crystals of the *B. pseudomallei* c-ring after one week of incubation at 18°C.
Crystals could be grown in 0.1 M NaCl, 0.325 M NaAc pH 7.8, 0.1 M Tris HCl pH 8.0, 21 % PEG_{300} using 3 mg/ml protein in 1 % DDM. **(A)**. Increasing the protein concentration to 6 mg/ml **(B)** or using PEG_{200} **(C)** did not increase crystal size. Slightly larger crytstals could be obtained in 0.2 M NaCl, 0.1 M HEPES pH 7.0 and 19 % PEG_{550MME} **(D)** and in 0.05 M $(NH_4)_2SO_4$, 0.1 M NaCl and 14 % PEG_{8000} **(E)** with 0.1 M glycine **(F)**.

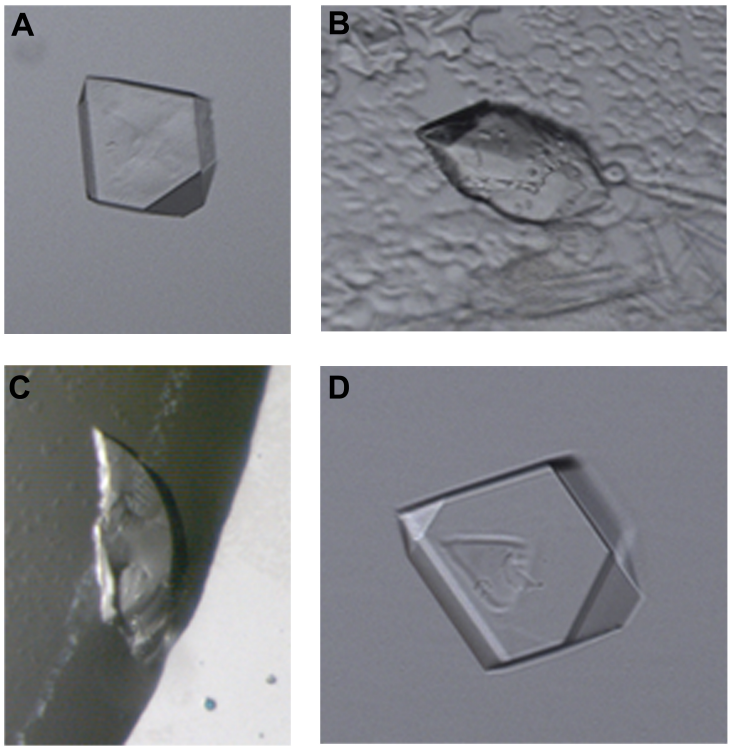

Figure 62. Crystals of the *B. pseudomallei* c-ring after three months of incubation.
Larger c-ring crystals could be obtained after three month of incubation at 18° C in 0.05 M $(NH_4)_2SO_4$, 0.1 M NaCl, 14 % PEG_{8000} **(A)** and 0.2 M NaCl, 0.1 M HEPES pH 7.0, 21 % PEG_{550MME} **(B)**. Large crystals could also be grown after three month at 18° C in 0.1 M NaCl, 0.325 M NaAc pH 7.8, 0.1 M Tris HCl pH 8.0, 20 % PEG_{400} **(C)** as well as in 0.1 M NaCl, 0.325 M NaAc pH 7.8, 0.1 M Tris HCl pH 8.0, 22.5 % PEG_{300} including a temperature shift after one week of incubation at 12° C to 18° C **(D)**.

3.3.2.3 Initial crystallographic data of the *B. pseudomallei* c-ring

X-ray diffraction experiments were carried out with a series of crystals grown under different conditions, including small and large crystals. It turned out that in all cases, larger crystals diffracted better than smaller ones. The best crystal could be grown in 0.1 M NaCl, 0.325 M NaAc pH 7.8, 0.1 M Tris HCl pH 8.0 and 21 % PEG_{400} in a 24-well plate containing 500 µl reservoir and with a drop size of 1 µl. The protein was incubated for 6 days at 12° C before it was shifted to 18° C for another three month of incubation. Several crystals attached to each other have grown in the drop which were separately fished with a nylon loop and directly frozen in liquid nitrogen. The crystals were measured at the beamline ID23.2 of the European Synchrotron Radiation Facility (ESRF, Grenoble, France). The diffraction pattern (figure 63 A) of the best

crystal (figure 63 B and C) showed spots to 6.5 Å. A data set of this crystal in space group $P2_1$ could be collected and initial processing steps were performed using the XDS package. A good signal to noise ratio (I/σ 1.49) to a resolution of 6.69 Å was obtained after data processing (figure 63 D). However, due to a low completeness (25.1 %) of the data set, further processing was not possible. Data collection statistics are summarized in figure 63 D.

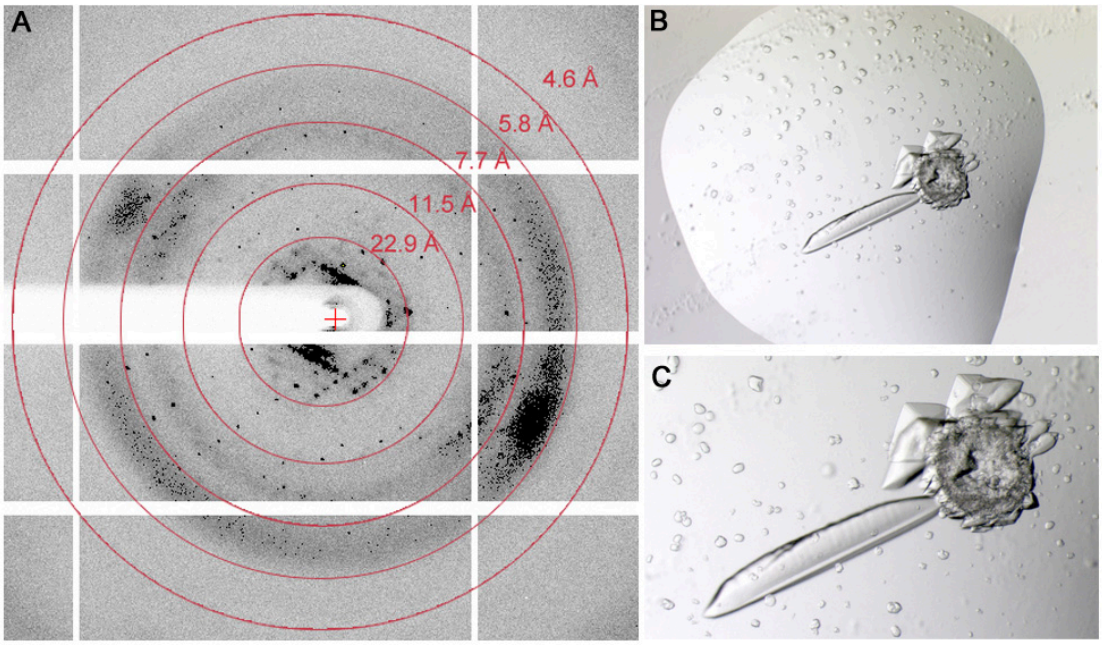

D

SUBSET OF INTENSITY DATA WITH SIGNAL/NOISE >= -3.0 AS FUNCTION OF RESOLUTION

RESOLUTION LIMIT	NUMBER OF REFLECTIONS OBSERVED	UNIQUE	POSSIBLE	COMPLETENESS OF DATA	R-FACTOR observed	R-FACTOR expected	COMPARED	I/SIGMA	R-meas	CC(1/2)	Anomal Corr	SigAno	Nano
15.04	1266	375	1642	22.8%	1.7%	2.0%	1252	41.14	2.0%	100.0*	-30	0.638	170
11.18	2161	577	2301	25.1%	4.0%	3.6%	2157	26.61	4.6%	99.8*	-17	0.737	362
9.29	2657	709	2848	24.9%	3.7%	3.7%	2650	24.45	4.4%	99.9*	-10	0.746	434
8.12	3018	839	3352	25.0%	6.8%	6.8%	2999	12.27	8.0%	99.8*	-7	0.713	436
7.30	3592	922	3725	24.8%	25.5%	26.0%	3581	4.53	29.6%	98.2*	1	0.722	638
6.69	4114	1033	4121	25.1%	94.5%	98.9%	4109	1.49	109.0%	75.0*	2	0.671	757
6.21	2934	888	4442	20.0%	179.0%	191.3%	2843	0.61	211.3%	42.0*	-1	0.635	406
5.82	681	328	4732	6.9%	676.1%	701.1%	553	0.10	844.7%	9.5	21	0.666	28
5.50	196	168	5080	3.3%	-99.9%	-99.9%	55	-99.00	-99.9%	28.2	0	0.000	0
total	20619	5839	32243	18.1%	2.8%	3.0%	20199	11.08	3.3%	100.0*	-4	0.698	3231

Figure 63. Diffraction pattern and initial crystallographic data of the best *B. pseudomallei* c-ring crystal.

(A) The data set was collected at the ESRF beamline ID23.2 (Grenoble, France) from the longish crystal shown in the crystallization drop **(B)** and in detail **(C)**. **(D)** A section of the XDS data statistics (CORRECT.LP) showing the quality of the data set. The signal to noise ratio (I/σ 1.49) was good till a resolution of 6.69 Å, but the data set was not complete (25.1 % completeness) and therefore not suitable for further processing (values are marked in blue).

The results described above showed that the *B. pseudomallei* c-ring could be crystallized obtaining protein crystals which diffracted up to 6.5 Å. However, there is still a lot more potential for improving the resolution of these c-ring crystals. Purification and crystallization of the protein in different detergents would be one of the crucial next steps. In this work, only maltosides (DM, DDM and UDM) and detergents from the cymal series (cymal-4, cymal-5 and cymal-7) were used for crystallization.

Under the crystallization conditions tested so far, a protein concentration between 2 and 4 mg/ml of c-ring resulted in crystal formation. Precipitation was observed if the protein concentration was increased and no crystals were obtained when less concentrated protein was used.

Besides, including a temperature shift was found to increase the size of the protein crystals. Therefore, different temperatures and time spans could be tested in the future to further optimize the crystal size and quality. In addition, small changes in the PEG concentration were observed to have a large impact on the crystal size. Accordingly, fine-tuning of the amount of precipitation could further improve the crystal size and quality.

3.3.3 Structural investigations of the *B. pseudomallei* N-ATPase c-ring using single-particle electron microscopy (EM)

Single-particle electron microscopy of the *B. pseudomallei* c-ring was done in collaboration with Martin Wilkes (Structural Biology, Max-Planck-Institute of Biophysics, Frankfurt), who has plunge-frozen the specimen containing *B. pseudomallei* c-rings and performed cryo-EM data processing of the complex in amphipol (A8-35), DDM and LDAO.

3.3.3.1 Negative stain EM of the *B. pseudomallei* c-ring in DDM

An alternative approach to obtain structural information about the N-ATPase c-ring, besides X-ray crystallography, is the investigation of the protein by single-particle electron microscopy. To produce reliable high-resolution images of intact biological structures, electron cryo-microscopy (cryo-EM) has proven indispensable (van Heel *et al*, 2000) as the resolution is limited to about 20 Å in negative stain EM. Besides, the homogeneity of the protein sample which is investigated is crucial for performing successful single-particle EM, in general. Different types of particles within one sample can hardly be discriminated from each other in cryo-EM since the contrast is much lower compared to negative staining. Furthermore, the protein size and its density are limiting factors of the method itself as the protein has to be distinct and visible as a single-particle in the EM. To apply only homogeneous, monodisperse protein for structural investigations, fractions of the *B. pseudomallei* c-ring after the second SEC were used, which contained only one population of the protein, i.e. single c-rings (peak at 15 ml in figure 60). Initially, the protein was analyzed by negative stain single-particle EM to check its suitability for subsequent structural investigations by cryo-EM and to preliminarily determine the protein concentration, which will be applicable to achieve a decently workable c-ring distribution for later particle picking from the recorded images. In these initial experiments it turned out that the most appropriate particle distribution in negative stain EM was obtained using a protein concentration of 0.05 to 0.1 mg/ml c-ring, dissolved in 0.05 % DDM (figure 64).

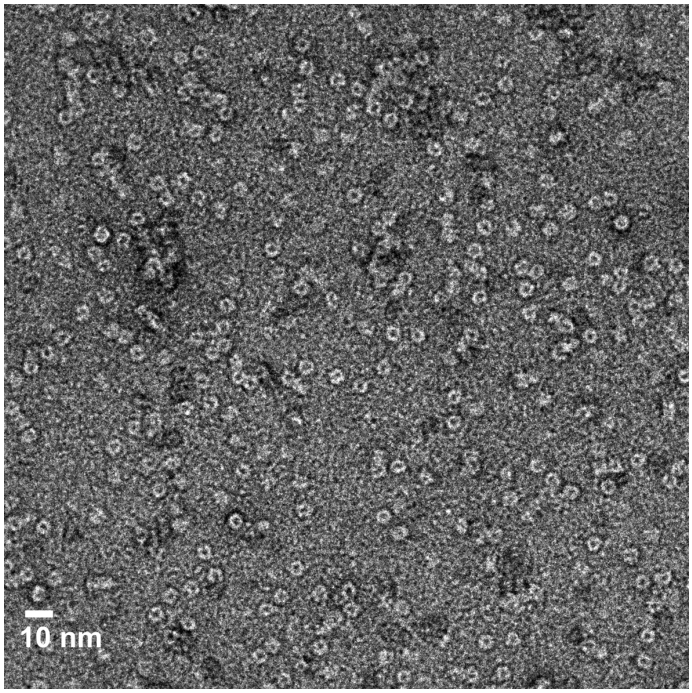

Figure 64. Negative stain single-particle EM analysis of the purified, DDM-solubilized *B. pseudomallei* c-ring.

Electron micrograph of single c-ring particles (c= 0.1 g/ml) in 0.05 % DDM, stained with 1 % uranyl acetate for one minute and imaged at 59 k magnification and 1.1 µm defocus with a Phillips CM120 electron microscope. A scale bar is indicated.

3.3.3.2 Sample preparation of the *B. pseudomallei* c-ring in amphipol (A8-35)

As previously described (Althoff *et al*, 2011; Liao *et al*, 2013; Lu *et al*, 2014), analyzing membrane proteins by single-particle cryo-EM in amphipol, instead of detergent, has distinct advantages, such as enhancing the contrast of the protein, which it encloses and facilitating its embedding into the ice holes of the Quantifoil carbon grid. To test whether this holds also true for the membrane rotor ring, the detergent-solubilized protein was transferred into amphipol A8-35. For this purpose, the purified, DDM-solubilized *B. pseudomallei* c-ring (after SEC, figure 60) was incubated with amphipol (A8-35) at 1:3 (w/w) for four hours at 4° C. To remove the detergent, activated Biobeads were added to the sample and stirred for 16 hours at 4°C. The Biobeads with the bound detergent were removed afterwards. Finally, the sample was loaded on a Superose 6 column to separate c-rings in amphipol from possible excessive, unbound amphipol molecules by SEC (figure 65). As the figure shows, an almost monodispers protein peak was obtained with a retention volume of

the amphipol-solubilized c-ring of 14 ml (figure 65 A). This peak is shifted by 1 ml in comparison to the DDM-solubilzed c-ring, which eluted with a retention volume of 15 ml (figure 60 A). There were no excessive amphipol molecules present in the sample as indicated by the absence of an additional peak in the SEC-profile (figure 65 A). SDS-PAGE analysis of the amphipol-solubilized c-ring revealed that the protein is pure and stable under these conditions (figure 65 B).

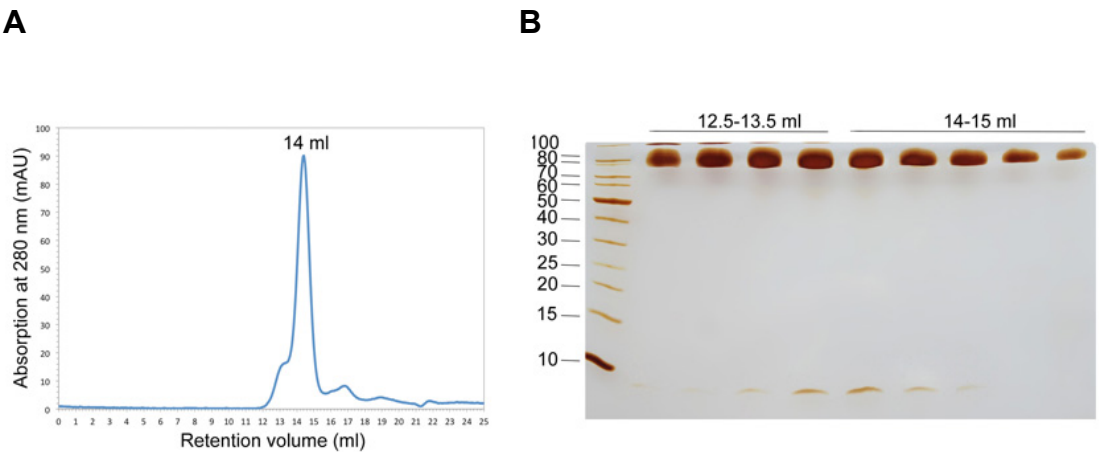

Figure 65. Size exclusion chromatography of the *B. pseudomallei* c-ring in amphipol (A8-35) and silver-stained SDS-PAGE of the corresponding fractions.

(A) SEC was performed using a Superose 6 10/300 column with a constant flow of 0.3 ml/min. The SEC-profile shows an almost monodisperse peak of the amphipol-bound c-ring, eluting with a retention volume of 14 ml, alongside with a small shoulder at 13 ml. The peak of the c-ring in amphipol was shifted 1 ml forward in reference to the ring in DDM (figure 55). Residual, unbound amphipol molecules are assumed to elute afterwards with a retention volume of 16-17 ml, represented by a very small peak not containing any protein. **(B)** The SDS-polyacrylamide gel indicates that the main peak at 14 (-15) ml contains homogeneous c-ring migrating at a level of 80-100 kDa, whereas the smaller shoulder (12.5-13.5 ml) includes c-ring and some rings stacking together, migrating slower on the gel.

3.3.3.3 Negative stain EM of the *B. pseudomallei* c-ring in amphipol (A8-35)

The c-ring in amphipol (SEC-fraction eluting at 14 ml in figure 65) was analyzed by negative stain single-particle EM, analogous to the protein sample in DDM (3.3.3.1). The micrographs obtained show the amphipol-bound c-rings stained with uranyl acetate (figure 66). Single c-ring particles were visible in the micrograph whereby a protein concentration of 0.05-0.1 mg/ml c-ring showed again the most appropriate particle distribution here.

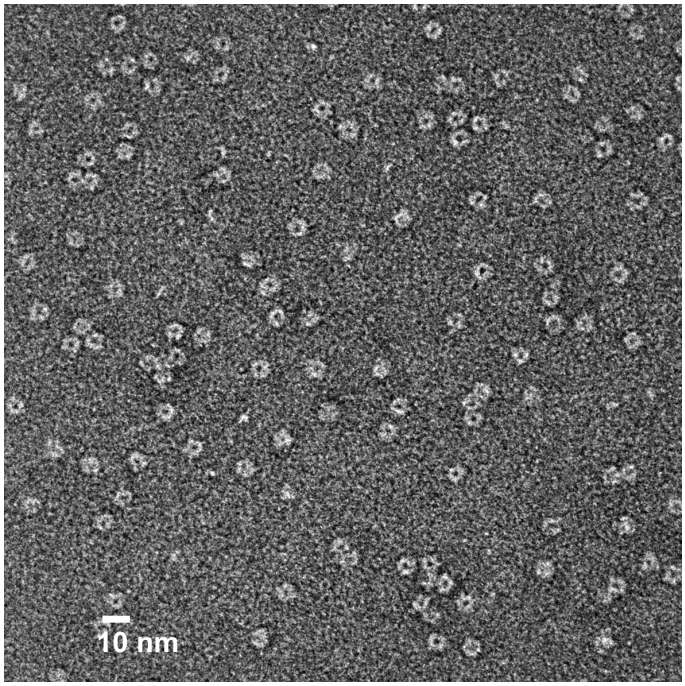

Figure 66. Negative stain single-particle EM of the amphipol-bound *B. pseudomallei* c-ring.
Electron micrograph of single c-ring particles in amphipol (A8-35). Particles were stained with 1 % uranyl acetate for one minute and imaged with a CM120 electron microscope (Phillips) at 59 k magnification and a defocus of 1.3 μm. The detergent was exchanged with amphipol as explained in the text. A scale bar is given.

3.3.3.4 Cryo-EM of the *B. pseudomallei* c-ring in amphipol (A8-35)

- **Data collection**

In a next step, the specimen containing monodisperse amphipol-bound c-rings on a Quantifoil R2/2 grid was plunge-frozen in liquid ethane using a Vitrobot Mark IV (FEI Company). Cryo-EM images of the protein were collected at liquid nitrogen temperature on a JEOL 3200 FSC electron microscope operating at 300 kV with an in-column energy filter. Images were recorded with a K2 Summit direct electron detector camera operating in counting mode with an exposure time of five seconds at a nominal magnification of 30.000, corresponding to a pixel size of 1.14 Å at the specimen. The defocus ranged from 0.5 to 3.7 μm. In the micrographs assumed top and side views of single c-rings as well as side views of two adjacent rings can be identified (figure 66). There are significantly more side views (blue) and dimers of side views (green) present in the sample than top views (red).

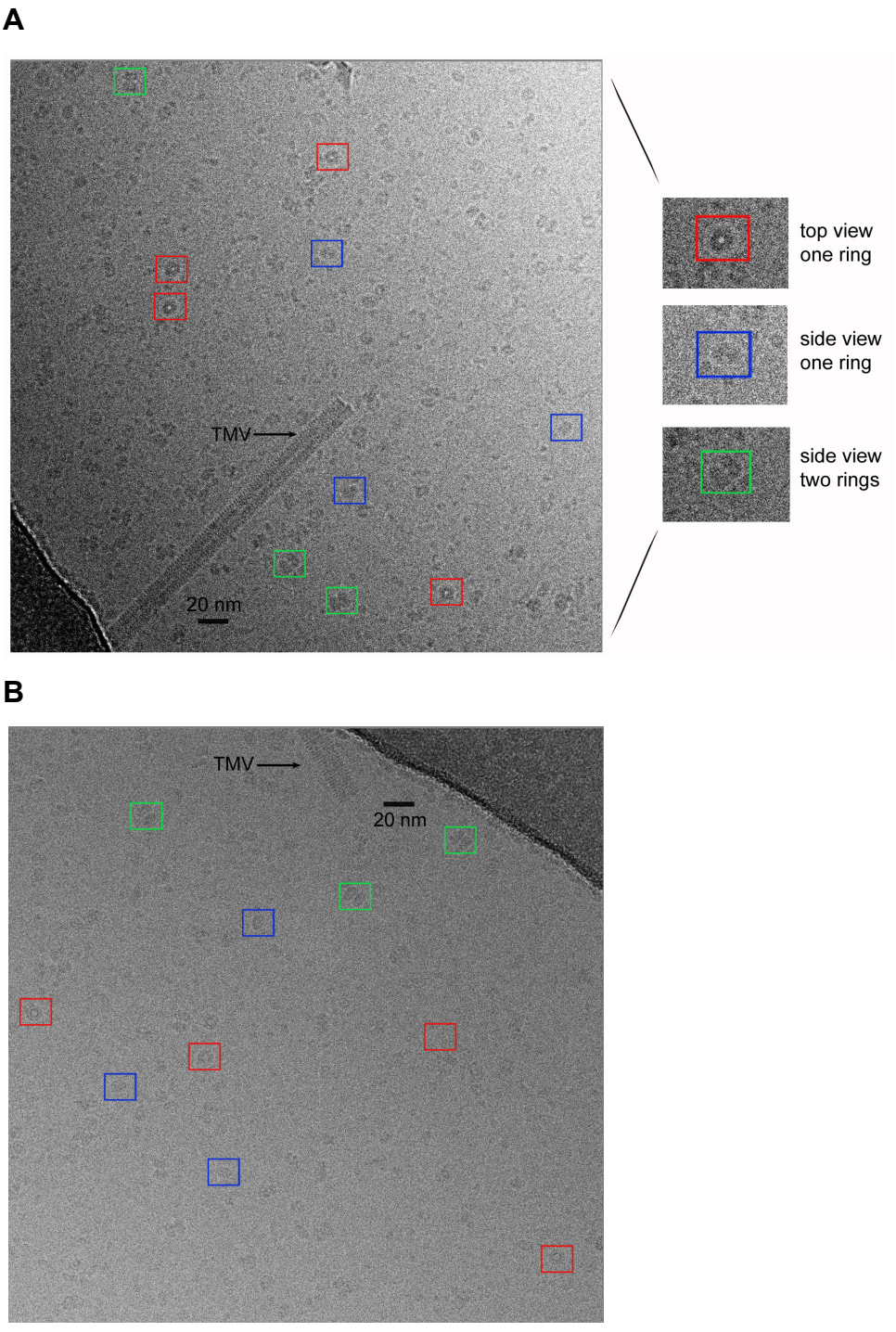

Figure 67. Cryo-EM analysis of the amphipol-bound *B. pseudomallei* c-ring.

Electron micrographs of the c-ring in amphipol (A8-35), embedded in vitreous ice and imaged with a Gatan JEOL 3200 FSC electron microscope with a K2 direct electron detector camera with a defocus of 3.7 µm **(A)** and 1.8 µm **(B),** respectively. Top views (red squares) and side views (blue squares) of single c-rings, as well as side views of two adjacent c-rings (green squares) are marked. Tabacco Mosaic Virus (TMV), which consists of a double layer with 10 nm for each layer, is indicated with an arrow and was used as a standard. A scale bar is given.

- **Data processing**

A total of 2.200 micrographs of the c-ring in amphipol were finally collected and 55.081 particles (see 3.3.3.8, table 53) were initially picked manually using the EMAN programm Boxer (Ludtke *et al*, 1999). Defocus was determined using CTFFIND3 (Mindell & Grigorieff, 2003) and motion correction was perfomed according to (Li *et al*, 2013).

Due to the very small size of the protein complex and therefore the low signal to noise ratio, many particles have to be averaged for structure determination. For reasons of efficiency, automatic particle picking implemented in RELION 1.3 (Scheres, 2012) was tested using the manually-picked c-ring particles as a reference. This resulted in a huge amount of selected particles, requiring manual inspection and editing of each micrograph.

Afterwards, a final dataset comprised about 226.000 automatically picked and inspected particles (see 3.3.3.8, table 53), which were then used for a two-dimensional reference-free classification in RELION 1.3. All of these particles were integrated into 250 different classes. As already apparent from the micrographs, most of the particles represented side views of the protein in vitreous ice. The best 2D class of side views comprised 25 % of all picked particles and clearly showed the overall shape of a c-ring as viewed along the membrane plane.

Intriguingly, distinct densities within the protein could actually be identified, running parallel from one long side to the opposite long side of the c-ring (figure 68 A). These densities reflected the subunits of the c-ring which are composed of just two transmembrane α-helices (1.3.2.4).

The density of a second c-ring (indicated with an arrow in figure 68 A) was present adjacent to it as the protein strongly tends to form dimers (over the time), which could already be observed in SEC (figure 59) and in the sample while imaged in the EM (figure 67).

Four densities were very prominent (marked with orange dots in figure 68) whereby a pair of two was present at each side of the ring. The densities in between were less pronounced and not continuous from one long side to the other, but nevertheless clearly visible as separate densities. In the side view of the c-ring eight single densities could be seen (numbered in figure 68).

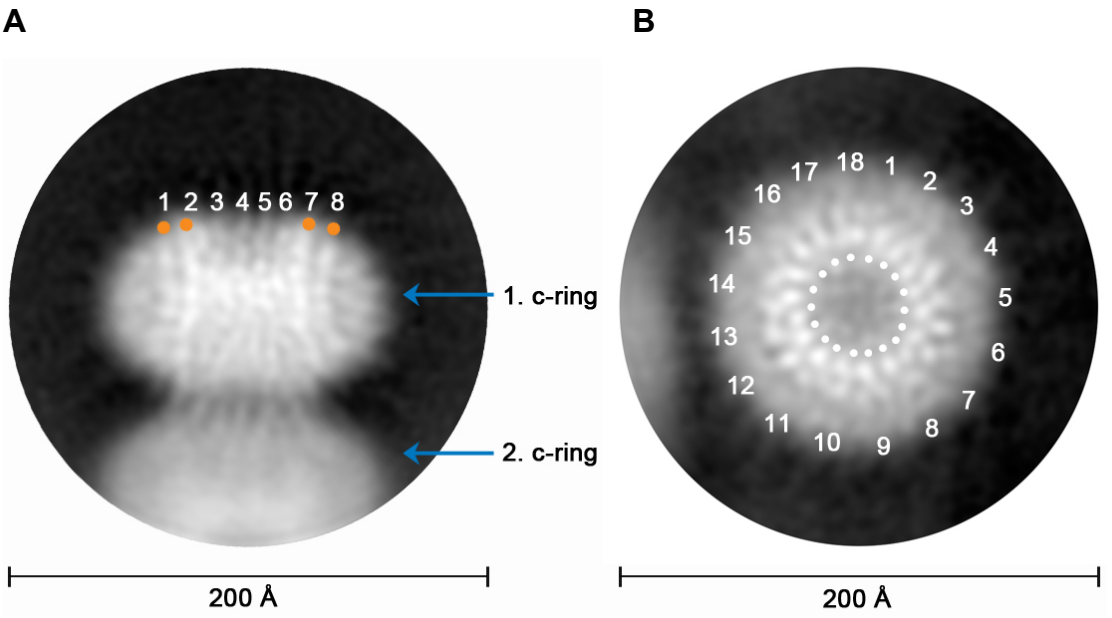

Figure 68. Two-dimensional class averages of a side and a top view of the *B. pseudomallei* c-ring in amphipol (A8-35).

Most of the selected particles are side views of the c-ring. The classification was perfomed with a circular mask of 200 Å using RELION 1.3. **(A)** A 2D class average of side views of the c-ring showing the overall shape of the protein complex. Eight distinct densities are visible running from one long side of the c-ring to the opposite long side. Four of these densities are more pronounced than the residuals (marked with orange dots). A second ring is visible bellow the other one as the protein tends to dimerize upon purification which was also seen in SEC (figure 54). This 2D class of side views comprises 25 % of all picked particles. **(B)** A 2D class average of top views of the c-ring containing 2.5 % of all particles. Two rings of 18 punctual densities each are visible probably corresponding to the inner and outer helices of the c-subunits. As not all densities are equally pronounced and the rings are not absolutely round, the stoichiometry of the complex in amphipol can not be determined.

In contrast to the abundant side views of the c-ring, top views of it were rare. The best 2D class of top views constituted only about 2.5 % of all the picked particles. Nevertheless, 2D class averages of these particles unambiguously showed a c-ring as viewed from the periplasm or cytoplasm with two concentric rings of distinct, punctual densities for its inner and outer helices constituting the c-subunits (figure 68 B).

However, the rings formed by the single densities were not perfectly round, as would be expected from c-ring structures previously solved by X-ray crystallography (Matthies *et al*, 2014; Meier *et al*, 2005; Pogoryelov *et al*, 2009; Preiss *et al*, 2010; Saroussi *et al*, 2012; Schulz *et al*, 2013; Symersky *et al*, 2012; Vollmar *et al*, 2009;

Watt *et al*, 2010), but rather slightly oval-shaped. It appeared that two rings of 18 punctual densities each were present, which would correspond to a stoichiometry of 18 c-subunits for the ring. However, this result has to be considered with great caution, as not all of these densities were equally pronounced. Thus, counting the subunits of the c-ring is still sophisticated and therefore the stoichiometry could not be determined at this point.

In order to be able to determine the c-ring stoichiometry, several 2D classifications of the particles were performed using different circular masks with diameters ranging from 150 to 200 Å. Besides, several iterating classifications were carried out and different class averages (containing similar orientated particles) were selected and then used for the next classification step. However, the densities reflecting the helices of the c-ring in amphipol could not be improved.
A major challenge during the performed 2D classification was the fact that the density of amphipol (1.24 g/ml) (Gohon *et al*, 2004) is very close to the density of protein (1.36 g/ml) (Schmidt-Krey & Rubinstein, 2011). This caused the amphipol densities to be included into the protein signal, leading to misinterpretations and misalignments during data processing.
In previous studies, membrane proteins, which were solubilized in amphipol and investigated by cryo-EM, had an exposed, soluble domain which allowed the alignment of the protein particles during the classification processes (Liao *et al*, 2013; Lu *et al*, 2014). Such a clearly visible, exposed structure part of hydrophilic nature is missing in the present case as the c-ring is generally highly hydrophobic at its outer surface and within its native environment almost totally embedded in the membrane. Due to this hydrophobicity the protein binds a large amount of amphipol and is therefore completely covered by these molecules impeding differentiation of the amphipol densities from the actual protein signal.

As some detergents have lower densities than amphipol, the protein in detergent was tried next for cryo EM data collection. The c-ring was already purified and analyzed by negative stain EM in DDM what has a density of 1.19 g/ml (Schmidt-Krey & Rubinstein, 2011) thus it was chosen for cryo-EM data collection to improve the protein to detergent signal.

3.3.3.5 Cryo-EM of the *B. pseudomallei* c-ring in DDM

- **Data collection**

As particle alignment was impeded by the prominent density of the amphipol (A8-35) molecules (1.24 g/ml), single-particle analysis of the c-ring was next tried with the protein complex solubilized in the DDM, which has a lower densitiy (1.19 g/ml). The monodisperse c-ring in DDM was likewise plunge frozen in liquid ethane and cryo-EM images were collected as described for the protein in amphipol (3.3.3.4).
The DDM-solubilized c-rings were indeed less dense and considerably less visible in the micrographs than the amphipol-bound rings (figure 69).

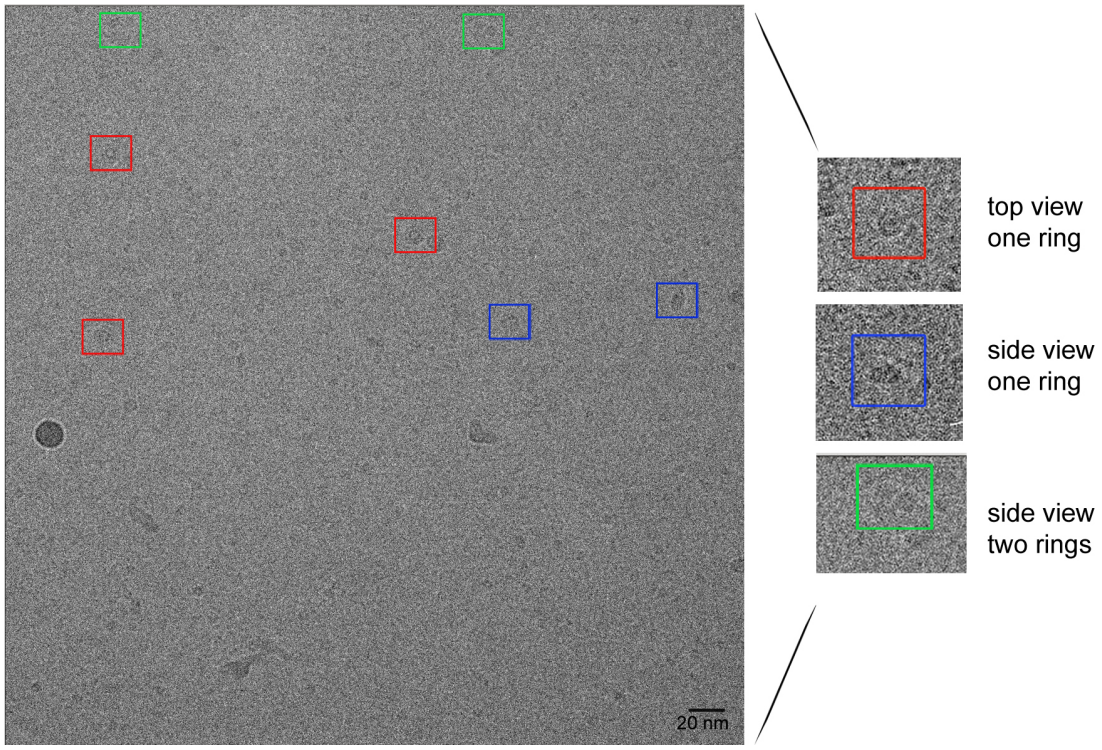

Figure 69. Cryo-EM of the DDM-solubilized *B. pseudomallei* c-ring.
Electron micrographs of the c-ring in 0.05 % DDM embedded in vitreous ice were imaged with a Gatan JEOL 3200 FSC electron microscope with a K2 direct electron detector camera with a defocus of 1.9 µm. Top views (red squares) and side views (blue squares) of single c-rings, as well as side views of two rings (green squares) are marked. A scale bar is given.

On the one hand the fact that the DDM-solubilized c-rings appeared less dense in the EM affects particle identification and picking, on the other hand it might exactly correspond to the expectations of lowering the detergent-to-protein signal or thus improving the protein-to-detergent signal. Therefore cryo-EM data of the c-ring in DDM were collected to perform 2D class averages.

- **Data processing**

A total of 1.060 micrographs were collected with the c-ring in DDM and particles were picked automatically in RELION 1.3 using the previously picked c-ring particles in amphipol as a reference. Again, manual revision of all the corresponding micrographs was required afterwards. Here, a final data set comprising 76.460 particles (see 3.3.3.8, table 53) with a defocus range of 0.5 to 4.0 µm was used for 2D classification processed in RELION 1.3. The best 2D class of side views of the c-ring included 17 % of all picked particles. The overall shape of the protein appeared to be improved in comparison to the c-ring in amphipol as the densities were more defined and less blurry. However, eight distinct densities were visible again with the two pairs of outer densities being more pronounced than the inner densities. As the sample was immediately frozen after purification by SEC less dimerization of the c-rings was observed in this case. Therefore the best side view class in DDM showed only one c-ring (figure 70 A).

The side views in DDM, as well as in Amphipol, appear nearly twofold symmetric along the horizontal axis. Therefore, different orientations can hardly be separated by 2D class-averaging.

Only a minor portion of particles comprises top views of the protein in DDM, as was the case for the data collected from the amphipol-bound c-rings. The best 2D class of top views contained only 2.5 % of all the picked particles.

However, a considerable improvement of the data quality is that the two rings of punctual densities corresponding to the inner and outer helices of the c-subunits are arranged more regularily thereby forming proper circles instead of an oval-shaped structure in case of the amphipol-solubilized protein (figure 68). Furthermore, the distinct densities of both helices of the c-ring are equally pronounced assuming that each density results from a real protein signal and is not caused or biased by the

detergent (figure 70 B). Here, two rings of 17 punctual densities each are present, which would correspond to a stoichiometry of 17 subunits.

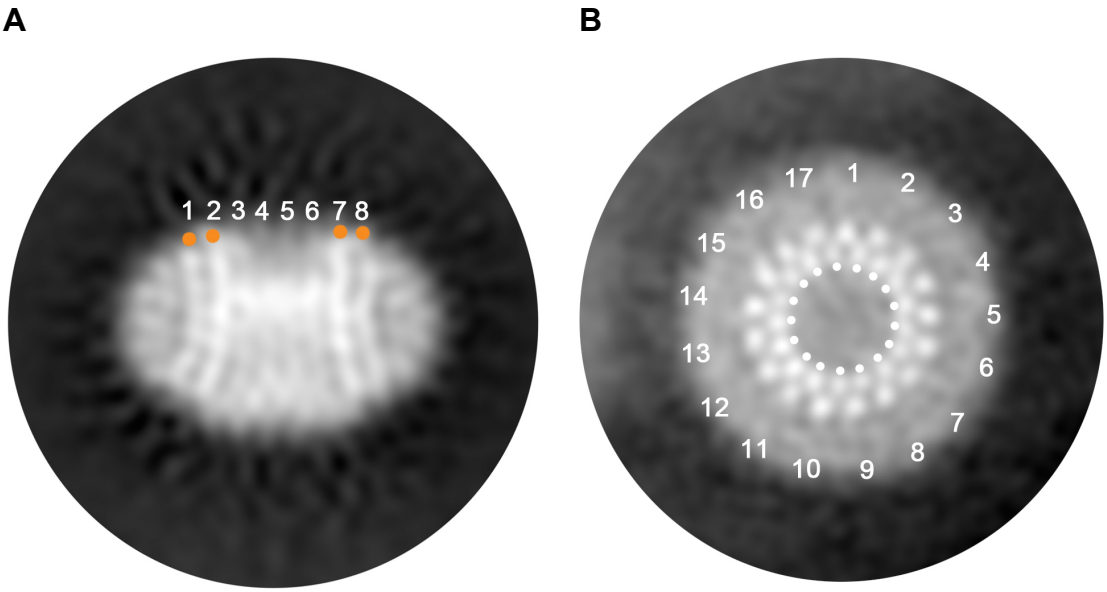

Figure 70. Two-dimensional class averages of a side and a top view of the *B. pseudomallei* c-ring in DDM.

Most of the selected particles are side views of the c-ring in 0.05 % DDM. The classification was perfomed with a circular mask of 200 Å using RELION 1.3. **(A)** A 2D class average of side views of the ring in DDM showing better defined and less blurry lines of the protein densities than for the c-ring in amphipol (figure 63). Eight distinct densities are visible running from one long side of the ring to the opposite. Four of these densities are more pronounced than the residuals (marked with orange dots). This 2D class of side views comprises 17 % of all the picked particles. **(B)** A 2D class average of top views of the c-ring containing again only 2.5 % of all picked particles. The two rings of 17 punctual densities representing the inner and outer helices of the c-subunits are forming perfect circles. Each of the densities presumably representing the transmembrane α-helices of the ring is defined and clearly separated from the adjacent density.

3.3.3.6 The stoichiometry and size of the *B. pseudomallei* c-ring in DDM

To determine the c-ring stoichiometry, the single densities reflecting the two transmembrane α-helices were counted in a top view class of the protein in DDM. 34 distinct densities are visible, whereby the inner ring of 17 densities could represent the inner transmembrane α-helices of the c-subunits and the external 17 densities could build the outer α-helices (figure 71).

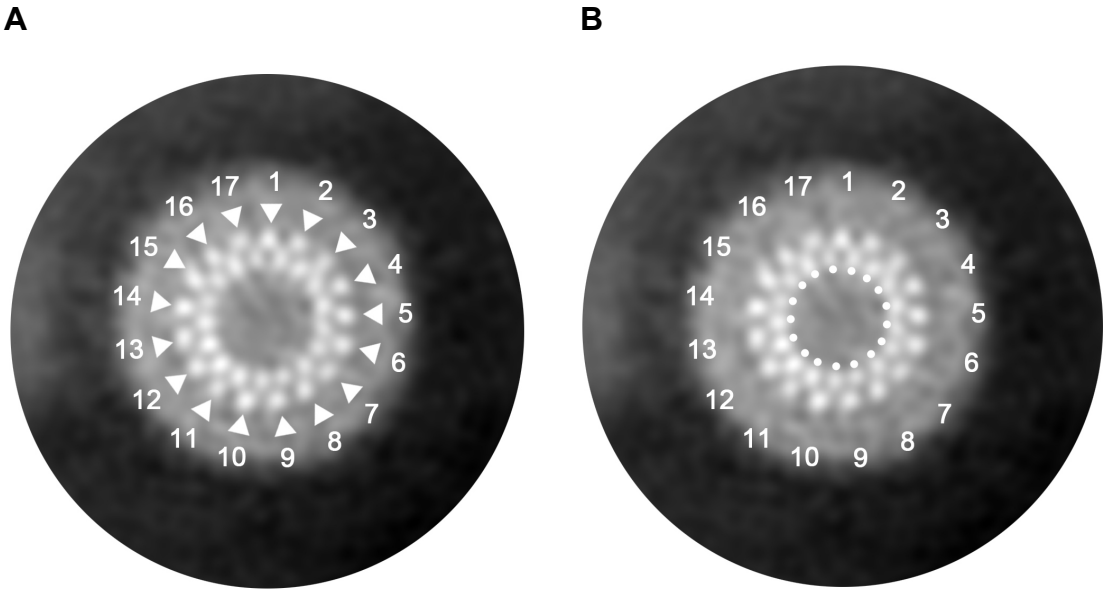

Figure 71. Determination of the *B. pseudomallei* c-ring stoichiometry based on the two-dimensional class averages of the top views of the c-ring in DDM.

A 2D class of top views of the c-ring in 0.05 % DDM shows two concentric rings each composed of 17 equal punctual densities. The external densities forming the outer helices of the subunits are indicated by white triangles **(A)** while the inner densities building the inner helices of the c-subunits are marked with white dots **(B)**. The numbers of the helices are written clockwise outside around the rings at the corresponding positions of the single c-subunits.

Further analysis of the cryo EM data was performed to describe the overall structure of the N-ATPase c-ring. The dimensions of the protein complex, including the diameter and height of the ring as well as the distances between the single inner and outer helices of the c-subunits, were measured (figure 72). Calculations were based on a pixel size of 1.14 Å at the specimen for the K2 direct electron detector camera which was used for imaging.

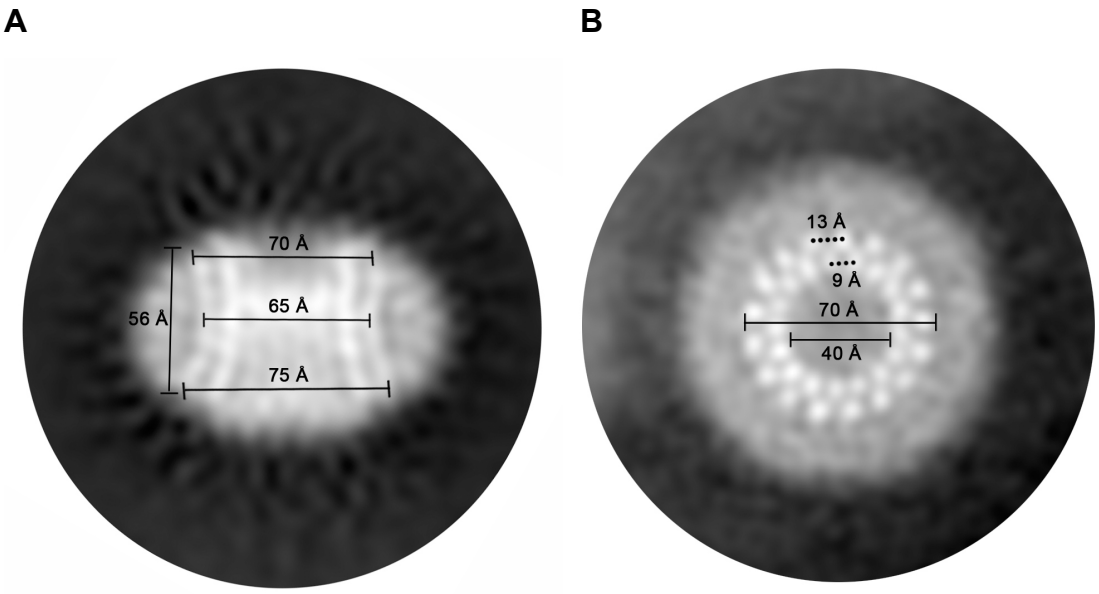

Figure 72. Dimensions of the *B. pseudomallei* c-ring determined in 2D class averages of a side and a top view of the c-ring in DDM.

(A) A 2D class of side views of the c-ring. The narrowest diameter of the c-ring (65 Å) is approximately in the middle of the membrane, where the ion-binding site is assumed to be localized. At the termini and loop regions of the protein the diameter ranges from 70 to 75 Å. The c-ring has a height of about 56 Å**. (B)** A 2D class of top views of the c-ring. The average diameter of the c-ring as seen in the top views was determined to be 70 Å, while the diameter of the protein pore is 40 Å. The mean distance between two outer α-helices is 13 Å and between two inner helices 9 Å (dottes lines).

In summary, to investigate the *B. pseudomallei* c-ring by cryo-EM, the protein in amphipol (A8-35) and in DDM was used as described above. Two data sets of c-ring particles (226.000 particles in amphipol and 76.250 particles in DDM; see 3.3.3.8 table 53) were collected and initial data processing was performed. The 2D class averages which were obtained showed better results, in terms of signal to noise, when the protein in DDM was analyzed, presumably because the lower density of it improved the protein to detergent signal.

However, 3D refinement trials to determine the structure of the c-ring failed du to the fact that the signal of DDM was still very strong. Therefore, to further improve the protein to detergent signal and to validate the c-ring stoichiometry, the complex was analyzed by cryo-EM in a second detergent. Lauryldimethylamine-N-oxide (LDAO) was chosen for two reasons: First, the *B. pseudomallei* c-ring remained stable in the presence of LDAO and second, LDAO has a very low density of only 0.88 mg/ml

(Schmidt-Krey & Rubinstein, 2011), which is much lower than the density of protein (1.36 mg/ml) and also than the density of amphipol (A8-35) (1.24 mg/ml) and DDM (1.19 mg/ml) used before.

3.3.3.7 Cryo-EM of the *B. pseudomallei* c-ring in LDAO

- **Data collection**

The c-ring was purified in LDAO as in DDM and the monodisperse protein (data not shown) was plunge frozen in liquid ethane. Cryo-EM images were collected as described for the protein in amphipol (3.3.3.4) and DDM (3.3.3.5).

The LDAO-solubilized c-rings appeared similar to the DDM-solubilized c-rings (figure 65) in the micrographs, but seemed to be slightly smaller in length and diameter (figure 73). Here, top and side views of single rings were visible, whereas no dimers of c-rings could be detected.

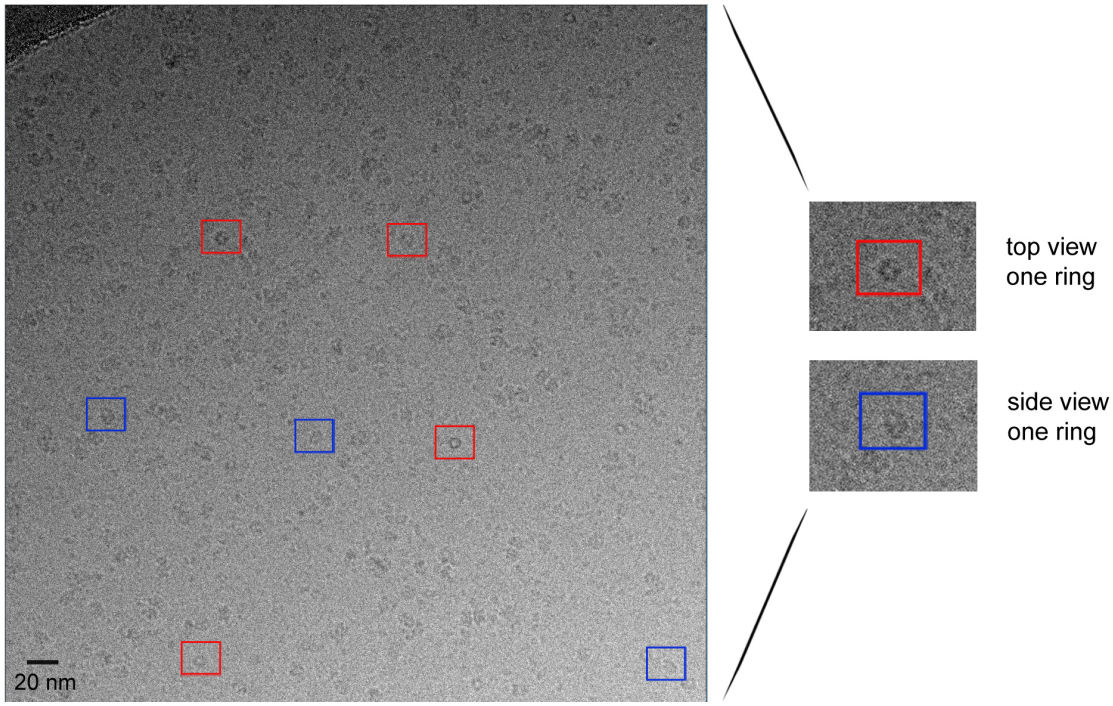

Figure 73. Cryo-EM analysis of the LDAO-solubilized *B. pseudomallei* c-ring.

Electron micrographs of the c-ring in 0.2 % LDAO, embedded in vitreous ice and imaged with a Gatan JEOL 3200 FSC electron microscope and a K2 direct electron detector camera with a defocus of 2.0 µm. Top views (red squares) and side views (blue squares) of single c-rings) are marked. Dimers of side views could not be detected here. A scale bar is given.

- **Data processing**

A total of 710 micrographs were collected with the c-ring in LDAO and 39.433 particles were initially picked manually in Boxer and then 74.139 automatically in RELION 1.3 by using the manually picked particles in LDAO as a reference (see 3.3.3.8, table 53). Automatic particle picking by using c-ring particles in amphipol (A8-35) or DDM as a reference was not successful. The final data set of 74.139 particles with a defocus range of 0.6 to 3.7 µm was used for 2D classification in RELION 1.3. The best 2D class of side views of the c-ring includes 25 % of all picked particles. The overall shape of the protein is further improved when compared to the ring in DDM (figure 70). Eight distinct densities are visible again with the two pairs of outer densities being more pronounced than the inner densities (figure 74 A).

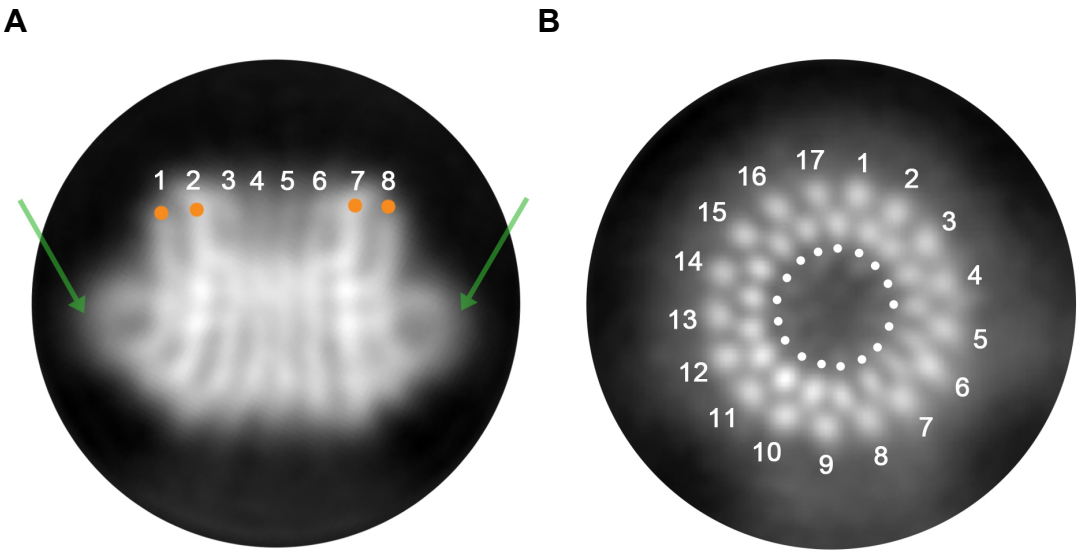

Figure 74. Two-dimensional class averages of a side and a top view of the *B. pseudomallei* c-ring in LDAO.

Most of the selected particles are side views of the c-ring. The classification was perfomed with a circular mask of 130 Å using RELION 1.3. **(A)** A 2D class average of side views of the ring in LDAO with sharper densities than for the c-ring in amphipol (figure 67) and DDM (figure 69). Eight distinct densities are visible again from one long side of the ring to the opposite, whereby four of these densities are more pronounced (orange dots). This 2D class of side views comprised 25 % of all picked particles. The density of LDAO (green arrows) was reduced compared to amphipol (figure 67) and DDM (figure 69). **(B)** A 2D class average of top views of the c-ring in LDAO containing 5.5 % of all picked particles. The two rings of 17 punctual densities represent the inner and outer helices of the c-subunits, as was the case for the c-ring in DDM (figure 67). Each of the densities is very defined and clearly separated from the adjacent density.

The best side view of the ring in LDAO shows only one protein complex. Remarkably, the signal of the detergent bound to the ring (figure 74 A, green arrows) is significantly reduced.
The best 2D class of top views contains only 5.5 % of all the picked particles. Like in the top view of the c-ring in DDM, two rings of 17 punctual densities each are present here, which would correspond to a stoichiometry of 17 c-subunits (figure 74 B).

No dimerization of the c-ring was observed.

The prominent top and side view classes of the c-ring were present in all three samples, amphipol (A8-35) (figure 68), DDM (figure 70) and LDAO (figure 74) when classification was performed by default with a full CTF correction (2.4.3.5). When 2D classification in RELION 1.3 was performed with phase-flipping, different other classes of the c-ring appeared very clearly when the c-ring in LDAO was analyzed (figure 75). As the amplitudes were not CTF corrected, more general features of the protein are considered during the alignment process thereby improving the overall shape of the different c-ring views. A series of these classes can be regarded as a tilt series of the c-ring meaning that the protein itself is frozen in a continuously tilted orientation in the vitreous ice whereas the specimen containing grid was not tilted during cryo-EM data collection.

Figure 75. Two-dimensional class averages of different views of the *B. pseudomallei* c-ring in LDAO.

The data set was phase-flipped during 2D classification of the c-ring in RELION 1.3. Different views of the c-ring representing a tilt series of the protein in the vitreous ice from the side to the top view are shown. Single densities of the protein can be discriminated in all of the five views.

3.3.3.8 The stoichiometry of the *B. pseudomallei* c-ring in LDAO

To further confirm the c-ring stochiometry, the best top view of the c-ring in LDAO, which was obtained when reference-free and full CTF-corrected 2D classification was performed in RELION 1.3, was reanalyzed using Imagic (van Heel *et al*, 1996). The top view 2D class from manually picked particles was used as an input and different symmetries (8-19) were applied. Remarkably, the results indicate again that this c-ring is probably composed of 17 subunits. The inner and outer helices are more defined in the c_{17} ring in comparison to rings obtained after having applied other symmetries (figure 76).

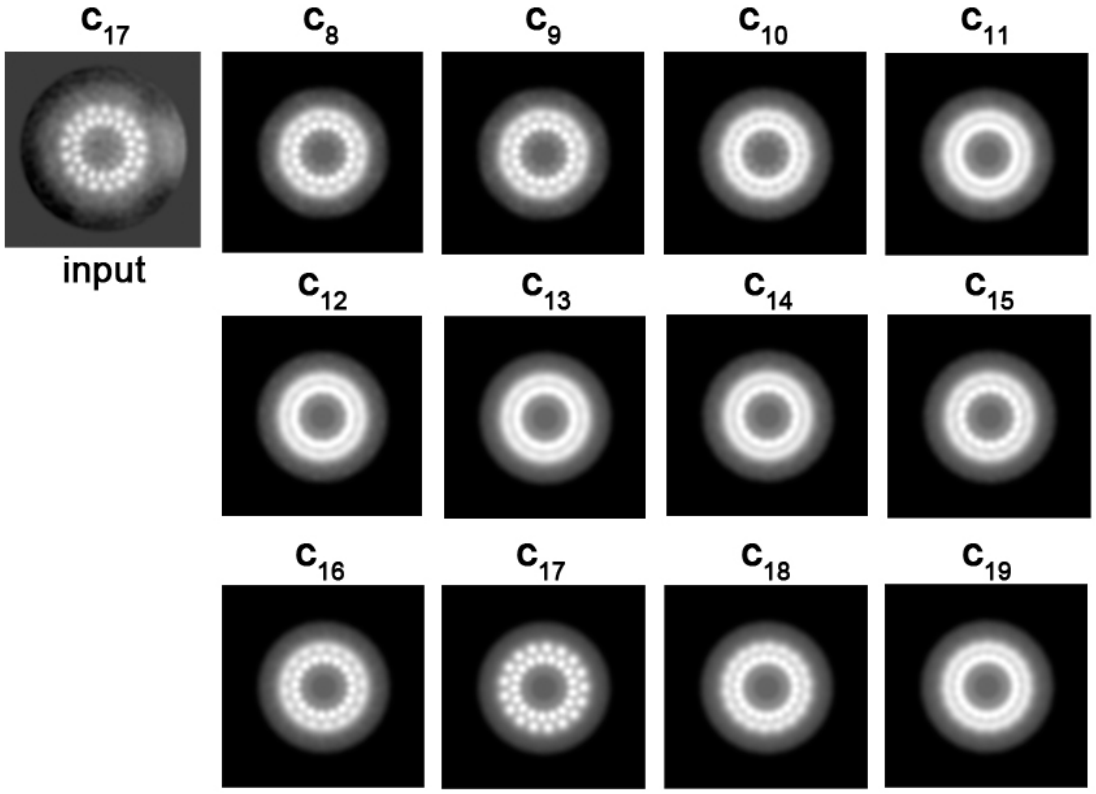

Figure 76. Different symmetries applied on the best top view 2D class of the *B. pseudomallei* c-ring in LDAO.

The best top view of the c-ring obtained from reference-free, full CTF-corrected 2D class averaging in RELION 1.3 (c_{17} input) was subsequently symmetrized in Imagic. The different outputs with symmetries ranging from 8 to 19 are shown. The best-looking top view of the c-ring was obtained when a 17-fold symmetry was applied in Imagic (c_{17}).

The same procedure was carried out with the c-ring in DDM, but in this case none of the symmetries applied yielded any useful results (data not shown). The most probable reason for this is that the automatically picked particles are not as well centered, which impedes symmetrization of the protein in Imagic.

The three single-particle cryo-EM analyses of the *B. pseudomallei* N-ATPase c-ring in amphipol (A8-35), DDM and LDAO (3.3.3.1-3.3.3.8), are summarized in table 53.

Table 50. Data collection and analysis of the *B. pseudomallei* c-ring by single-particle cryo-EM

	amphipol A8-35	**detergent DDM**	**detergent LDAO**
Protein sample	1.4 mg/ml c-ring in amphipol A8-35	1.6 mg/ml c-ring in 0.05 % DDM	3.5 mg/ml c-ring in 0.2 % LDAO
Densities of detergents	1.36 g/ml	1.19 g/ml	0.88 g/ml
Data collection			
Electron microscope	JEOL 3200 FSC (Gatan)	JEOL 3200 FSC (Gatan)	JEOL 3200 FSC (Gatan)
Detector camera	K2 Summit direct electron detector camera (Gatan)	K2 Summit direct electron detector camera (Gatan)	K2 Summit direct electron detector camera (Gatan)
Pixel size	1.14 Å	1.14 Å	1.14 Å
Defocus range	0.5 - 3.7 µm	0.5 - 4.0 µm	0.6 - 3.7 µm
Images	2.200	1.060	710
Data processing			
Software packages	RELION 1.3	RELION 1.3	RELION 1.3 and Imagic
particles picked			
manually	55.081	-	39.433
automatically	226.000	76.460	74.139
Mask for class-averaging	200 Å	200 Å	130 Å
Particles in top view	2.50 %	2.50 %	5.50 %
Particles in side view	25.0 %	17.0 %	25.0 %
Symmetry of the c-ring	18	17	17

3.3.3.9 Cryo-EM data interpretation and evaluation

- **Structural model of the *B. pseudomallei* N-ATPase c-ring**

For an additional validation of the c-ring cryo EM data, a structural model of the N-type complex was computed using the *B. pseudomallei* c-subunit sequence, the structure of the c_{10} ring of yeast (pdb 3u2y) (Symersky *et al*, 2012) as a basis and applying a 17-fold symmetry (2.4.7). The c_{17} ring model obtained (figure 77) shows a prominent kink slightly above the middle of the helices. The kink, which was initially introduced by the used c_{10} model, is localized where the ion-binding sites come to lie (figure 69 A). This kink further leads to an asymmetric c-ring with a wider diameter at the cytoplasmic loop region (80 Å) and the smallest diameter at the periplasmic N- and C-termini (65 Å). The total height of the ring is about 60 Å.

An electrostatic surface representation of the modeled c_{17} ring was calculated showing the distribution of the charged residues of the protein (figure 77 B). However, as the generated c-ring is only a model, this electrostatic potential distribution has to be interpreted with caution. The transmembrane region of the ring is assumed to extend from F80 on the periplasmic side to S54 near the cytoplasmic loop region. Thus, negatively (red) and positively (blue) charged residues are found at the periplasmic termini and the cytoplasmic loop region as well as in the middle of the helices, where the ion-binding sites are presumably located. The hydrophobic, uncharged regions of the c-ring are shown in white. Most of the detergent seen in the 2D classes of the protein is supposed to be bound to the hydrophobic (white) region above the ion-binding sites of the c-ring (indicated with an arrow in figure 77 B), which fits remarkably well with the obtained model.

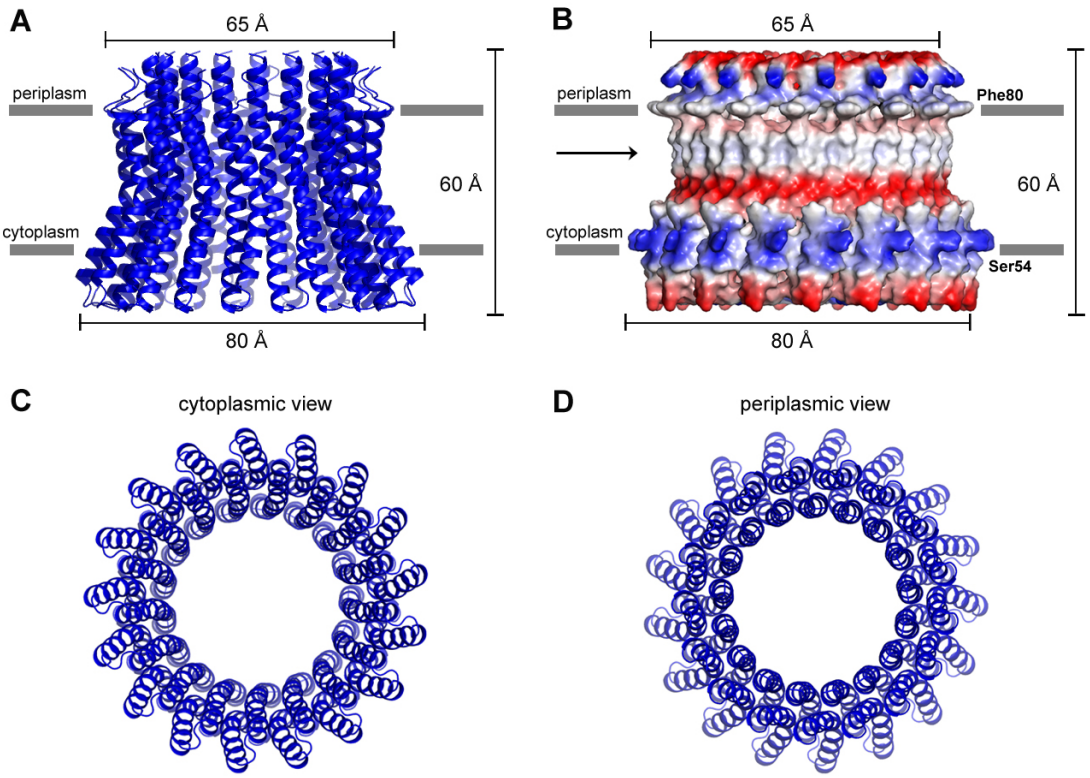

Figure 77. Structural model of the *B. pseudomallei* N-type c-ring.

The rotor ring was built of 17 identical c-subunits of *B. pseudomallei*. **(A)** Side view of the c_{17} ring model, parallel to the membrane plane. The model has a diameter of 65 Å at the periplasmic termini and a diameter of 80 Å at the cytoplasmic loop region. The height of the complex is 60 Å. **(B)** Electrostatic surface potential distribution of the side view of the modeled *B. pseudomallei* c_{17} ring. Charged regions (red: negative; blue: positive) are localized at the termini and loop regions of the ring, while uncharged, hydrophobic residues are found in the middle of the complex (white), where most of the amphipol and detergent is supposed to be bound (arrow). **(C)** Cytoplasmic and **(D)** periplasmic view of the modeled c_{17} ring showing the two concentric rings formed by the inner and outer helices of the protein.

- **Reprojections of different c-ring X-ray structures and comparison with the *B. pseudomallei* c_{17} ring cryo-EM data**

Supposing that the investigated c-ring has a stoichiometry of 17, the question arises how many subunits can be expected to be visible in a side view of the cryo EM 2D class averages. To investigate this question, reprojections of c-rings with known stoichiometries were calculated using EMAN2 (Tang *et al*, 2007) to find out how many subunits can be seen when visualizing these rings by EM. Several c-ring

structures, which have been previously solved by X-ray crystallography (c_{11} from *I. tartaricus*, c_{12} mutant from *B. pseudofirmus* OF4, c_{13} from *B. pseudofirmus* OF4, c_{14} from *S. oleraceae* and c_{15} from *S. platensis*), as well as a structural model for the c_{17} ring, which was created in this work (figure 77), were used. The X-ray structures as well as the model structure were low-pass filtered to 7 Å, where only α-helices and no side chain residues of the protein are visible.

Based on the reprojections showing the top and side views of each c-ring (figure 78) several significant observations can be made:

In the top views the number of densities, which can be seen, reflects the actual number of c-subunits of the corresponding complex. Each c-subunit is formed by an inner and an outer transmembrane α-helix. Accordingly, two concentric rings representing the two helices can be discriminated.
The quality of the top views apparently varies between the c-rings, resulting from a different helix packing within these complexes. While in case of the *I. tartaricus* c-ring, eleven subunits are present in a ring with an outermost diameter of 50 Å (Meier *et al*, 2005) the 13 subunits of the wildtype *B. pseudofirmus* OF4 c-ring are evenly distributed in a ring with an outermost diameter of 63 Å (Preiss *et al*, 2010), which makes 4.5 Å and 4.85 Å per c-subunit, respectively. Consequently, the distances between the single helices are slightly but significantly wider in the c_{13} ring leading to a better separation of the helices in the reprojection of this ring in comparison to the more tightly packed c_{11} ring. This means, the closer the distances of the inner and outer helices of one c-subunit are, the less separated the densities of these helices appear in the reprojections.
Besides that point, it can be seen in the top views of the c_{11} and the c_{13} ring (figure 78), that the two helices of each subunit can not be brought to congruence with each other as they are slightly off set thereby introducing a so-called vorticity in the c-ring.
In the side views of the different c-rings several densities are visible, whereby in each case some of them are more pronounced than others. Conspicuously, two side views showing different numbers of densities were obtained when reprojections were calculated from rings with an even number of subunits (c_{12} and c_{14}) whereas only one

side view resulted when a c-ring with an odd stoichiometry (c_{11}, c_{13},c_{15} and c_{17}) was used (figure 78).

The reprojection of the c_{17} ring model shows nine distinct densities in the side view of the protein (figure 78).

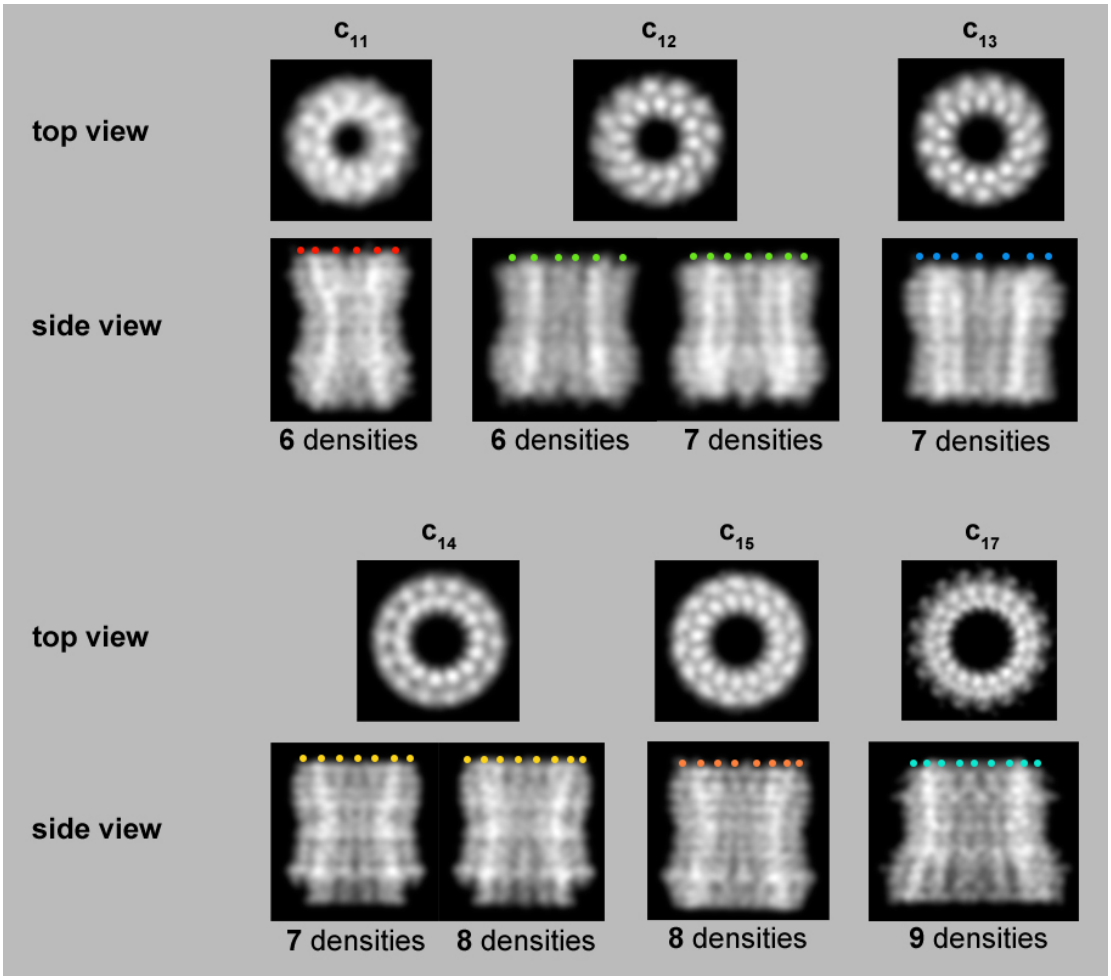

Figure 78. Reprojections of the X-ray structures of c-rings with different stoichiometries (c_{11}-c_{15}) and a structural model of the c_{17} ring.

The c-ring X-ray structures of *I. tartaricus* (c_{11}, pdb 1yce Meier *et al*., 2005), *B. pseudofirmus* (mutant c_{12}, pdb 3zo6, Preiss *et al*., 2013; wildtype c_{13}, pdb 2x2v; Preiss *et al.*, 2010), *S. oleraceae* (c_{14}, pdb 2w5j; Vollmar *et al*., 2009) and *S. platensis* (c_{15}, pdb 2wie, Pogoryelov *et al*., 2009) as well as a structural model of the *B. pseudomallei* c-ring (c_{17}, this work, figure 76) were low-pass filtered to 7 Å and reprojections were calculated using EMAN2. The single densities representing the helices in the side views of the rings are marked with coloured dots. In case of an equal number of c-subunits (12 and 14) two different side views were obtained whereby one of them shows one density more than the other. Considering a c-ring with an odd number of-subunits (11, 13, 15 and 17) only one side view was obtained. In all reprojections the single densities are differently pronounced.

- **Evaluation of the *B. pseudomallei* c-ring cryo-EM data**

The reprojection of the side view of the modeled c_{17} ring shows nine densities (figure 75). In contrast, only eight densities are visible in the side view of the cryo-EM 2D class averages of the investigated c-ring in DDM (figure 70) and LDAO (figure 74). This discrepancy as well as the occurrence of differently pronounced densities in both cases, the cryo-EM 2D classes and the calculated reprojections, can be explained by the principle of image formation in electron cryo-microscopy and the geometry of the investigated protein complex.

In single-particle cryo-EM, structural information is obtained from the elastic scattering of electrons while interacting with the biological sample in vitreous ice. The scattering of electrons is proportional to the density of the material. The denser the molecule is, the more electrons are scattered and thus the stronger is the resulting signal, meaning the object appears darker against the less dense aqueous background (Booy & Elena, 2006). Consequently, the smaller the distances between two neighbouring (inner and outer) helices are, the denser the protein is packed at this position.

As the investigated protein complex is ring-shaped, it is not possible to see only one helix pair in the c-ring side view but several helix pairs being superimposed to each other (figure 78 and 79). Due to the geometry of a circle, in a side view the distances between two adjancent c subunits become smaller at the curvatures of the c-ring than in the middle of the protein resulting in a stronger signal in the EM. In comparison, helix pairs which have larger distances between each other, as is the case for the helices located in the middle of the c-ring, result in a lower density. A comparably weak signal is obtained at the outermost left and right positions of the c-ring where only one helix pair is localized. Figure 79 illustrates this phenomenon schematically with a c_{17} ring. This theoretical consideration explains the occurrence of the densities seen in the side view 2D class of the c-ring when imaged by cryo-EM.

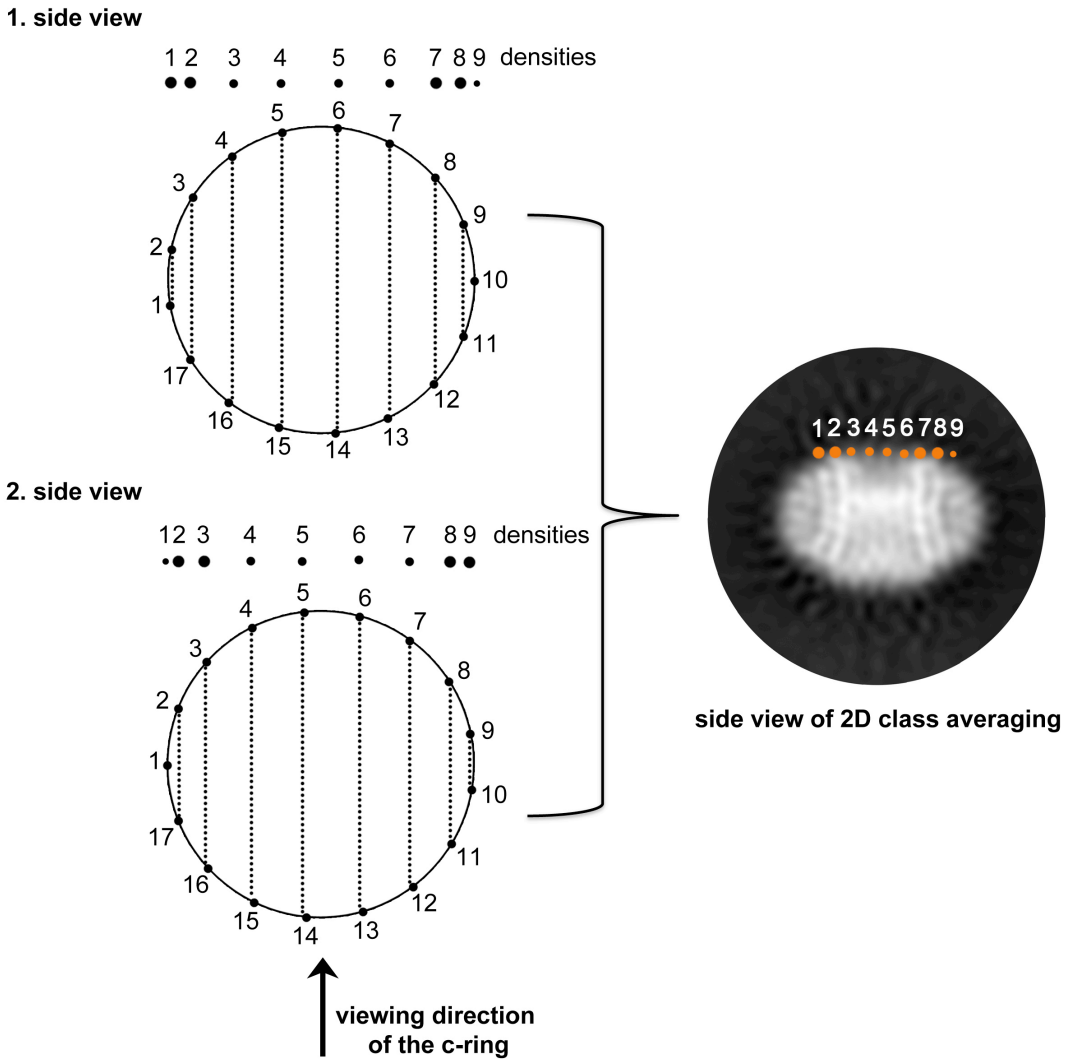

Figure 79. The theoretical number of subunits seen in the side views of a c_{17} ring.

Scheme of how the helices of a c_{17} ring can be superimposed to each other in a side view. Each pair of helices forming one c-subunit is shown as a dot on the circle (ring). The viewing direction at the ring is indicated (arrow). The densities expected to be seen in a side view are indicated by dots above the rings. The dot size represents the signal intensity. The density signal is enhanced for the helix pairs located at the curvatures (pairs 2+1 and 3+17 on the left and pairs 8+12 and 9+11 on the right of the upper ring; pairs 2+17 and 3+16 on the left and pairs 8+11 and 9+10 on the right of the lower ring). Larger dots indicate more signal intensity. These four helix pairs produce stronger intensities. The outermost single helix pairs produce only a weak signal (10 in the upper ring; 1 in the lower ring) hence smaller dots. The residual densities in the middle (pairs 4-7 and 13-16 in the upper ring and pairs 4-7 and 12-15 in the lower ring) are equally pronounced. As the protein has an odd number of subunits, two different side views are obtained which can not be separated but become averaged in the actual 2D class side view of the c-ring. Here, two pronounced densites are visible at each side of the c-ring, at its curvatures. The single helix pair is not visible as it might be averaged out due to a low signal intensity.

There is only one striking helix arrangement possible in the side view of a ring with an even number of subunits. In this case no single helix pair can be present at either side of the ring.
However, if a ring with an uneven number of c-subunits, like 17, is considered from the side, different helix arrangements can be found, whereby two of them are most conspicuous. Here, the extent helix pair can be localized at each side of the c-ring. However, these two side views could not be separated during the 2D classification of the c-rings, probably due to very small signal differences within the two views. Accordingly, the resulting side view represents an average of both views with two prominent helix pairs at each side of the ring, located at the curvatures. Due to this average it is also feasible that the single helix pair at the outermost position changed between the left and right side of the c-ring and is therefore averaged out in the final resulting side view in/of the 2D class.

Summary of the single-particle cryo-EM analysis of the *B. pseudomallei* N-type c-ring

Considering all the results obtained from the 2D class averaging of the c-ring particles as well as from the reprojections calculated from different c-ring X-ray structures, the following conclusions from these investigations can be drawn at this point:

- Using single-particle cryo-EM as a method to obtain structural information about a protein complex requires a homogenous sample to trace recurrent features of the protein. Due a strong hydrophobicity of the here investigated protein complex, the N-type rotor ring of *B. pseudomallei*, a high amount of solubilizing detergent is bound to the protein surface. The overall structure of the c-ring could be visualized by performing 2D class averaging of the protein particles. At this point it became apparent that the quality of the resulting classes was dependent on the choice of the detergent (DDM, LDAO or amphipol A8-35) used for analysis (chapters 3.3.3.4-3.3.3.7).

- A possible reason for the fact that image quality improved by using DDM instead of amphipol A8-35 is that DDM molecules have a lower density than amphipol molecules. Consequently, the densities resulting from the protein could be better discriminated from the densities caused by the surrounding detergent. An additional improvement was obtained by the use of LDAO, which has a density even lower than DDM and protein (chapters 3.3.3.4-3.3.3.7).

- In the top view of the c-ring in DDM and LDAO, 34 punctual densities could be clearly discriminated, just as in the reprojections of different c-rings which were calculated for comparison with the 2D class averages of the actual cryo-EM data. Each of these 34 densities represents one transmembrane α-helix, thereby forming an inner and outer ring of 17 helices each (chapters 3.3.3.5-3.3.3.9).

- According to the reprojections, nine densities should be visible when considering a c_{17} ring from the side. Due to the geometry of a ring and the fact that more tightly packed regions within a protein produce stronger signals in the electron microscope, not all of these densities are equally pronounced in a side view of the ring. Besides, the visible densities are the result of several helices being superimposed to each other. Accordingly, the more helices are superimposed and the lower the distances between these densities are, the stronger the resulting densities appear after averaging the side views of the c-ring particles. Consequently, the strongest signal is obtained at the curvatures of the c-ring, which is apparent in the 2D class averages as well as in the calculated reprojections of the different c-rings (3.3.3.9).

- In line with this, the weakest signal is obtained at the outermost part of the c-ring, where only one helix pair is located. Two different side views are obtained in the reprojections in which the single helix pair is present either on the left or on the right side of the protein. In the 2D classes of the c-ring in DDM and LDAO these two views were merged thereby averaging out the

single helix pair. Accordingly, in the resulting side view, the density from this single helix pair is missing so that only eight densities are clearly visible (3.3.3.5, 3.3.3.7, 3.3.3.9).

- These obervations lead to the assumption that it is not possible to determine the stoichiometry of the investigated c-ring in the side view of the protein. However, this is not an option either when considering an X-ray c-ring structure from its side by electron microscopy. The helices are too tightly packed and can not be discriminated unamiguously to define the stoichiometry of a given c-ring (3.3.3.9).

- Nevertheless, the densities seen in the top and the side views of the c-ring indicate that the ring might be composed of 17 c-subunits, whereby each subunit is formed by an inner and outer helix builing two concentric rings with the helices off-set (3.3.3.5, 3.3.3.7).

- The ultimate determination of the c-ring stoichiometry requires a three-dimensional structure of the protein complex. Therefore, further data collection and processing for structural analysis needs to be continued from this point on.

4 Discussion

4.1 The hybrid F_1F_o ATP synthase and the *F. nucleatum* rotor ring

F. nucleatum is an anaerobic bacterium growing by the fermentation of glutamate via the 2-hydroxyglutatarate pathway which involves the membrane bound enzyme complex glutaconyl-CoA decarboxylase (Buckel & Barker, 1974). While catalyzing the decarboxylation reaction of glutaconyl-CoA to crotonyl-CoA, a transmembrane Na^+ gradient is generated by the enzyme (Beatrix *et al*, 1990; Boiangiu *et al*, 2005; Buckel & Barker, 1974).

In the first part of this work, we performed combined biochemical and structural experiments with the isolated ATP synthase rotor ring of *F. nucleatum.* The structure, stoichiometry and ion specificity of the protein complex were determined, revealing a novel type of Na^+ coordination not having been characterized so far. Thus, the experimentally determined Na^+-specificity of the *F. nucleatum* ATP synthase rotor ring led to the unequivocal conclusion that the transmembrane sodium gradient established during glutamate fermentation is subsequently used for the production of ATP by the F_1F_o ATP synthase.

In particular, the question of the involvement of two glutamate residues within an ion-binding site with a Na^+-signature was investigated and their mechanistic implications are considered in the following. In this context, the protonation state within this particular ion-binding site is discussed with respect to the ion translocation mechanism of the *F. nucleatum* ATP synthase.

Furthermore, the noticeable feature of the observed undecameric hairpin construction type of Na^+-binding c-rings is another important question, which is adressed in this discussion section.

4.1.1 The strategy for the heterologous expression of the *F. nucleatum* c-ring

For structural investigations, in particular for three-dimensional crystal growth, substantial amounts of protein are necessary, usually several mg per protein preparation. Previously performed experiments showed that the heterologous expression of the c-subunit encoding *atpE* gene of *F. nucleatum* in *E. coli* did not yield a properly assembled c-ring (Schulz, 2010). Therefore, an alternative approach

was used in this work, in which the rotor ring was produced using a hybrid ATP synthase, consisting of the F_1ab_2 complex of *I. tartaricus* and the c-ring of *F. nucleatum*. The enzyme of *I. tartaricus* was chosen for the experiments for two reasons. First, a plasmid containing all *atp* subunits for the heterologous expression of the *I. tartaricus* enzyme in *E. coli* was already available (Oberfeld, 2006). In addition, as the c-subunit sequences of *I. tartaricus* and *F. nucleatum* share about 80 % identity, it seemed to be feasible to produce a hybrid enzyme by substituting the *I. tartaricus atpE* gene by the one of *F. nucleatum*.

A hybrid enzyme comprising all *atp* subunits of *I. tartaricus* and the c-ring of *F. nucleatum* could be purified from *E. coli* membranes. Biochemical analysis revealed that the hybrid protein complex was not as tightly coupled and less stable than the *I. tartaricus* wildtype enzyme. In previous mutagenesis studies several residues of the ATP synthase rotor components (cR45 and cQ46, γE204 and γF203, εD31, εE29 and εH38, *I. tartaricus* numbering) were identified to be important for its assembly (Pogoryelov *et al*, 2008). However, the corresponding residues of the c-subunits are conserved between *I. tartaricus* and *F. nucleatum* hence the reason for a reduced enzyme stability is not the absence of one of these residues important for rotor assembly and functionality.

It turned out that the *F. nucleatum* c-ring was remarkably stable when purified from the hybrid ATP synthase. The oligomeric state of the protein could be maintained while incubated at 70°C and in the presence of 2 % SDS. Several mechanisms have been described for conferring (thermal) stability to a protein complex, including ionic stabilization of the secondary structure, salt bridges and a tight packing of the protein. The *F. nucleatum* c-ring is tightly packed and stabilized by intermolecular hydrogen bonds and ionic interactions conferring (thermal) stability to the protein complex. Besides, it has been shown that in the *I. tartaricus* c-ring stability can be deduced from Na^+-ion cross-bridging in the binding sites. As the c-subunit sequences of *I. tartaricus* and *F. nucleatum* are very similar, comparable interactions are supposed to further stabilize the *F. nucleatum* rotor ring. The inherent stability of the complex enhances its suitability for structural analysis. This assumption has hold true, as the c-ring could successfully be crystallized at low (5.3) and high pH (8.7), whereby crystal quality was good enough to determine both structures by X-ray crystallography. The

long N- and C-termini of this c-ring allowed the formation of stable crystal contacts with the loop regions of the subunits in a head-to-tail orientation. The conformation of the ion-binding site was further stabilized due to the presence of Na^+-ions in the crystallization buffer which cross-bridged the ion-binding residues as described in the structure of the *I. tartaricus* c-ring. In total, this led to tightly packed firm crystals, which diffracted X-rays to a resolution of 2.2 and 2.64 Å.

4.1.2 The *F. nucleatum* c-ring structure and the Na^+-binding site

F_1F_o ATP synthase rotor rings of different organisms are formed with a varying number of identical c-subunits in different species. However, the number of subunits per c-ring is constant within one species (Meier *et al*, 2011). In this work two high resolution X-ray structures of the *F. nucleatum* c-ring were solved at pH 5.3 and pH 8.7. Both structures were identical with respect to the overall stoichiometry and architecture of the ring as well as the conformation and protonation state of the ion-binding residues.

It was already observed in previous experiments that the detergent used in the crystallization procedure uncouples the ion-binding site from the external pH (Pogoryelov *et al*, 2010; Preiss *et al*, 2013; Symersky *et al*, 2012). The c-ring assembles into an hour-glass shaped ring structure in the membrane with the termini of the protein ending in the periplasm while the short loop is located in the cytoplasm (figure 28). The c-subunit and c-ring architectures are very similar to those of the *I. tartaricus* rotor ring with an RMSD of 0.275 and 0.326, respectively. This fact is reasonable as the c-subunit primary sequences of both species share an identity of about 80 % (figure 15). Besides that, both c-rings have the same undecameric stoichiometry.

The resolution of the data in both c-ring structures (2.2 and 2.64 Å, respectively) allowed the unambiguous assignment of a Na^+ and a structural water molecule in each of the eleven ion-binding sites. However, model bias is generally a major challenge in macromolecular crystallography, resulting when an atomic model is used for the calculation of the crystallographic phases. The obtained electron density map tends to have features from the template model even if they are absent in the actual protein structure. One way of avoiding model bias is to never introduce it thereby yielding

more confidence in the electron densities of the protein. To prevent model bias in the *F. nucleatum* c-ring structure, which was solved by molecular replacement using the *I. tartaricus* c-ring structure as a template, the coordinated sodium ion as well as the structural water molecule were initially omitted from the template molecule. After several iterative cycles of model building and refining, the Na^+ and H_2O were modeled into the corresponding densities subsequently improving the overall densities of the protein.

For further validation of the *F. nucleatum* c-ring structure an F_{obs}-F_{calc} omit electron density map for the Na^+ and H_2O of the c-ring at pH 5.3 was calculated afterwards. Such a map is able to visualize where a map has densities resembling atomic densities arising from atoms in the template model used in phasing and not from atoms in the actual protein structure. Indeed, the omit map showed densities emerging at the positions where the Na^+ and H_2O were withdrawn from the reference structure (figure 30).

Supporting evidence confirming the Na^+-selectivity of the *F. nucleatum* c-ring was further obtained from biochemical experiments performed in this work, in which a fluorescent analogue of the ATP synthase inhibitor DCCD competes with Na^+ for the ion-binding glutamate, which does not occur in H^+-specific c-rings (3.1.3).

Na^+ is often bound by five ligands within a protein resulting in a very stable coordination of the ion. However, analysis of the distances in the *F. nucleatum* c-ring ion-binding site revealed that only four amino acid residues can build protein-ion-interactions. One inner (N-) terminal α-helix and two outer (C-) terminal helices are involved, namely the side chain oxygen atoms of two glutamate residues (E32 and E65), the backbone carbonyl oxygen of a valine (V63) and the side chain oxygen of a serine residue (S66) are directly coordinating the Na^+. A fifth ligand, though, is a buried water molecule in the binding site bridging the distances between the Na^+ and further coordinating residues in the ion-binding site, namely A64 and T67. This finding is consistent with a former investigation showing that a structural water molecule is essential for conferring Na^+-specificity to a given c-ring (Meier *et al*, 2009). Hence, it appears that the presence or absence of a water molecule in an ion-binding site is a general strategy for defining the ion selectivity in ATP synthase rotor rings. If bulkier residues are present instead of T67 within the ion-binding site, a

structural water molecule is excluded thus altering the selectivity of the c-ring from Na^+ to H^+.

In contrast to the Na^+-binding sites of *I. tartaricus* (Meier *et al*, 2009; Meier *et al*, 2005) and also *A. woodii* (Matthies *et al*, 2014), in the present case two carboxylates are involved in ion-coordination. E65 is the highly conserved ion-binding carboxylate which is present in all c-rings. E32 is the second carboxylic residue not being present in the other so far structurally characterized Na^+-binding sites. This raises the question whether this second, new glutamate is constitutively protonated to compensate for its charge or whether it is able to co-translocate an ion, along with the Na^+. In this context, possible implications on the ion translocation mechanism in the *F. nucleatum* ATP synthase by these two glutamate residues in the rotor ring have to be assessed.

4.1.3 The protonation state in the Na^+-binding site of the *F. nucleatum* c-ring

Complementary to the X-ray crystallographic data, molecular dynamics simulations with the *F. nucleatum* c-ring were performed in the group of Dr. José Faraldo-Gómez (NIH, Washington, USA). Different states of the Na^+-binding sites were modeled and their likelihood was assessed by all-atom simulations of the complete rotor ring in a lipid membrane environment.

In principle, the second glutamate (E32) would cause an additional negative charge within the ion-binding site which would further lead to considerable rearrangements of the other ligands including the structural water molecule (figure 80 C). Due to electrostatic repulsion between both negatively charged glutamate residues, E65 would bend outwards, while the water molecule would likewise reorient and both would no longer be able to coordinate the Na^+ (Schulz *et al*, 2013). As seen in both X-ray structures the arrangement of all Na^+-coordinating ligands is not altered in comparison to the ion-binding site of *I. tartaricus* and it can be assumed that the second glutamate (E32) is protonated thereby being neutral within the ion-binding site. A protonated E32 would thus structurally resemble a glutamine residue, which can be found at this position in the Na^+-binding c-ring of *I. tartaricus*. To confirm that a proton is indeed present in the binding site, the pKa of E32 was determined showing a clearly higher value relative to its intrinsic value in solution. To determine where the H^+ is actually bound, the energetics of proton transfer between both glutamate

residues was assessed, revealing that E32 is more likely to be protonated than E65 (figure 80 A and B).

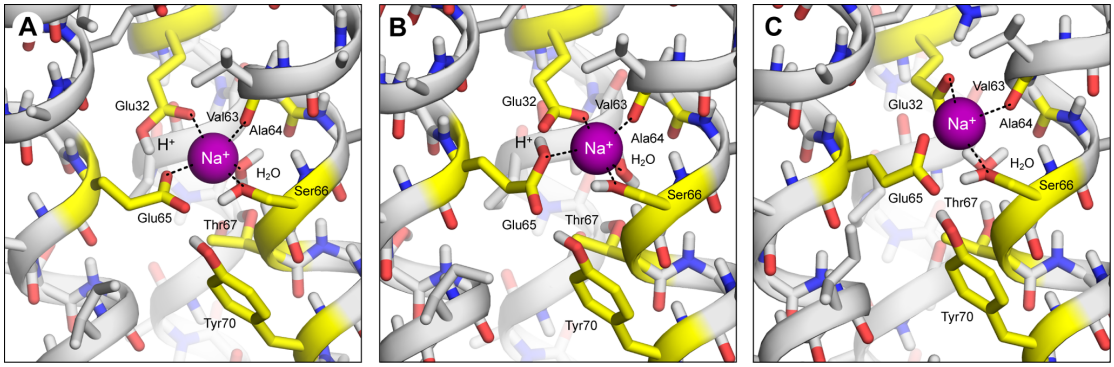

Figure 80. Alternative models of the *F. nucleatum* c-ring Na^+-binding site.
Three models in alternate protonation states of E32 and E65. **(A)** Model with E32 protonated (in *cis*) structurally resembling a glutamine and E65 deprotonated. The Na^+ is coordinated directly by E65, E32, S66, V63 and a bound water molecule. The protonated E32 hydrogen bonds with E65. **(B)** Model with E32 deprotonated and E65 protonated (in *cis*). This model switched in time into model A with the proton building a hydrogen bond to E32. **(C)** Model with both E32 and E65 deprotonated. In this configuration E65 is displaced outwards and Na^+ is coordinated only by E32 and S66 while the water molecule reorients. Model A shows the most probable Na^+-bound state with E32 protonated. Simulation were performed by Dr. Alexander Krah in the group of Dr. José Faraldo-Gómez (NIH, Washington, USA). The figure was taken from (Schulz *et al*, 2013).

4.1.4 The ion translocation mechanism in the *F. nucleatum* c-ring

The finding that a Na^+ and a H^+ are concomitantly bound in the same ion-binding site of the c-ring raises the question whether both ions can be translocated during enzyme operation. Be it that two ions instead of only one are transported during c-ring rotation, an altered ion-to-ATP ratio would be expected being twice as large as usual (22/3 instead of 11/3 for the *F. nucleatum* ATP synthase). As the simultaneous release of both ions would be most likely when the corresponding c-ring ion-binding site is facing the stator a-subunit arginine, a structural model of this state was generated (figure 81 A) and the pKa value of E32 in this state was calculated (figure 81 B). The result showed that the pKa of E32 is shifted upwards in this open, hydrated state in comparison to the pKa value in the ion-locked state. Nevertheless a deprotonation of E32 and thus the translocation of the H^+ as a second ion remains highly unlikely (figure 81 B).

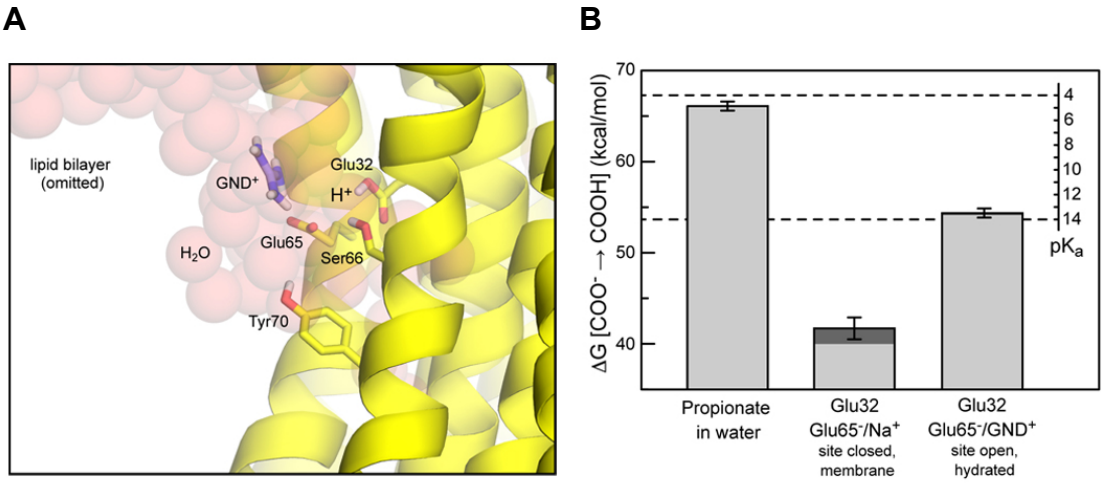

Figure 81. Simulation model of the hydrated open-state of the *F. nucleatum* Na^+-binding site and free-energy gain of the protonation of E32.

(A) A model of the c-ring viewed from the membrane plane with a simulated hydrated environment of the a/c-ring interface on the cytoplasmic side of the protein-lipid interface. A guanidinium ion (GND^+) mimics the conserved arginine side-chain of subunit a. E65 is interacting with the GND^+ while E32 is likely to remain protonated. **(B)** Calculated free-energy gain of the the protonation of E32 in relation to a side chain analogue (propionate) in solution. Protonation of E32 is very likely in both states, the Na^+-bound, locked conformation and the hydrated, open conformation of the ion-binding E65. Simulations were performed by Dr. Alexander Krah in the group of Dr. José Faraldo-Gómez (NIH, Washington, USA). The figure was taken from (Schulz *et al*, 2013).

Experimental validation of the computations was obtained by measuring the ATP-driven H^+-uptake into inverted membrane vesicles of *E. coli* and *F. nucleatum*. Proton accumulation in the *E. coli* membranes could be observed as the quenching of the pH reporter acridine orange. In contrast, no quenching could be seen in *F. nucleatum* membranes under conditions were the ATP synthase is expected to be coupled to transmembrane Na^+-transport (Figure 82) (Schulz *et al*, 2013).

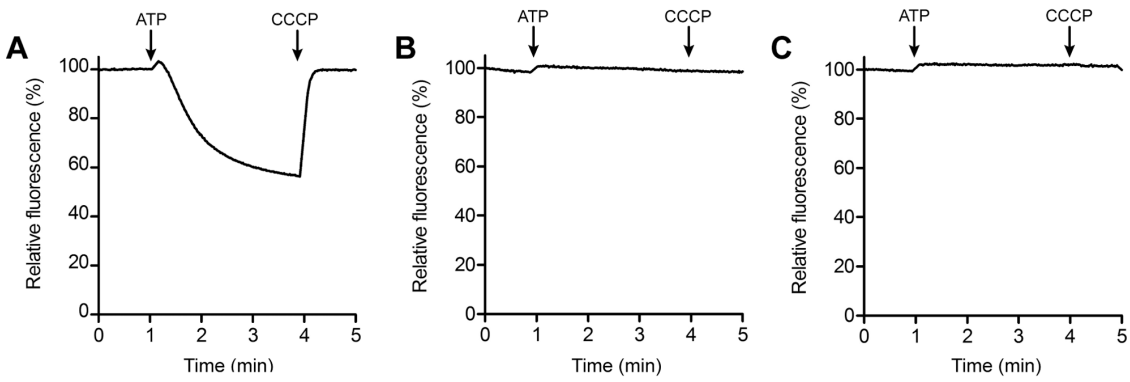

Figure 82. ATP-driven proton translocation in inverted membrane vesicles of *E. coli* and *F. nucleatum.*

Proton translocation was determined by the quenching of acridine orange fluorescence. The reaction was started by the addition of 1.25 mM ATP and stopped with 30 µM CCCP. **(A)** *E. coli* membranes at pH 7.5 with Na^+-ATP resulting in the quenching of acridine orange which was reversed upon CCCP addition. **(B)** *F. nucleatum* membranes at pH 6.0 with Na^+-ATP and **(C)** same as (B) with 10 mM NaCl. No quenching was observed in *F. nucleatum* membranes. The experiments were performed by Dr. Marina Iglesias-Cans in the group of Prof. Dr. Gregory M. Cook (Dunedin, New Zealand). The figure was taken from (Schulz *et al*, 2013).

Combining the experimentally and computationally obtained results it is very unlikely that the F. *nucleatum* ATP synthase rotor ring mediates co-translocation of a H^+, in addition to a Na^+. The protonated E32, which is the most probable state of the residue within the ion-binding site, presumably structurally resembles a glutamine which is present at this position in other Na^+ selective c-rings.

4.1.5 Mechanistic implications of the two-carboxylate Na^+-binding signature in the *F. nucleatum* c-ring

A two-carboxylate-motif as seen in the c-ring structure of *F. nucleatum* seems to be also present in the binding sites of several H^+-translocating ATP synthases. Among these candidates there are several species belonging to human pathogens, which cause severe infections, e.g. *Streptococcus pneumoniae* and *Mycobacterium tuberculosis.* Studies of *Steptococcus mutans,* which also possesses two carboxylates in the ion-binding sites, indicated that its F_1F_o ATPase seems to regulate the intracellular pH in these cells, but not above pH 7.5 (Dashper & Reynolds, 1992). The second carboxylate might thereby react as a pH sensor for this pH regulation by becoming

protonated at acidic pH. Thus, E32 of the *F. nucleatum* ion-binding site may likewise be involved in such a regulatory mechanism.
In support of this, a similar pH dependent function of the ATP synthase was described in a cA24D mutant of the *E. coli* enzyme, where it was suggested to play a role for limiting the ATPase-coupled H^+-transport in these cells (Zhang & Fillingame, 1994). It was further concluded that the second, in this case engineered carboxylate (D24), must be constitutively protonated for the enzyme to be functional, while the conserved carboxylate (D61) seems to mediate H^+-translocation.
In another study, a comparable effect could be observed when cI28 was substituted by an aspartate or glutamate in the *E. coli* ATP synthase likewise indicating that a second carboxylate may be involved in the regulation of enzyme function in response to the cytoplasmic pH (Jones, 2001).
These studies underline the importance of the two-carboxylate ion-binding motif for a potential function of the ATP synthase in internal pH regulation.

However, despite these previously made findings, an alternative explanation can be given based on the findings of the present work. Having introduced a second carboxylate in the *E. coli* c-subunit, which is assumed to be constitutively protonated for enzyme function, the pKa of the complete ion-binding site is thus lowered. This down-shift minimizes the probability of the conserved carboxylate (D61 in *E. coli*) to be protonated resulting in a lower H^+-transport activity, which was observed in the corresponding *E. coli* mutants. This alternative hypothesis is further supported by H^+-transport measurements with inverted membrane vesicles of *F. nucleatum* showing that the Na^+ is the only translocated ion whereas no H^+ co-transport could be measured (figure 81). These results are consistent with the assumption that only one ion is transported under physiological conditions and that the constitutively protonated E32 does not differ from a glutamine residue, which can be found in many species at the corresponding position of the c-subunit sequence.

To preclude that the isolated c-ring has an altered ion specificity compared with the rotor ring in the assembled ATP synthase, experiments with the purified *F. nucleatum* enzyme were performed in collaboration with the group of Prof. Gregory M. Cook showing that Na^+ indeed stimulates ATP hydrolysis activity (Figure 23) (Schulz *et al*,

2013). These results indicate that the *F. nucleatum* ATP synthase is physiologically coupled to a sodium motive force. This is feasible as the transmembrane sodium gradient which is generated during its metabolism, the fermentation of glutamate, can then directly be used by the ATP synthase.

The facts that the assembled *F. nucleatum* ATP synthase is activated by Na^+ and the two X-ray structures show in detail the Na^+-coordination network of the c-ring, underline the hypothesis that the second glutamate in the ion-binding site is constitutively protonated structurally functioning as a glutamine to further stabilize the entire ion-binding site.

4.1.6 The undecameric stoichiometry of Na^+ translocating c-rings

Another remarkable aspect of all Na^+-binding F_1F_o ATP synthase c-rings, such as those from *I. tartaricus*, *P. modestum*, *A. woodii* and *C. paradoxum* and the one from *F. nucleatum,* is the fact that, so far, they are all composed of eleven hairpin-like c-subunits. In contrast, V- and A-type Na^+-ATPases consist of rotor rings that contain very different numbers of hairpins per ring (Vonck *et al*, 2009). Conclusively, this means that while in F-ATP synthases this seems a frequently chosen, perhaps even preferred number of c-subunits, the undecameric stoichiometry can not be considered as a general prerequisite for all Na^+- binding rings in rotary ATPases.

Besides, the oligomeric state of a c-ring is not defined by the ion-binding residues but by a conserved stretch of glycine/alanine residues at the c-c-interfaces (Liu *et al*, 2011; Pogoryelov *et al*, 2012; Preiss *et al*, 2013). Single point mutations within the glycine-motif in the *I. tartaricus* c_{11} ring caused an altered stoichiometry of the complex, but finally did not impair its Na^+-specificity (Pogoryelov *et al*, 2012). Enlarged c-rings can still form enzyme complexes, which are functional in ATP synthesis and hydrolysis while maintaining their Na^+-specificity.

Moreover, the Na^+-specific ATP synthase rotor ring of *A. woodii* is a 9:1 heteromer of F- and V-type c-subunits. Each of the nine single-hairpin c-subunits harbours a Na^+-binding site whereas one double-hairpin subunit has one additional site and one vacancy. Here, the ion-to-ATP ratio is altered as only ten Na^+-ions are transported across the membrane in a complete revolution of this rotor ring, although it is composed of 11 hairpins (Matthies *et al*, 2014).

These results further underline that a functional Na^+-ATP synthase is not linked with an undecameric rotor ring as a matter of principle.

The only conformity of all species characterized so far to have a Na^+-coupled ATP synthase is that the ecological niches, in which they live in, seem to be of anaerobic nature and with a moderately high environmental Na^+-concentration. Thus, the coincidence of an undecameric c-ring stochiometry and a Na^+-specificity might have some general evolutionary reasons that derive from these commonalities. However, the possibility should not be excluded *a priori*, that alternative ecological niches, in which species operate Na^+ rotary ATPases, will be found in the future. An ATP synthase with a small c-ring such as the c_{11} ring is able to work very efficiently as less ions are needed per ATP molecule to be synthesized. In evolutionary-early times Na^+ played a crucial role in bioenergetics thus such a proliferous Na^+-driven ATP synthase with a small c-ring might have been beneficial for these early organisms.

Summary

The *F. nucleatum* F_1F_o ATP synthase rotor ring was analyzed using biochemical assays and X-ray crystallography. The two X-ray structures of the c-ring present a previously uncharacterized type of Na^+-coordination in the protein complex. The results were finally supplemented by computer-simulation data providing further understanding of the mechanistic implications of this ion-binding mode in the *F. nucleatum* rotor ring.

Conclusively, the ATP synthase of *F. nucleatum* uses a transmembrane sodium gradient generated by the glutaconyl CoA-decarboxylase to drive the synthesis of ATP. Na^+-translocation is mediated by the enzyme rotor ring which is composed of eleven identical c-subunits. Each of these subunits has a Na^+-binding signature with a two-carboxylate ion-binding motif, including two glutamate residues. While E65 is a highly conserved carboxylate, which is found in all known c-subunits, E32 is a second, new carboxylic residue. The pKa of this additional glutamate within the ion-binding site is significantly higher than its intrinsic value in solution thereby enhancing its protonation probability. Thus, two ions are concurrently bound in the same ion-binding site of the *F. nucleatum* c-ring. However, the Na^+ is the only transported ion during enzyme operation while the protonated E32 rather resembles a structural constituent of this ion-binding site.

4.2 The *Burkholderia* N-type ATPase and its rotor ring

An *in silico* study proposed a new type of rotary ATPase in different, phylogenetically independent species. As the *atp* operon, which encodes for this type of enzyme was found to be always present next to a common F-type ATP synthase encoding *atp* operon and the corresponding rotor ring was suggested to bind Na^+, it was thereafter referred to as N-type ATPase. However, the assignment of the physiological function of this novel type of rotary ATPase is not possible as neither any structural information about the entire enzyme or single subunits are available.

In the second part of this work the phenotypic existence of this enzyme was examined and various forms of heterologous expressions using different systems for the production of the *B. pseudomallei* N-ATPase were performed. A biochemical study, which was further carried out with the wildtype and mutant *B. pseudomallei* N-type rotor ring, revelead that the protein complex is H^+-specific. In addition, structural investigations using single-particle cryo-EM indicated a new stoichiometry of 17 c-subunits for the complex.

The determined ion specificity and stoichiometry of the *B. pseudomallei* N-ATPase rotor ring provide first insights into the structure and function of an isolated N-type c-ring. Possible physiological functions of the N-ATPase as an additional type of rotary ATPase in many different current species as well as potential evolutionary mechanisms of these enzymes are discussed in the following chapters. In this context, the physiological and mechanistical implications of the N-type c-ring as the largest ATPase rotor ring known so far are reflected.

4.2.1 The phenotypic existence of the *B. thailandensis* N-ATPase

A transcription analysis of the N-*atp* operon in *B. thailandensis* confirmed the actual phenotypic existence of the N-ATPase in these cells. A R(everse)T(ranscription)-PCR experiment was carried out in which RNA transcription could be detected. Hereby, the isolated total-RNA of a species is initially transformed into c(omplementary)DNA using a reverse transcriptase and afterwards defined sequences of this cDNA are specifically amplified using PCR. This method is widely used for studying gene expression and the most sensitive method for detecting (low abundance) mRNA (Bustin, 2000a).

Six out of seven RT-PCR products have been obtained using isolated total-RNA of *B. thailandensis* as a template and oligonucleotide primer, which specifically bind to the sequence of the N-*atp* operon. The lack of one PCR-product might be due to insufficient primer binding at the corresponding cDNA sequence or caused by imperfect cDNA synthesis from the isolated RNA, as the latter one itself is difficult to handle due to its enormous (chemical) instability. Generally, all genes of an operon are under the control of a single promoter and transcribed together into a single polycistronic mRNA. Thus, the transcription of the entire operon can already be deduced from the partial existence of the corresponding mRNA. Further, as transcription and translation in bacterial cells is going hand in hand, the fact that the N-*atp* operon is actually transcribed in *B. thailandensis* cells suggests that the corresponding N-ATPase complex is likely to be also produced in these cells.

However, these results do not allow any quantitative statement about the expression of the N-*atp* operon as neither the amount of isolated RNA having been used was normalized nor the efficiency of each RT-PCR was determined. The use of the glyceraldehyd-3-phosphate dehydrogenase (GAPDH) as an endogenous control could only serve to indicate whether the RT-PCR has functioned as the corresponding gene is ubiquitously expressed and moderately abundant in different cells, but not for a quantitative analysis of the gene expression level as GAPDH concentrations can vary significantly under certain conditions in the cell (Bustin, 2000b).

4.2.2 The two types of rotary ATPases in *B. thailandensis* cells

Several experimental approaches were applied in this work to purify the two rotary ATPases (F- and N-type), which were assumed to be present in *B. thailandensis*. The F-type ATP synthase could successfully be isolated from native *B. thailandensis* membranes with all the *atp* subunits being visible on an analytical SDS-polyacrylamide gel. In addition, several subunits (α, β, γ and ε) could be identified by ESI-MS peptide mass fingerprint. Hence, while the F-type ATP synthase could be purified using a classic ATPase purification protocol, the N-ATPase could not be properly extracted from these cells, even if different approaches for the purification were carried out, including several chromatography and protein precipitation procedures. A possible reason for this might be that the expression level of the F-ATP synthase is significantly higher which leads to a rapid enrichment of this enzyme

during the purification. Besides that, the N-ATPase might not be stable under the conditions chosen for the procedures so that the protein complex might have disassembled during the preparation.

The F-type ATP synthase isolated from *B. thailandesis* membranes was found to show only little ATP hydrolysis activity (0.14-0.18 U/mg protein). Several chemical compounds were tested for their potential to enhance the hydrolysis activity whereby trypsin was found to have a prominent effect. Upon trypsin addition to the isolated enzyme its activity increased by a factor varying between 4.5 and 10.7 to a specific activity of 0.81 and 1.61 U/mg protein, respectively. So far, it`s not allegeable what causes the varying strength of activation in the single experiments. Both values, however, are in the range of activities determined for ATP synthases from different species, including the Na^+-coupled enzyme of *I. tartaricus* (1.28 U/mg) (Neumann *et al*, 1998) and the H^+-dependent ATP synthases of *E. coli* (1.9 U/mg) (Ishmukhametov *et al*, 2005) and *C. thermarum* sp. strain TA2.A1 (0.78 U/mg) (Cook *et al*, 2003). The determined hydrolysis activity was significantly decreased by the ATP synthase inhibitors dicyclohexylcarbodiimide (DCCD) and tributyltin chloride (TBT-Cl) in amounts that are known to strongly inhibit F-type ATP synthases. The enzyme was pre-incubated with DCCD as this compound needs some time to reach the ion-binding glutamate where it inhibited enzyme`s activity by 36 to 50 %. TBT-Cl was suggested to bind in the region where ion translocation takes place in the F_o-part of the enzyme (von Ballmoos *et al*, 2004) and was found to inhibit *B. thailandensis* ATPase activity by 50 % instantly after having been added to the enzyme. These results revealed that the *B. thailandensis* F_1F_o ATP synthase showed only moderate ATPase activity which could be enhanced by the addition of trypsin. Inhibition of this hydrolytic activity by DCCD and TBT-Cl indicated that a functionally coupled enzyme could be purified.

4.2.3 The *B. pseudomallei* N-ATPase

Since the unmodified N-ATPase could not be isolated from native *B. thailandensis* cells, several experiments, including different heterologous expression systems, were performed with a genetically tagged enzyme of *B. pseudomallei*. *E. coli* is the most commonly used host for the heterologous overexpression of bacterial proteins. However, by prediction and analogous to the F-type ATP synthase, an N-ATPase would be a huge membrane protein complex of at least eight different structural

subunits which have to be expressed and folded correctly before the entire complex can be functionally assembled. The actual cloning of the complete N-*atp* operon was challenging due to the large nucleotide sequence and high GC content of the operon which has to be amplified correctly from genomic DNA of *B. pseudomallei*. Therefore, the operon was divided into four parts which were then coalesced and PCR-introduced point mutations were eliminated afterwards by side directed mutagenesis. This strategy turned out to be more successful than amplifying the entire *atp* operon in a single reaction.

The expression of the N-ATPase in *E. coli* cells resulted in a strong degradation of the His-tagged β-subunit of the enzyme as shown by Western Blot analysis. Accordingly, protein degradation was likewise observed when the enzyme was extracted and purified from *E. coli* membranes. The fact that degradation was already observed in whole *E. coli* cells and not just when extracted from membranes, led to the conclusion that this host is not suitable for the heterologous expression of the *Burkholderia* enzyme. This might be due to the absence of inevitable chaperones for protein folding and complex formation in *E. coli*. A more generally reasoning is that the entire protein expression process in *E. coli* is not optimized for *B. pseudomallei* proteins eventually leading to a disequilibrium of the single *atp* genes which then, in consequence, leads to their degradation.

As these results indicated that *E. coli* is not a suitable host for the heterologous expression of the *Burkholderia* N-ATPase, an alternative expression system was needed. Due to their clinical relevance (Chaowagul *et al*, 1989; Wilkinson, 1981), *Burkholderia* species are under intensive investigation, particularly with respect to their pathogenicity. Cloning and expression vectors have therefore been created by others allowing the heterologous protein expression in *Burkholderia* strains. One of these vectors, namely pHERD28T, was chosen for the production of the N-type ATPase in *B. thailandensis* cells (Qiu *et al*, 2008).

The major challenge for genetic selection in these cells is their intrinsic resistance to many different antibiotics, including penicillins and aminoglycosides, which are most frequently used for genetic experiments (Choi *et al*, 2008; Moore *et al*, 1999). The designed *Burkholderia* vector encodes for a dihydrofolate reductase necessary in the thymidine synthesis thereby enabling transformed bacteria to grow on trimethoprim-containing selective agar (Bushby & Hitchings, 1967; Osborn & Huennekens, 1958).

This is one of the rare antibiotics to which *Burkholderia* strains are less resistant to as the inactivation mechanism of trimethoprim is a specific effect in some bacteria, such as soil and clinical representatives of the genera *Burkholderia*, *Pseudomonas* and *Xanthomonada* and not a general mechanism (Walsh & Duffy, 2013). Thus, the application of 50 µg/ml trimethoprim enabled genetic selection in *B. thailandensis*. Besides, the frequency of spontaneous resistance to trimethoprim is very low (personal communication, Prof. Dr. Herbert P. Schweizer, Colorado State University). When comparing Western Blot analyses of the expression of the N-ATPase in *E. coli* and *B. thailandensis* cells clear differences can be seen: In *Burkholderia* cells no degradation of the His-tagged β-subunit occurred, which led to the conclusion that the enzyme could be stably expressed in these cells. Even if the enzyme was extracted from inverted membrane vesicles using a selection of different detergents no protein degradation was visible.

Another hint for the correct assembly of the enzyme was obtained from immunogold labeling experiments. Nanogold particles can bind to His-tagged proteins, in this case to the His-tagged β-subunit of the F_1-part and then be visualized by electron microscopy. As the soluble F_1-subcomplex as such is not membrane-bound it can be concluded that both parts of the enzyme are present in the sample as gold particles were visible close to the membrane vesicles. The occurrence of randomly distributed gold particles as would be expected when only the His-tagged F_1-subcomplex is bound with a nanogold particle, can be negated. Besides, there were no particles visible in the control sample in which expression of the His-tagged N-ATPase was not induced. These results revealed that the N-ATPase is expressed and assembled in *B. thailandensis* membranes.

However, the analyses of several performed affinity chromatographic studies showed that the F_1-subcomplex is tightly bound via the His-tagged β-subunit to the Ni^{2+}NTA resin whereas the F_o-part of the enzyme does not or only weakly bind to the column as most of the protein was found in the flow through of the column. Having seen that the enzyme is assembled in membranes it appears that the use of detergents apparently causes some loosening of the interactions between the two subcomplexes. Binding of the His-tagged β-subunit to the Ni^{2+}NTA resin might finally provoke the complete detachment of the F_o-part from the enzyme.

Taken together, the heterologous expression of the *B. pseudomallei* N-ATPase in *B. thailandensis* seemed to be more successful than in *E. coli* as judged from the Western Blot analyses and immunogold labeling experiments. The enzyme appeared to be more stable after its expression in *B. thailandensis* cells, however after extracting the complex from membranes using detergents, degradation could also be observed in this case.

In future work, milder conditions for the isolation of the heterologously expressed N-ATPase could be tried to prevent disassembling and degradation of the enzyme. Another promising approach is to analyze homologous N-ATPases from other species, such as for example *Azotobacter vinelandii*, *Nitrosomonas eutropha* and *Methanosarcina barkeri*, to find out if any of them are more stable during isolation and purification. The heterologous expression and protein complex purification protocol developed here could then be used as a basis for the analysis of homologous enzymes.

4.2.4 The ion specificity of N-ATPase c-rings

In silico studies of N-ATPases from different species suggested that these are very ancient enzymes being physiologically coupled to Na^+ (Dibrova *et al*, 2010). In addition, it was shown that the hydrolytic activity of an *A. halophytica* ATPase which, according to its operon organization also belongs to the N-ATPases, could be stimulated by Na^+ when expressed in inverted *E. coli* membrane vesicles. Moreover, it was shown that DCCD-inhibition of the ATP hydrolysis activity in this membrane vesicles could be protected by Na^+ (Soontharapirakkul *et al*, 2011).

However, the ion specificity of these enzymes has not been determined until today, neither structurally nor biochemically, using a purified enzyme or a purified rotor ring. In this work, the first analysis of an isolated N-ATPase rotor ring, e.g. the protein complex of *B. pseudomallei*, was described. Biochemical studies of the detergent-solubilized c-ring revealed that Na^+ could not protect the protein complex from being inhibited by DCCD and a fluorescent analogue, namely NCD-4. These results contrast with the above-mentioned proposals made in the bioinformatics study, as well as the investigation of the ion specificity of the *A. halophytica* enzyme in inverted membrane vesicles.

To further explore the ion specificity of this novel type of enzyme, the c-subunit sequences of different N-ATPases were aligned to each other as well as with the Na^+-binding c-subunit of *F. nucleatum* and the H^+-binding c-subunit of *S. platensis*, both belonging to F-type ATP synthases (figure 83).

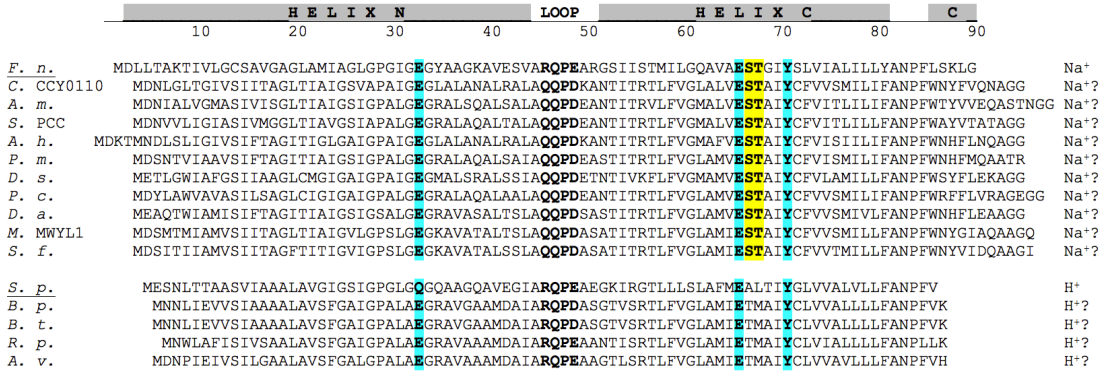

Figure 83. Alignment of selected N-type ATPase c-subunit sequences with the F-type ATP synthase c-subunits of *F. nucleatum* (Na^+-specific) and *S. platensis* (H^+-specific).
The c-subunit sequences from selected N-ATPases, including the *Burkholderia* strains *B. pseudomallei* and *B. thailandensis*, which were used in this work, were compared with the Na^+-binding c-subunit of *F. nucleatum* and the H^+-binding c-subunit of *S. platensis* (F-ATP synthases, underlined). The c-subunit sequences were aligned according to their cytoplasmic loop region (bold black). The N- and C-terminal helices are indicated above. Amino acids conserved within all given c-subunits are highlighted in cyan, residues only conserved within (presumed) Na^+-specific c-subunits are marked in yellow. The (predicted) type of ion-coordination is indicated on the right side (with a question mark). The species names on the left side are as follows: *Fusobacterium nucleatum* subsp. *nucleatum* (F-type) (numbering), *Cyanothece* sp. CCY0110 (N-type), *Acaryochloris marina* strain MBIC 11017 (N-type), *Synechococcus* sp. PCC7335 (N-type), *Aphanothece halophytica* (N-type), *Planctomyces maris* DSM 8797 (N-type), *Desulfovibrio salexigens* strain ATCC 14822 (N-type), *Pelobacter carbinolicus* strain DSM 2380 (N-type), *Desulfuromonas acetoxidans* DSM 684 (N-type), *Marinomonas* sp. strain MWYL1 (N-type), *Shewanella frigidimarina* strain NCIMB 400 (N-type), *Spirulina platensis* (F-type), *Burkholderia pseudomallei* strain K96243 (N-type), *Burkholderia thailandensis*strain E264 (N-type), *Rhodopseudomonas palustris* strain TIE-1 (N-type), *Azotobacter vinelandii* strain DJ (N-type).

This alignment reveals that all given c-subunits harbor a carboxylic residue (E or D, E32 numbering) in the N-terminal helix as well as a tyrosine (Y70 numbering) in the C-terminal helix, besides the conserved ion-binding glutamate (E65 numbering) (figure 83, highlighted in cyan). Some of the N-ATPase c-subunits further show a

serine (S66 numbering) and threonine (T67 numbering) as is the case in the *F. nucleatum* c-subunit (figure 83, highlighted in yellow). In the *F. nucleatum* c-ring S66 is directly involved in Na^+-binding while T67 is coordinating a structural water molecule which in turn serves as a fifth ligand for Na^+-coordination. Due to the presence of these amino acid residues, the corresponding N-ATPase c-subunits are likely to be also Na^+-specific. The enzyme of *A. halophytica*, which was previously suggested to be Na^+-coupled (Soontharapirakkul *et al*, 2011) shows this set of Na^+-binding ligands supporting the experimental findings in this publication. In contrast, in several N-ATPase c-subunits these two residues are substituted by other amino acids like a methionine, alanine or leucine. This constellation rather resembles a H^+-binding site like in the c-subunit of *S. platensis*. In this c-ring the proton is coordinated by the conserved glutamate and an opposite backbone oxygen of a phenylalanine on the adjacent c-subunit. The N-ATPase c-subunits of *B. pseudomallei* and *B. thailandensis* carry a methionine residue at the corresponding position of the Na^+-binding threonine (figure 83).

We therefore speculated that, for steric reasons, the methionine residue within the ion-binding site (M63 in *B. pseduomallei*) might preclude a structural water molecule and hence Na^+-coordination in this c-ring. However, mutational studies with the *B. pseudomallei* c-ring in which this methionine residue was mutated into a threonine (M63T), which can be found at the corresponding position in the *F. nucleatum* c-ring, negated that this is the only reason to exclude Na^+-specificity. Remarkably, even after having mutated the entire ion-binding site according to the Na^+-binding site in the *F. nucleatum* rotor ring (M59T I60A T62S M63T), the *B. pseudomallei* complex remained H^+-specific. It therefore seems, up to this point, that the N-ATPase rotor ring of *B. pseudomallei* is H^+-binding and thus the enzyme seems to be coupled to a *pmf*.

Although the primary c-subunit sequence gives a good indication on the coupling ion used for ATP synthesis by the corresponding enzyme and such a Na^+-signature is necessary for Na^+-binding, it nevertheless seems not to be sufficient. This work exemplifies that other factors probably contribute to determine the ultimate ion specificity.

A structural comparison of the *I. tartaricus* c_{11} ring with the *S. platensis* c_{15} ring revealed that the overall size of the ion-binding site also contributes to the ion

specificity (Pogoryelov *et al*, 2009). In general, the size of an ion-binding site is defined by the kink of the outer helix of the ring. The more kinked the helix is, the longer are the distances within the ion-binding sites, especially between the conserved E/D residue and the opposite residue involved in ion-coordination. Shorter distances, as in the c_{15} ring, allow direct hydrogen bonding between the carboxyl side chain oxygen (of E62 in *S. platensis*) and the backbone carbonyl oxygen (of F60 in *S. platensis*), whereas this is not possible in the Na^+-binding c_{11} ring having longer distances as it is more kinked. The bending of the *B. pseudomallei* c-ring helices could thus also influence the c-ring ion specificity by enabling direct H^+-coordination within the binding site.

4.2.5 Models for a H^+-binding site of the *B. pseudomallei* N-ATPase c-ring

Due to the results of the NCD-4 and DCCD-modification reactions of the purified *B. pseudomallei* c-ring we concluded that the investigated protein complex is H^+-specific. To assess whether H^+-coordination is theoretically possible in this case, two structural models for a H^+-binding site in the *B. pseudomallei* rotor ring were drafted. For this purpose, a homology model of the *B. pseudomallei* c-ring was created using the c-subunit sequence of *B. pseudomallei* and the c-ring of *F. nucleatum* as a template (see 2.4.6 and 3.3.14). In all previously described c-ring structures the ion-binding unit is formed by two adjacent c-subunits. Likewise, the N- and C-terminal helices of one subunit and the C-terminal helix of the adjacent subunit are assumed to be involved in ion-coordination in this c-ring (figure 84). The c-subunits form hairpins with a height of about 63 Å and are kinked approximately in the middle of the membrane, where the ion-binding sites are localized. The transmembrane region of the protein appears to extend from phenylalanine 76 (F76) to serine 50 (S50) (figure 84).

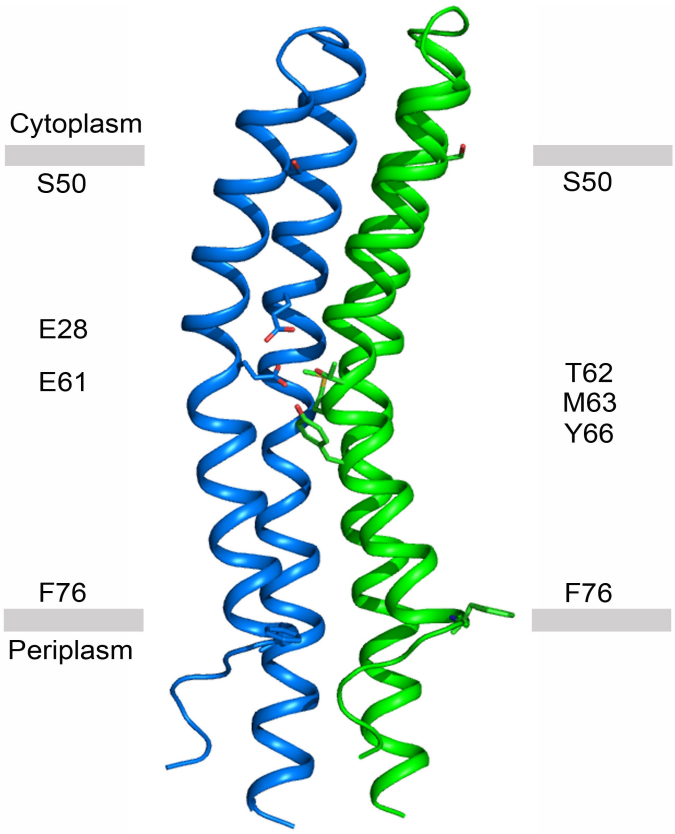

Figure 84. Model for the ion-binding unit of the *B. pseudomallei* N-ATPase c-ring.
The hypothetical ion-binding unit of the modeled N-ATPase c-ring is formed by the N- (inner) and C- (outer) terminal helices of one c-subunit (blue) as well as the C-terminal helix of the adjacent subunit (green). Residues presumed to be important for ion-binding are indicated as sticks and labeled on the right and left at the corresponding height of the helices. The membrane borders are given as grey bars at a height of S50 and F76 of the c-subunits.

The distance between the conserved ion-binding glutamate, which is generally the actual carrier of the translocated ion, and the ligand on the opposite side of the adjacent c-subunit is crucial for the ion-binding mode. However, the exact distances between the residues within the ion-binding site can not be determined in a structural model as this is strongly biased by the template used for model building. Besides, the geometry and conformation of the side chain residues in a homology model do not ultimately reflect the actual positions of these residues. Nevertheless, based on previous knowledge about different c-ring ion-binding sites as well as the preliminary structural information obtained from the created homology model, two hypothetical H^+-binding sites in the *B. pseudomallei* c-ring (figure 85) are described in the following:

In the first model (figure 85 A) the translocated ion is directly coordinated by one side chain oxygen (Oε1) of the key glutamate (E61) and the side chain oxygen of a threonine of the neighboring subunit (T62), as hydrogen bonding might be possible between these residues (figure 84 A, purple dotted lines). It has already been observed in previously solved c-ring structures that this ion-locked conformation of a protonated glutamate is very stable (Meier *et al*, 2009; Meier *et al*, 2005; Pogoryelov *et al*, 2009; Preiss *et al*, 2010; Schulz *et al*, 2013). A second glutamate (E28) is further present in the ion-binding site of the *B. pseudomallei* c-ring. In the first part of this thesis two high resolution structures of the *F. nucleatum* rotor ring (at pH 5.3 and pH 8.7) were described. In that case, two glutamates are involved in the coordination of a Na^+ in the binding site (two-carboxylate ion-binding motif). However, the presence of a second carboxylate within the ion-binding site is not restricted to Na^+-specific c-rings as it can also be found in the *Mycobacterium phlei* (D32) c-ring, which was shown to be H^+-binding (Preiss, 2013). As learned from the two *F. nucleatum* c-ring structures and accompanying MD simulations, the second glutamate is constitutively protonated thus allowing hydrogen bonding between the two glutamates. This hydrogen bond also applies to the *B. pseudomallei* H^+-binding site, namely between Oε2 of E28 and Oε1 of E61. Besides, Oε2 of E61 might form another hydrogen bond with the side chain oxygen of Y70 to further stabilize the H^+-binding site (figure 85 A, black dotted lines). The bulky side chain of a methionine within the ion-binding site (M63) might further preclude the presence of a water molecule as a coordination ligand for Na^+, as it is the case in the Na^+-binding c-rings of *I. tartaricus* (1yce (Meier *et al*, 2005), 2wgm (Meier *et al*, 2009)), *F. nucleatum* (3zk1 and 3zk2 (Schulz *et al*, 2013)) and *A. woodii* (4bem (Matthies *et al*, 2014)).

In the second model (figure 85 B) the translocated proton is coordinated by the key glutamate (E61) Oε1 and a side chain sulphur of a methionine of the neighboring subunit (M63). It has already been shown that a methionine sulphur can coordinate a protein substrate by polar interactions with the molecule, e.g. with a γ-butyrobetaine molecule in the Na^+-independent antiporter CaiT (Schulze *et al*, 2010). The distance between E61 and M63 in the modeled ion-binding site does not allow direct hydrogen bonding. However, the methionine side chain has a certain flexibility within the ion-binding site and the *F. nucelatum* c-ring, which served as a template for model building, has introduced some bias in this region. Thus, the actual distance between

E61 Oε1 and M63S might be smaller. Besides, it has been described that hydrogen bonds involving sulphur atoms are longer than those including nitrogen or oxygen as sulphur is larger and has a more diffuse electron cloud (Gregoret *et al*, 1991). The same methionine sulphur could hydrogen bond with the side chain oxygen of T62 of the same helix to further stabilize the coordination network. The distance between these two residues could likewise be shortened in the actual *B. pseudomallei* ion-binding site for enabling direct hydrogen bonding. As in the first model (A), the second glutamate (E28) is probably constitutively protonated allowing hydrogen bonding between Oε2 of E28 and Oε1 of E61. In addition hydrogen bonds are seen between Oε2 of E61 and the side chain oxygen of Y70 (figure 85 B).

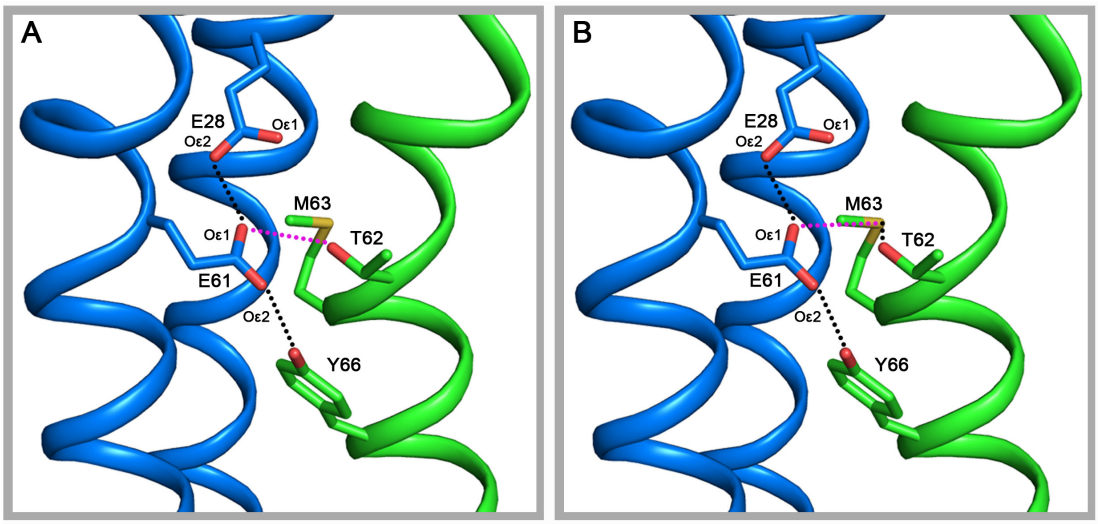

Figure 85. Two models for a H^+-binding site in the *B. pseudomallei* N-ATPase c-ring.
The hypothetical binding sites are displayed from the membrane plane. **(A)** In the first model the H^+ is coordinated directly by one side chain oxygen (Oε1) of the conserved glutamate (E61) of the C-terminal helix of one c-subunit and the side chain oxygen of a threonine (T62) of the C-terminal helix of the adjacent subunit (purple dotted line). Oε1 of E61 is further forming a hydrogen bond to one side chain oxygen (Oε2) of E28 of the same subunit, while Oε2 of E61 hydrogen bonds with the side chain oxygen of Y66 of the adjacent c-subunit (black dotted lines). **(B)** In the second model the H^+ is coordinated directly by E61 Oε1 of the C-terminal helix of one c-subunit and the sulphur of a methionine (M63) of the C-terminal helix of the adjacent subunit (purple dotted line). The same S of M63 forms a polar interaction with the side chain oxygen of T62 of the same helix. Oε1 of E61 is further forming a hydrogen bond to Oε2 of E28 of the same subunit, while Oε2 of E61 hydrogen bonds with the side chain oxygen of Y66 of the adjacent subunit (black dotted lines), just as in (A).

The two models for a H^+-binding site in the *B. pseduomallei* c-ring described here are just two of many possibilities for ion-coordination in this ring. For a conclusive statement on the ion specificity of the rotor ring, the result obtained from biochemical analysis has to be confirmed by a structural method, namely X-ray crystallography. However, it is possible that this type of rotary ATPase comprises both, H^+- and Na^+-coupled enzymes, varying between different species, just as it is the case for F-, V- and A-type ATPases (see 4.2.10). This would explain why different ion specificities were determined for the *A. halophytica* and the *B. pseudomallei* N-type ATPases. Further investigations of other, homologous N-ATPase c-rings would be useful to determine their ion specificities and find out if the specificities of N-ATPases can actually vary between different species.

4.2.6 The size of the purified *B. pseudomallei* N-ATPase c-ring

The heterologously expressed and purified *B. pseudomallei* N-ATPase rotor ring was initially analyzed by SDS-PAGE, where it was migrating at a molecular weight level of 80-100 kDa on a SDS-polyacrylamide gel (figure 51-53).

Previous investigations of other bacterial c-rings showed that the isolated protein complexes migrate between 40 and 60 kDa on SDS polyacrylamide-gels. However, the actual molecular masses range from 78 kDa for the smallest bacterial c-ring known so far, the c_9 ring of *Mycobacterium phlei* (Preiss, 2013) to 122 kDa for the largest bacterial ring, the c_{15} ring of *Spirulina platensis* (Pogoryelov *et al,* 2007). According to SDS-PAGE the N-ATPase rotor ring would have a molecular weight of 160-200 kDa, corresponding to an estimated stoichiometry between 18 and 22. Another plausible explanation for the slow migration during SDS-PAGE is that significantly less detergent molecules are bound to the *B. pseudomallei* rotor ring surface. Besides, it is known (lab internal knowledge) that an estimation of the c-ring stoichiometry from the proteins migration behaviour can be misleading and is difficult as it is influenced by the overall shape of the protein. SDS-PAGE calibration of c-rings, however, just worked out well if structurally enough related protein complexes were used for comparing their particular migration behaviour as for example c-rings isolated from various cyanobacterial sources and using the same methodology (Pogoryelov *et al*, 2007).

Noteworthy, the isolated *B. pseudomallei* c-ring shows the same molecular size as if it was expressed in the entire N-ATPase (figure 45). This confirmed that the high molecular weight level of the purified c-ring was not due to an artificial assembly if the c-ring alone is heterologously expressed in *E. coli*. Besides, it was already demonstrated in previous studies that the rotor ring stoichiometry is not altered if the corresponding protein was heterologously expressed in *E. coli*, e.g. the c-ring of *I. tartaricus* was shown to be composed of eleven identical c-subunits in both cases, if purified from native membranes (Stahlberg *et al*, 2001) as well as from *E. coli* membranes (Pogoryelov *et al*, 2007).

4.2.7 Determination of the *B. pseudomallei* N-ATPase c-ring stoichiometry by single-particle cryo-EM

Besides the approach to crystallize the *B. pseudomallei* N-ATPase rotor ring to solve the structure by X-ray crystallography, the ring was structurally investigated by single-particle electron cryo-microscopy (cryo-EM).

Cryo-EM as a method for the structural analysis of the *B. pseudomallei* c-ring

In contrast to X-ray- or electron-crystallography, in single-particle EM there is no need for protein crystallization which can be very challenging. Though for a long time only protein complexes in the megadalton (MDa) size range were suitable for structure determination by single-particle cryo-EM. However, substantial progress was made recently by determining the 4.5 Å structure of the glycosylated form of the human γ-secretase with a total molecular weight of 230 kDa for the complex (Lu *et al*., 2014). 3D structure determination by single-particle EM is performed by enhancing the signal obtained from the elastic scattering of electrons while interacting with an object (e.g. the protein particle) via aligning and averaging a huge number of these particles in all possible orientations. The signal-to-noise is thereby better for larger proteins and gets worse if the object becomes smaller. This impedes structure determination of very small proteins and currently also limits the method. A major contribution to improve the signal-to-noise in electron microscopy imaging is the development of new direct electron detectors. Besides that, data processing software has improved a lot increasing the reliability of the results obtained.

Cryo-EM data of the human γ-secretase were collected with both, a K2 Summit and a Falcon II direct electron detector camera (Lu *et al*, 2014). The results clearly revealed that the best resolution could be obtained when the K2 Summit direct electron detector was used for data collection. In addition, the authors could show that the use of amphipols for keeping the membrane protein soluble facilitates its embedding in the vitrous ice of the Quantifoil carbon grid and furthermore enhances the contrast for particle alignment during data processing.

Cryo-EM of the *B. pseudomallei* c-ring in amphipol (A8-35)

In consideration of all the previously reported results and encouraged particularly by the work of (Liao *et al*, 2013) and (Lu *et al*, 2014) the N-ATPase rotor ring was also incubated in amphipol after its purification, thereby substituting the bound detergent. We were also able to use a K2 Summit direct electron detector camera at a large defocus range for data collection. Due to the very small size of the protein complex the signal-to-noise-ratio was very low and only few pixel could be used for particle alignment, thus a huge number of protein particles (about 75.000) was needed.

Sorting and grouping of particles was performed by 2D class averaging in RELION 1.3 with a large cryo EM data set. Structurally, the investigated complex is composed of a not yet known number of identical repeats of two transmembrane α-helices. During the class averaging of the c-ring particles these two helices have to be aligned correctly to enhance the protein signal and clearly distinguish it from noisy background signal. In the present case, a substantial but unintended background signal is produced by the detergent micelles formed around the highly hydrophobic c-ring, in addition to detector noise and background signal from the vitrified buffer which generally arises during EM data collection (Booy & Elena, 2006).

Remarkably, single densities of the protein could be discriminated from each other in both, the top and the side view of the c-ring in RELION 1.3. Accordingly, the 2D classes of the c-ring must have a resolution of at least 7 Å, which is required to visually separate the helices from each other. The major advantage of 2D class averaging is the fact that the process is reference-free. Accordingly, the resulting number of helices visible in the top view of the protein is created by the actual cryo-EM densities and thereby not biased by any reference or symmetry applied.

We experienced that the use of amphipol (A8-35) for cryo-EM data collection instead of detergent was not advantageous in our case. The high density of the amphipol molecules impeded discrimination of protein from amphipol signal leading to misalignments during data processing. The single densities in the c-ring were not equally pronounced but rather partially blurry and not clearly separated from each other. In comparison, previously solved cryo-EM structures of proteins in amphipol possessed water-accessible domains which did not have amphipol molecules bound (Liao *et al*, 2013; Lu *et al*, 2014). Due to its strong hydrophobicity, the rotor ring is completely surrounded by an amphipol belt, which is clearly visible in the 2D class averages as prominent density around the protein (figure 68 and 86).

Cryo-EM of the *B. pseudomallei* c-ring in DDM and LDAO

An improvement of the signal-to-noise ratio was achieved by collecting cryo-EM data with the c-ring in detergent. Both, the c-ring in DDM and LDAO yielded significantly better results in 2D class averages of the protein complex (figure 68, 74 and 86). DDM still produced a strong signal in cryo-EM imaging, but the protein-to-detergent signal was much better in comparison to amphipol. However, a significantly lower signal originated from LDAO as a detergent for the c-ring, which led to a further improvement in the protein-to-detergent signal (figure 86).

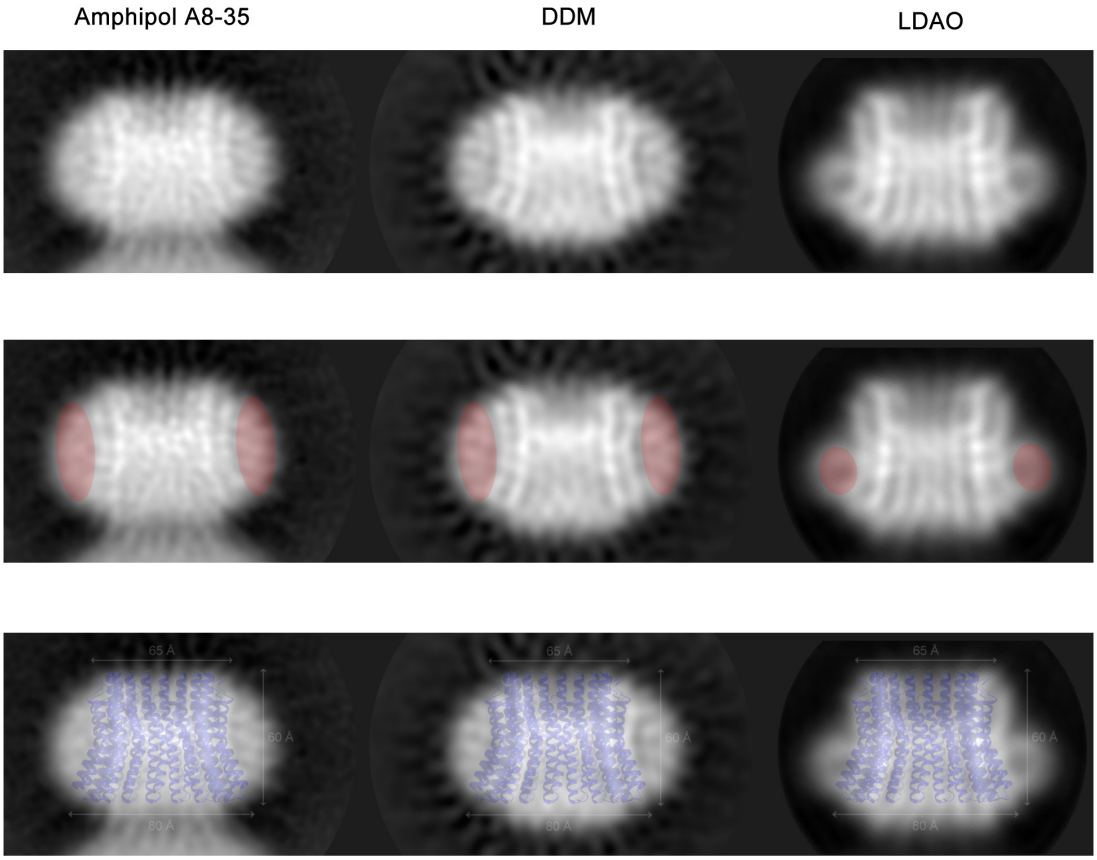

Figure 86. Comparison of the densities of amphipol (A8-35), DDM and LDAO in the side view of the *B. pseudomallei* N-ATPase c-ring obtained by 2D class averages.
In the first row the side views of the 2D class averages of the c-ring in amphipol (A8-35) (left) , DDM (middle) and LDAO (right) are shown. In the second row the densities resulting from the amphipol and detergent molecules bound to the c-ring are indicated in transparent red. In the third row, the structural model of the c_{17} ring is superimposed on each of the 2D classes indicating the dimensions of the densities arising from the protein complex. The density produced by the amphipol molecules was very prominent resulting in a low protein-to-amphipol signal. The density caused by DDM was weaker than by amphipol leading to an improved protein-to-detergent signal. LDAO was bound to a smaller region of the c-ring and produced the lowest density thus the protein-to-detergent signal was best when the c-ring in LDAO was imaged in cryo-EM.

In the top views of the protein complex 17 distinct inner and outer helices could be counted. The diameter of the ring is about 70 Å, thus larger than the diameter of the c_{15} ring of *S. platensis* (65 Å) (Pogoryelov *et al*, 2009) which underpins that the rotor ring investigated here has a higher stoichiometry, such as 17 (figure 87).

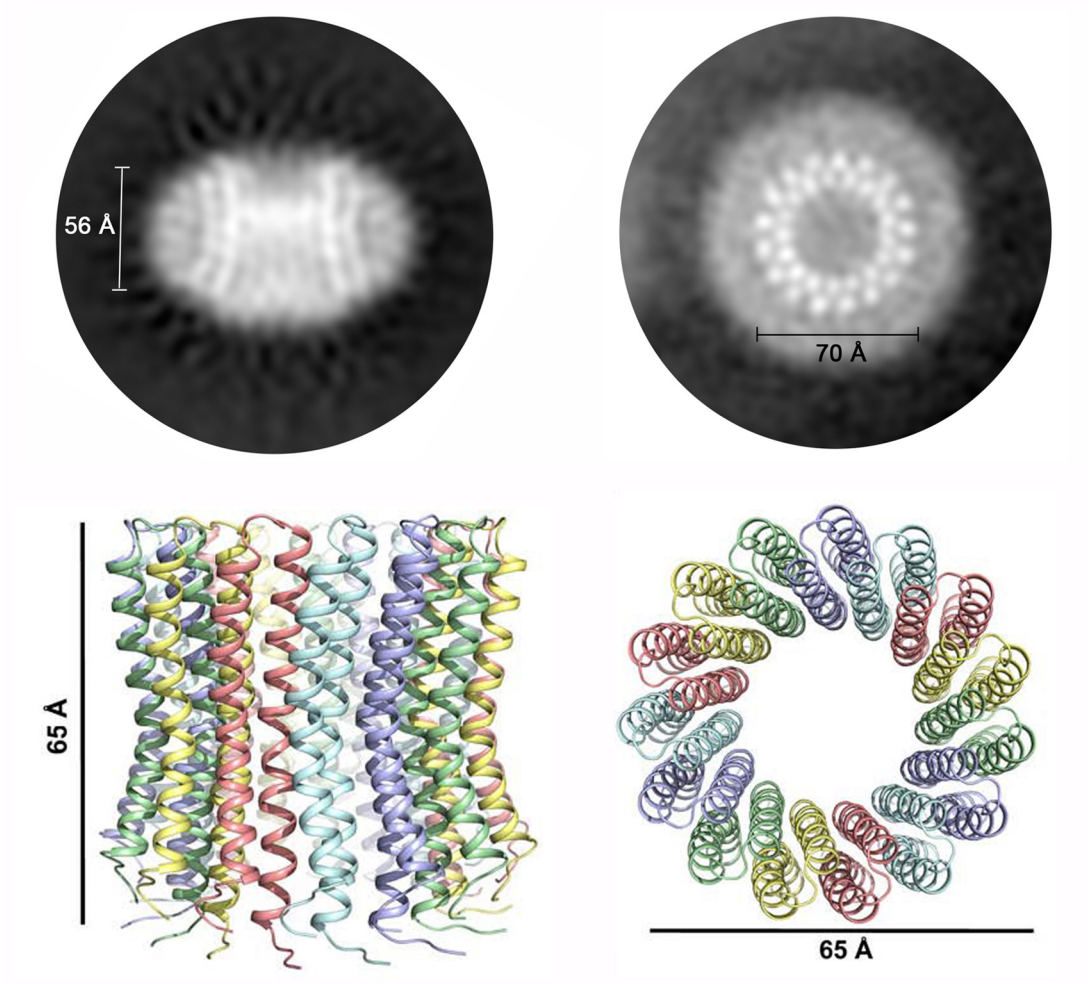

Figure 87. Comparison of the 2D class averages of the *B. pseudomallei* c-ring with the X-ray structure of the *S. platensis* c_{15} ring.

The side and top views of the 2D class averages of the *B. pseudomallei* c-ring in DDM (see figure 65) show a height of 56 Å and a diameter of 70 Å for the protein complex (top). The c_{15} ring of *S. platensis* (Pogoryelov *et al*, 2009) has a height and diameter of 65 Å, in comparison (bottom). The fact that the diameter of the c-ring seen in the top view of the 2D class averages is larger than that of the c_{15} ring substantiates that the *B. pseudomallei* complex has a higher stoichiometry (17 subunits).

However, 2D classification processed in RELION 1.3 has not been used in the past to determine the oligomeric size of a protein complex but was rather used for sorting and grouping selected particles. It has also been described that artificial results can be obtained during 2D class averaging in RELION as the cleanest class may attract other images even if they belong to other classes. As a consequence, different particles might be integrated into the same class while indeed this class represents a mixture of several different classes (Sorzano *et al*, 2010). Despite this observation, RELION 1.3

is currently the most frequently used software package for single-particle protein structure determination. In previous studies larger proteins were analyzed by single-particle cryo-EM producing significantly better signal-to-noise ratios and thereby better alignment possibilities of the structural protein features. According to the low molecular weight of the membrane rotor ring it is a very challenging subject for structure determination by single-particle cryo EM. Nevertheless, a major advantageous in the present case is the intrinsic high symmetry of the protein complex as this could significantly facilitate the subsequent 3D reconstruction process (van Heel *et al*, 2000). Continuous development of the software package will probably enable structure determination of small membrane proteins, like an ATPase rotor ring, in the near future.

Validation of the c-ring stoichiometry indicated in RELION 1.3 could be performed by applying different symmetries on the top view class and compare the resulting quality of the classes in Imagic, which is another commonly used software program for 2D class averaging of single-particles. This way, a c_{17} ring was again shown to be the most probable result as the signal of the single protein densities was significantly clearer than in the other c-rings in the tested range from c_8 to c_{19} (figure 76).

4.2.8 The physiological functions of the two co-existing rotary ATPases

F-type ATP synthases are the universal ATP-producing enzymes. Under physiological conditions, they use an ion-motive force built by H^+ or Na^+ to synthesize ATP from ADP and P_i. The magnitudes of the single components of this ion-motive-force (the membrane potential, $\Delta\psi$ and the transmembrane ion gradient, ΔpH) itself seem to have an influence on the c-ring stoichiometry (Meier *et al*, 2011). Thus, striktly speaking and for a most efficient ATP synthesis only, a lower rotor ring stoichiometry would be energetically favourable as less ions are needed per rotation to generate three ATP molecules in F_1 per complete cycle. Assuming that the F-type ATP synthase is the main enzyme to produce ATP in *Burkholderia* cells, it would be beneficial to have a small c-ring in this enzyme.

In contrast and along the same line of arguments, a high(er) c-ring stoichiometry would be advantageous for efficient transmembrane ion-pumping only, as more ions can be translocated for the energetic output of an ATP molecule. The experiments performed in this work indicated that the N-type rotor ring has a high stoichiometry of

17 c-subunits. Assuming that the N-type ATPases are constructed and coupled analogous to the F-type ATP synthases and likewise exhibit an ion-to-ATP ratio, the latter one would be 17:3 for the *B. pseudomallei* N-ATPase. This way, working in ATP hydrolysis mode, 17 ions would be transported for the cost of three hydrolyzed ATP molecules during a complete c-ring rotation. Hence, the N-type enzyme would establish a transmembrane ion gradient more efficiently than the F-type ATP synthase, given first that the F-ATP synthase indeed harbors a smaller c-ring and second that these c-ring stoichiometries can not be adapted to cell-physiological requirements within a given species (see chapter 1.3.3.1).

Reconsidering the ion specificity of the N-type ATPase it would be feasible that both, Na^+ and H^+-binding rotor rings have evolved, depending on the environmental conditions of a particular organism. For bacteria living in a salt-rich habitat, efficient outwards pumping of Na^+ is indispensable for coping with salt stress. Thus, the N-type ATPases from organisms that live in these salt-rich habitats could play a functional role as ATP-driven Na^+-pumps, additional to other Na^+-extruding enzymes like Na^+/H^+-antiporters, in agreement with what was already hypothesized by others (Soontharapirakkul *et al*, 2011).
In contrast and apart from this putative role of the N-type ATPase, surviving in an acidic environment requires efficient H^+-outwards pumping machineries. Thus, the N-type ATPases could also function as ATP-driven proton pumps to maintain intracellular pH homeostasis. In the context of the results obtained in this work and the measured H^+ (but not Na^+) dependency of *the B. pseudomallei* c-ring, this could be the assumed function for the H^+-specific *B. pseudomallei* N-ATPase. An alignment of different N-ATPase c-subunits together with the detailed knowledge of the Na^+-binding signature (Meier *et al*, 2009) illustrates that both types of ion-coordination are feasible to be present in the N-type enzymes (figure 83).

The presence of the N-ATPase as a second copy of rotary ATPase further strengthens the notion that this enzyme can not functionally replace an F-type ATP synthase, which is always additionally present in the corresponding species. Therefore, the F-type enzyme could physiologically work as an ATP synthesizing enzyme while the N-

ATPase could consume the same to function as an ion outwards pumping enzyme, whereby both enzymes would functionally complement each other.
Finally it is interesting to note that the N-*atp* operon also occurs in pathogenic bacteria like *B. pseudomallei* and *B. mallei*. An additional rotary ATPase working as an ATP-driven ion-pump might facilitate their survival in the human blood stream and could thus be acquired from their non-pathogenic relatives.

4.2.9 Membrane bioenergetics and the evolution of the N-ATPases

Until today, it is still unknown whether H^+- or Na^+-coupled bioenergetics arose first and, consequently, which of the two types was the primary form of rotary ATPase. Various hypotheses have been developed to explain the origin of membrane bioenergetics and the implicated proteins, which will be discussed in the context of the discovery of the N-ATPases in the following.

One common hypothesis suggests alkaline hydrothermal vents to be the primordial energy source for life (Baross & Hoffmann, 1985). In these vents, natural geochemical proton gradients could have been constituted initial ion gradients. Despite the first organic membranes were leaky thus preventing the establishment of an electrochemical gradient, the flow of alkaline fluids and ocean water through the early compartments could have generated initial proton and redox gradients. Hence, these sharp differences in the proton concentration over short distances could have sustained primordial carbon and energy metabolism. These early membranes could than first have become impermeable to sodium ions and the continuous flow of protons could have powered Na^+-efflux via primitive Na^+/H^+-antiporters. Thus, a biochemical sodium ion gradient would have evolved from the primordial geochemical proton gradient (Lane & Martin, 2012).
Considering phylogenetic analyses of rotary ATPases in this context it is striking that these enzymes are interleaved concerning their ion specificity (Mulkidjanian *et al*, 2008a). This observation is in accordance with the finding that some methanogens, such as *Methanothermobacter thermautotrophicus*, rely on both, a Na^+ and H^+ gradient, which are modulated by Na^+/H^+-antiporters (Surin *et al*, 2007). Besides, in the Archaeum *Methanosarcina acetivorans* an ATP synthase with an equal affinity for both ions was found (Schlegel *et al*, 2012). This promiscuity of Na^+- and H^+-

coupled ATP (synth)ases makes it difficult to deduce on what primordial bioenergetics they have relied. According to this hypothesis the ancestral ATPases have arisen in alkaline vents using the natural geochemical proton gradient to produce ATP (Lane *et al*, 2010) while Na^+-coupled enzymes have evolved afterwards.

In contrast to this, an alternative hypothesis suggests that Na^+-gradients from ocean salinity were the primordial driving force (Mulkidjanian *et al*, 2008a; Mulkidjanian *et al*, 2009; Mulkidjanian *et al*, 2007). As biogeochemical considerations revealed that the sodium concentration in the ancient ocean, in times when first primitive cells have evolved, was comparable to that in the current ocean (Mulkidjanian *et al*, 2008a), the ancestral ATPases could also have functioned as sodium ion outwards pumping enzymes. The fact that they occur in Bacteria and in Archaea indicates that they probably have evolved prior to the divergence of the three domains of life. In contrast to other Na^+-translocating enzymes, the rotary ATPases are in principle able to work in both directions so that rotation in the opposite direction would result in the synthesis of ATP by the use of a sodium ion gradient. The evolution of these ATP synthesizing enzymes would then have completed a sodium bioenergetics cycle in the cell membrane (Mulkidjanian *et al*, 2008a).

The N-ATPases are presumed to have been acquired via lateral gene transfer as they are present in many physiologically diverse bacteria (Dibrova *et al*, 2010). As the GC content of the corresponding N-*atp* operon is consistent with the GC content of the entire genome of the corresponding organism, it is plausible that the operon was acquired very early. Consequently, the N-type ATPase might actually represent an evolutionary early form of membrane ATPase. However, as it can not be stated whether Na^+ or H^+-bioenergetics have preceded, the primordial form of N-ATPase can also not be derived.

Nevertheless, considering that the N-ATPase rotor ring of *B. pseudomallei*, according to the investigations presented in this thesis, has a large stoichiometry of 17 c-subunits, a hypothesis for the evolution of membrane rotary ATPases can be established:

The differences in the pH solutions and redox potentials in the alkaline hydrothermal vents were probably very low, resulting in a low overall *proton motive force*. As already suggested by others (Lane *et al*, 2010) the ancestral form of rotary ATPases could have used this proton gradient to synthesize ATP.

At a low *pmf* a large rotor ring is advantageous for ATP synthesis as the energy required to turn the c-ring one step and thus to translocate one ion across the membrane is lower than when a small c-ring is operating. The synthesis of 1 ATP molecule requires 30.5 kJ/mol. 3 ATP molecules are synthesized upon one complete rotation of the c-ring, accordingly necessitating 91.5 kJ/mol. Thus, the energy required for one step of c-ring rotation in a c_{11} ring, such as the one from *F. nucleatum* (Schulz *et al*, 2013), is 1/11 of the total energy for the synthesis of 3 ATP molecules (8.3 kJ/mol), while in a c_{17} ring it is only 1/17 (5.4 kJ/mol), that is significantly lower. Consequently, an N-ATPase with a c_{17} ring could have enabled early ATP synthesis in alkaline hydrothermal vents at a low (local) *pmf*.

In the course of the evolvement of primordial Na^+/H^+-antiporter and a tightening of the membrane a sodium motive force could have been established leading to the genesis of Na^+-specific N-ATP synthases. As a result of the conversion of the natural geochemical proton gradient into a biochemical Na^+-gradient a larger *ion motive force* could be generated. Under these conditions, smaller rotor rings turned out to be more beneficial for ATP synthesis as a low ion-to-ATP ratio implies a more efficient use of energy.

Possibly, the F_1F_o ATP synthases with smaller c-rings could then have evolved from these primordial N-type ATP synthases, using either protons or sodium ions to generate ATP. At this point, the N-type enzymes could then have turned to physiologically function as ATP-driven ion-pumps for efficiently generating an ion motive force, thereby complementing the separate F-ATP synthases, which physiologically function as ATP synthesizing machines in the same cell (figure 88).

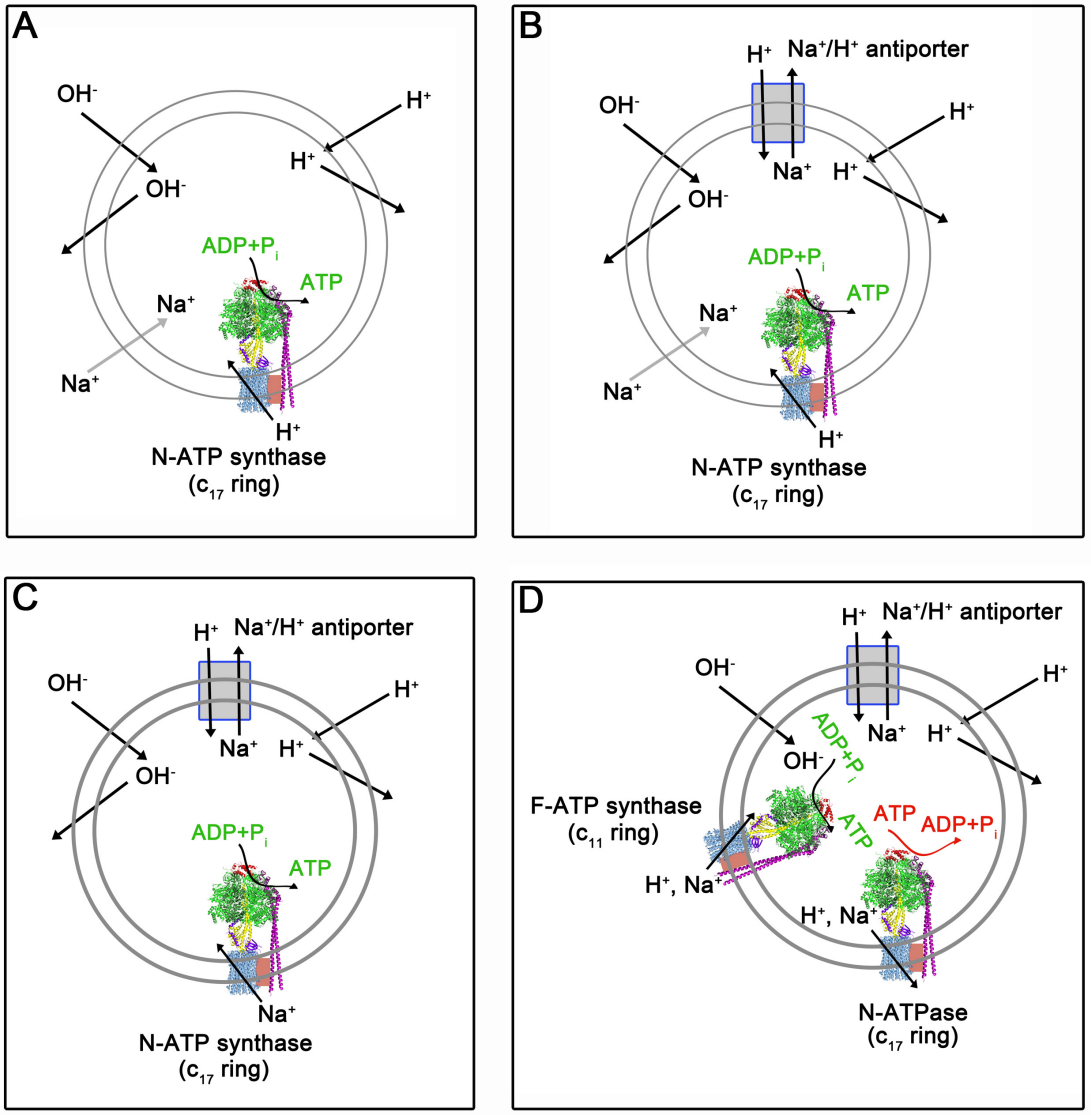

Figure 88. Model for the evolution of early bioenergetics and the N- and F-type ATP (synth)ases. **(A)** Ions (mainly H^+ and OH^-, less Na^+) cross the membrane due to local concentration gradients and electrical potential in a permeable membrane (2 thin circles). This natural geochemical proton gradient can be used by the primordial H^+-specific N-ATP synthase to produce ATP. A large rotor ring of 17 identical subunits is hereby beneficial for ATP synthesis at a low *pmf*. **(B)** Early Na^+/H^+-antiporters generate a biochemical Na^+-gradient from the geochemical H^+-gradient. This leads to promiscuity of membrane proteins for Na^+ and H^+. **(C)** Ion-pumping by antiporters drives the tightening of the membranes (2 thicker circles) and the evolution of Na^+-specific N-ATP synthases. **(D)** Evolvement of the F-ATP synthase with smaller c-rings to synthesize ATP efficiently at higher ion motive forces (*pmf* and *smf*). Transition of the N-type enyzme into an efficient ATP-driven ion-pump.

As outlined above and illustrated in an alignment (figure 83) today`s N-ATPases might still comprise both, Na^+ and H^+-binding enzymes, depending on the environmental needs of a given organism.

This idea contrasts with the hypothesis made by others that a Na^+-coupled N-ATPase, which was working as an ATP-driven Na^+-pump, was the common ancestor of all rotary ATPases (Dibrova *et al*, 2010). The proposal made in this thesis would furthermore contrast with the notion of the primacy of sodium bioenergetics over proton bioenergetics (Mulkidjanian *et al*, 2008b).

Summary

In this work, a N(ovel)-type of rotary ATPase and its rotor ring in particular was investigated biochemically and structurally for the first time. Initially, a transcription analysis of the non-pathogenic *B. thailandensis* revealed that the N-*atp* operon encoding for the N-ATPase is expressed in these cells. For further analysis, the N-*atp* operon of the pathogenic *B. pseudomallei* was cloned and expressed using different heterologous expression systems. Immunogold labeling electron microscopy showed that the N-ATPase is assembled in the *B. thailandensis* membranes. Different approaches were applied to purify the recombinant enzyme which yielded initial success but have to be further optimized in future work in order to isolate a complete N-ATPase complex. Besides the investigation of the complete enzyme, the N-type rotor ring of *B. pseudomallei* was scrutinized and found to be H^+-specific. Structural analysis of the protein complex using single-particle electron cryo-microscopy revealed a yet undescribed stoichiometry of 17 identical c-subunits in a rotor ring, which harbors a total of 17 ion-binding sites. This large numer of ion-bindings sites has a bioenergetical impact on the corresponding ATPase which can operate with a very high ion-to-ATP ratio of 17:3 (i.e. 5.7 ions per ATP pumped) and thus today physiologically function as the most efficient ATP-driven ion-pump characterized so far.

5 Conclusions and perspectives

In the first part of this work the *F. nucleatum* ATP synthase rotor ring was structurally shown to have an undecameric stoichiometry whereby each of the eleven subunits coordinates a Na^+ which is the coupling ion for ATP synthesis in this bacterium. Biochemical and structural methods were used complementary to determine the ion specificity revealing a novel type of Na^+-coordination in this c-ring, which is shared by several other bacteria, including numerous pathogens. Two high resolution X-ray structures revealed that two ions, a Na^+ and a H^+, are concurrently bound to the same site. Biochemical and simulation experiments addressed the possible ion translocation mode in this rotor ring demonstrating that the Na^+ is the only transported ion while the H^+ is constitutively bound in the ion-binding site, resembling a structural feature of the protein.

Until now all Na^+-specific rotor rings investigated so far are composed of eleven hairpin-like subunits while the particular organisms are all growing under anaerobic conditions. In future work on this topic, ATP synthase rotor rings from species which do not grow anaerobically could be analyzed to elucidate if there is any causal relationship between the undecameric stoichiometry and Na^+-specificity of a rotor ring and the anaerobic way of life of the corresponding organism.

In the second part of this work a novel type of rotary ATPase, the N-ATPase, was analyzed. For the first time, the phenotypic existence of this enzyme could be demonstrated in *Burkholderia* cells and an N-ATPase rotor ring has been isolated and biochemically characterized for the first time: These experiments indicate that this N-ATPase is H^+-coupled during its operational cycle as we could show that the isolated, detergent-solubilized c-ring does not bind Na^+. To further address the ion specificity of N-ATPases, future work could be performed on c-rings of other species, such as *Desulfovibrio salexigens* and *Pelobacter carbinolicus*, which do not exhibit a methionine residue in their predicted ion-binding site regions, but instead a threonine residue. This residue provides an essential hydroxyl group at its side chain that is known to be essential for Na^+-binding in c-rings.

Structural investigations of the N-ATPase rotor ring using single-particle cryo-EM demonstrated that the complex is composed of 17 identical c-subunits. This is the largest c-ring known so far with respect to the number of ion-binding sites, making the N-type ATPase of *B. pseudomallei* to the most efficient ATP-hydrolytic ion-pump

known to date. At this point, it is higly promising that the still ongoing work on cryo-EM data analysis will visualize the architecture and structure of the N-ATPase rotor ring.

6 Appendix

A

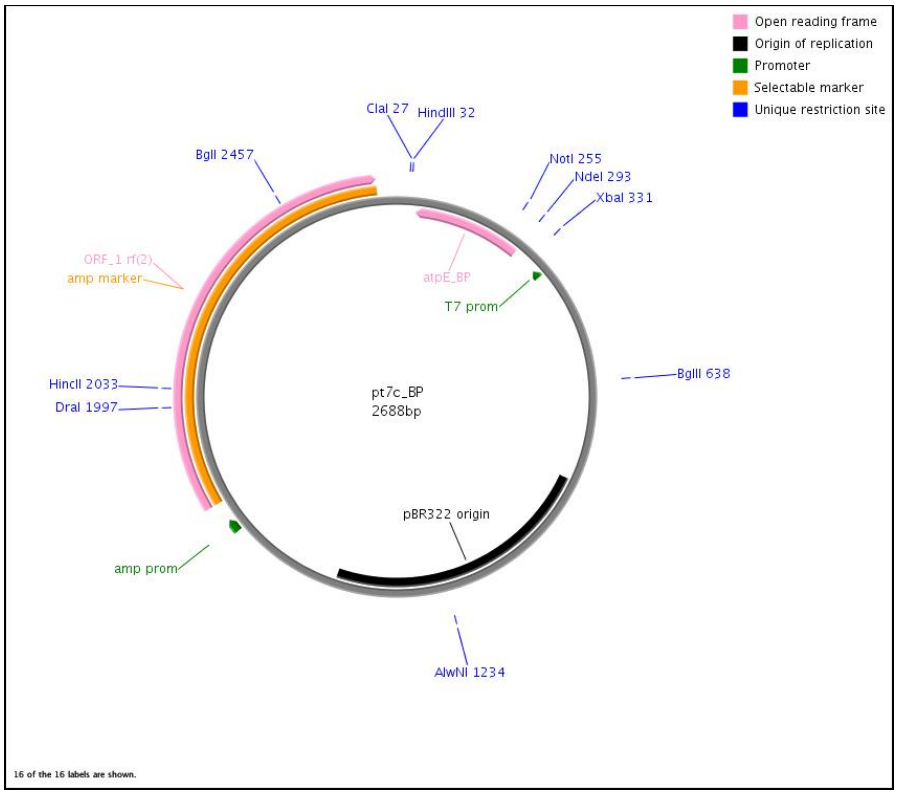

B

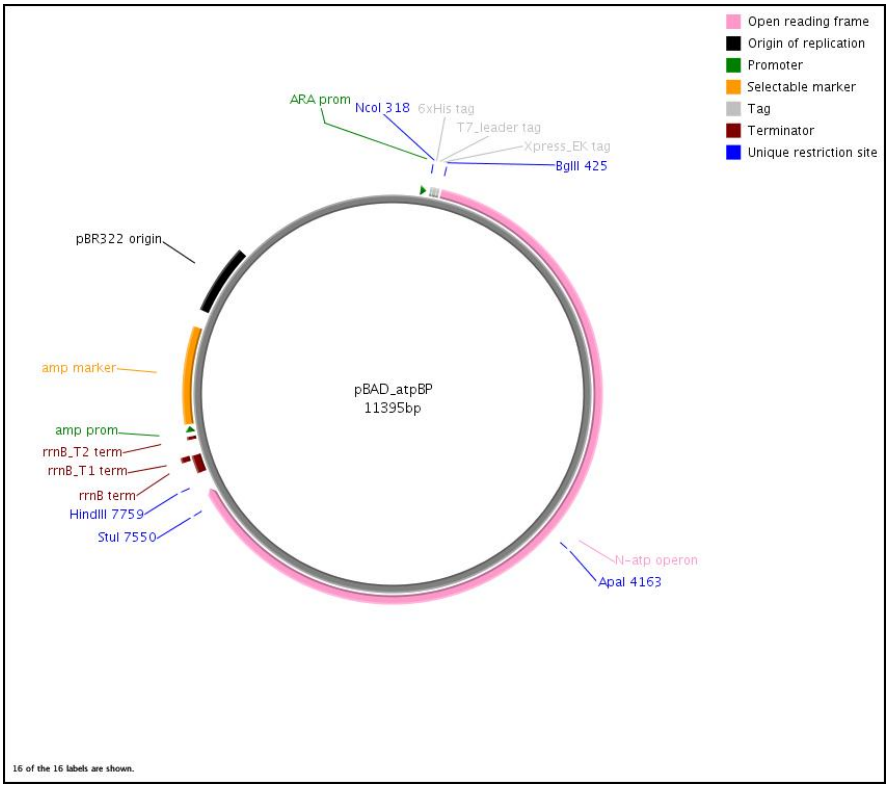

C

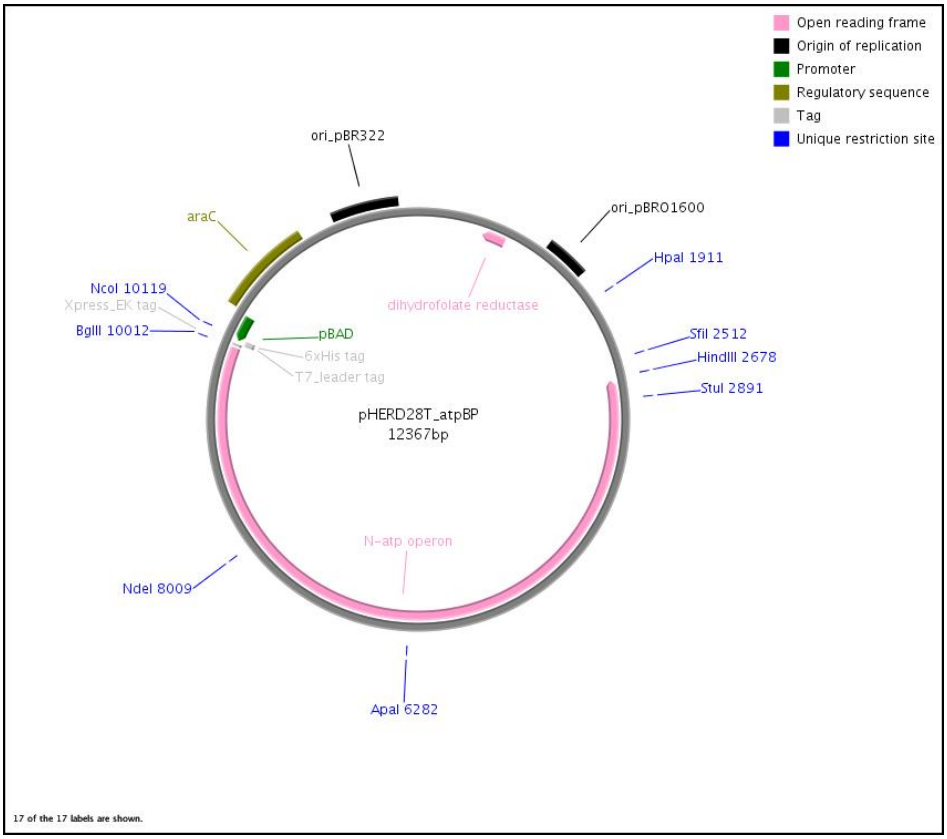

Figure 89. Vector maps of the constructs cloned for the heterologous expression of the *B. pseudomallei* N-ATPase c-ring and the entire N-ATPase enzyme.

(A) Plasmid pt7c_BP (2688 bp) used for the heterologous expression of the N-ATPase c-ring in *E. coli*. **(B)** Plasmid $pBAD_{HisB}$_atpBP (11395 bp) and **(C)** Plasmid pHERD28T_atpBP (12367 bp) used for the heterologous expression of the N-ATPase enzyme in *E. coli* and *B. thailandensis*, respectively. The open reading frames of the *atpE* gene (A) or the entire N-*atp* operon (B and C) are shown in rosé. Unique restriction sites, origins of replication, promotor and terminator sequences, affinity tags as well as selection marker are indicated in different colours.

GCCGTGCGCGACGCGTCGCCGCCGTGCCCGCGCGTCGATCGTTTCGCATCGCGAGACGCCGCGTTTCATCTGGCGATTTCCCGTTTCTTGACCGAGAT
CAGCCGGCGGGCGGCGCGCGCCGTTATGGTGAAGCCATCTTCGAAACAGCCAGATGGGAGCGACGGTGGCGGACCTGCAAGCGACGAACGGCACGGCG
CAGGCGCAAGCGAAGCACGGCGTGAGCGACGGGCGCGTCGTCGCGGTGCGCGGCGCGGTCGTCGACGTCGCGTTCGACGGCGGCGTGCTGCCCGCGCT
GAACGACGCGCTCGTGATTCCGATCGACGGCGCCGCGCCGATCCTCGCCGAGGTGCACGCGCACCTGAGCGACGCGGCGGTGCGCGCGCTCGCGCTCG
GCCCGACGGGCGGGCTGCGGCGCGGCGCCGCCGTGCGCGCGACGGGCGGGCCGATTCGCGTGCCTGTCGGCGACGCGGTGCTCGGCCGCCTGCTGAGC
GTCACGGGCGAGCCCGGCGACGACGGCGCGGCGCTGGCGGCGGACGTCGCGCGGCGGCCGATCCATCGCGGCGCGCCGCCGCTCGCCGAGCAGAAGAG
CGCGACCGCGCTGTTCGCGACCGGCATCAAGGTGATCGATCTGCTCGCGCCGCTCGCGCAGGGCGGCAAGGCCGCGATGTTCGGCGGCGCGGGCGTCG
GCAAGACGGTGCTCGTGATGGAGCTGATCCACGCGATGGTCGAGCGCTATCGCGGGATCTCGGTGTTCGCCGGCATCGGCGAGCGCTCGCGCGAAGGG
CACGAGATGCTGCTCGACATGCGCGGCTCCGGCGTGCTCGGCCGCACGGTGCTCGTCTACGGGCAGATGAACGAGCCGCCCGGCGCGCGCTGGCGCGT
GCCGCTCACCGCGCTCGCGATCGCCGAGTATTTCCGCGACGAGCGCGCGCAGAACGTGCTGCTCCTGATGGACAACGTGTTTCGCTTCGTGCAGGCGG
GCGCGGAGGTGTCGGGCCTGCTCGGGCGGCTGCCGTCGCGGGTCGGCTATCAGCCGACGCTCGCGAGCGAGGTCGCGGCGCTGCAGGAGCGCATCGCG
TCGGTCGAGGGCGCGGCGGTGACGGCGATCGAGGCCGTCTACGTGCCCGCCGACGATTTCACCGATCCCGCCGTCACCGCGATCGCCGCGCACGTCGA
CAGCATGGTCGTGCTGTCGCGCGCGATGGCGGCCGAAGGCATGTACCCGGCGATCGACCCGGTCGCGTCGTCGTCGATCCTGCTCGATCCGCTCGTCG
TCGGCGAAGCGCACGTCGAGGTCGCGATCGAGGTGCGCCGCGTGATCGAGCATTACCGCGAACTGCAGGACGTGATCGCGCTGCTCGGCATCGACGAG
CTCGGCGCGGACGATCGCCGCATCGTCGGCCGCGCGCGCCGGCTGCAGCGCTTTCTCACGCAGCCGTTCGCGGTGACCGAGGCGTTCACGGGACAGGC
GGGCGCGTCGGTCGAGATCGCCGACACGATCGCCGGCTGCCGCGCGATCCTGCGCGGCGATTGCGACGACTGGCGCGAGAGCTCGCTGTACATGGTCG
GCACGCTCGACGATGCGCGGCGCAAGGAAGAGGCGGCGCGCGAAGCGGATGCGCGGCGCGATGCGGCGGCGGGCGCCGCGTCCGGCTCCGCCGGGCCG
CAAGGCGCGCAGCATGGCCGCTGAGCTGCGCGTGACGATCGCGACGCCGGCGCGCGTGTGCGTCGACGATCTGCCGATCGTGTCGCTGCGCGCCGAGG
ACGCGAGCGGCGCGTTCGGCATCCGCGCGGGCCATGTCGATTTCGTCACGCTGCTGCGCGCGTCGGTCGTGCGCTGGCGCACCGCCGACGACGCGATG
CATTACGCCGCGCTCGACGGCGGCGTGCTGCGCGTGACGCGCGGCGCGCGCATCGAGATCGCGTGCCGCGACGCGGTGCTCGGCGAGTCGCTCGCGGA
GCTCGAAGCGGTGGTGCGCGGCGTGCGCGAGACGCAGCTCGACGAGAAGCGCCGCGCGCGCGTCGACGAGACGCGGCTGCATGCGCAGGCGGTGCGGC
GGCTGCTTACGTATCTGCGGCCCGAGCATGCGAAGGACGGCATGCTCGCGCCGATGAAGCCGGAGACGCTCGAATGACGAAGCGCCGGCCGTTCGAAG
CGAAGCGCGACGATGCGGCGCGCGGCGACGCGCGCCGCGCCGGGGCGAGCGCCGCGCGGGACGACGCGCGCGACGGTGCGCCGCGCGAGCCGTCGCCG
GAATCATCCGGATCTCCCGCCGCGCGCGATGGCGGAAGGCCCCCGGCCGTGCGGCCCGCCGACGCCGCGCCGAAGCCCGCCGCCGACCGCGTCGCGCA
GGCGGCGCGCACGGCGGCGACGCGCGCGGCGCGCGGCGCGCGCGATCCGGAGCCGTCGCTCGGCCGGCGGCTTGCGCAGATCGGCGTGCTCGGCTGGA
CGATCGTCGCGCCGACGCTCGCCGCGCTCGCGATCGGGCGCTGGCTTGACCGCGTGTTCGCGTCGCGCGTGTTCTTTTCCGCGCCGCTCGTGATGCTC
GGCGCGGCGCTCGGCTTCTGGCTCGCGTGGCGCTGGATGAAAGGTCAACAAGAAGGAGATCGCGATGATTGACATGTGGGACACCGCGCGCGCGTCGT
TCGACGGCATCGCCGCCGTGATCGGGCTGGCGGCCGGGTTCGCCGCCGGCGCGTGCCATTTCGTATCGCTCGGCTGGAACAGCCGGCTGTTCGTCGCG
GGGCGCGCGGGCGCGGCGCTCGCGTTGCAGTTCGTGCGGATCGCGCTCGCGGTGGCGGTGCTCGTCGTGCTCGCGCGCGCGGGTTTCGGCATGCTCGT
CGCGGGCTCGGCCGGCTTCTTCGCCGCGCGCGCGCTCGCGGTGCGCCGCGCGGCCGCGCTGACGGGAGCGCGGCAATGAACGCGTCGCCGCTGTCGAC
CGTGCCGATGTTCTCGATCGGCCCCGTCGGCATCTCCGCACCCGTGCTCGCGACGTGGGCGATCATGGCCGCGCTCGTCGCGCTCGCGCTCGCCGCGC
GCGGGCGGCTGAGCGTCGAAGCGCCGTCGCGGCTGCAAAGCGTGCTCGAGCTGTTCGTCGCGACGATCGACGCGCAGATCGCCGACACGATGCAGACG
CCGCCCGCGCGCTATCGCGCGCTGATCGGCACGATCTTCGTGTTCGTGTTCTGCGCGAACGGCACGTCGCTCGTGCCGGGCGTCGAGCCGCCCACCGC
GCACCTCGAGACCGACGCCGCGCTCGCGCTCGTCGTGCTCGCGGCGACGCTCTACTACGGCGTGCGCGTGCGCGGCGTGCGCGGCTATCTCGCGACGT
TCGCCGAGCCGACGTGGGTGATGATTCCGCTGAACGTCGTCGAGCAGCTGACGCGCACGTTCTCGCTGATCGTGCGTCTGTTCGGCAACGTGATGAGC
GGCGTGTTCGTGATCGGCATCGTGCTGTCGCTCGCCGGCCTGTTCGTGCCGATTCCGCTGATGGCGCTCGATCTGCTGACGGGCACGGTGCAGGCGTA
CATCTTCATGGTGCTGTCGATGGTGTTCATCGGCGCGGCGGTGTCCGGTGACGAAACTTCCGCGCCGCGGCGCGGGCAGGAGAATGCATGAACAATCT
CATCGAAGTGGTCAGCATCGCGGCGGCCGCGCTCGCCGTGTCGTTCGGCGCGATCGGTCCAGCGCTTGCCGAGGGGCGCGCGGTCGGCGCGGCGATGG
ACGCGATCGCGCGGCAGCCCGACGCGTCCGGCACCGTGTCGCGCACGCTGTTCGTCGGGCTCGCGATGATCGAGACGATGGCGATCTACTGCCTCGTC
GTCGCGCTGCTGCTGCTGTTCGCGAATCCGTTCGTCAAGTGACGAGGGGGCGGCGATGCGAATCGACTGGTCCACGCTCGCGCTGCAGACGATCAACG
TCGTCGTGCTCGTGTGGCTGCTGTCGCGCTTCCTGTTTCGCCCCGTGAGCGACATCATCGCGAAGCGCCAGGCCGCCGCGCGCGCAAGCTGATCGACGAC
GCGGCGCACGAGCGCGACGCCGCGCGCGCCGAGCGTGAGCGGGTGCGCGGCGAGCGCGCGTCGCTCGCCGCGGCGCGCGACGACGCGCTGAAGGACGC
GCTCGCGCAAGCCGCCACCGAGCGCGAGCGCCTGATCGACGCCGCGCGCGCCGACGCGCGGGCGCTGCGCGACGCGGCGCGCGCGCAGGCGGACGCCG
ACGCCGCGCGGCGCGCGAAGGCGCTCGACGCGCACGCGACGCGCCTCGCGATCGACATCGCTGCGAAGCTGCTCGCGCGGCTGCCGGACAGCGCGCGC
GTCGCGGGCTTCGTCGACGGCGTCGCGGCGTCTCTCGCGAAGCTGCCGGCCGACGTGCGCGCGTCGCTCGCCGGCGACGACGCGCAGGTGAGGCTCGT
CGCGCCGCGCGCGCGCTGACCGCGCAGGAGGCGGCCGCGTGCCGCGCGGCGTTCGCGGCGAGCGTCGGGCGGCCGCTCGAGCCCGACGTGCGCATCGATC
CCGCGCTGATCGCGGGGCTTGAGCTCGAATCGAAATACGCGAACGTGCGCAACAGCCTGCGCCAGGATCTCGCGACCATCGAGGCGGCACTGCTGAAC
GACGATGACGCAAACGCCTGATGCAACCGGGGCCGCCGCCGATGCGCGCTGGCTCGCGCGCCGCCGCGGCGCGCTCGCGTGCGTCGCGCTCGCGCCCG
TCGCGCAGGCGCTCGGGCGAGTCGAGCGCGTCGCGGACGGGATCGCGTTCGTGTCGGGCCTCGAGGACGCGATGCTCAACGAAGTGCTGCGCTTCGAC
GGCGGCGTCACCGGCTTCGCGCATACGCTCGACGAGGATCTGATCAGCGTCGTGCTGCTCGATCCCGACGCGGGCGTTCAGGCGCAGACGGCGGTCAC
GCGCACGGGCGCGGTGCTCGAAGTGCCGGTCGGGCCGCAACTGCTCGGGCGCGTCGTCGATCCGCTCGGCCGTCCGCTCGACGGCGGCGCGCCGCTCG
GCACGGCGGACACGCTGCCGATCGAGCGCCCCGCGCCCGAGATCATCGAGCGCGACCTCGTCAGCGAGCCGCTCGATACCGGCGTGCTGATCGTCGAC
GCGCTCTTCACGATCGGGCGCGGCCAGCGCGAGCTGATCATCGGCGATCGCGCGACCGGCAAGACCTCGCTCGCGATCGACGCGATCGTCAACCAGCG
GCATTCGGACGTGATCTGCGTGTACGTCGCGATCGGCCAGCGCGCGAGCGCGGTGCGGCGCGTGATCGACGCGGTGCGCCGTTACGGCGCGCCCGAGC
GCTGCATCTTCGTCGTCGCGCCGGCCGCGTGCGCGCCGGGGCTGCAGTGGATCGCGCCGTTCGCGGGCTTTTCGGTCGCCGAGTACTTCCGGGACCGC
GGGCAGCACGCGCTCGTCGTCGTCGACGATCTGACGAAGCACGCGGCGACGCACCGCGAGCTCGCGCTGCTCACGCGCGAGCCGCCCGGCCGCGAGGC
GTACCCCGGCGATATCTTCTACGTGCACGCGCGCCTGCTCGAACGGGCGGCGAAGCTGTCGGCCAAGCTCGGCGGCGGATCGCTGTCCGCGCTGCCGA
TCGCGGAGACCGACGCGGGCAACCTCGCCGCGTACATTCCGACGAACCTGATTTCGATCACCGACGGGCAGATCGTGCTCGATTCGGCGCTGTTCGCC

GCGAACCAGCGGCCGGCCGTCGACGTTGGGCTGAGCGTGAGCCGCGTCGGCGGCAAGGCGCAGCATCCGGCGCTGCGCGCCGCGTCAGGCCGCCTGCG
GCTCGACTACGCGCAGTTCCTCGAGCTGGAGGCGTTCACGCGCTTCGGCGGGCTCACCGACGCGCGGCTGCGCGCGCAGATCACGCGCGGCGAGCGGA
TTCGCGCGTTGATCACGCAGCCGCGCTTTCGCGCGCTGCGCACGCTCGACGAGGTCGTGCTGCTGAAGGCGCTCGCGGCGGGCGTGCTCGATGCGATG
TCGCCGGATCTCGTCGCGCCGTTGCGCGAGCGGCTGCCGTCGTGGCTCGACGCGCGGCTCGCGCCGCCGCGCGACCGGCTCGCGGACGACGCGGCGCT
TTCGATGCTCGCGGAATCGATCGGCGAACTGGTCGAGCGGGTTGCTGCGGACGCCGCGCATCGCGCGGCGGCGGGCGGGCACGCGGAGGACGCGGCGG
ACGACATGGGCGGTGCGCTCGACGGCGAACACGCGAGCGGCGATGCGACAAGCATCGCCCCGACGCCGCCGGGCGGCGCCGAAGCCGGCGCGCCGCGC
AAGCGATGAGCGACAAGCTCGCCGCGATCGAAGCGCGCACCGACACCGCGCGCCAACTGCAGACCGTGATCGGCGCGATGCAGGGCGTTGCCGCCGCG
CGCGCGCACGAGGCGCAGCAGCGCTTGCCGGGCATCCGCGCGTCGGCGGCGACGGTCGGCGCGGCGATCGGCGACGCGCTGTCGGCGGGCGCGCCGTC
GGGCGAGACGGCCGCCGCGAGGCGCGGCGTGCCGCGCGCGCGGCTCGTCGTCGTGCTCTGCAGCGAGCAGGGCTTCGTCGGCGCATACAACGCGCAGT
TGATCGACCGCGCGACGCAGCCCGACGCGGACGTGTCGCGCGAATACATGATGATCGGCTCGCGCGGCGCGATGCTCGCCGAAGCGGGCGGCGTGCCG
CTCGTGTGGCGCACGCCGATGGCGTCGCACGCGGACGACGTCGTGCATCTCGCGAACCGGATCACCGACGCGCTGTACGCGCATCTCGCGAAGCGCGG
CGCGCAGCCGGTGTCGATCGTCCATGCGATGCCGGGCGGCGCGCCGCGGCTCGACGTGATCGAACGCCGTCTGCTGCCGTTCGACTACGCGCGCTTCG
ACACCGCGCCGCGCGTGCAGCCGCCGCTCGTGCACCTGCCGCCCGCGACGCTGCTCGCGGAGCTCGCGCAGGCGTACGTGTTCGTCGAGCTGTGCGAG
GCGGCGATGCTCGCGTTCGCCGCGGAGAACGAGGCGCGCACGCGCGCGATGATCGCCGCGCGCGAATCGGTCGAGCGCACGCTCGGCGAGCTGTTGCA
GGCATACCGGATCGCCCGGCAGGACGAGATCACGGCGGACATCGTCGAGCTTGCGGCGAGCGGGTTGTGAACCCGGACGTGGCGGCGTGACGACGCAA
TCGCGCGATCTCGCGATTTCGCGATTGCTCGATCGAGCGCCGCGCGCACGCATCGCGCCGGGCACGCGAA

Figure 90. Sequence of the *B. thailandensis* N-*atp* operon.

The coding region (yellow) as well as the start (green) and stop (red) codons are indicated. Overlapping nucleotides are marked in purple.

GGAGCGACGGTGGCGGATCCGCAGGCGACGAACGGCACGGGCGCGGCGTGCGCGGAGCGCGACGCGAGCGACGTGGGCGATGTGAGCGACGTGGGCGA
TGCGCGTGACGAGGGCGCCGGCCGCGTCGTCGCGGTGCGCGGCGCGGTGGTCGACGTCGCGTTCGACGGCGGCGCGCTGCCCGCGCTGAACGAAGCGC
TCACGATCCCGGTCGACGGCGCCTCGCCGATTCTCGCCGAGGTGCACGCACACCTGAGCGACGCGGCGGTGCGCGCGCTCGCGCTCGGCCCGACGGGC
GGCCTGCGGCGCGGCGCCGCCGTGCGCGCGACGGGCGGGCCGATTCGCGTGCCCGTCGGCGACGCGGTGCTCGGCCGCCTGCTGAGCGTGACGGGCGC
GCCCGGCGACGACGGCGCGGCGCTTGCGGCGGACGTCGAGCGGCGGCCGATCCATCGCGGCGCGCCGCCGCTCGCCGAGCAGAAGAGCGCGAACGCGC
TGTTCGCGACCGGCATCAAGGTGATCGATCTGCTCGCGCCGCTCGCGCAGGGCGGCAAGGCCGCGATGTTCGGCGGCGCGGGCGTGGGCAAGACGGTG
CTCGTGATGGAGTTGATCCATGCGATGGTCGAGCGCTATCGCGGGATCTCGGTGTTCGCGGGCATCGGCGAGCGCTCGCGCGAGGGGCACGAGATGCT
GCTCGACATGCGCGGCTCCGGCGTGCTCGGCCGCACAGTGCTCGTCTACGGGCAGATGAACGAGCCGCCCGGCGCGCGCTGGCGCGTGCCGCTCACCG
CGCTCGCGATCGCCGAGTATTTTCGCGACGAGCGCGCGCAGAACGTGCTGCTGCTGATGGACAACGTGTTTCGCTTCGTGCAGGCGGGCGCCGAGGTG
TCGGGCCTGCTCGGGCGGCTGCCGTCGCGGGTCGGCTACCAGCCGACGCTCGCGAGCGAGGTCGCGGCGCTGCAGGAGCGGATCGCCTCGGTCGAGGG
CGCGGCGGTGACCGCGATCGAGGCCGTCTACGTGCCCGCCGACGATTTCACCGATCCCGCCGTCACCGCGATCGCCGCGCACGTCGACAGCATGGTCG
TGCTGTCGCGCGCGATGGCGGCCGAAGGAATGTATCCGGCGATCGATCCGGTCGCGTCGTCGTCGATCCTGCTCGATCCGCTCGTCGTCGGCGAAGCG
CACGTGGAGGTGGCCATCGAGGTGCGCCGCGTGATCGAGCATTACCGCGAATTGCAGGACGTGATCGCGTTGCTCGGCATCGATGAGCTCGGCGCGGA
CGACCGGCGGCTCGTCGGCCGCGCGCGCCGGCTGCAGCGCTTTCTCACGCAGCCGTTCGCGGTGACCGAGGCGTTCACGGGGCAGGCGGGCGCGTCGG
TCGAGATCGCCGACACGATCGCCGGTTGCCGCGCGATCCTGCGCGGCGACTGCGACGACTGGCGCGAGAGTTCGCTGTACATGGTCGGCACGCTCGAC
GACGCGCGGCGCAAGGAAGCGGCGGCGCGCGAAGCGGACGCGCGCCGCGAGGCGGCTGCCGCGGCGTCGGTCGCGGGACCGGGCACGACATCGGGCAC
GACATCCGACCCCGCATCCGGCTCCGCCGAGCCGCAAGGCGCGCGGCATGGGCGCTGAGCTGCGCGTGACGATCGCGACGCCGGCGCGCGTGTGCGTC
GACGATCTGCCGATCGTGTCGCTGCGCGCCGAGGACGCGAGCGGCGCGTTCGGCATCCGCGCGGGCCACGTCGATTTCGTCACGCTGCTGCGCGCGTC
AGTCGTGCGCTGGCGCACCGCCGACGGCGCGACGCATTACGCGGCGCTTGACGGCGGCGTGCTGCGCGTGACGCGCGGCGCGCGCATCGAGATCGCGT
GCCGCGACGCGGTGCTGGGCGAGTCGCTCGCCGAGCTCGAGGCGGTGGTGCGCGGCGTGCGCGCGACGCAGCTCGACGAGAAGCGCCGCGCGCGCGTC
GACGAGACGCGGCTGCATGCGCAGGCGGTGCGGCGGCTGCTCACGTATCTGCGGCCCGAGCACGCGAAGGACGGCGTGCACGCGCCGCTGAAGCCGGA
GACGCTCGAATGATGAAGCGCAGGCCGCCCGAGGTGAAGCGCGAGGCGCGCGAGGCGCGCGACGATGCCGCGCGCGGCGACGCGCGGCACGCCGGCGC
CGGCGCCGCGCCGGATGACCCACGCGGCGCCGCGCGGCGCGACCCGCCGCCCGGCTCGCGCGCCGCGCGCGGCGGCGCAACGCATCCGGCCGCGCGAG
CCGCCGAGCCCGCCGCGCCGAAGCCCGCCGCCGATCGCGTCGAGCGGGCCGCGCACACGGCCGCGGCGCGCGCGGCGCGGCGCGCGCGATCCGGAA
CCGTCGCTCGGCCGACGGCTCGCGCAGATCGGCGTGCTCGGCTGGACGATCGTCGCGCCGACGCTCGCCGCGCTCGCGCTCGGCCGCTGGCTCGACCG
GATGTTCGCGACGCGGGTGTTTTTTTCCGCGCCGCTCCTGATGCTCGGCGCGGCGCTCGGCCTCTGGCTCGCGTGGCGCTGGATGAAAGCTCAACAGC
ATGGAGATCGCGATGATTGAGATGTGGGAAACCGCGCGCGCGTCGTTCGACGGCATCGCCGCCGCGATCGGGCTCGCGCTCGGGTTCGCCGCCGGCGC
GTGCCATTTCGTGTCGCTCGGCTGGAACAGCCGGCTGTTCGTCGCGGGCCGCGCGGGCGTGGCGCTCGCGCTGCAGTTCGCGCGCGTCGCGCTCGCGG
TGGCGGTGCTCGTCGTGCTGGCGCGGGCGGGCTTCGGCATGCTCGTTGCGGGCTCCGCGGGGTTTTTCGCCGCGCGGGGCGATCGCGGTCCGCCGCGCG

GCCGCGTTGACGGGAGCGCGGCGATGAACGCGTCGCCGCTGTCGACCGTGCCGCTGTTCTCGGTCGGCCCCGTCGGCATCTCGGCGCCCGTGCTCGCG
ACGTGGGCGATCATGGCCGTGCTCGTCGCGCTCGCGCTCGTCGCGCGCCGGCGGCTGAGCGTCGATGCGCCGTCGCGGCTGCAAAGCGTGCTCGAGCT
GTTCGTCGCGACCGTCGACGCGCAGATCGCCGACACGATGCAGACGCCGCCCGCGCGCTATCGCGCGCTGATCGGCACGATCTTCGTGCTCGTGTTCT
GCGCGAACGGCGCGTCGCTCGTGCCGGGCGTCGAGCCGCCGACCGCGCATCTCGAGACCGACGCCGCGCTCGCGCTCGTCGTGCTCGCGGCGACGCTC
TATTACGGCGTGCGCGCGCGCGGCGTGCGCGGCTATCTGGCGACGTTCGCCGAGCCGACCTGGGTGATGATTCCGTTGAACGTCGTCGAGCAGCTCAC
GCGCACGTTCTCGCTGATCGTGCGCCTGTTCGGCAACGTGATGAGCGGCGTGTTCGTGATCGGCATCGTGCTGTCGCTCGCCGGCTTGTTCGTGCCGA
TTCCGCTGATGGCGCTCGATCTGCTGACGGGCACGGTGCAGGCGTACATTTTCATGGTGCTGTCGATGGTGTTCATCGGCGCGGCCGTATCCGGTGAC
GAAACTTCCGCGCCGCGGCGCGGGCAGGAGAACACATGAACAATCTCATCGAAGTGGTCAGCATCGCGGCGGCCGCGCTCGCCGTGTCGTTCGGCGCG
ATCGGCCCCGCGCTCGCGGAAGGGCGCGCGGTCGGCGCGGCGATGGATGCGATCGCGCGGCAGCCGGACGCGTCCGGCACGGTGTCGCGCACGCTGTT
CGTCGGGCTCGCGATGATCGAGACGATGGCGATCTACTGCCTCGTCGTCGCGCTGCTGCTGCTGTTCGCGAATCCGTTCGTCAAGTGACGCGGAGGCC
GCGATGCGAATCGACTGGTCCACGCTCGCGCTGCAGACGGTCAACGTCGTCGTGCTCGTGTGGCTGTTGTCGCGCTTCCTGTTTCGCCCGGTGAGCGA
CATCATCGCGAAGCGCCAGGCCGCCGCGCGCAAGCTGATCGACGATGCGTCACGCGAGCGCGATGCCGCCCACGCCGAGCGCGAACGGGCGCGCGCCG
AGCGCGCGTCGCTCGCCGCCGCGCGCGACGACGCGCTGAAGGACGCGCTCGCGCAGGCCGCCGCCGAGCGCGAGCGGCTGATCGCCGCCGCGCGCCC
GACGCGCAGGCGCTGCGCGACGCGGCGCGCGCGCAAGCCGATGCCGACGCCGTGCAGCGCGCGAAGGCGCTCGACGCGCGCGCGACGCGCCTCGCGAT
CGACATCGCCGCGAAGCTGCTCGCGCGGCTGCCGGACAGCGCGCGGGTCGCGGGTTTCGTCGACGGCGTCGCGGCATCGCTCGCGCGATTGCCGGCCG
ACGTGCGCGCGTCGCTCGCCGACGAGGACGCGCAGGTGCGGCTCGTCGCGCCGCGCGCGCTGACCGCGCAGGAGGCGGCCGCGTGCCGCGCGGCGTTC
GCGGCGAGCGTCGGGCGGCCGCTCGAGCCCGACGTGCGTGTCGATCCCGCGCTGATCGCCGGGCTCGAGCTCGAATCGAAATACGCGAACGTGCGCAA
CAGCCTGCGCCAGGATCTCGCGACCATCGAGGCAGCGTTGCTGAACGAAGATGACGCCGACGCCTGACGCACCTGCCGCCGCCGCCGCTGATGCCGCA
ACCGGCGCCGGCTGGCTCGCGCGCCGCCGGGGCGCACTCGCGCGCGTCGCGCTCGCGCCCGTCGCGCAGGCGATCGGGCGGGTCGAGCGCGTCGCGGA
CGGGATCGCGTTCGTGTCCGGTCTCGAAGACACGATGCTCAACGAAGTGCTGCGTTTCGAAGGCGGCGTGACCGGCTTCGCGCATACGCTCGATGAGG
ATCTGATCAGCGTCGTGCTGCTCGATCCGGACGCGGGCGTTCGCGCGCAGACGGCGGTCGCGCGCACGGGCGCGGTGCTCGAAGTGCCGGCCGGGCCG
CAACTGCTCGGGCGCGTGGTCGATCCGCTCGGCCGCCCGCTCGACGGCGGCGCACCGCTCGATGCGGCGCACACGCTGCCGATCGAGCGCGCCGCGCC
GGCGATCATCGAGCGCGATCTCGTCAGCGAGCCGCTCGACACCGGCGTGCTGATCGTCGACGCGCTCTTCACGATCGGGCGCGGCCAGCGCGAGCTGA
TCATCGGCGATCGCGCGACCGGCAAGACCTCGCTCGCGATCGACGCGATCGTCAACCAGCGGCATTCGGACGTGATCTGCGTGTACGTCGCGATCGGC
CAGCGCGCGAGCGCGGTGCGCCGCGTGATCGACGCGGTGCGCCGCTACGGCGCGCCCGAGCGCTGCGTCTTCGTCGTCGCGCCGGCCGCGTGCGCGCC
GGGGCTGCAGTGGATCGCGCCGTTCGCGGGCTTCTCGATCGCCGAATATTTCCGCGACCGCGGCCAACACGCGCTCGTCGTCGTCGATGACCTGACAA
AGCATGCGGCGACGCACCGCGAGCTCGCGCTGCTCACGCGCGAGCCGCCCGGCCGCGAGGCGTATCCGGGCGACATCTTCTACGTGCACGCGCGCCTG
CTCGAACGCGCGGCGAAGCTGTCGGCGGCGCTCGGCGGCGGATCGCTGTCCGCGCTGCCGATCGCGGAGACCGATGCGGGCAACCTCGCCGCCTACAT
TCCGACGAACCTGATTTCGATCACCGACGGGCAGATCGTGCTCGATTCGGCGCTGTTCGCCGCGAACCAGCGGCCGGCCGTCGACGTCGGGCTGAGCG
TGAGCCGCGTCGGCGGCAAGGCGCAGCATCCGGCGCTGCGCGCCGCGTCGGGCCGCCTGCGGCTCGACTATGCGCAGTTCCTCGAGCTGGAGGCGTTC
ACGCGCTTCGGCGGGCTCACGGACGCGCGGCTGCGCGCGCAGATCACGCGCGGCGAGCGCATTCGCGCGTTGATCACGCAGCCGCGCTTTCGCGCGCT
GCGCACGCTCGACGAAGTGGTGCTGCTCAAGGCGCTCGCGGCGGGCGCGCTCGATGCGATGTCGCCGGATCTCGTCGCGCCGCTGCGCGAGCGCTTGC
CTGCGTGGCTCGATGCGCGGATCGCGGCGCTCACGCCGGCGCTTGCGCCGCCGCGCGACTGGCTTGCGGACGATGCGGCGCTCGACGCGCTCGCGGAA
TCGGTCGGCGAGCTGATCGAGCGGATCGCCGCGGACGCCGCGCGTCGCGCGACGGCGGGCATGCCGGCGGAGGACGCGGCGGGCGACATCGGCGGCGC
GTTCGGCGGCGAGCAGGCGCGCGGCGATGCGGATCGTGATGCGGATCATGGCGCGAATCGCGAGGTCAGTCGCGAGGTCAGTCCCGAGGCGAGTCGCG
AAGTGAGCCGTGAAGTGAGCTGTGAAGTGAGCCACGAGGCCGATCGAGACGCGGCCGCCGATGCGGCGCGCGTCGCCGGTCGGGCGCCCGGGCGCGCC
GAGCCGGATCGCGCGGCCCCACGCGCGATGCCCGACGGGCCGCCGCGCGCGCAGGCCGACGGCGATCGCGCATCGGCGTCTCGGCCGCGGCCCGATGC
GCGCGGCGACGCGGCGCGCACCGCACCGTCTCCGCAAGGCGGTGCCGACGCCAACGTCGATGCCGAAGCCGAAGCGAGGCACAAGCGATGAGCGACAA
GCTCGCCGCGATCGAGGCGCGCACCGATACCGCTCGTCAACTGCAGACCGTGATCGGTGCGATGCAGGGCGTGGCCGCCGCGCGCGCGCACGAGGCGC
AGCAGCGTTTGCCGGGCATTCGCGCGTCGGCGGCCACCGTCGGCGCGGCGATCGGCGACGCGCTGTCGGCCGGCGCGCGTTCGGGCGAAACGGCGGCC
GGCGCGCGCGCCGCGCCGCGCGCGCGGCTCGTCGTCGTGCTGTGCAGCGAGCAAGGTTTCGTCGGCGCATACAACGCGCAACTGATCGAGCACGCGAC
GCGGCCCGGGCCGAGCGTGTCGCGCGAGTACATGATGGTCGGCTCGCGCGGCGCGATGCTCGCCGACGCGGGCGGCGTGCCGCTCGTCTGGCGCACGC
CGATGGCGGCGCGCGCGGACGACGTCGTGCATCTCGCGAACCGGATCACCGATGCACTGTACGCGCATCTCGCGAAGCGCGGCGCGCAGCCGGTATCG
ATCGTGCATGCGATGCCGGGGGGCGCGGCGCGGCTCGAGGTGACCGAGCGCCGGCTGCTGCCGTTCGACTATGCGCGCTTCGATACCGCGCCGCGCGC
GCAGCCGCCGCTCGTGCATCTGCCGCCCGCGACGCTGCTCGCGGAGCTCGCGCAGGCCTACGTGTTCGTCGAGCTGTGCGAGGCGGCGATGCTCGCGT
TCGCCGCGGAAAACGAGGCGCGCACGCGCGCGATGATCGCCGCGCGCGAATCGGTCGAGCGCGCGCTCGGCGATCTGCTGCAGGCGTACCGGATCGCG
CGGCAGGACGAGATCACGGCGGATATCGTCGAGCTGGCCGCGAGCGGACTATGAAACCGGGCGCATCGAAGCGGCGGTGCGGCGGTGCGCCGCGCGGC
GCGCCGAATCGCGTGCACGAATCGCGCGCCGCTTCGCATGCGGTTTCGCCGCGGACGCGCGGATCGTCAACGCAATCGCGCCTCGCGCCGGGCGCGGT
TGACGCACGTCAACGCCGGGCG

Figure 91. Sequence of the *B. pseudomallei* N-*atp* operon.

The coding region (yellow) as well as the start (green) and stop (red) codons are indicated. Overlapping nucleotides are marked in purple.

	density	reference
protein	1.36 g/ml	(Schmidt-Krey & Rubinstein, 2011)
Amphipol A8-35	1.24 g/ml	(Gohon *et al*, 2004)
n-Dodecyl-ß-D-maltoside (DDM)	1.19 g/ml	(Schmidt-Krey & Rubinstein, 2011)
Lauryldimethylamine-N-Oxide (LDAO)	0.88 g/ml	(Schmidt-Krey & Rubinstein, 2011)

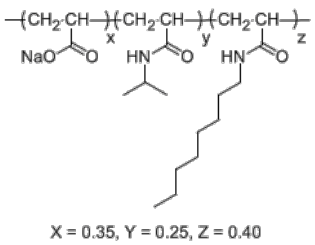

Amphipol A8-35

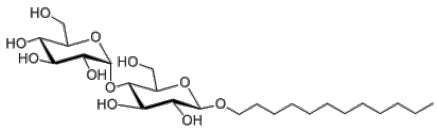

DDM

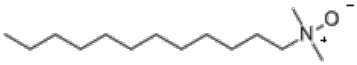

LDAO

Figure 92. The densities and chemical structures of the amphipol and detergent molecules used for structural analysis of the *B. pseudomallei* c-ring by single-particle cryo-EM.

The densities of the different amphiphatic molecules (Amphipol A8-35, DDM and LDAO) as well as their chemical structures are given.

7 References

Abrahams JP, Leslie AG, Lutter R, Walker JE (1994) Structure at 2.8 A resolution of F1-ATPase from bovine heart mitochondria. *Nature* **370:** 621-628

Agarwal N, Kalra VK (1983) Purification and functional properties of the DCCD-reactive proteolipid-subunit of the H+-translocating ATPase from Mycobacterium phlei. *Biochimica et biophysica acta* **723:** 150-159

Aksimentiev A, Balabin IA, Fillingame RH, Schulten K (2004) Insights into the molecular mechanism of rotation in the Fo sector of ATP synthase. *Biophysical journal* **86:** 1332-1344

Allegretti M, Klusch N, Mills DJ, Vonck J, Kuhlbrandt W, Davies KM (2015) Horizontal membrane-intrinsic alpha-helices in the stator a-subunit of an F-type ATP synthase. *Nature* **521:** 237-240

Althoff T, Mills DJ, Popot JL, Kuhlbrandt W (2011) Arrangement of electron transport chain components in bovine mitochondrial supercomplex I1III2IV1. *The EMBO journal* **30:** 4652-4664

Angevine CM, Fillingame RH (2003) Aqueous access channels in-subunit a of rotary ATP synthase. *The Journal of biological chemistry* **278:** 6066-6074

Angevine CM, Herold KA, Vincent OD, Fillingame RH (2007) Aqueous access pathways in ATP synthase-subunit a. Reactivity of cysteine substituted into transmembrane helices 1, 3, and 5. *The Journal of biological chemistry* **282:** 9001-9007

Arechaga I, Butler PJ, Walker JE (2002) Self-assembly of ATP synthase-subunit c rings. *FEBS letters* **515:** 189-193

Baker D, Sali A (2001) Protein structure prediction and structural genomics. *Science* **294:** 93-96

Baradaran R, Berrisford JM, Minhas GS, Sazanov LA (2013) Crystal structure of the entire respiratory complex I. *Nature* **494:** 443-448

Baross JA, Hoffmann SE (1985) Submarine hydrothermal vents and associated environments as sites for the orign and evolution of life. *Origins of Life* **15:** 327-345

Beatrix B, Bendrat K, Rospert S, Buckel W (1990) The biotin-dependent sodium ion-pump glutaconyl-CoA decarboxylase from Fusobacterium nucleatum (subsp. nucleatum). Comparison with the glutaconyl-CoA decarboxylases from gram-positive bacteria. *Arch Microbiol* **154:** 362-369

Becher B, Muller V (1994) Delta mu Na+ drives the synthesis of ATP via an delta mu Na(+)-translocating F1F0-ATP synthase in membrane vesicles of the archaeon Methanosarcina mazei Go1. *Journal of bacteriology* **176:** 2543-2550

Boiangiu CD, Jayamani E, Brugel D, Herrmann G, Kim J, Forzi L, Hedderich R, Vgenopoulou I, Pierik AJ, Steuber J, Buckel W (2005) Sodium ion-pumps and hydrogen production in glutamate fermenting anaerobic bacteria. *J Mol Microbiol Biotechnol* **10:** 105-119

Bolstadt AI, Jensen HB, Bakken V (1996) Taxonomy, Biology and Periodontal Aspects of Fusobacterium nucleatum. *Clin Microbiol Rev* **9:** 55-71

Bolstadt AI, Kleivdal H, Jensen HB (1994) Similarities between Fusobacterium nucleatum and Bacteroides fragilis studied by two DNA probes dervied from Fusobacterium nucleatum. *Scand J Dent Res* **102:** 5-9

Booy F, Elena O (2006) Cryomicroscopy. *Chemical Biology***:** 11-28

Bottcher B, Schwarz L, Graber P (1998) Direct indication for the existence of a double stalk in CF0F1. *Journal of molecular biology* **281:** 757-762

Boyer PD (1975) A model for conformational coupling of membrane potential and proton translocation to ATP synthesis and to active transport. *FEBS letters* **58:** 1-6

Boyer PD (1993) The binding change mechanism for ATP synthase--some probabilities and possibilities. *Biochimica et biophysica acta* **1140:** 215-250

Boyer PD, Cross RL, Momsen W (1973) A new concept for energy coupling in oxidative phosphorylation based on a molecular explanation of the oxygen exchange reactions. *Proceedings of the National Academy of Sciences of the United States of America* **70:** 2837-2839

Branden CI, Jones TA (1990) Between objectivity and subjectivity. *Nature* **343:** 687-689

Brett PJ, DeShazer D, Woods DE (1998) Burkholderia thailandensis sp. nov., a Burkholderia pseudomallei-like species. *International journal of systematic bacteriology* **48 Pt 1:** 317-320

Brodie AF, Gray CT (1956) Phosphorylation coupled to oxidation in bacterial extracts. *The Journal of biological chemistry* **219:** 853-862

Brunger AT (1992) Free R value: a novel statistical quantity for assessing the accuracy of crystal structures. *Nature* **355:** 472-475

Buckel W (2001) Unusual enzymes involved in five pathways of glutamate fermentation. *Applied microbiology and biotechnology* **57:** 263-273

Buckel W, Barker HA (1974) Two pathways of glutamate fermentation by anaerobic bacteria. *Journal of bacteriology* **117:** 1248-1260

Bushby SRM, Hitchings GH (1967) Trimethoprim, a sulphonamide potentiator. *Br J Pharmac Chemother* **33:** 72-90

Bustin SA (2000a) Absolute quantification of mRNA using real-time reverse transcription polymerase chain reaction assays. *Journal of molecular endocrinology* **25:** 169-193

Bustin SA (2000b) Absolute quantification of mRNA using real-time reverse transcription polymerase chain reaction assays. *J Mol Endocrinol* **25:** 169-193

Cain BD (2000) Mutagenic analysis of the F0 stator-subunits. *Journal of bioenergetics and biomembranes* **32:** 365-371

Cain BD, Simoni RD (1986) Impaired proton conductivity resulting from mutations in the a-subunit of F1F0 ATPase in Escherichia coli. *The Journal of biological chemistry* **261:** 10043-10050

Cain BD, Simoni RD (1988) Interaction between Glu-219 and His-245 within the a-subunit of F1F0-ATPase in Escherichia coli. *The Journal of biological chemistry* **263:** 6606-6612

Cain BD, Simoni RD (1989) Proton translocation by the F1F0ATPase of Escherichia coli. Mutagenic analysis of the a-subunit. *The Journal of biological chemistry* **264:** 3292-3300

Capaldi RA, Schulenberg B, Murray J, Aggeler R (2000) Cross-linking and electron microscopy studies of the structure and functioning of the Escherichia coli ATP synthase. *The Journal of experimental biology* **203:** 29-33

Carmeli C, Lifshitz Y (1972) Effects of P 1 and ADP on ATPase activity in chloroplasts. *Biochimica et biophysica acta* **267:** 86-95

Chaowagul W, White NJ, Dance DA, Wattanagoon Y, Naigowit P, Davis TM, Looareesuwan S, Pitakwatchara N (1989) Melioidosis: a major cause of community-acquired septicemia in northeastern Thailand. *The Journal of infectious diseases* **159:** 890-899

Cheng AC (2010) Melioidosis: advances in diagnosis and treatment. *Current opinion in infectious diseases* **23:** 554-559

Cheng AC, Dance DA, Currie BJ (2005) Bioterrorism, Glanders and melioidosis. *Euro surveillance : bulletin Europeen sur les maladies transmissibles = European communicable disease bulletin* **10:** E1-2; author reply E1-2

Chew J, Zilm PS, Fuss JM, Gully NJ (2012) A proteomic investigation of Fusobacterium nucleatum alkaline-induced biofilms. *BMC microbiology* **12:** 189

Choi KH, Kumar A, Schweizer HP (2006) A 10-min method for preparation of highly electrocompetent Pseudomonas aeruginosa cells: application for DNA fragment transfer between chromosomes and plasmid transformation. *Journal of microbiological methods* **64:** 391-397

Choi KH, Mima T, Casart Y, Rholl D, Kumar A, Beacham IR, Schweizer HP (2008) Genetic tools for select-agent-compliant manipulation of Burkholderia pseudomallei. *Applied and environmental microbiology* **74:** 1064-1075

Coenye T, Vandamme P (2003) Diversity and significance of Burkholderia species occupying diverse ecological niches. *Environmental microbiology* **5:** 719-729

Conover TE, Prairie RL, Racker E (1963) Partial Resolution of the Enzymes Catalyzing Oxidative Phosphorylation. Iii. A New Coupling Factor Required by Submitochondrial Particles Extracted with Phosphatides. *The Journal of biological chemistry* **238:** 2831-2837

Cook GM, Keis S, Morgan HW, von Ballmoos C, Matthey U, Kaim G, Dimroth P (2003) Purification and Biochemical Characterization of the F1Fo-ATP Synthase from Thermoalkaliphilic Bacillus sp. Strain TA2.A1. *Journal of bacteriology* **185:** 4442-4449

Cross RL, Nalin CM (1982) Adenine nucleotide binding sites on beef heart F1-ATPase. Evidence for three exchangeable sites that are distinct from three noncatalytic sites. *The Journal of biological chemistry* **257:** 2874-2881

Dance DA, Wuthiekanun V, Chaowagul W, White NJ (1989) The antimicrobial susceptibility of Pseudomonas pseudomallei. Emergence of resistance in vitro and during treatment. *The Journal of antimicrobial chemotherapy* **24:** 295-309

Dashper SG, Reynolds EC (1992) pH regulation by Streptococcus mutans. *Journal of dental research* **71:** 1159-1165

Deckers-Hebestreit G, Altendorf K (1996) The F0F1-type ATP synthases of bacteria: structure and function of the F0 complex. *Annual review of microbiology* **50:** 791-824

Deckers-Hebestreit G, Greie J, Stalz W, Altendorf K (2000) The ATP synthase of Escherichia coli: structure and function of F(0)-subunits. *Biochimica et biophysica acta* **1458:** 364-373

Del Rizzo P, Bi J, Dunn S, BShilton B (2002) The "Second Stalk" of Escherichia coli ATP Synthase: Structure of the isolated Dimerization Domain. *Biochemistry* **41:** 6875-6884

Del Rizzo PA, Bi Y, Dunn SD (2006) ATP synthase b-subunit dimerization domain: a right-handed coiled coil with offset helices. *Journal of molecular biology* **364:** 735-746

DeLano WL (2002) The PyMol Molecular Graphics System (DeLano Scientific, San Carlos, CA).

Dibrova DV, Galperin MY, Mulkidjanian AY (2010) Characterization of the N-ATPase, a distinct, laterally transferred Na+-translocating form of the bacterial F-type membrane ATPase. *Bioinformatics* **26:** 1473-1476

Diez M, Zimmermann B, Borsch M, Konig M, Schweinberger E, Steigmiller S, Reuter R, Felekyan S, Kudryavtsev V, Seidel CA, Graber P (2004) Proton-powered-subunit rotation in single membrane-bound F0F1-ATP synthase. *Nature structural & molecular biology* **11:** 135-141

Dimroth P, von Ballmoos C, Meier T (2006) Catalytic and mechanical cycles in F-ATP synthases. Fourth in the Cycles Review Series. *EMBO reports* **7:** 276-282

Dmitriev O, Jones PC, Jiang W, Fillingame RH (1999) Structure of the Membrane Domain of-subunit b of the Escherichia coli F0F1 ATP Synthase. *Journal of Biological Chemistry* **274:** 15598-15604

Dong X, Stothard P, Forsythe IJ, Wishart DS (2004) PlasMapper: a web server for drawing and auto-annotating plasmid maps. *Nucleic acids research* **32:** W660-664

Duncan TM, Zhou Y, Bulygin VV, Hutcheon ML, Cross RL (1995) Probing interactions of the Escherichia coli F0F1 ATP synthase beta and gamma-subunits with disulphide cross-links. *Biochemical Society transactions* **23:** 736-741

Dunn SD (1992) The polar domain of the b-subunit of Escherichia coli F1F0-ATPase forms an elongated dimer that interacts with the F1 sector. *The Journal of biological chemistry* **267:** 7630-7636

Dunn SD, Chandler J (1998) Characterization of a b2delta complex from Escherichia coli ATP synthase. *The Journal of biological chemistry* **273:** 8646-8651

Dunn SD, Kellner E, Lill H (2001) Specific heterodimer formation by the cytoplasmic domains of the b and b'-subunits of cyanobacterial ATP synthase. *Biochemistry* **40:** 187-192

Dzink JL, Socransky SS, Haffajee AD (1988) The predominant cultivable microbiota of active and inactive lesions of destructive periodontal diseases. *Journal of clinical periodontology* **15:** 316-323

Dzink JL, Tanner AC, Haffajee AD, Socransky SS (1985) Gram negative species associated with active destructive periodontal lesions. *Journal of clinical periodontology* **12:** 648-659

Eickhoff TC, Bennett JV, Hayes PS, Feeley J (1970) Pseudomonas pseudomallei: susceptibility to chemotherapeutic agents. *The Journal of infectious diseases* **121:** 95-102

Emsley P, Cowtan K (2004) Coot: model-building tools for molecular graphics. *Acta crystallographica Section D, Biological crystallography* **60:** 2126-2132

Eya S, Maeda M, Futai M (1991) Role of the carboxyl terminal region of H(+)-ATPase (F0F1) a-subunit from Escherichia coli. *Archives of biochemistry and biophysics* **284:** 71-77

Feniouk BA, Suzuki T, Yoshida M (2007) Regulatory interplay between proton motive force, ADP, phosphate, and-subunit epsilon in bacterial ATP synthase. *The Journal of biological chemistry* **282:** 764-772

Feniouk BA, Yoshida M (2008) Regulatory mechanisms of proton-translocating F(O)F (1)-ATP synthase. *Results and problems in cell differentiation* **45:** 279-308

Fillingame RH, Jones PC, Jiang W, Valiyaveetil FI, Dmitriev OY (1998)-subunit organization and structure in the F0 sector of Escherichia coli F1F0 ATP synthase. *Biochimica et biophysica acta* **1365:** 135-142

Fritz M, Klyszejko AL, Morgner N, Vonck J, Brutschy B, Muller DJ, Meier T, Muller V (2008) An intermediate step in the evolution of ATPases: a hybrid F(0)-V(0) rotor in a bacterial Na(+) F(1)F(0) ATP synthase. *The FEBS journal* **275:** 1999-2007

Fujisaki H, Ito H, Hirata Y, Tanaka M, Hata M, Lin M, Adachi S, Akimoto H, Marumo F, Hiroe M (1995) Natriuretic peptides inhibit angiotensin II-induced proliferation of rat cardiac fibroblasts by blocking endothelin-1 gene expression. *The Journal of clinical investigation* **96:** 1059-1065

Gay NJ, Walker JE (1981a) The atp operon: nucleotide sequence of the promoter and the genes for the membrane proteins, and the delta-subunit of Escherichia coli ATP-synthase. *Nucleic acids research* **9:** 3919-3926

Gay NJ, Walker JE (1981b) The atp operon: nucleotide sequence of the region encoding the alpha-subunit of Escherichia coli ATP-synthase. *Nucleic acids research* **9:** 2187-2194

Gharbia SE, Shah HN (1988) Characteristics of glutamate dehydrogenase, a new diagnostic marker for the genus Fusobacterium. *Journal of general microbiology* **134:** 327-332

Gharbia SE, Shah HN (1991) Pathways of glutamate catabolism among Fusobacterium species. *Journal of general microbiology* **137:** 1201-1206

Giraud MF, Velours J (1997) The absence of the mitochondrial ATP synthase delta-subunit promotes a slow growth phenotype of rho- yeast cells by a lack of assembly of the catalytic sector F1. *European journal of biochemistry / FEBS* **245:** 813-818

Girvin ME, Rastogi VK, Abildgaard F, Markley JL, Fillingame RH (1998) Solution structure of the transmembrane H+-transporting-subunit c of the F1F0 ATP synthase. *Biochemistry* **37:** 8817-8824

Glockner FO, Kube M, Bauer M, Teeling H, Lombardot T, Ludwig W, Gade D, Beck A, Borzym K, Heitmann K, Rabus R, Schlesner H, Amann R, Reinhardt R (2003) Complete genome sequence of the marine planctomycete Pirellula sp. strain 1.

Proceedings of the National Academy of Sciences of the United States of America **100:** 8298-8303

Gohon Y, Pavlov G, Timmins P, Tribet C, Popot JL, Ebel C (2004) Partial specific volume and solvent interactions of amphipol A8-35. *Anal Biochem* **334:** 318-334

Gregoret LM, Rader SD, Fletterick RJ, Cohen FE (1991) Hydrogen bonds involving sulfur atoms in proteins. *Proteins* **9:** 99-107

Haagsma AC, Driessen NN, Hahn MM, Lill H, Bald D (2010) ATP synthase in slow- and fast-growing mycobacteria is active in ATP synthesis and blocked in ATP hydrolysis direction. *FEMS microbiology letters* **313:** 68-74

Haffajee AD, Socransky SS, Dzink JL, Taubman MA, Ebersole JL (1988) Clinical, microbiological and immunological features of subjects with refractory periodontal diseases. *Journal of clinical periodontology* **15:** 390-398

Hakulinen JK, Klyszejko AL, Hoffmann J, Eckhardt-Strelau L, Brutschy B, Vonck J, Meier T (2012) Structural study on the architecture of the bacterial ATP synthase Fo motor. *Proceedings of the National Academy of Sciences of the United States of America* **109:** E2050-2056

Hara KY, Kato-Yamada Y, Kikuchi Y, Hisabori T, Yoshida M (2001) The role of the betaDELSEED motif of F1-ATPase: propagation of the inhibitory effect of the epsilon-subunit. *The Journal of biological chemistry* **276:** 23969-23973

Haraga A, West TE, Brittnacher MJ, Skerrett SJ, Miller SI (2008) Burkholderia thailandensis as a model system for the study of the virulence-associated type III secretion system of Burkholderia pseudomallei. *Infection and immunity* **76:** 5402-5411

Hartzog PE, Cain BD (1994) Second-site suppressor mutations at glycine 218 and histidine 245 in the alpha-subunit of F1F0 ATP synthase in Escherichia coli. *The Journal of biological chemistry* **269:** 32313-32317

Hatch LP, Cox GB, Howitt SM (1995) The essential arginine residue at position 210 in the alpha-subunit of the Escherichia coli ATP synthase can be transferred to position 252 with partial retention of activity. *The Journal of biological chemistry* **270:** 29407-29412

Hausrath AC, Capaldi RA, Matthews BW (2001) The conformation of the epsilon-and gamma-subunits within the Escherichia coli F(1) ATPase. *The Journal of biological chemistry* **276:** 47227-47232

Hensel M, Deckers-Hebestreit G, Altendorf K (1991) Purification and characterization of the F1 portion of the ATP synthase (F1Fo) of Streptomyces lividans. *European journal of biochemistry / FEBS* **202:** 1313-1319

Hicks DB, Liu J, Fujisawa M, Krulwich TA (2010) F1F0-ATP synthases of alkaliphilic bacteria: lessons from their adaptations. *Biochimica et biophysica acta* **1797:** 1362-1377

Hofstadt T (1981) The procaryotes. A handbook on habitats, isolation and identification of bacteria. The genus Fusobacterium. *Springer Verlag, New York***:** 1464-1467

Holden MT, Titball RW, Peacock SJ, Cerdeno-Tarraga AM, Atkins T, Crossman LC, Pitt T, Churcher C, Mungall K, Bentley SD, Sebaihia M, Thomson NR, Bason N, Beacham IR, Brooks K, Brown KA, Brown NF, Challis GL, Cherevach I, Chillingworth T, Cronin A, Crossett B, Davis P, DeShazer D, Feltwell T, Fraser A, Hance Z, Hauser H, Holroyd S, Jagels K, Keith KE, Maddison M, Moule S, Price C, Quail MA, Rabbinowitsch E, Rutherford K, Sanders M, Simmonds M, Songsivilai S, Stevens K, Tumapa S, Vesaratchavest M, Whitehead S, Yeats C, Barrell BG, Oyston PC, Parkhill J (2004) Genomic plasticity of the causative agent of melioidosis, Burkholderia pseudomallei. *Proceedings of the National Academy of Sciences of the United States of America* **101:** 14240-14245

Hoppe J, Schairer HU, Sebald W (1980) The proteolipid of a mutant ATPase from Escherichia coli defective in H+-conduction contains a glycine instead of the carbodiimide-reactive aspartyl residue. *FEBS letters* **109:** 107-111

Hoppe J, Sebald W (1980) Amino acid sequence of the proteolipid-subunit of the proton-translocating ATPase complex from the thermophilic bacterium PS-3. *Eur J Biochem* **107:** 57-65

Howitt SM, Lightowlers RN, Gibson F, Cox GB (1990) Mutational analysis of the function of the a-subunit of the F0F1-APPase of Escherichia coli. *Biochimica et biophysica acta* **1015:** 264-268

Howitt SM, Rodgers AJ, Hatch LP, Gibson F, Cox GB (1996) The coupling of the relative movement of the a and c-subunits of the F0 to the conformational changes in the F1-ATPase. *Journal of bioenergetics and biomembranes* **28:** 415-420

Hunte C, Koepke J, Lange C, Roßmanith T, Michel H (2000) Structure at 2.3 A resolution of the cytochrome bc1 complex from the yeast Saccharomyces cerevisiae co-crystallized with an antibody Fv fragment. *Cell* **8:** 669-684

Ishmukhametov RR, Galkin MA, Vik SB (2005) Ultrafast purification and reconstitution of His-tagged cysteine-less Escherichia coli F1Fo ATP synthase. *Biochimica et biophysica acta* **1706:** 110-116

Itoh H, Takahashi A, Adachi K, Noji H, Yasuda R, Yoshida M, Kinosita K (2004) Mechanically driven ATP synthesis by F1-ATPase. *Nature* **427:** 465-468

Jabbar Z, Currie BJ (2013) Melioidosis and the kidney. *Nephrology* **18:** 169-175

Jager H, Birkenhager R, Stalz WD, Altendorf K, Deckers-Hebestreit G (1998) Topology of-subunit a of the Escherichia coli ATP synthase. *European journal of biochemistry / FEBS* **251:** 122-132

Jones PC (2001) Introduction of a carboxyl group in the first transmembrane helix of Escherichia coli F1Fo ATPase-subunit c and cytoplasmic pH regulation. *Journal of bacteriology* **183:** 1524-1530

Jounouchi M, Takeyama M, Chaiprasert P, Noumi T, Moriyama Y, Maeda M, Futai M (1992) Escherichia coli H(+)-ATPase: role of the delta-subunit in binding Fl to the Fo sector. *Archives of biochemistry and biophysics* **292:** 376-381

Junge W, Lill H, Engelbrecht S (1997) ATP synthase: an electrochemical transducer with rotatory mechanics. *Trends in biochemical sciences* **22:** 420-423

Kabsch W (1993) Automatic processing of rotation diffraction data from crystals of initially unknown symmetry and cell constants. *Journal of Applied Crystallography* **26:** 795-800

Kagawa Y, Racker E (1966) Partial resolution of the enzymes catalyzing oxidative phosphorylation. 8. Properties of a factor conferring oligomycin sensitivity on mitochondrial adenosine triphosphatase. *The Journal of biological chemistry* **241:** 2461-2466

Kaim G, Dimroth P (1999) ATP synthesis by F-type ATP synthase is obligatorily dependent on the transmembrane voltage. *The EMBO journal* **18:** 4118-4127

Kaim G, Wehrle F, Gerike U, Dimroth P (1997) Molecular basis for the coupling ion selectivity of F1F0 ATP synthases: probing the liganding groups for Na+ and Li+ in the c-subunit of the ATP synthase from Propionigenium modestum. *Biochemistry* **36:** 9185-9194

Kanazawa H, Kayano T, Mabuchi K, Futai M (1981a) Nucleotide sequence of the genes coding for alpha, beta and gamma-subunits of the proton-translocating ATPase of Escherichia coli. *Biochemical and biophysical research communications* **103:** 604-612

Kanazawa H, Mabuchi K, Kayano T, Noumi T, Sekiya T, Futai M (1981b) Nucleotide sequence of the genes for F0 components of the proton-translocating ATPase from Escherichia coli: prediction of the primary structure of F0-subunits. *Biochemical and biophysical research communications* **103:** 613-620

Kim HS, Schell MA, Yu Y, Ulrich RL, Sarria SH, Nierman WC, DeShazer D (2005) Bacterial genome adaptation to niches: divergence of the potential virulence genes in three Burkholderia species of different survival strategies. *BMC genomics* **6:** 174

Kleywegt GJ, Jones TA (1995) Where freedom is given, liberties are taken. *Structure* **3:** 535-540

Kleywegt GJ, Jones TA (1996) Phi/psi-chology: Ramachandran revisited. *Structure* **4:** 1395-1400

Klionsky DJ, Brusilow WS, Simoni RD (1984) In vivo evidence for the role of the epsilon-subunit as an inhibitor of the proton-translocating ATPase of Escherichia coli. *Journal of bacteriology* **160:** 1055-1060

Kluge C, Dimroth P (1993) Specific protection by Na+ or Li+ of the F1F0-ATPase of Propionigenium modestum from the reaction with dicyclohexylcarbodiimide. *The Journal of biological chemistry* **268:** 14557-14560

Knorr M (1922) Über die fusospirilläre Symbiose, die Gattung Fusobacterium (K. B. Lehmann) und Spirillium sputigenum. (Zugleich ein Beitrag zur Bakteriologie der Mundhöhle). I. Mitteilung: die Epidemiologie der fusospirillären Symbiose, besonders der Plaut-Vincentschen Angina. *Zentralbl Bakteriol Parasitenkd Infektionskkr Hyg Abt 1 Orig* **87:** 436-545

Kramer DM, Crofts AR (1989) Activation of the chloroplast ATPase measured by electrochromic change in leaves of intact plants. *Biochimica et biophysica acta* **967:** 28-41

Kuki M, Noumi T, Maeda M, Amemura A, Futai M (1988) Functional domains of epsilon-subunit of Escherichia coli H+-ATPase (F0F1). *The Journal of biological chemistry* **263:** 17437-17442

Lane N, Allen JF, Martin W (2010) How did LUCA make a living? Chemiosmosis in the origin of life. *BioEssays : news and reviews in molecular, cellular and developmental biology* **32:** 271-280

Lane N, Martin WF (2012) The origin of membrane bioenergetics. *Cell* **151:** 1406-1416

Langen P, Hucho F (2008) Karl Lohmann and the discovery of ATP. *Angewandte Chemie* **47:** 1824-1827

Lau WC, Rubinstein JL (2012) Subnanometre-resolution structure of the intact Thermus thermophilus H+-driven ATP synthase. *Nature* **481:** 214-218

Laubinger W, Dimroth P (1987) Characterization of the Na+-stimulated ATPase of Propionigenium modestum as an enzyme of the F1F0 type. *European journal of biochemistry / FEBS* **168:** 475-480

Laubinger W, Dimroth P (1988) Characterization of the ATP synthase of Propionigenium modestum as a primary sodium pump. *Biochemistry* **27:** 7531-7537

Lee LK, Stewart AG, Donohoe M, Bernal RA, Stock D (2010) The structure of the peripheral stalk of Thermus thermophilus H+-ATPase/synthase. *Nature structural & molecular biology* **17:** 373-378

Leelarasamee A, Bovornkitti S (1989) Melioidosis: review and update. *Reviews of infectious diseases* **11:** 413-425

Li X, Mooney P, Zheng S, Booth CR, Braunfeld MB, Gubbens S, Agard DA, Cheng Y (2013) Electron counting and beam-induced motion correction enable near-atomic-resolution single-particle cryo-EM. *Nat Methods* **10:** 584-590

Liao M, Cao E, Julius D, Cheng Y (2013) Structure of the TRPV1 ion channel determined by electron cryo-microscopy. *Nature* **504:** 107-112

Lightowlers RN, Howitt SM, Hatch L, Gibson F, Cox G (1988) The proton pore in the Escherichia coli F0F1-ATPase: substitution of glutamate by glutamine at position 219 of the alpha-subunit prevents F0-mediated proton permeability. *Biochimica et biophysica acta* **933:** 241-248

Lightowlers RN, Howitt SM, Hatch L, Gibson F, Cox GB (1987) The proton pore in the Escherichia coli F0F1-ATPase: a requirement for arginine at position 210 of the a-subunit. *Biochimica et biophysica acta* **894:** 399-406

Lipman F (1941) Metabolic generation and utilization of phosphate bond energy. *Adv Enzymol* **1:** 99-162

Liu J, Fackelmayer OJ, Hicks DB, Preiss L, Meier T, Sobie EA, Krulwich TA (2011) Mutations in a helix-1 motif of the ATP synthase c-subunit of Bacillus pseudofirmus OF4 cause functional deficits and changes in the c-ring stability and mobility on sodium dodecyl sulfate-polyacrylamide gel electrophoresis. *Biochemistry* **50:** 5497-5506

Long JC, Wang S, Vik SB (1998) Membrane Topology of-subunit a of the F1F0 ATP Synthase as Determined by Labeling of Unique Cysteine Residues. *Journal of Biological Chemistry* **273:** 16235-16240

Lu P, Bai XC, Ma D, Xie T, Yan C, Sun L, Yang G, Zhao Y, Zhou R, Scheres SH, Shi Y (2014) Three-dimensional structure of human gamma-secretase. *Nature* **512:** 166-170

Ludtke SJ, Baldwin PR, Chiu W (1999) EMAN: semiautomated software for high-resolution single-particle reconstructions. *J Struct Biol* **128:** 82-97

MacKenzie KR, Prestegard JH, Engelman DM (1997) A transmembrane helix dimer: structure and implications. *Science* **276:** 131-133

Matthies D, Preiss L, Klyszejko AL, Muller DJ, Cook GM, Vonck J, Meier T (2009) The c13 ring from a thermoalkaliphilic ATP synthase reveals an extended diameter due to a special structural region. *J Mol Biol* **388:** 611-618

Matthies D, Zhou W, Klyszejko AL, Anselmi C, Yildiz O, Brandt K, Muller V, Faraldo-Gomez JD, Meier T (2014) High-resolution structure and mechanism of an F/V-hybrid rotor ring in a Na(+)-coupled ATP synthase. *Nature communications* **5:** 5286

McCarn DF, Whitaker RA, Alam J, Vrba JM, Curtis SE (1988) Genes encoding the alpha, gamma, delta, and four F0-subunits of ATP synthase constitute an operon in the cyanobacterium Anabaena sp. strain PCC 7120. *Journal of bacteriology* **170:** 3448-3458

McInerney MJ, Rohlin L, Mouttaki H, Kim U, Krupp RS, Rios-Hernandez L, Sieber J, Struchtemeyer CG, Bhattacharyya A, Campbell JW, Gunsalus RP (2007) The genome of Syntrophus aciditrophicus: life at the thermodynamic limit of microbial growth. *Proceedings of the National Academy of Sciences of the United States of America* **104:** 7600-7605

McLachlin DT, Bestard JA, Dunn SD (1998) The b and delta-subunits of the Escherichia coli ATP synthase interact via residues in their C-terminal regions. *The Journal of biological chemistry* **273:** 15162-15168

McLachlin DT, Dunn SD (1997) Dimerization interactions of the b-subunit of the Escherichia coli F1F0-ATPase. *The Journal of biological chemistry* **272:** 21233-21239

Meier T, Dimroth P (2002) Intersubunit bridging by Na+ ions as a rationale for the unusual stability of the c-rings of Na+-translocating F1F0 ATP synthases. *EMBO reports* **3:** 1094-1098

Meier T, Faraldo-Gòmez JD, Börsch M (2011) Molecular Machines in Biology. ATP Synthase - A Paradigmatic Molecular Machine. *Cambridge University Press* **1st edition:** 208-238

Meier T, Ferguson SA, Cook GM, Dimroth P, Vonck J (2006) Structural investigations of the membrane-embedded rotor ring of the F-ATPase from Clostridium paradoxum. *Journal of bacteriology* **188:** 7759-7764

Meier T, Krah A, Bond PJ, Pogoryelov D, Diederichs K, Faraldo-Gomez JD (2009) Complete ion-coordination structure in the rotor ring of Na+-dependent F-ATP synthases. *J Mol Biol* **391:** 498-507

Meier T, Matthey U, Henzen F, Dimroth P, Muller DJ (2001) The central plug in the reconstituted undecameric c cylinder of a bacterial ATP synthase consists of phospholipids. *FEBS letters* **505:** 353-356

Meier T, Matthey U, von Ballmoos C, Vonck J, Krug von Nidda T, Kuhlbrandt W, Dimroth P (2003) Evidence for structural integrity in the undecameric c-rings isolated from sodium ATP synthases. *Journal of molecular biology* **325:** 389-397

Meier T, Polzer P, Diederichs K, Welte W, Dimroth P (2005) Structure of the rotor ring of F-Type Na+-ATPase from Ilyobacter tartaricus. *Science* **308:** 659-662

Miller OL, Jr., Hamkalo BA, Thomas CA, Jr. (1970) Visualization of bacterial genes in action. *Science* **169:** 392-395

Mindell JA, Grigorieff N (2003) Accurate determination of local defocus and specimen tilt in electron microscopy. *J Struct Biol* **142:** 334-347

Minkov IB, Fitin AF, Vasilyeva EA, Vinogradov AD (1979) Mg2+-induced ADP-dependent inhibition of the ATPase activity of beef heart mitochondrial coupling factor F1. *Biochemical and biophysical research communications* **89:** 1300-1306

Miroux B, Walker JE (1996) Over-production of proteins in Escherichia coli: mutant hosts that allow synthesis of some membrane proteins and globular proteins at high levels. *Journal of molecular biology* **260:** 289-298

Mitchell P (1961) Coupling of phosphorylation to electron and hydrogen transfer by a chemi-osmotic type of mechanism. *Nature* **191:** 144-148

Mitome N, Ono S, Sato H, Suzuki T, Sone N, Yoshida M (2010) Essential arginine residue of the F(o)-a-subunit in F(o)F(1)-ATP synthase has a role to prevent the proton shortcut without c-ring rotation in the F(o) proton channel. *Biochem J* **430:** 171-177

Mizutani K, Yamamoto M, Suzuki K, Yamato I, Kakinuma Y, Shirouzu M, Walker JE, Yokoyama S, Iwata S, Murata T (2011) Structure of the rotor ring modified with N,N'-dicyclohexylcarbodiimide of the Na+-transporting vacuolar ATPase. *Proceedings of the National Academy of Sciences of the United States of America* **108:** 13474-13479

Moore RA, DeShazer D, Reckseidler S, Weissman A, Woods DE (1999) Efflux-mediated aminoglycoside and macrolide resistance in Burkholderia pseudomallei. *Antimicrobial agents and chemotherapy* **43:** 465-470

Moore WE, Holdeman LV, Cato EP, Good IJ, Smith EP, Ranney RR, Palcanis KG (1984a) Variation in periodontal floras. *Infection and immunity* **46:** 720-726

Moore WE, Moore LV (1994) The bacteria of periodontal diseases. *Periodontology 2000* **5:** 66-77

Moore WEC, Haagsma AC, Cato EP, Smibert J, Burmeister JA, Palcanis KG, Ranney RR (1985) Conparative bacteriology of juvenile periodontitis. *Infect Immun* **48:** 507-519

Moore WEC, Holdeman LV, Cato EP, Goog IJ, Smith EP, Rannes RR, Palcanis KG (1984b) Variation in periodontal floras. *Infect Immun* **46:** 720-726

Mulkidjanian AY, Dibrov P, Galperin MY (2008a) The past and present of sodium energetics: may the sodium-motive force be with you. *Biochimica et biophysica acta* **1777:** 985-992

Mulkidjanian AY, Galperin MY, Koonin EV (2009) Co-evolution of primordial membranes and membrane proteins. *Trends in biochemical sciences* **34:** 206-215

Mulkidjanian AY, Galperin MY, Makarova KS, Wolf YI, Koonin EV (2008b) Evolutionary primacy of sodium bioenergetics. *Biology direct* **3:** 13

Mulkidjanian AY, Makarova KS, Galperin MY, Koonin EV (2007) Inventing the dynamo machine: the evolution of the F-type and V-type ATPases. *Nature reviews Microbiology* **5:** 892-899

Muller DJ, Dencher NA, Meier T, Dimroth P, Suda K, Stahlberg H, Engel A, Seelert H, Matthey U (2001) ATP synthase: constrained stoichiometry of the transmembrane rotor. *FEBS letters* **504:** 219-222

Mullis KB, Faloona FA (1987) Specific synthesis of DNA in vitro via a polymerase-catalyzed chain reaction. *Methods in enzymology* **155:** 335-350

Murata T, Yamato I, Kakinuma Y, Leslie AGW, Walker JE (2005) Structure of the rotor of the V-type Na^+-ATPase from Enterococcus hirae. *Science* **308:** 654-659

Murshudov GN, Vagin AA, Dodson EJ (1997) Refinement of macromolecular structures by the maximum-likelihood method. *Acta crystallographica Section D, Biological crystallography* **53:** 240-255

Nakagawa H, Lee SH, Kalra VK, Brodie AF (1977) Trypsin-induced changes in the orientation of latent ATPase in protoplast ghosts from Mycobacterium phlei. *The Journal of biological chemistry* **252:** 8229-8234

Nakamoto RK (1996) Mechanisms of active transport in the FOF1 ATP synthase. *The Journal of membrane biology* **151:** 101-111

Nakanishi-Matsui M, Kashiwagi S, Hosokawa H, Cipriano DJ, Dunn SD, Wada Y, Futai M (2006) Stochastic high-speed rotation of Escherichia coli ATP synthase F1 sector: the epsilon-subunit-sensitive rotation. *The Journal of biological chemistry* **281:** 4126-4131

Nesterenko MV, Tilley M, Upton SJ (1994) A simple modification of Blum's silver stain method allows for 30 minute detection of proteins in polyacrylamide gels. *Journal of biochemical and biophysical methods* **28:** 239-242

Neumann S, Matthey U, Kaim G, Dimroth P (1998) Purification and properties of the F1F0 ATPase of Ilyobacter tartaricus, a sodium ion-pump. *Journal of bacteriology* **180:** 3312-3316

Nielsen J, Hansen FG, Hoppe J, Friedl P, von Meyenburg K (1981) The nucleotide sequence of the atp genes coding for the F0-subunits a, b, c and the F1-subunit delta of the membrane bound ATP synthase of Escherichia coli. *Molecular & general genetics : MGG* **184:** 33-39

Noji H, Yasuda R, Yoshida M, Kinosita K, Jr. (1997) Direct observation of the rotation of F1-ATPase. *Nature* **386:** 299-302

O'Sullivan LA, Mahenthiralingam E (2005) Biotechnological potential within the genus Burkholderia. *Letters in applied microbiology* **41:** 8-11

Oberfeld B (2006) F1Fo ATP synthase: Identification of a plug within the c-ring and heterologous expression of a sodium-translocating enzyme. *PhD thesis***:** ETH Zürich

Oberfeld B, Brunner J, Dimroth P (2006) Phospholipids occupy the internal lumen of the c ring of the ATP synthase of Escherichia coli. *Biochemistry* **45:** 1841-1851

Oot RA, Huang LS, Berry EA, Wilkens S (2012) Crystal structure of the yeast vacuolar ATPase heterotrimeric EGC(head) peripheral stalk complex. *Structure* **20:** 1881-1892

Osborn MJ, Huennekens FM (1958) Enzymatic reduction of dihydrofolic acid. *J Biol Chem* **233:** 969-974

Patrie WJ, McCarty RE (1984) Specific binding of coupling factor 1 lacking the delta and epsilon-subunits to thylakoids. *The Journal of biological chemistry* **259:** 11121-11128

Peacock SJ, Schweizer HP, Dance DA, Smith TL, Gee JE, Wuthiekanun V, DeShazer D, Steinmetz I, Tan P, Currie BJ (2008) Management of accidental laboratory exposure to Burkholderia pseudomallei and B. mallei. *Emerging infectious diseases* **14:** e2

Penefsky H, Pullmann M, Datta A, Racker E (1960) Partial Resolution of the enzymes catalyzing oxidative phosphorylation. *The Journal of biological chemistry* **235:** 3330-3336

Pogoryelov D, Klyszejko AL, Krasnoselska GO, Heller EM, Leone V, Langer JD, Vonck J, Muller DJ, Faraldo-Gomez JD, Meier T (2012) Engineering rotor ring stoichiometries in the ATP synthase. *Proceedings of the National Academy of Sciences of the United States of America* **109:** E1599-1608

Pogoryelov D, Krah A, Langer JD, Yildiz O, Faraldo-Gomez JD, Meier T (2010) Microscopic rotary mechanism of ion translocation in the F(o) complex of ATP synthases. *Nat Chem Biol* **6:** 891-899

Pogoryelov D, Nikolaev Y, Schlattner U, Pervushin K, Dimroth P, Meier T (2008) Probing the rotor-subunit interface of the ATP synthase from Ilyobacter tartaricus. *The FEBS journal* **275:** 4850-4862

Pogoryelov D, Reichen C, Klyszejko AL, Brunisholz R, Muller DJ, Dimroth P, Meier T (2007) The oligomeric state of c rings from cyanobacterial F-ATP synthases varies from 13 to 15. *Journal of bacteriology* **189:** 5895-5902

Pogoryelov D, Yildiz O, Faraldo-Gomez JD, Meier T (2009) High-resolution structure of the rotor ring of a proton-dependent ATP synthase. *Nat Struct Mol Biol* **16:** 1068-1073

Pogoryelov D, Yu J, Meier T, Vonck J, Dimroth P, Muller DJ (2005) The c15 ring of the Spirulina platensis F-ATP synthase: F1/F0 symmetry mismatch is not obligatory. *EMBO reports* **6:** 1040-1044

Preiss L (2013) Structural and functional characterization of the rotor rings from a Bacillus and a Mycobaterium F1Fo ATP synthase. *PhD thesis***:** Max-Planck-Institute of Biophysics, Frankfurt am Main

Preiss L, Klyszejko AL, Hicks DB, Liu J, Fackelmayer OJ, Yildiz O, Krulwich TA, Meier T (2013) The c-ring stoichiometry of ATP synthase is adapted to cell physiological requirements of alkaliphilic Bacillus pseudofirmus OF4. *Proc Natl Acad Sci U S A* **110:** 7874-7879

Preiss L, Yildiz O, Hicks DB, Krulwich TA, Meier T (2010) A new type of proton coordination in an F(1)F(o)-ATP synthase rotor ring. *PLoS Biol* **8:** e1000443

Pullman ME, Monroy GC (1963) A Naturally Occurring Inhibitor of Mitochondrial Adenosine Triphosphatase. *The Journal of biological chemistry* **238:** 3762-3769

Pullman ME, Penefsky HS, Datta A, Racker E (1960) Partial resolution of the enzymes catalyzing oxidative phosphorylation. I. Purification and properties of soluble dinitrophenol-stimulated adenosine triphosphatase. *The Journal of biological chemistry* **235:** 3322-3329

Pullmann M, Penefsky H, Datta A, Racker E (1960) Partial resolution of the enzymes catalyzing oxidative phosphorylation. *The Journal of biological chemistry* **235:** 3322-3329

Qiu D, Damron FH, Mima T, Schweizer HP, Yu HD (2008) PBAD-based shuttle vectors for functional analysis of toxic and highly regulated genes in Pseudomonas and Burkholderia spp. and other bacteria. *Applied and environmental microbiology* **74:** 7422-7426

Ralser M, Querfurth R, Warnatz HJ, Lehrach H, Yaspo ML, Krobitsch S (2006) An efficient and economic enhancer mix for PCR. *Biochemical and biophysical research communications* **347:** 747-751

Rees DM, Leslie AG, Walker JE (2009) The structure of the membrane extrinsic region of bovine ATP synthase. *Proceedings of the National Academy of Sciences of the United States of America* **106:** 21597-21601

Reidlinger J, Muller V (1994) Purification of ATP synthase from Acetobacterium woodii and identification as a Na(+)-translocating F1F0-type enzyme. *European journal of biochemistry / FEBS* **226:** 1079

Richter ML, Patrie WJ, McCarty RE (1984) Preparation of the epsilon-subunit and epsilon-subunit-deficient chloroplast coupling factor 1 in reconstitutively active forms. *The Journal of biological chemistry* **259:** 7371-7373

Robrish SA, Oliver C, Thompson J (1987) Amino acid-dependent transport of sugars by Fusobacterium nucleatum ATCC 10953. *Journal of bacteriology* **169:** 3891-3897

Robrish SA, Thompson J (1990) Regulation of fructose metabolism and polymer synthesis by Fusobacterium nucleatum ATCC 10953. *Journal of bacteriology* **172:** 5714-5723

Rodgers AJ, Capaldi RA (1998) The second stalk composed of the b- and delta-subunits connects F0 to F1 via an alpha-subunit in the Escherichia coli ATP synthase. *The Journal of biological chemistry* **273:** 29406-29410

Rodgers AJ, Wilkens S, Aggeler R, Morris MB, Howitt SM, Capaldi RA (1997) The-subunit delta-subunit b domain of the Escherichia coli F1F0 ATPase. The B-subunits interact with F1 as a dimer and through the delta-subunit. *The Journal of biological chemistry* **272:** 31058-31064

Rodriguez R, Chinea G, Lopez N, Pons T, Vriend G (1998) Homology modeling, model and software evaluation: three related resources. *Bioinformatics* **14:** 523-528

Rogers AH, Zilm PS, Gully NJ, Pfennig AL, Marsh PD (1991) Aspects of the growth and metabolism of Fusobacterium nucleatum ATCC 10953 in continuous culture. *Oral microbiology and immunology* **6:** 250-255

Rondelez Y, Tresset G, Nakashima T, Kato-Yamada Y, Fujita H, Takeuchi S, Noji H (2005) Highly coupled ATP synthesis by F1-ATPase single molecules. *Nature* **433**: 773-777

Sabbert D, Engelbrecht S, Junge W (1996) Intersubunit rotation in active F-ATPase. *Nature* **381:** 623-625

Sambrook J, Fritsch EF, Maniatis T (1989) *Molecular Cloning - A laboratory manual*, 2nd edition edn. New York: Cold Spring Harbor Laboratory Press.

Saraste M, Gay NJ, Eberle A, Runswick MJ, Walker JE (1981) The atp operon: nucleotide sequence of the genes for the gamma, beta, and epsilon-subunits of Escherichia coli ATP synthase. *Nucleic acids research* **9:** 5287-5296

Saroussi S, Schushan M, Ben-Tal N, Junge W, Nelson N (2012) Structure and flexibility of the C-ring in the electromotor of rotary F(0)F(1)-ATPase of pea chloroplasts. *PloS one* **7:** e43045

Saum R, Schlegel K, Meyer B, Muller V (2009) The F1FO ATP synthase genes in Methanosarcina acetivorans are dispensable for growth and ATP synthesis. *FEMS microbiology letters* **300:** 230-236

Sawada K, Watanabe H, Moritani-Otsuka C, Kanazawa H (1997)-subunit interactions of Escherichia coli F1-ATPase: mutants of the gamma-subunits defective in interaction with the epsilon-subunit isolated by the yeast two-hybrid system. *Archives of biochemistry and biophysics* **348:** 183-189

Schagger H, von Jagow G (1987) Tricine-sodium dodecyl sulfate-polyacrylamide gel electrophoresis for the separation of proteins in the range from 1 to 100 kDa. *Analytical biochemistry* **166:** 368-379

Schemidt RA, Hsu DK, Deckers-Hebestreit G, Altendorf K, Brusilow WS (1995) The effects of an atpE ribosome-binding site mutation on the stoichiometry of the c-subunit in the F1F0 ATPase of Escherichia coli. *Archives of biochemistry and biophysics* **323:** 423-428

Schemidt RA, Qu J, Williams JR, Brusilow WS (1998) Effects of carbon source on expression of F0 genes and on the stoichiometry of the c-subunit in the F1F0 ATPase of Escherichia coli. *Journal of bacteriology* **180:** 3205-3208

Scheres SH (2012) A Bayesian view on cryo-EM structure determination. *Journal of molecular biology* **415:** 406-418

Schlegel K, Welte C, Deppenmeier U, Muller V (2012) Electron transport during aceticlastic methanogenesis by Methanosarcina acetivorans involves a sodium-translocating Rnf complex. *The FEBS journal* **279:** 4444-4452

Schmidt-Krey I, Rubinstein JL (2011) Electron cryomicroscopy of membrane proteins: specimen preparation for two-dimensional crystals and single-particles. *Micron* **42:** 107-116

Schulz S (2010) Biochemische Untersuchungen zur Ionenspezifität bakterieller Rotor Ring aus F1Fo ATP-Synthasen. *Diploma thesis***:** Max-Planck-Institute of Biophysics, Frankffurt am Main

Schulz S, Iglesias-Cans M, Krah A, Yildiz O, Leone V, Matthies D, Cook GM, Faraldo-Gomez JD, Meier T (2013) A new type of Na(+)-driven ATP synthase membrane rotor with a two-carboxylate ion-coupling motif. *PLoS Biol* **11:** e1001596

Schulze S, Koster S, Geldmacher U, Terwisscha van Scheltinga AC, Kuhlbrandt W (2010) Structural basis of Na(+)-independent and cooperative substrate/product antiport in CaiT. *Nature* **467:** 233-236

Schwem BE, Fillingame RH (2006) Cross-linking between helices within-subunit a of Escherichia coli ATP synthase defines the transmembrane packing of a four-helix bundle. *The Journal of biological chemistry* **281:** 37861-37867

Sebald W, Machleidt W, Wachter E (1980) N,N'-dicyclohexylcarbodiimide binds specifically to a single glutamyl residue of the proteolipid-subunit of the mitochondrial adenosinetriphosphatases from Neurospora crassa and Saccharomyces cerevisiae. *Proceedings of the National Academy of Sciences of the United States of America* **77:** 785-789

Seelert H, Poetsch A, Dencher NA, Engel A, Stahlberg H, Muller DJ (2000) Structural biology. Proton-powered turbine of a plant motor. *Nature* **405:** 418-419

Shannon RD (1976) Revised effective ionic radii and systematic studies of interatomic distances in halides and chalcogenides. *Acta Crystallogrography* **32:** 751-767

Sheng Z, Knowlton K, Chen J, Hoshijima M, Brown JH, Chien KR (1997) Cardiotrophin 1 (CT-1) inhibition of cardiac myocyte apoptosis via a mitogen-activated protein kinase-dependent pathway. Divergence from downstream CT-1 signals for myocardial cell hypertrophy. *The Journal of biological chemistry* **272:** 5783-5791

Signat B, Roques C, Poulet P, Duffaut D (2011) Fusobacterium nucleatum in periodontal health and disease. *Current issues in molecular biology* **13:** 25-36

Smith MD, Wuthiekanun V, Walsh AL, White NJ (1995) Quantitative recovery of Burkholderia pseudomallei from soil in Thailand. *Transactions of the Royal Society of Tropical Medicine and Hygiene* **89:** 488-490

Socransky SS, Haffajee AD, Cugini MA, Smith C, Kent RL, Jr. (1998) Microbial complexes in subgingival plaque. *Journal of clinical periodontology* **25:** 134-144

Soontharapirakkul K, Promden W, Yamada N, Kageyama H, Incharoensakdi A, Iwamoto-Kihara A, Takabe T (2011) Halotolerant cyanobacterium Aphanothece halophytica contains an Na+-dependent F1F0-ATP synthase with a potential role in salt-stress tolerance. *The Journal of biological chemistry* **286:** 10169-10176

Sorgen PL, Caviston TL, Perry RC, Cain BD (1998) Deletions in the second stalk of F1F0-ATP synthase in Escherichia coli. *The Journal of biological chemistry* **273:** 27873-27878

Sorzano CO, Bilbao-Castro JR, Shkolnisky Y, Alcorlo M, Melero R, Caffarena-Fernandez G, Li M, Xu G, Marabini R, Carazo JM (2010) A clustering approach to multireference alignment of single-particle projections in electron microscopy. *Journal of structural biology* **171:** 197-206

Stahlberg H, Muller DJ, Suda K, Fotiadis D, Engel A, Meier T, Matthey U, Dimroth P (2001) Bacterial Na(+)-ATP synthase has an undecameric rotor. *EMBO reports* **2:** 229-233

Steffens K, Hoppe J, Altendorf K (1988) F0 part of the ATP synthase from Escherichia coli. Influence of-subunits a, and b, on the structure of-subunit c. *European journal of biochemistry / FEBS* **170:** 627-630

Sternweis PC (1978) The epsilon-subunit of Escherichia coli coupling factor 1 is required for its binding to the cytoplasmic membrane. *The Journal of biological chemistry* **253:** 3123-3128

Stewart AG, Sobti M, Harvey RP, Stock D (2013) Rotary ATPases: models, machine elements and technical specifications. *Bioarchitecture* **3:** 2-12

Stock D, Leslie AW, Walker JE (1999) Molecular Architecture of the Rotary Motor in ATP Synthase. *Science* **286:** 1700-1705

Studier FW, Moffatt BA (1986) Use of bacteriophage T7 RNA polymerase to direct selective high-level expression of cloned genes. *Journal of molecular biology* **189:** 113-130

Sumi M, Yohda M, Koga Y, Yoshida M (1997) F0F1-ATPase genes from an archaebacterium, Methanosarcina barkeri. *Biochemical and biophysical research communications* **241:** 427-433

Surin S, Cubonova L, Majernik AI, McDermott P, Chong JP, Smigan P (2007) Isolation and characterization of an amiloride-resistant mutant of Methanothermobacter thermautotrophicus possessing a defective Na+/H+ antiport. *FEMS microbiology letters* **269:** 301-308

Susaengrat W, Dhiensiri T, Sinavatana P, Sitprija V (1987) Renal failure in melioidosis. *Nephron* **46:** 167-169

Suzuki T, Murakami T, Iino R, Suzuki J, Ono S, Shirakihara Y, Yoshida M (2003) F0F1-ATPase/synthase is geared to the synthesis mode by conformational rearrangement of epsilon-subunit in response to proton motive force and ADP/ATP balance. *The Journal of biological chemistry* **278:** 46840-46846

Suzuki T, Ozaki Y, Sone N, Feniouk BA, Yoshida M (2007) The product of uncI gene in F1Fo-ATP synthase operon plays a chaperone-like role to assist c-ring assembly. *Proceedings of the National Academy of Sciences of the United States of America* **104:** 20776-20781

Swingley WD, Chen M, Cheung PC, Conrad AL, Dejesa LC, Hao J, Honchak BM, Karbach LE, Kurdoglu A, Lahiri S, Mastrian SD, Miyashita H, Page L, Ramakrishna P, Satoh S, Sattley WM, Shimada Y, Taylor HL, Tomo T, Tsuchiya T, Wang ZT, Raymond J, Mimuro M, Blankenship RE, Touchman JW (2008) Niche adaptation and genome expansion in the chlorophyll d-producing cyanobacterium Acaryochloris marina. *Proceedings of the National Academy of Sciences of the United States of America* **105:** 2005-2010

Symersky J, Pagadala V, Osowski D, Krah A, Meier T, Faraldo-Gomez JD, Mueller DM (2012) Structure of the c(10) ring of the yeast mitochondrial ATP synthase in the open conformation. *Nature structural & molecular biology* **19:** 485-491, S481

Tabor S, Richardson CC (1985) A bacteriophage T7 RNA polymerase/promoter system for controlled exclusive expression of specific genes. *Proceedings of the National Academy of Sciences of the United States of America* **82:** 1074-1078

Tang G, Peng L, Baldwin PR, Mann DS, Jiang W, Rees I, Ludtke SJ (2007) EMAN2: an extensible image processing suite for electron microscopy. *Journal of structural biology* **157:** 38-46

Toei M, Gerle C, Nakano M, Tani K, Gyobu N, Tamakoshi M, Sone N, Yoshida M, Fujiyoshi Y, Mitsuoka K, Yokoyama K (2007) Dodecamer rotor ring defines H+/ATP ratio for ATP synthesis of prokaryotic V-ATPase from Thermus thermophilus. *Proceedings of the National Academy of Sciences of the United States of America* **104:** 20256-20261

Tsukihara T, Aoyama H, Yamashita E, Tomizaki T, Yamaguchi H, Shinzawa-Itoh K, Nakashima R, Yaono R, Yoshikawa S (1996) The whole structure of the 13-subunit oxidized cytochrome c oxidase at 2.8 A. *Science* **272:** 1136-1144

Tsunoda SP, Rodgers AJ, Aggeler R, Wilce MC, Yoshida M, Capaldi RA (2001) Large conformational changes of the epsilon-subunit in the bacterial F1F0 ATP synthase provide a ratchet action to regulate this rotary motor enzyme. *Proceedings of the National Academy of Sciences of the United States of America* **98:** 6560-6564

Uhlin U, Cox GB, Guss JM (1997) Crystal structure of the epsilon-subunit of the proton-translocating ATP synthase from Escherichia coli. *Structure* **5:** 1219-1230

Valiyaveetil FI, Fillingame RH (1997) On the role of Arg-210 and Glu-219 of-subunit a in proton translocation by the Escherichia coli F0F1-ATP synthase. *The Journal of biological chemistry* **272:** 32635-32641

Valiyaveetil FI, Fillingame RH (1998) Transmembrane Topography of-subunit a in the Escherichia coli F1F0 ATP Synthase. *Journal of Biological Chemistry* **273:** 16241-16247

van Heel M, Gowen B, Matadeen R, Orlova EV, Finn R, Pape T, Cohen D, Stark H, Schmidt R, Schatz M, Patwardhan A (2000) Single-particle electron cryo-microscopy: towards atomic resolution. *Quarterly reviews of biophysics* **33:** 307-369

van Heel M, Harauz G, Orlova EV, Schmidt R, Schatz M (1996) A new generation of the IMAGIC image processing system. *Journal of structural biology* **116:** 17-24

Vik SB, Antonio BJ (1994) A mechanism of proton translocation by F1F0 ATP synthases suggested by double mutants of the a-subunit. *The Journal of biological chemistry* **269:** 30364-30369

Vik SB, Simoni RD (1987) F1Fo-ATPase from Escherichia coli with mutant Fo-subunits. Partial purification and immunoprecipitation of F1Fo complexes. *J Biol Chem* **17**: 8340-8346

Vik SB, Ishmukhametov RR (2005) Structure and function of-subunit a of the ATP synthase of Escherichia coli. *Journal of bioenergetics and biomembranes* **37:** 445-449

Vollmar M, Schlieper D, Winn M, Buchner C, Groth G (2009) Structure of the c14 rotor ring of the proton translocating chloroplast ATP synthase. *The Journal of biological chemistry* **284:** 18228-18235

von Ballmoos C, Appoldt Y, Brunner J, Granier T, Vasella A, Dimroth P (2002a) Membrane topography of the coupling ion-binding site in Na+-translocating F1F0 ATP synthase. *The Journal of biological chemistry* **277:** 3504-3510

von Ballmoos C, Brunner J, Dimroth P (2004) The ion channel of F-ATP synthase is the target of toxic organotin compounds. *Proceedings of the National Academy of Sciences of the United States of America* **101:** 11239-11244

von Ballmoos C, Meier T, Dimroth P (2002b) Membrane embedded location of Na+ or H+ binding sites on the rotor ring of F1F0 ATP synthases. *European Journal of Biochemistry* **269:** 5581-5589

von Meyenburg K, Jorgensen B, Michelsen O, Sorensen L, McCarthy J (1985) Proton conduction by-subunit a of the membrane-bound ATP synthase of Escherichia coli revealed after induced overproduction. *The EMBO journal* **4:** 2357-2363

Vonck J, Pisa KY, Morgner N, Brutschy B, Muller V (2009) Three-dimensional structure of A1A0 ATP synthase from the hyperthermophilic archaeon Pyrococcus

furiosus by electron microscopy. *The Journal of biological chemistry* **284:** 10110-10119

Vonck J, von Nidda TK, Meier T, Matthey U, Mills DJ, Kuhlbrandt W, Dimroth P (2002) Molecular architecture of the undecameric rotor of a bacterial Na+-ATP synthase. *Journal of molecular biology* **321:** 307-316

Wachter A, Bi Y, Dunn SD, Cain BD, Sielaff H, Wintermann F, Engelbrecht S, Junge W (2011) Two rotary motors in F-ATP synthase are elastically coupled by a flexible rotor and a stiff stator stalk. *Proceedings of the National Academy of Sciences of the United States of America* **108:** 3924-3929

Wada T, Long JC, Zhang D, Vik SB (1999) A novel labeling approach supports the five-transmembrane model of-subunit a of the Escherichia coli ATP synthase. *The Journal of biological chemistry* **274:** 17353-17357

Walker JE, Cozens AL, Dyer MR, Fearnley IM, Powell SJ, Runswick MJ (1987) Structure and genes of ATP synthase. *Biochemical Society transactions* **15:** 104-106

Walker JE, Saraste M, Gay NJ (1984) The unc operon. Nucleotide sequence, regulation and structure of ATP-synthase. *Biochimica et biophysica acta* **768:** 164-200

Walsh F, Duffy B (2013) The culturable soil antibiotic resistome: a community of multi-drug resistant bacteria. *PloS one* **8:** e65567

Watt IN, Montgomery MG, Runswick MJ, Leslie AG, Walker JE (2010) Bioenergetic cost of making an adenosine triphosphate molecule in animal mitochondria. *Proceedings of the National Academy of Sciences of the United States of America* **107:** 16823-16827

Wehrle F, Kaim G, Dimroth P (2002) Molecular mechanism of the ATP synthase's F(o) motor probed by mutational analyses of-subunit a. *Journal of molecular biology* **322:** 369-381

White NJ (2003) Melioidosis. *Lancet* **361:** 1715-1722

Whitmore A (1913) An Account of a Glanders-like Disease occurring in Rangoon. *The Journal of hygiene* **13:** 1-34 31

Wilkens S, Capaldi RA (1998) ATP synthase's second stalk comes into focus. *Nature* **393:** 29

Wilkens S, Dahlquist FW, McIntosh LP, Donaldson LW, Capaldi RA (1995) Structural features of the epsilon-subunit of the Escherichia coli ATP synthase determined by NMR spectroscopy. *Nature structural biology* **2:** 961-967

Wilkens S, Rodgers A, Ogilvie I, Capaldi RA (1997) Structure and arrangement of the delta-subunit in the E. coli ATP synthase (ECF1F0). *Biophysical chemistry* **68:** 95-102

Wilkinson L (1981) Glanders: medicine and veterinary medicine in common pursuit of a contagious disease. *Medical history* **25:** 363-384

Winer J, Jung CKS, Shackel I, Williams PM (1999) Development and validation of real-time quantitative reverse transciptase-polymerase chain reaction for monitoring gene expression in cardiac myocytes in vitro. *Analytical Biochemistry* **270:** 41-49

Wollert KC, Taga T, Saito M, Narazaki M, Kishimoto T, Glembotski CC, Vernallis AB, Heath JK, Pennica D, Wood WI, Chien KR (1996) Cardiotrophin-1 activates a distinct form of cardiac muscle cell hypertrophy. Assembly of sarcomeric units in series VIA gp130/leukemia inhibitory factor receptor-dependent pathways. *The Journal of biological chemistry* **271:** 9535-9545

Wuthiekanun V, Smith MD, White NJ (1995) Survival of Burkholderia pseudomallei in the absence of nutrients. *Transactions of the Royal Society of Tropical Medicine and Hygiene* **89:** 491

Yabuuchi E, Kosako Y, Oyaizu H, Yano I, Hotta H, Hashimoto Y, Ezaki T, Arakawa M (1992) Proposal of Burkholderia gen. nov. and transfer of seven species of the genus Pseudomonas homology group II to the new genus, with the type species Burkholderia cepacia (Palleroni and Holmes 1981) comb. nov. *Microbiology and immunology* **36:** 1251-1275

Yamada H, Moriyama Y, Maeda M, Futai M (1996) Transmembrane topology of Escherichia coli H(+)-ATPase (ATP synthase) subunit a. *FEBS letters* **390:** 34-38

Yasuda R, Noji H, Kinosita K, Jr., Yoshida M (1998) F1-ATPase is a highly efficient molecular motor that rotates with discrete 120 degree steps. *Cell* **93:** 1117-1124

Yasuda R, Noji H, Yoshida M, Kinosita K, Jr., Itoh H (2001) Resolution of distinct rotational substeps by submillisecond kinetic analysis of F1-ATPase. *Nature* **410:** 898-904

Yokoyama K, Oshima T, Yoshida M (1990) Thermus thermophilus membrane-associated ATPase. Indication of a eubacterial V-type ATPase. *The Journal of biological chemistry* **265:** 21946-21950

Yoshida M, Allison WS (1986) Characterization of the catalytic and noncatalytic ADP binding sites of the F1-ATPase from the thermophilic bacterium, PS3. *The Journal of biological chemistry* **261:** 5714-5721

Zhang Y, Fillingame RH (1994) Essential aspartate in subunit c of F1F0 ATP synthase. Effect of position 61 substitutions in helix-2 on function of Asp24 in helix-1. *The Journal of biological chemistry* **269:** 5473-5479

Zhang Y, Fillingame RH (1995) Changing the ion-binding specificity of the Escherichia coli H(+)-transporting ATP synthase by directed mutagenesis of subunit c. *The Journal of biological chemistry* **270:** 87-93

Zhu G, Chang Y, Zuo J, Dong X, Zhang M, Hu G, Fang F (2001) Fudenine, a C-Terminal Truncated Rat Homologue of Mouse Prominin, Is Blood Glucose-Regulated and Can Up-Regulate the Expression of GAPDH. *Biochemical and biophysical research communications* **281:** 951-956

Zilm PS, Rogers AH (2007) Co-adhesion and biofilm formation by Fusobacterium nucleatum in response to growth pH. *Anaerobe* **13:** 146-152

Zwart PH, Afonine PV, Grosse-Kunstleve RW, Hung LW, Ioerger TR, McCoy AJ, McKee E, Moriarty NW, Read RJ, Sacchettini JC, Sauter NK, Storoni LC, Terwilliger TC, Adams PD (2008) Automated structure solution with the PHENIX suite. *Methods in molecular biology* **426:** 419-435